ISSN 0911-5730
UVSOR-18
March 1991

UVSOR
ACTIVITY REPORT
1990

Ultraviolet Synchrotron Orbital Radiation Facility
Institute for Molecular Science

CONTENTS

APPENDIX

Preface

It is a great pleasure for me to publish the 1990 Activity Report which presents a number of synchrotron radiation studies carried out with our UVSOR Facility in 1990 as well as the recent situation of the Facility.

During the last year, our UVSOR synchrotron radiation source has been regularly operated with an electron energy of 750 MeV and at an initial ring current of 200 mA. Nine well-established beam lines (1B, 2B1, 3A1, 3A2, 6A1, 7A, 7B, 8A, and 8B1) have been provided for general users, while five beam lines (1A, 2A, 2B2, 3B, and 6A2) have been used by the in-house groups. Furthermore, three new recently completed beam lines (4A, 4B and 6B) will soon be used for surface photochemistry and for far-infrared microscopic spectroscopy mainly by in-house groups. Another beam line (5B) which belongs to the National Institute for Fusion Science has been used for calibration.

I am also pleased to mention that last spring the three researchers Dr. Shin-ichiro TANAKA, Dr. Shiro TAKANO, and Dr. Hiroyuki HAMA were appointed as Research Associates working at UVSOR.

The various joint programs operating at UVSOR throughout the 1990 fiscal year can be classified as followed; 3 Special-Project Programs, 28 Cooperative-Research Programs, and 104 Use-of-Facility Programs. Furthermore, two synchrotron radiation symposia were held at this Institute: One was a users' meeting, and the other was a workshop on synchrotron light sources.

I would like to express my thanks to all the UVSOR staff for their great efforts and contributions to the UVSOR Facility and its activity. I would also like to thank all the users for their cooperation.

January 1991

Katsumi KIMURA
Professor
Director of UVSOR

LIGHT SOURCE & BEAMLINES

Measurement of the Bunch Length of the UVSOR Storage Ring

Akihiko LIN*, Hiroyuki HAMA, Shirou TAKANO and Goro ISOYAMA

* Institute for Solid State Physics, University of Tokyo, Roppongi, Minatoku, Tokyo 106
Institute for Molecular Science, 38 Myodaiji, Okazaki 444

The bunch length of the UVSOR storage ring has been measured with the single photon counting method over wide ranges of beam energies from 500 to 750 MeV and stored beam currents from 100 μA to about 60 mA in the single bunch operation mode. The synchrotron radiation emitted in one of the bending magnets is detected with a fast photomultiplier. A time difference between signals from the photomultiplier and the revolution frequency is analyzed with a conventional time analyzing system. The overall time resolution of the detection system is estimated to be 194 pses (FWHM). The synchrotron frequency was also measured when a beam current is less than 1 mA.

The following three kinds of measurements have been made;

(a) dependence of the bunch length and the synchrotron frequency at E=750 MeV on the RF accelerating voltage. The beam current is kept less than 1 mA in order to avoid influences of the collective effect.

(b) dependence of the bunch length and the synchrotron frequency on the beam energy. The beam current is kept less than 1 mA and the RF voltage is fixed at a nominal value, about 50 kV.

(c) dependence of the bunch length on the beam current in the energy region from 500 to 750 MeV. The RF voltage is kept at the nominal value.

In the analysis, it is assumed that an energy spread of the electron beam is given by the single particle theory, an equilibrium distribution determined by quantum

excitation and radiation damping, and the energy of an electron is lost only by emission of the synchrotron radiation, when the beam current is low at E=750 MeV. From the experimental result in the measurement (a) and the above assumptions, the time resolution of the measurement system and the momentum compaction factor α are estimated, and the RF voltage is calibrated. From the measurements (a) and (b), it is confirmed that the electron energy and the RF voltage dependences of the bunch length agree well with the predictions of the single particle theory.

Figure 1 shows the current dependent bunch lengthening of the UVSOR storage ring at various beam energies. The bunch length becomes longer when the beam current is larger than a few mA, and the bunch lengthening is larger when the beam energy is lower. This behavior does not agree with a prediction of the microwave instability[1] that the bunch length becomes long as the 1/3 power of the beam current. The experimental bunch lengthening of the UVSOR storage ring shown in Fig. 1 is well reproduced by the potential distortion theory[2] if the effective impedance is taken as a free parameter. The effective impedances estimated above are shown in Fig. 2 as a function of bunch length. Although they are estimated from data taken at various beam currents and energies, all the points in Fig. 2 are located around a single curve, which varies smoothly from about 1.2 to 0.2 Ω as the bunch length changes from 0.033 to 0.055 m. This fact assures us that the bunch lengthening of the UVSOR storage ring is dominated by the potential distortion.

References

1) A.W. Chao, AIP Conf. Proc. **105**, 1982, p.353.
2) J.L. Laclare, Cern **87-03**, 1987, p.264.

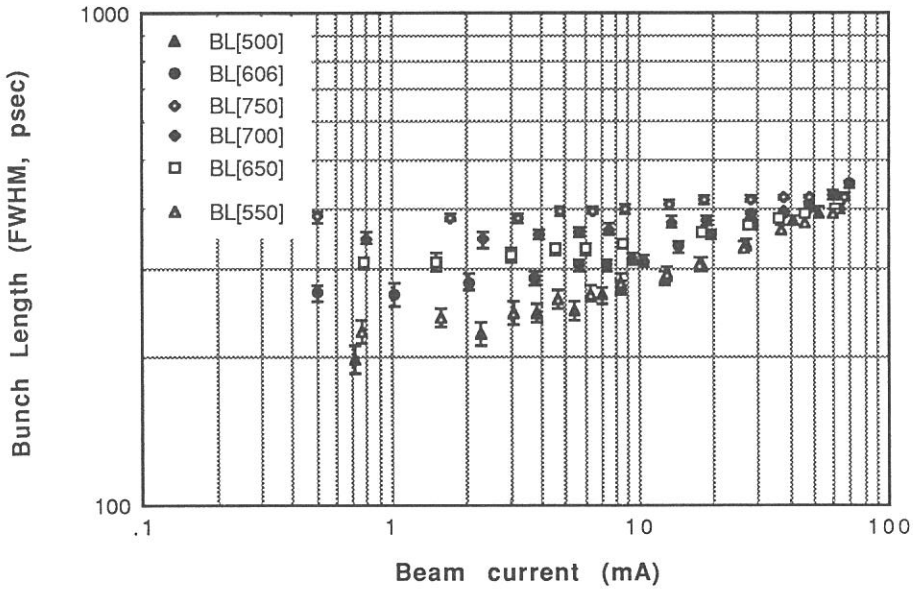

Fig.1. Bunch Lengthening of the UVSOR Storage Ring

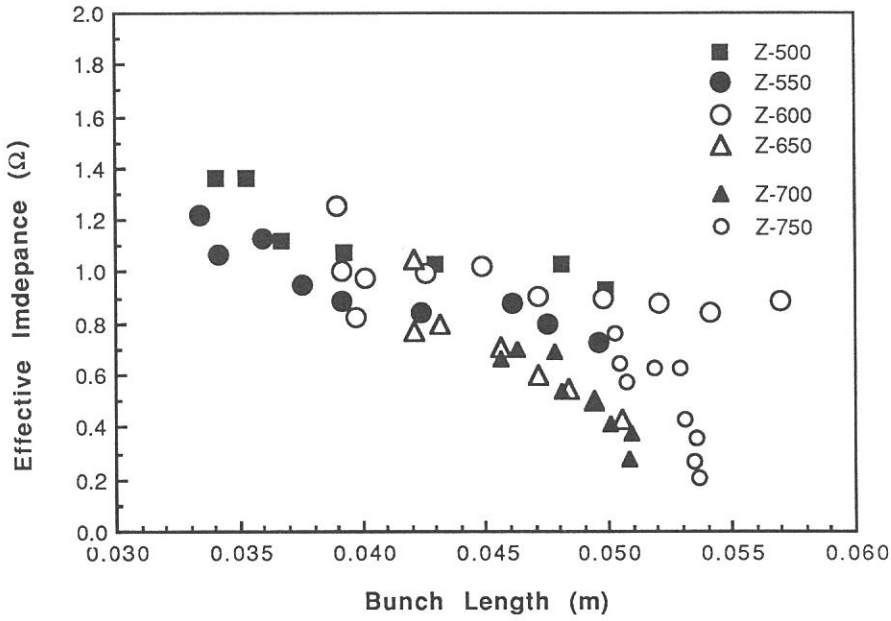

Fig. 2. Effective impedance as a function of bunch length

Free Electron Laser Experiment on the UVSOR Storage Ring

Shirou TAKANO, Hiroyuki HAMA, Goro ISOYAMA, and Akihiko LIN*

Institute for Molecular Science, 38 Myodaiji, Okazaki 444
*Institute for Solid State Physics, The University of Tokyo, Roppongi, Minatoku, Tokyo 106

A free electron laser (FEL) experiment is now being carried out on the UVSOR storage ring. The wavelength of light has been chosen to be 488 nm for an electron energy of 500 MeV.

For a gain measurement experiment, a conventional transverse undulator made of permanent magnets is employed for the moment, and is installed in one of the long straight sections of the storage ring. The period length and the number of periods of the undulator are 111 mm and 19, respectively. Electrons are stored in one of the 16 RF buckets (the single bunch operation) by the full energy injection. So far, the maximum stored beam current (average) I is about 60 mA. The beam life time is 25 min. at I = 50 mA, and is 70 min. at I = 10 mA. The peak current, which is estimated from a measurement of the longitudinal bunch length[1], is 5 A for the beam current I = 10 mA, whereas it is 19 A for I = 50 mA due to the bunch lengthening. The horizontal and the vertical beam sizes at the center of the straight section are σ_h = 0.7 mm and σ_v = 0.1 mm, respectively. The theoretical small-signal gain per pass estimated for the above conditions is $3\times10^{-3}(I/10mA)\mathcal{F}$, where $\mathcal{F}$ is a filling factor calculated from an overlap between the laser beam and the electron beam. Figure 1 shows an experimental arrangement for the gain measurement. An argon ion laser of 1 W (CW) output power is used as the external light, which is injected through a glass window into the straight section. The laser beam is focused to a waist near the center of the undulator by a mode matching telescope, and a direction of is varied with a frequency of about 100 kHz by a photoelastic modulator. The output light from the exit glass window passes through two irises and a bandpass filter, which reduce unwanted

spontaneous emission from the undulator, and is focused to a fast photodiode. The signal from the detector is amplified and processed by an spectrum analyzer. The signal due to stimulated emission or absorption is doubly modulated by the revolution frequency of the electron bunch (f_{rev} = 5.6 MHz) and by the modulation frequency of the laser beam (f_{mod} ~ 100 kHz), and it is observed as the side bands of the revolution frequency at $f_{rev} \pm f_{mod}$. A preliminary result of the experiment is given in figure 2. The upper panel shows the intensity of spontaneous emission as a function of the undulator gap. The lower panel shows the intensity of the sideband (open circles), which is proportional to an amplitude of the gain or loss, as well as a fit using an theoretical gain curve calculated from the spontaneous emission spectrum shown above (Maday's theorem). The measured peak gain without correction of the filling factor is estimated to be roughly 10^{-3} for the stored beam current I of 10 mA. We are now trying to obtain an accurate calibration of the peak gain.

For the next step, we plan to employ an undulator with the optical klystron configuration in order to increase the gain. The central three periods of the present undulator will be transformed into the dispersive section of the optical klystron by re-arranging magnet blocks. The magnet gap of the dispersive section can be varied independently of the normal undulator sections. We have chosen an optimum value of N_d to be 72, which is the number of light waves passing over an electron in the dispersive section. The estimated gain becomes 6-8 times higher than that with the conventional undulator for the energy spread of the electron beam σ_E/E = (5-10)$\times 10^{-4}$. After an amplifier experiment with this optical klystron, we will proceed to an oscillator experiment.

Acknowledgement: We are grateful to Dr. N. A. Vinokurov for his technical and theoretical suggestions for the experiment.

References

1) A. Lin 1991, Master Thesis, The University of Tokyo; A. Lin, H. Hama, S. Takano and G. Isoyama, a report in this volume.

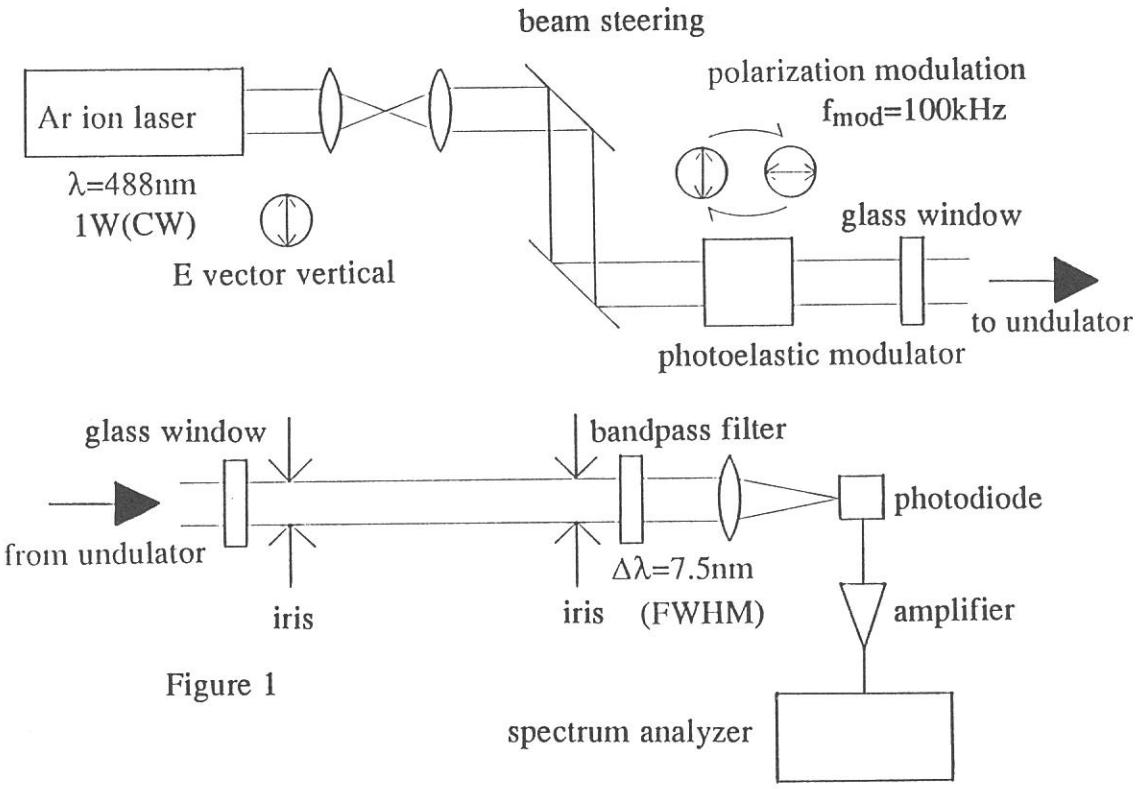

Figure 1

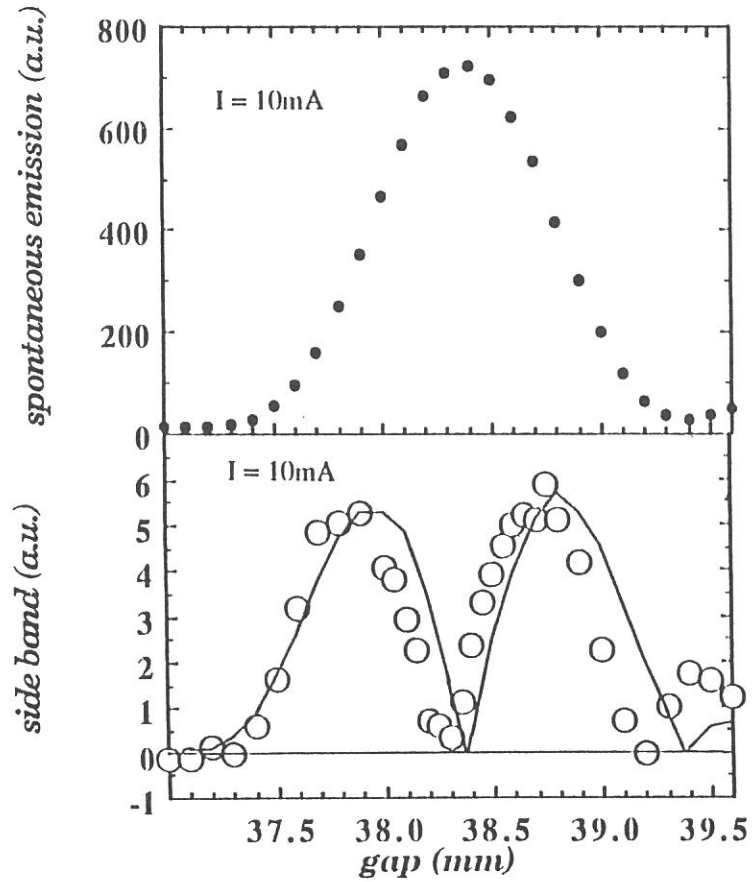

Figure 2

Construction of Beam Lines

M. Kamada and M. Watanabe

Institute for Molecular Science, Myodaiji, Okazaki 444

We are constructing four beam lines (BL1A, BL4A, BL4B, and BL6B). BL1A is designed for soft x-ray spectroscopy on gas and solids. Beam line valves, a pre-mirror chamber, and a double-crystal monochromator chamber have been constructed last autumn. The test of monochromator will be carried out this winter. BL4A and BL4B serve for photolysis and photo-chemical reaction experiments on solid surfaces. These beam lines consist of valves, pre-mirror chambers, reaction chambers, and analysing instruments. Both focused and unfocused synchrotron radiation can be supplied. BL6B is used for infrared spectroscopy. Beam line valves, a pre-mirror chamber, and a window chamber have been constructed last autumn. An interferometer equipped with a microscope will be installed this winter. Synchrotron radiation through various ir-window materials can be used at this beam line.

Thus, we have now nineteen beam lines at UVSOR Facility (see Table II in Appendix). Nine of them (BL1A, BL2A, BL2B2, BL3B, BL4A, BL4B, BL6A2, BL6B, and BL8B2) are mainly used by in-house staffs of IMS (outside researchers can also use them), one of them (BL5B) is belonging to National Institute for Fusion Science, and the others (BL1B, BL2B1, BL3A1, BL3A2, BL6A1, BL7A, BL7B, BL8A, and BL8B1) are opened to both inside and outside users of IMS. There are four 1m Seya-Namioka, one 3m normal incidence, three plane grating, three grazing incidence and two double-crystal motochromators for vacuum ultraviolet and soft x-ray, and one interferometer for far infrared. An interferometer for infrared will be installed soon at BL6B.

Construction of New Soft X-ray Beam Line at BL1A

Atsunari HIRAYA, Toshio HORIGOME, Norio OKADA, Nobuo MIZUTANI, Kusuo SAKAI, Osamu MATSUDO, Masami HASUMOTO, Kazutoshi FUKUI† and Makoto WATANABE

Institute for Molecular Science, Myodaiji, Okazaki 444
†Department of Electrical and Electronics Engineering, Fukui University, Fukui 910

A new soft X-ray beam line equipped with a double crystal monochromator (DXM) has been constructed at BL1A. In order to gather synchrotron radiation and focus it at the sample position a pre-mirror is used for this beam line, which is the main difference between BL1A and the existing soft X-ray beam line BL7A. Both the minimum reflection loss in the soft X-ray region and the good focusing without astigmatism at the sample position are required for this mirror. In order to fulfill these requirements the grazing angle of 1 ° was selected and a cylindrical mirror (550 mm long, 30 mm wide, 15 mm thick, 50.5 mm curvature, Pt coated) was elliptically bent for horizontal focusing by pressing on an elliptic surface of the mirror holder. With this pre-mirror horizontal acceptance angle of BL1A is 4.2 mrad which is about two times wider than that of BL7A. Focused spot size of the monochromatized X-ray measured by a multi-channel-plate with phosphor screen was 2 mm wide and 1 mm high at the sample position.

Figure 1 shows the scanning mechanism of the new DXM which is essentially the same with the DXM at BL7A.[1] Fixed direction and constant offset of the monochromatized X-ray beam during the change of Bragg angle is realized as follows. By linear-guides indicated by horizontal arrows, vertical positions of the centers of the first and second crystal surfaces are confined on the levels of the incident and

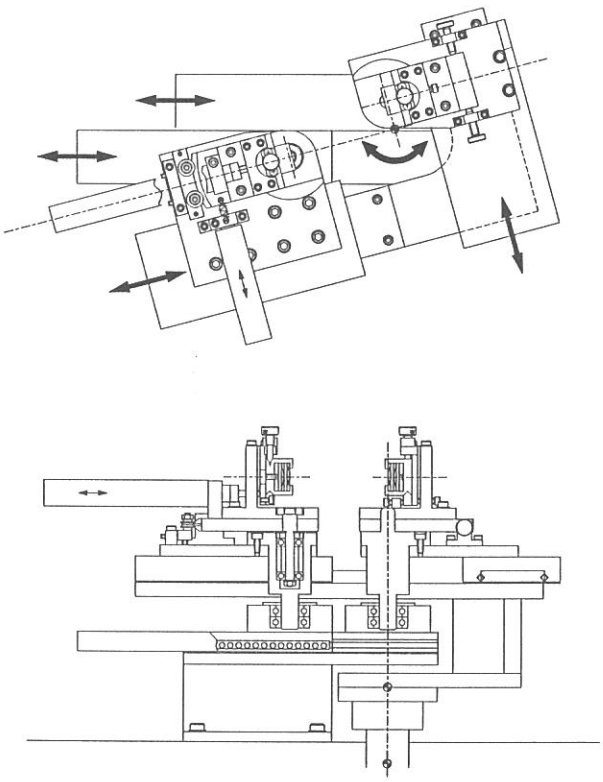

Figure 1. Drawing of the scanning mechanism of the double crystal monochromator at BL1A.

monochromatized beams, respectively. By other linear-guides indicated by slanting arrows moving along each arm of a L-shaped base, the crystal surfaces are kept parallel with each other. Scanning of Bragg angle is introduced by the rotation of the L-shaped base indicated by a curved arrow. For each crystal a pair of the former and the latter linear-guides are linked at the rotation axis on the crystal surface. Therefore the angles and horizontal positions of two crystals are synchronously driven so that the first and second crystals reflect the beam at their center of crystal surface at any Bragg angle to the fixed direction with constant offset. In order to angle adjustments of the second crystal with keeping vacuum of the monochromator chamber, two motorized-screws with encoders (Oriel Encoder Mike™) are used.

Figure 2 shows the throughput spectrum of BL1A behind the double crystal monochromator with beryl crystals measured by an electron multiplier tube (EMT) with an Au first dynode. Compared with the throughput spectrum of BL7A (DXM with another pair of beryl crystals) measured by the same EMT, the throughput of BL1A is found to be 3 ~ 4 times higher than that of BL7A over the scanning range of the DXM.

1) T.Murata, T.Matsukawa, M.Mori, M.Obashi, S.Naoe, H.Terauchi, Y.Nishihata, O.Matsudo and J.Yamazaki. J. de Phys. **C8** (1986) 135.

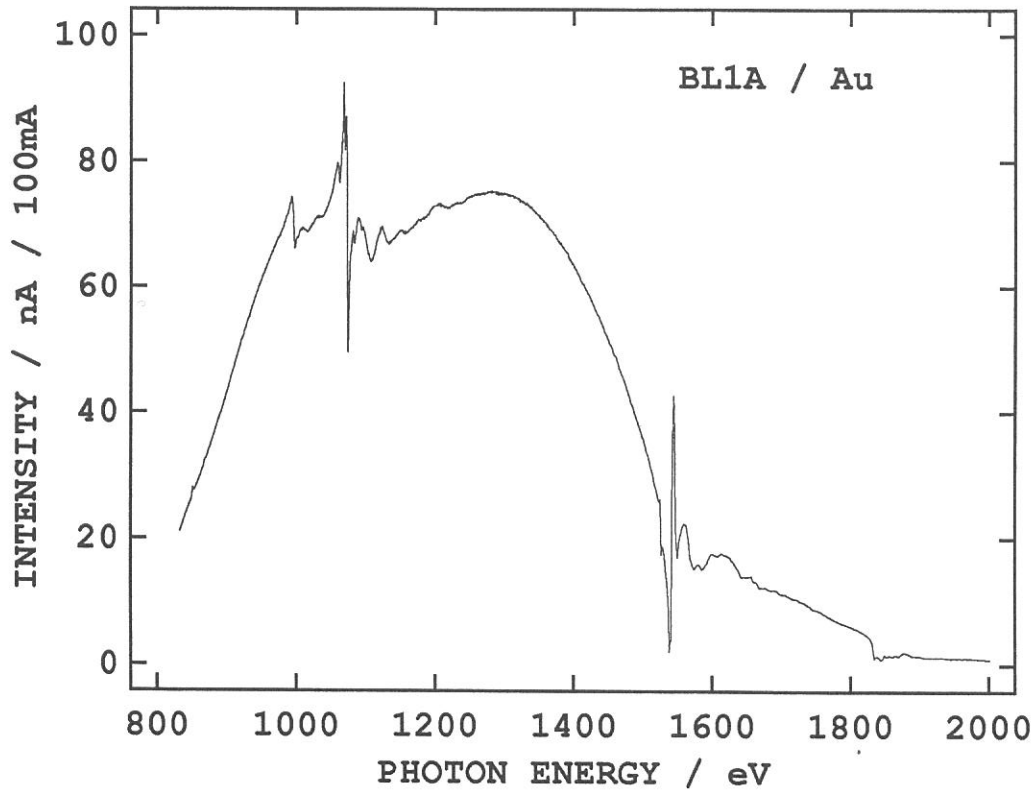

Figure 2. Throughput spectrum of double crystal (Beryl) monochromator at BL1A.

Utilization of Multilayers as the Dispersive Element of Soft X-Ray Monochromator

M. Watanabe, O. Matsudo, J. Yamazaki, S. Takahama* and K. Yamashita**

UVSOR, Institute for Molecular Science
*Department of Physics, Faculty of Science, Osaka University
**Institute for Space and Astronautical Science

Recently, multilayers have been developed extensively in the VUV and soft X-ray region as the efficient reflectors.[1] Since the reflectivity is enhanced at the wavelength which satisfies the usual Bragg condition $n\lambda=2d\sin\theta$, the multilayers can be used as a dispersive element. The resolution is the order of 10^{-2}.

For a double crystal monochromator (DXM) at BL7A,[2] a pair of beryl crystals is used as the dispersive element below 15 Å. Above 15 Å a KAP crystal is a candidate of the dispersive element. However, it is weak against the strong irradiation of synchrotron radiation, so that it can not be used as the first crystal of the DXM. In this experiment, instead of the KAP crystal a multilayer (W/Si) with 2d=53.2 Å is used as the first dispersive element and the KAP crystal (2d=26.6 Å) was used as the second dispersive element. In this case, the second order light (n=2) dispersed with the multilayer is again dispersed by the KAP crystal in the first order. Figure 1 a) shows the output photon flux distribution detected by a nude photomultiplier with a photocathode coated with Nacl. One can see O-K absorption of BeO which is the substrate material of the photocathode around 550 eV and Na-K absorption of NaCl around 1070 eV. The intensity decreases with the decrease in the photon energy below Na-K edge. This feature may be due to the reflection characteristics of the multilayer in the second order and the absorption of a Be foil of 5 μm thickness, which is located in front of the DXM to separate the vacuum of the DXM from that of the front end of BL7A. Figure 1 b) shows the detailed spectra around Na-K edge. The curve 1 is

the spectrum obtained without the collimation of the beam. The resolution is low. The curve 2 shows the spectrum obtained with the collimation of the incident and dispersed beams with two pinholes of which diameters are 0.8 mm. The resolution is improved, but not so good as that by using a pair of beryl crystals (curve 3).

Another experiment is now under way to get higher photon flux with less resolution by the use of a pair of multilayers (W/B_4C) with 2d=31.2 Å in the first order.

References

1) Proc. Int. Conf. Soft X-ray Optics and Technology, Berlin 1986, Proc. SPIE **733** (1987), p.307.

2) T. Murata et al.: J. de Phys. **C8** (1986) 135.

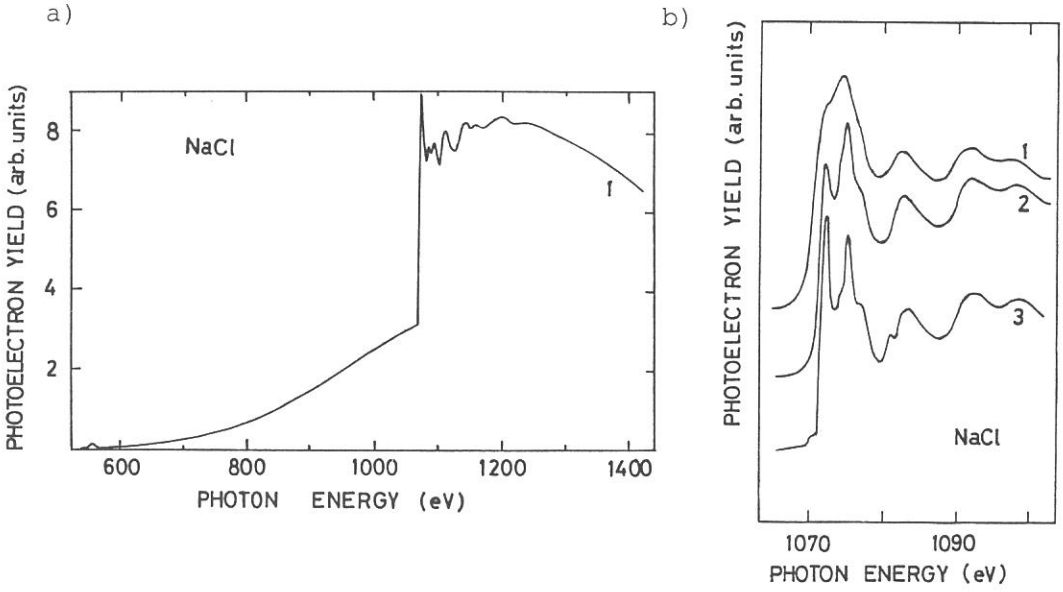

Fig.1. Output spectra from DXM detected by a nude photomultiplier with a NaCl coated photocathode, a) in the 550-1400 eV and b) 1070-1100 eV region. Curves 1 and 2 are spectra obtained by using a multilayer (W/Si, 2d=53.2 Å) as the first disperse element and a KAP crystal as the second one, without and with collimator of two pinholes with 0.8 mm diameter, respectively and curve 3, spectrum obtained by using a pair of beryl crystals.

Construction of the Second Experimental Chamber and Interchanging Mechanism for Focusing Mirrors

Makoto SAKURAI and Eiji ISHIGURO *

National Institute for Fusion Science, Nagoya 464-01
*Faculty of Engineering, Osaka City University, Osaka 558

BL5B is dedicated for various radiometric research projects in the wavelength range from VUV to SX. The experimental chamber of the beam line enables calibration and characterization of various type of optical elements and detectors [1], however, ultimate pressure of the chamber ($1x10^{-8}$ Torr) is insufficient for basic research such as to identify physical processes in surface sensitive detectors and clarify the correlation between surface structures and optical characteristics.

Under this necessity, the second experimental chamber was constructed and installed on the beam line at 3.3m downstream from the focusing mirror (M_3) of the plane grating monochromator (PGM) [2] as shown in Fig. 1. Since the original mirror has a focal point at 1.1m position (Q_1), we needed the second toroidal mirror for the other focal point (Q_2). Then, we calculated optimum parameters and manufactured a new mirror and a mirror holder which accomodates two focusing mirrors and enables to interchange the mirrors in vacuum. Fig. 2 shows calculated beam size at Q_2 for each combination of gratings and mirrors of the PGM with the optimized parameters; the radii of the toroid are R_V=23278mm and R_H=67mm for vertical and horizontal directions, respectively. Fig. 3 shows cross sectional view of the interchanging mechanism. The mirrors have three degrees of freedom: tilting around two axes and translation along horizontal direction perpendicular to the optical axis. Observed beam size was 2x5 mm^2 for the visible part of the 0th order light. The second experimental chamber, 450mmϕx700mm in size, is evacuated by a turbo-molecular pump, a sputter ion pump and a titanium sublimation pump with liquid nitrogen shroud, and is equipped with two (co-axial) rotational stages at the bottom of the chamber. Between the two experimental chambers, a rare gas ionization chamber is inserted to measure the absolute intensity of incident photon flux in the VUV regions. Positions of both entrance and exit windows of the chamber are adjustable in vacuum. This part also works as a

differential pumping stage which enables an experiment with SR light in the 10^{-10} Torr range at the second chamber while the first chamber remaining in the 10^{-8} Torr range.

References

1) M. Sakurai et al., Vacuum **41**, 1234 (1990).

2) M. Sakurai et al., Rev. Sci. Instrum. **60**, 2089 (1989).

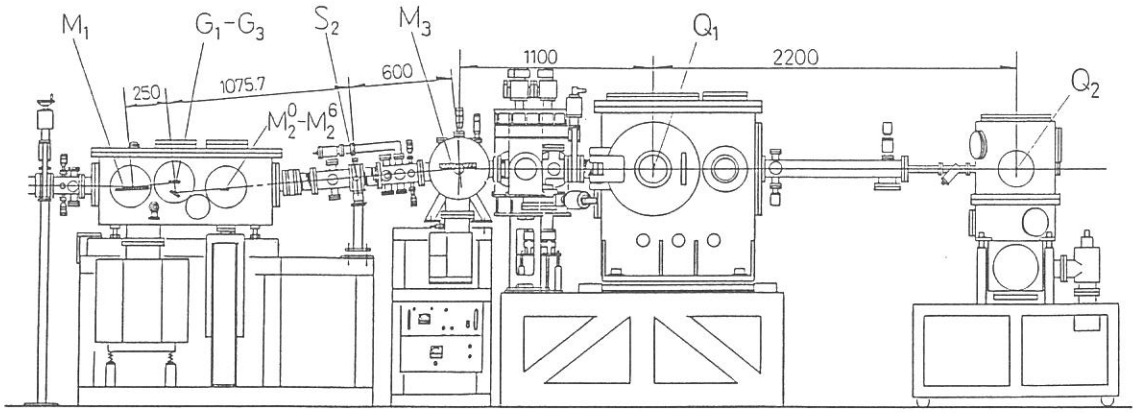

Fig. 1. Schematic diagram of BL5B.

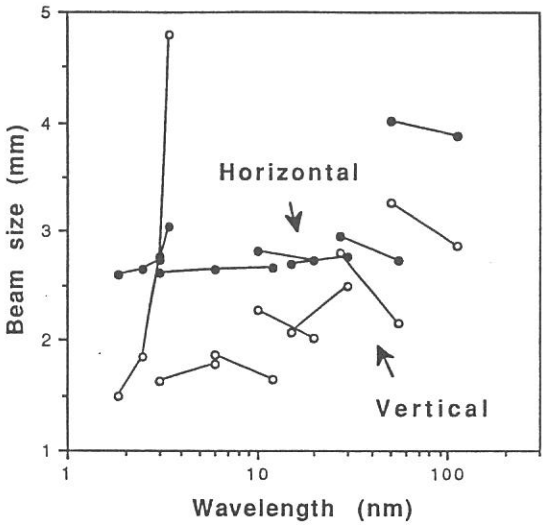

Fig. 2. Calculated beam size at Q_2.

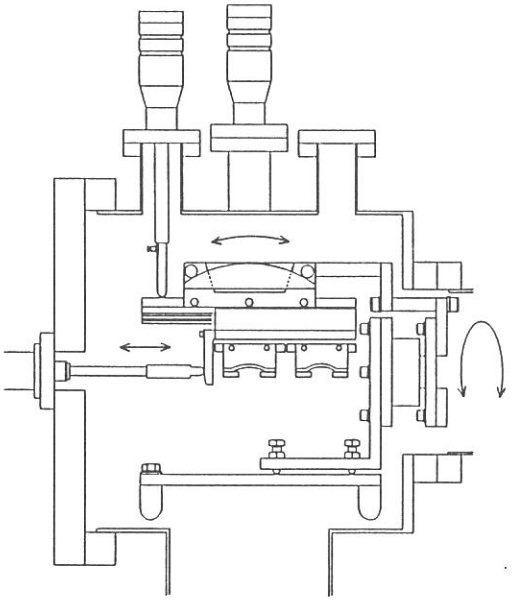

Fig. 3. Cross sectional view of interchanging mechanism for focusing mirrors.

RESEARCH ACTIVITIES

EXCITATION SPECTRUM OF CN($A^2\Pi_i$) AND CN($B^2\Sigma^+$) PRODUCED BY PHOTODISSOCIATION OF BrCN IN THE 105 - 155 nm REGION

Kazuhiro KANDA, Syunji KATSUMATA,
Takashi NAGATA*, Tamotsu KONDOW*,
Atsunari HIRAYA**, Kiyohiko TABAYASHI** and Kosuke SHOBATAKE**

Department of Fundamental Science, College of Science and Engineering, Iwaki Meisei University, Iwaki 970
* Department of Chemistry, Faculty of Science, the University of Tokyo, Bunkyo-ku 113
** Institute for Molecular Science, Myodaiji, Okazaki 444

Photodissociation of cyanogen bromide,

$$BrCN + h\nu \rightarrow Br + CN(A^2\Pi_i, B^2\Sigma^+) \qquad (1)$$

was studied in the wavelength range of 110-115 nm by the measurement of the excitation function for the subsequent CN(A-X) and CN(B-X) emission. The synchrotron radiation dispersed by a 1-m Seya-Namioka monochrometer at the BL2A line of UVSOR was used as an excitation source. Emission from the product CN radicals were monitored as a function of excitation wavelength. The fluorescence excitation spectra thus obtained are depicted in Fig. 1. The absolute scale for the ordinate was determined by a comparison of the emission intensities observed in process (1) with those in the photodissociation of HCN, for which the absolute emission cross section has been reported in the range of 105-150 nm.[1] The emission cross sections determined in the present study correspond to the cross sections for the production of CN(A) and CN(B) radicals from BrCN, because no processes other than radiative decay is expected for the $A^2\Pi_i$ and $B^2\Sigma^+$ states of CN. The band structures appearing in the fluorescence excitation spectrum were assignable to the transitions to high-lying Rydberg states of BrCN. The excitation function shows that the production of CN(B) radical is favored in the Rydberg states located below 135 nm, whereas the cross section for the CN(A) production exceeds that for CN(B) in the longer wavelength region. These observations can be explained qualitatively in terms of the correlation between the molecular orbitals of BrCN and those of CN radical. For example, the $2\pi \rightarrow 3s\sigma$ excitation of BrCN preferentially leads to the formation of CN(A) radical; The 2π orbital of the parent molecule correlates to the 1π orbital of CN and,

hence, the Rydberg state having a $(2\pi)^{-1}3s\sigma$ configuration directly correlates to the dissociation channel of Br + $CN(A^2\Pi_i)$, which has a $(1\pi)^{-1}5\sigma$ configuration. On the other hand, the production of CN radical in the $B^2\Sigma^+[(4\sigma)^{-1}(1\pi)^4 5\sigma]$ state is favorable in the photodissociation via the Rydberg states with a $(6\sigma)^{-1}$ configuration. This is also consistent with the fact that the 6σ orbital of BrCN primary correlates to the 4σ orbital of CN radical.

reference

1) L. C. Lee, J. Chem. Phys., *72*, 6414 (1980).

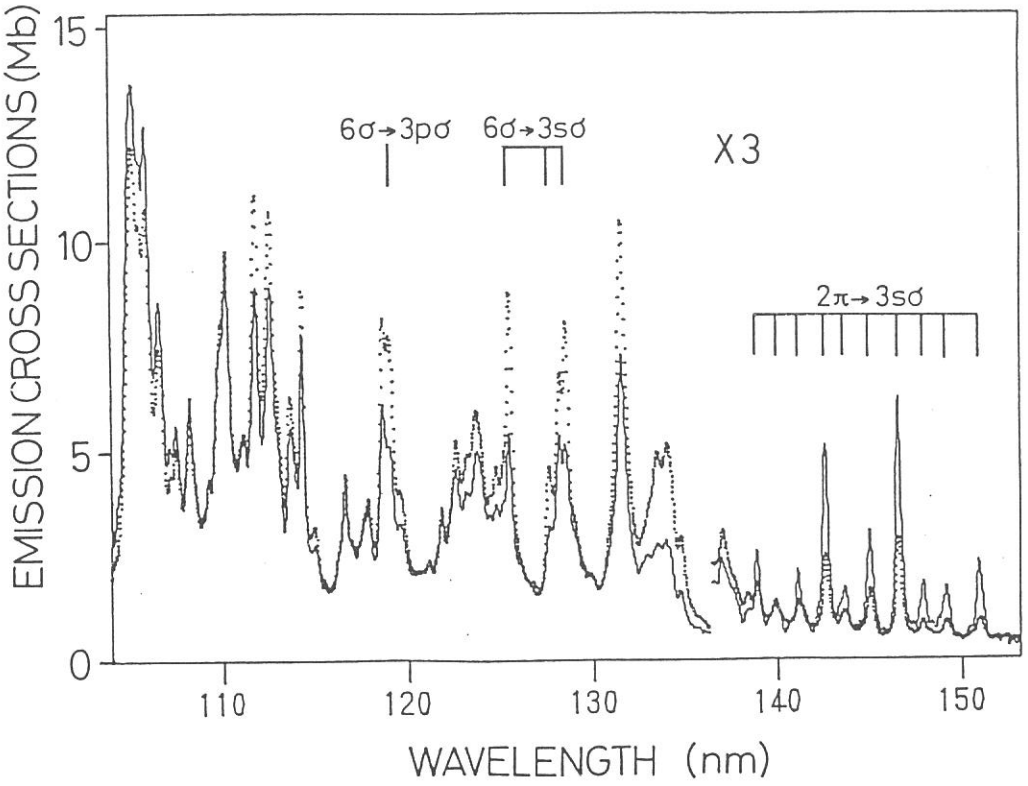

Fluorescence excitation spectra of $CN(A^2\Pi_i)$ (solid line) and $CN(B^2\Sigma^+)$ (dotted line) from BrCN. The cross sections were measured at the pressure of 28 mTorr.

RYDBERG TRANSITIONS OF CH_3Br and CD_3Br

Ikuo TOKUE, Atsunari HIRAYA* and Kosuke SHOBATAKE*

Department of Chemistry, Niigata University, Niigata 950-21
**Institute for Molecular Science, Myodaiji, Okazaki 444*

Vibronic structures of the lowest *s* and *p* Rydberg states of alkyl bromides have been studied in detail by vacuum ultraviolet (VUV) photoabsorption spectra or electron energy-loss spectra. There has been however only a little amount of information about assignments of higher Rydberg members. The splitting of the lone-pair ionization potentials caused by the spin-orbit interaction was either very small, as in methyl chlorides, or very large, as in methyl iodides. Thus, the splittings in methyl bromides can be of intermediate size. In such a case, Rydberg peaks are badly overlapped and assignments then become that much more difficult and tentative.

In this study photoabsorption cross sections (c.s.) of CH_3Br and CD_3Br were measured using synchrotron radiation (BL2A station) in the 105-230 nm region. The observed transitions were grouped and then the value of ionization potential (IP) and the quantum defect (δ) were refined by a least-square method using the form

$$\bar{\nu}_n = \mathrm{IP} - R/(n - \delta)^2.$$

Fig. 1 shows the VUV absorption spectra of CH_3Br and CD_3Br with the Rydberg progressions identified. The observed transitions were grouped in three and two Rydberg series converging to the first and second IP, respectively. The assignments for the Rydberg series thus obtained are summarized in Table 1. The $s\sigma$ type Rydberg series converging to the first and second IP are remarkably prominent and complete among the five series identified.

Vibrational progressions coupled with many of lower Rydberg members have been identified by comparing with the fundamental frequencies for the ground state. For CH_3Br, prominent vibrational spacings of 2830—2580, 1100—1245 and 570—450 cm^{-1} have been assigned to the CH_3 sym. str. (ν_1), CH_3 sym. def. (ν_2) and CBr str. (ν_3) vibrations, respectively.

Moreover, the vibrational spacing of 1400—1280 and 810—630 cm-1 observed can be assigned to CH_3 asym. def. (ν_5) and CH_3 rocking (ν_6) vibrations, respectively. Although the assignment for CD_3Br is more difficult than that for CH_3Br, the prominent spacings of 930—800 and 510—400 cm^{-1} have been assigned to ν_2 and ν_3, respectively. These prominent vibrational progressions indicate that the geometries for the Rydberg states are fairly different from that for the ground state.

Table 1 Rydberg series, IP and δ for CH_3Br and CD_3Br

Parent	Rydberg series	IP (cm^{-1})	δ	n
CH_3Br	$(^2E_{3/2})ns\sigma$	85072	3.06	5—13
	$np\sigma$	85064	2.53	5—10
	$nd\sigma$	85062	1.26	4—7
	$(^2E_{1/2})ns\sigma$	87643	3.07	5—13
	$np\sigma$	87665	2.55	5—9
CD_3Br	$(^2E_{3/2})ns\sigma$	85072	3.07	5—13
	$np\sigma$	85094	2.52	5—9
	$nd\sigma$	84937	1.22	4—6
	$(^2E_{1/2})ns\sigma$	87793	3.06	5—13
	$np\sigma$	87790	2.51	5—9

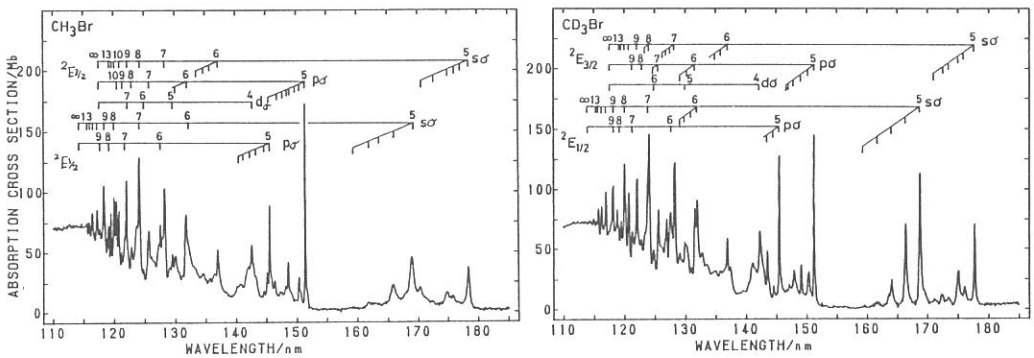

Fig. 1. The absorption c.s. in the 110-185 nm region measured at a spectral resolution of 0.2 nm: (a) CH_3Br at a vapor pressure of 9 mTorr and (b) CD_3Br at 8 mTorr.

UV AND VUV ABSORPTION MEASUREMENT OF JET COOLED CHLOROBENZENE

Teijiro ICHIMURA, Atsunari HIRAYA,* and Kosuke SHOBATAKE*

Dept. of Chemistry, Tokyo Inst. of Technology, Ookayama, Meguro-ku, Tokyo 152
**Institute for Molecular Science, Myodaiji, Okazaki 444 Japan*

The direct absorption spectrum of chlorobenzene C_6H_5Cl in a supersonic free jet is measured in the wavelength region of 130-271 nm, where the S_1, S_2, S_3, and Rydberg states are excited, using synchrotron radiation as a light source. The absolute molar extinction coefficient (ε) of some S_1 vibronic bands have been determined: the ε value for 0-0 transition are found to be 730 M^{-1} cm^{-1} for a spectral resolution of 0.2 nm. The minimum observable ε was 150 M^{-1} cm^{-1}.

A supersonic free jet apparatus installed to the BL2A beam line was used to measure the absorption spectrum of jet cooled chlorobenzene. The chlorobenzene vapor (100 Torr) in an Ar carrier gas at a total stagnation pressure of 350 Torr was expanded into a free jet chamber through a conical nozzle (throat diameter: 0.38 mm, exit diameter: 1.10 mm, and channel length: 3 mm) attached to a fuel injector. The fuel injector was operated at 10 Hz with an open duration of 40 msec. The nozzle temperature was usually set at higher temperatures than that of the sample tube in order to avoid forming chlorobenzene clusters. The free jet chamber was isolated from the chambers of the monochromator and the last focusing mirror by a LiF window. UV and VUV light monochromated by a 1 m Seya-Namioka type monochromator enters the free jet chamber through the LIF window and crosses the free jet. The transparent light is monitored by a combination of sodium salicylate coating on the exit window and a photomultiplier tube. Signals from the transmitted light were fed to two counting scalers, each enabled by each timing signal (gate width 30 msec). After accumulating for 10 on-off signals at each wavelength, the transparent photon counts corresponding to the free jet on, I_{on}, and that for to the free jet off, I_{off} were obtained. The absorbance of a sample in a free jet at the wavelength was determined as $\log(I_{off}/I_{on},)$, regardless of any fluctuations in the incident light intensity, and the absorption spectrum was obtained by scanning the wavelength of the monochromated synchrotron radiation.

Figure 1 shows the direct absorption spectrum of jet-cooled chlorobenzene seeded in Ar. The absorption spectrum in the observed wavelength region includes the S_1 (240-271 nm), S_2 (225-195 nm), S_3 (195-160) and Rydberg (170 - 130 nm) states. The ordi-nates of the figure are the absorbance, $\log(I_{off}/I_{on})$ and the molar extinction coefficient, ε.. The absolute value of ε at a given wavelength λ_{exc} is determined by normalizing the observed absorbance, $\log(I_{off}/I_{on})$ to that for the 215.0 nm band of the S_2 state, where the absolute ε value is measured in the room temperature vapor (ε = 6.07 x 10^3 Mol^{-1} cm^{-1}), assuming that (i) the ε values at 215.0 nm are identical in both the vapor phase and the free jet, and (ii) the effective

product of the concentration c and path length l, $c\,l$, determined at the reference wavelength (215.0 nm) can be used at other wavelengths. The former assumption is justified because of the breadth of the band. The minimum value of 0-0 transition at the S_2 state is determined as 150 Mol^{-1} cm^{-1} corresponding to 0.3 % standard deviation in the (1- I_{on}/I_{off}) value. That value is the minimum observable absorption in this study. For the strong absorption at the broad maximum of the S_3 state (185.0 nm) saturation effects should be taken into account under the present experimental conditions.

It should be emphasized here that the absorption spectrum measured under the present conditions is free from absorption due to chlorobenzene clusters $(C_6H_5Cl)_n$ ($n \geq 2$). In contrast when the Ar carrier gas pressure is increased to 760 Torr broad absorption bands are found to appear around 200 nm in addition to the bands of isolated chlorobenzene. These new feature may be attributed to chlorobenzene clusters rather than $C_6H_5Cl\cdots Ar_n$ ($n \geq 1$) clusters, since the absorption spectra of jet cooled benzene at a stagnation pressure of 760 Torr with different carrier gases were essentially the same, indicating that the major clusters formed are benzene clusters rather than $C_6H_6\cdots Rg_n$ (Rg = He, Ar, Xe).[1]

References

1) A. Hiraya and K. Shobatake, *Chem. Phys. Lett.* (in press).

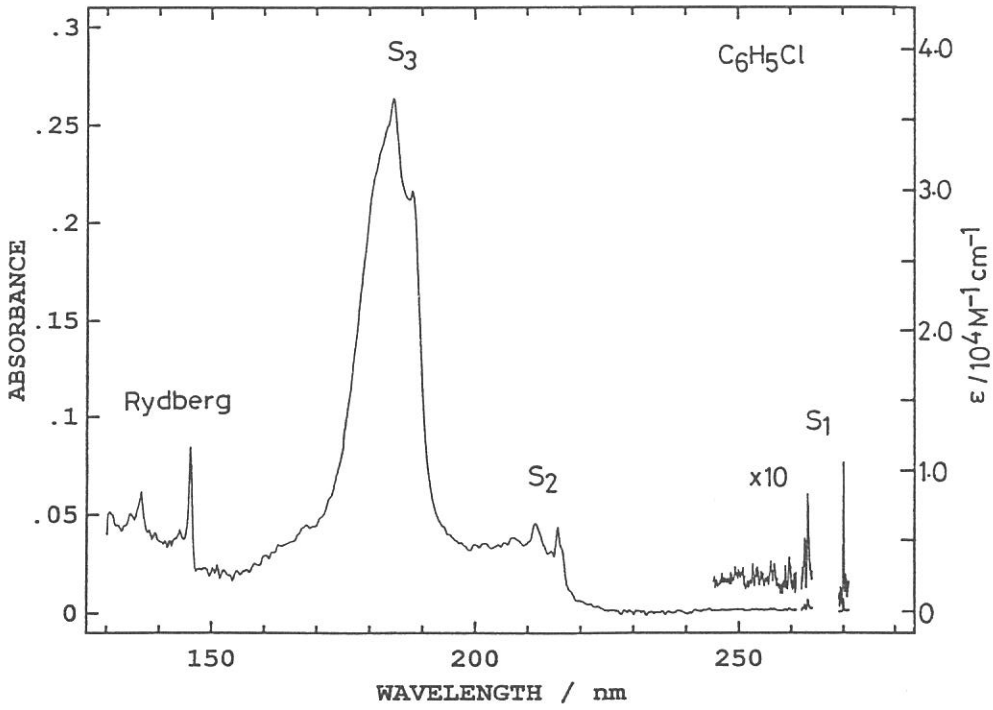

Figure 1. Absorption spectrum of jet cooled chlorobenzene seeded in Ar. The partial pressure of chlorobenzene was 100 Torr and that of Ar was 250 Torr. The stagnation temperature was kept at 80°C. The spectral resolution was 0.2 nm.

PHOTOCHEMISTRY OF RARE GAS-DIHALOGEN VAN DER WAALS MOLECULES III. VUV EXCITATION DYNAMICS OF RARE GAS··· DIHALOGEN COMPLEXES

Kiyohiko TABAYASHI, Atsunari HIRAYA, and Kosuke SHOBATAKE
Institute for Molecular Science, Myodaiji, Okazaki 444 Japan

In the VUV region we have found two types of new van der Waals (vdW) molecular bands originated from 1:1 Rg···Cl_2 (Rg = Kr and Xe) complexes[1] formed in the free jet expansion of regulated Cl_2/Rg/Ne mixtures, and they are assigned to the transition to the excited states of $RgCl^+Cl^-$ and/or $RgCl_2^-$ entities. The characteristics of the bands so far observed are summarized as follows:

(A) The Xe···Cl_2 complex exhibits two broad *absorption* bands (**A bands**) in the 125-150 nm region, whereas only very weak *fluorescence* was detected for these bands although relatively strong absorption was observed. Similar observations have been made for the Cl_2/Kr/Ne system.

(B) Careful measurements have enabled us to observe a rather fine vibrational structure (**B bands**) in the fluorescence excitation spectrum in the 138-145 nm region (Figure 1b), when only the fluorescence is monitored between 230 and 400 nm using a band-path filter, which covers the excimer emissions, XeCl(C→A and B→X) and $Cl_2(2^3\Pi_g \rightarrow 1^3\Pi_u)$. Since the fine structure is embedded in the rather strong,broad absorption feature, it was not resolved in the absorption spectrum.

From the similarity for the absorption spectra of both Xe···Cl_2 and Kr···Cl_2 complexes, **A bands** may be attributed to the excited state of ion-pair $RgCl^+Cl^-$ type. The significant depletion of fluorescent channels must be attributed to (pre-)dissociation of the photoexcited vdW complex to the non-fluorescent dissociated products via highly vibrationally excited states and then after curve-crossing to repulsive potential surfaces,

$$Xe\cdots Cl_2 + h\nu \rightarrow XeCl^+Cl^- (v' = m),$$
$$XeCl^+Cl^- \rightarrow Xe + 2\ Cl.$$

In the **B bands** a large vibrational spacing of $\Delta\nu \sim 640\ cm^{-1}$ is observed, which indicates that the excited state is of Rydberg-type Cl_2^* character. We propose that two kinds of excimer formation channels contribute to the emissions in the 230 - 400 nm region:

$$Xe\cdots Cl_2^* \rightarrow XeCl^* + Cl$$
$$\rightarrow Xe + Cl_2^*(2^3\Pi_g).$$

More detailed study is underway in order to determine the relative importance of each fluorescent channel as a function of excitation energy and to further clarify the quenching mechanism of the electronically excited rare gas-dihalogen vdW complexes.

Reference

[1] K. Tabayashi, A. Hiraya, and K. Shobatake, *UVSOR Activity Report 1989*, **17**, 8 (1990)

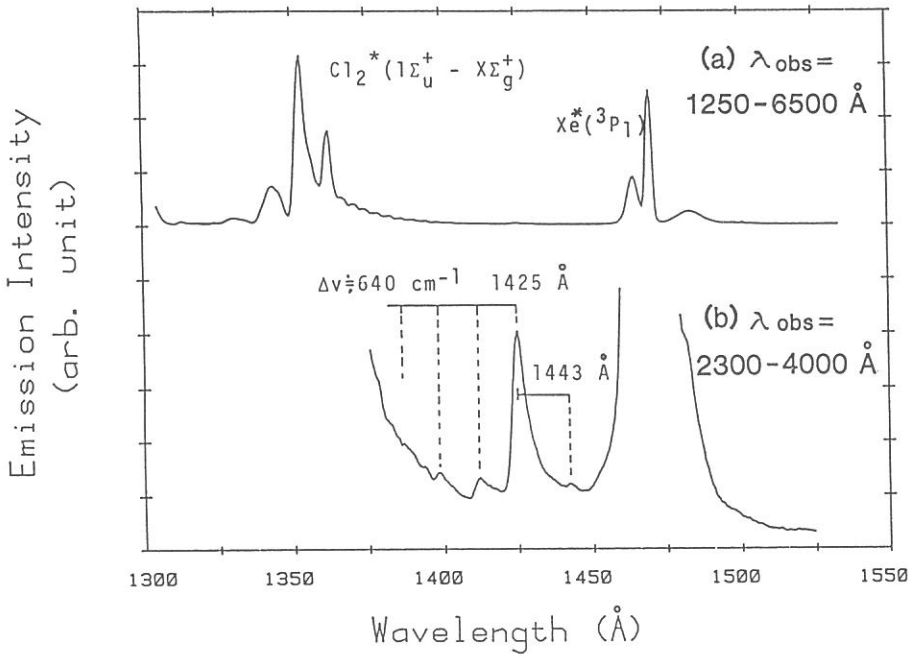

Figure 1. Fluorescence excitation spectra of free jets of Cl_2/Xe mixture under two conditions for emission detection. a) Spectrum obtained using Hamamatsu PMT (model R585MGF2) which is sensitive to the 125 - 650 nm region. The stagnation condition: the gas mixing ratio is 4.6% Cl_2 in Xe, the stagnation pressure p_0 = 265 Torr, and T_0 = 1°C. b) Spectrum obtained through a bandpath filter so that emissions in the wavelength region 230 nm < λ_{obsd} < 400 nm are detected. Stagnation conditions; the gas mixing ratio is 2.4 % Cl_2 in Xe, p_0 = 265 Torr, and T_0 = 2°C.

FORMATION AND PHOTOEXCITATION OF RARE GAS MICROCLUSTERS DOPED WITH Cl_2

Kiyohiko TABAYASHI, Atsunari HIRAYA, and Kosuke SHOBATAKE

Institute for Molecular Science, Myodaiji, Okazaki 444 Japan

In the present project VUV absorption and fluorescence spectroscopy has been applied to investigate photophysical processes of rare gas clusters and Cl_2 doped microclusters with average size $N < 1000$ formed in supersonic free jets under regulated expansion conditions. The spectral features of Xe clusters for large average cluster size N are found to well correspond to the exciton bands observed in the solid crystals. When N is larger than 150 (cluster radius $r \sim 12$Å), an exciton band for the principal number $n = 2$ appears. A linear relation has been observed between the intensities for absorption and fluorescence excitation spectra of Xe_N clusters when the emissions in the shorter wavelength region than 220 nm ($\lambda_{obsd} < 220$ nm) is detected, which suggests nearly a constant (probably a unity) quantum yield for the radiative process. This finding indicates that Xe_N clusters formed in free jets have a crystal-like lattice structure.

Figure 1 illustrates the absorption spectra obtained for free jets of pure Xe and a gas mixture of 1.2% Cl_2 in Xe. The comparison of the two absorption spectra tells us that the absorption feature does not change much upon doping a very small amount of Cl_2 gas in the supersonic flow, except for (i) a slight decrease in cluster band intensities, probably due to less cooling inherent to the addition of gaseous molecules with a larger heat capacity, and (ii) the appearance of a broad, weak absorption feature in the wavelength region $\lambda_{exc} < 146$ nm. The Cl_2 doped clusters, $Xe_N \cdots Cl_2$, exhibit excitonic transitions in the absorption spectrum.

On the contrary when a very small amount of Cl_2 gas is added to the free jet flow of pure Xe, a dramatic change is observed in the spectral profile of the fluorescence excitation. That is, the fluorescence intensities of the exciton bands almost disappear, leaving almost only the emissions assigned to excited atoms (M), dimer (D), and small clusters dominated. The present observations demonstrate that large sized Cl_2-doped clusters are definitely formed but fluorescent products, which emit in the 125-800 nm region, are not formed. Therefore it is concluded that non-radiative processes such as excitation transfer from the exciton to impurity Cl_2 and/or Xe/Cl_2 entities are quite effective. The dissociative process of excited Cl_2 in Xe "matrix" followed by excess energy disposal into Xe lattice can be considered as the main quenching channel.

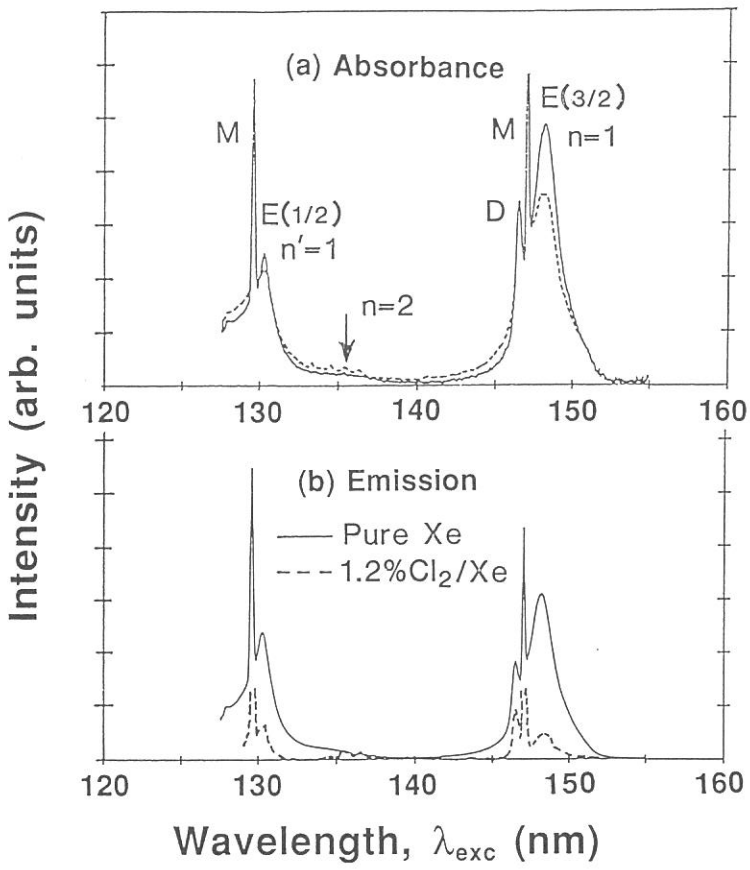

Figure 1. Comparison of the absorption and fluorescence ($\lambda_{obsd} < 220$ nm) excitation spectra of Cl_2 doped clusters with those of pure Xe clusters Xe_N. Spectral resolution is 0.2 nm. Stagnation conditions: $p_0 = 350$ Torr, and $T_0 = 22°C$. A diverging nozzle (throat diameter = 0.38 mm, exit diameter = 1.18 mm, and channel length = 3.0 mm) is used.

Fluorescence of SiH_4 subsequent to the Si-2p core excitation

Eiji ISHIGURO, Muneo HITOMI, Toshio IBUKI*, Haruhiko OHASHI**, Atsunari HIRAYA*** and Makoto WATANABE***

Department of Applied Physics, Osaka City University, Osaka 558
*Kyoto University of Education, Kyoto 612
**Toyohashi University of Technology, Toyohashi 440
***Institute for Molecular Science, Okazaki 444

Fluorescence measurement is a useful method to detect excited neutrals resulting from photodissociation of molecules. We have observed fluorescence of SiH_4 following the Si-2p core excitation. Dispersed fluorescence spectra in the uv and visible region were obtained with a monochromator(JY,HR-320) equipped with a 1024 multichannel detector (Princeton Instru. Inc.,).

Figure 1 shows the fluorescence spectrum of SiH_4 in the 1,900A-8,500A region obtained with the excitation by white light. Most of lines below 3,000A arise from the excited neutral Si atom(Si I). A band around 4,100A is attributed to emissions of SiH molecule. Some weak lines of ionic Si atom(Si II) can also seen in the spectrum. Dispersed Fluorescence Spectra were also taken for excitation by monochromatic light with various photon energies which corresponded to an unoccupied valence band, Rydberg bands, the ionization continuum or the L1 bands. However, no remarkable difference could be found between the spectra, because of weak monochromatic lights and as a result, because of a small SN ratio.

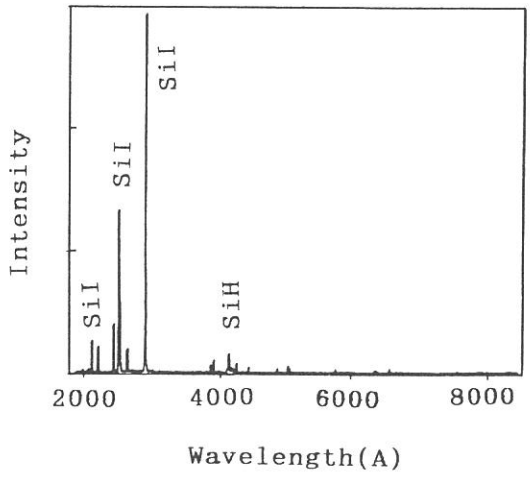

Fig.1 Fluorescence spectrum of SiH_4 obtained with excitation of the zeroth order light

Figure 2 shows a dependence of non-dispersed fluorescence intensities on

the excitation energy, together with an absorption spectrum(a). The fluorescence in Fig.2(b),(c) and (d) was detected by a PM sensitive to the region from 160 to 650nm, by a solar blind PM with a MgF_2 window to the region from 115 to 195 nm and by a channeltron with a MgF_2 window to the region around 120nm, respectively. In the three excitation spectra, there is a drastic enhancement just below the ionization edge. This region consists of a number of Rydberg bands which could not be resolved in the present experiment. Similar enhancement in the Rydberg region was observed for fluorescence of neutral fragments resulting from photodissociation of SiF_4 following excitation of a Si-2p electron[1]. This enhancement was explained by assuming that the Rydberg excitation resulted in production of excited fragments because of less overlap of the Rydberg orbital with the molecular ion core. To check this assumption, a high resolution experiment is necessary. We are going to do this sort of experiment in the near future.

Reference
1)R.A.Rosenberg, C.R.Wen,T.Tan and J.M.Chen, J.Chem.Phys. 92,5196(1990)

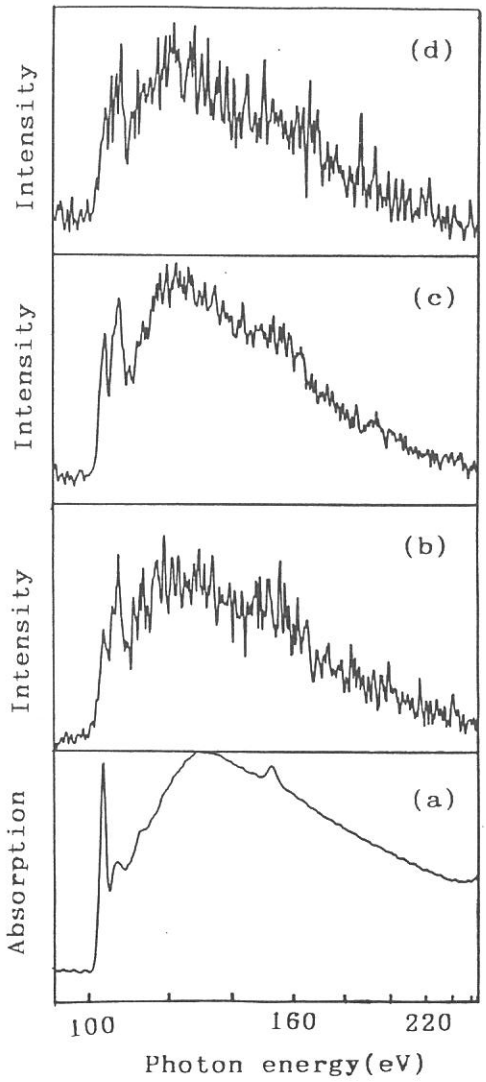

Fig.2 Absorption spectrum(a) and excitation spectra(b)-(d) of fluorescence of SiH_4. In the spectra (b) and (c), non-dispersed fluorescence in the uv/visible region(160-650nm) and in the vuv region(115-195nm) was detected, respectively, while in the spectrum(d) a narrow band fluorescence around 120nm was detected to obtain the H-Lyα emission at 121.6nm.

Performance of a New Threshold-Photoelectron Photoion Coincidence Apparatus at BL2B2

Kenji FURUYA, Takato HIRAYAMA,* and Katsumi KIMURA

Institute for Molecular Science, Myodaiji, Okazaki 444
*Department of Physics, Gakushuin University, Toshima-ku, Tokyo 171

We have designed and constructed a new threshold-photoelectron photoion coincidence (TPEPICO) spectrometer, which was basically designed by Hirayama *et al.*,[1] in order to improve the resolution of a time-of-flight mass spectrometer. The new spectrometer makes it easier to estimate the kinetic energy released in the fragmentation of polyatomic molecules, particularly hydrocarbons. It is also possible to study the photoionization processes of mass-selected atomic and molecular clusters.

Schematic view of the new spectrometer is shown in Figure 1. The dispersed light from a 1-m Seya-Namioka monochromator is re-focused at the center of a 2 cm wide ionization/acceleration region at a field of 10 V/cm. With this new spectrometer, it is possible to obtain a resolution of 20 meV for threshold electrons at a photon resolution of about 14 meV, and to separate adjacent mass units beyond 100 amu. Figure 2 shows a TPEPICO spectrum of Kr obtained at 84.5 nm. The known abundances of the krypton isotopes are 82, 11.6 %; 83, 11.5 %; 84, 57.0 %; 86, 17.3 %. The intensity ratios in the TPEPICO spectrum are consistent with the corresponding abundances.

Coincidence experiments on the fragmentation of hydrocarbon molecules are in progresss.

Reference

1) T. Hirayama, S. Nagaoka, and K. Kimura, UVSOR Activity Report 1988, p.38.

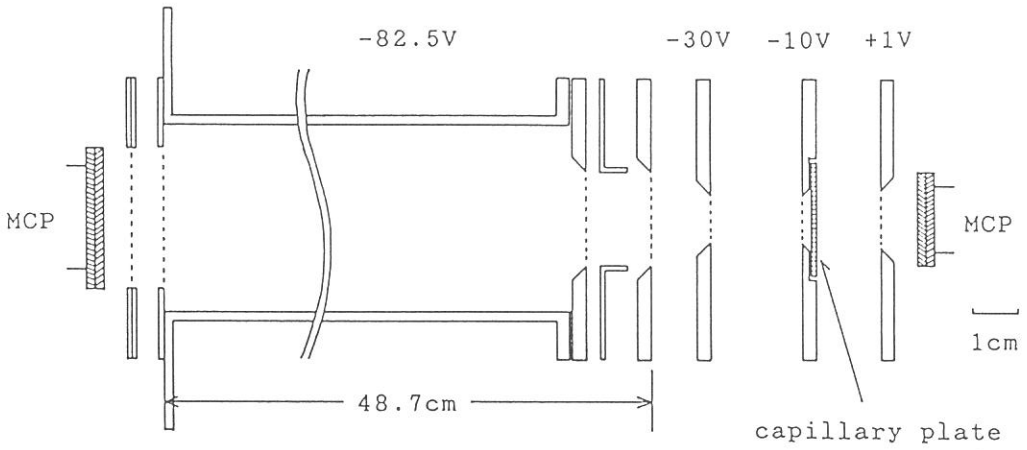

Figure 1. Schematic view of the threshold-photoelectron photoion coincidence spectrometer.

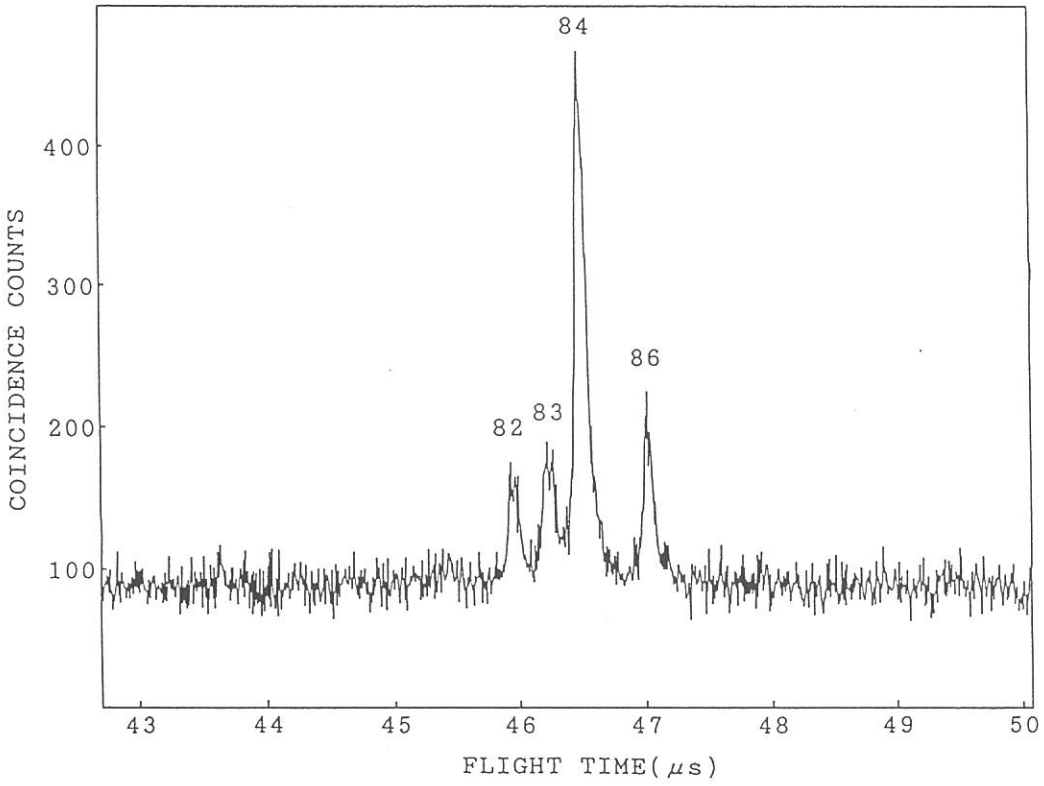

Figure 2. TPEPICO spectrum of Kr at 84.5 nm.

DISSOCIATIVE SINGLE AND DOUBLE PHOTOIONIZATION OF NITRIC OXIDE IN THE RANGE $h\nu$=30-110 eV

Toshio MASUOKA and Inosuke KOYANO*

Department of Applied Physics, Osaka City University, Sumiyoshi, Osaka 558
*Department of Material Science, Himeji Institute of Technology, Shosha, Himeji 671-22

Double photoionization processes have received increasing attention in the past decade and have been shown to contribute significantly to ion yields even in the region of the valence orbitals. The results have been interpreted as due to electronic many-body effects (the electron correlations). In the present study, we report the dissociative and non-dissociative double photoionization of nitric oxide examined by use of synchrotron radiation and time-of-flight mass spectrometry. In order to obtain accurate photoionization branching ratios over the wide photon energy range of 30-110 eV, the following precautions were taken in the measurements. 1) The photoion branching ratios were measured at the pseudo magic angle (~55°), which ensures uniform collection of photoions and photoelectrons without any effect of their angular distributions. In order to avoid energy discrimination effects of photoions, the photoion branching ratios were measured as a function of the length of the TOF drift tube, and the ratios were obtained by extrapolating those to the 'zero' length of the TOF drift tube. 3) Several optical filters were used throughout the photon energy range for order sorting and reduction of the unwanted scattered light.

The results obtained with 60 cm long drift tube are shown in Fig. 1 for the stable NO^{2+} and fragmented N^{2+} and O^{2+} ions. The

photoion branching ratio for NO^{2+} at 60 eV amounts to 4.5%, which is pretty large compared with those (1.6%) measured in the previous photon-impact experiments.[1,2] The present ratio for NO^{2+} should be considered as a higher limit. The effects of the presence of two electrons used as the start signal for the time-to-amplitude converter on the photoion branching ratios is under examination. The appearance potential of NO^{2+} is at 38.5 $\pm$ 0.1 eV, which agrees well with the most recent value (38.6 $\pm$ 0.1 eV).[3] There is a break in the curve at 40.5 eV indicating the appearance of the second stable NO^{2+} state ($A^2\Pi$).[3] The photoions N^{2+} and O^{2+} have not been observed in the previous experiments.[1,2] The present data show that the appearance energies for the N^{2+} and O^{2+} ions lie at 59.0 $\pm$ 0.5 and 66.5 $\pm$ 0.5 eV, respectively.

References
1) J.A.R. Samson, T.Masuoka, and P.N.Pareek, J. Chem. Phys. **83**, 5531 (1985).
2) Y. Iida, F.Carnovale, S.Daviel, and C.E.Brion, Chem. Phys. **105**, 211 (1986).
3) M.J.Besnard, L.Hellner, Y.Malinovich, and G.Dujardin, J. Chem. Phys. **85**, 1316 (1986).

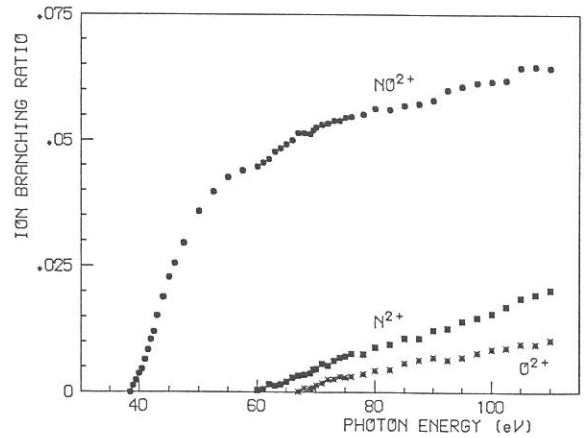

Fig. 1. Photoion branching ratios for NO^{2+} (●), N^{2+} (■), and O^{2+} (✱) as a function photon energy measured with 60 cm long drift tube.

KINETIC ENERGY RELEASE IN DISSOCIATIVE DOUBLE PHOTOIONIZATION OF OCS

Toshio MASUOKA, Inosuke KOYANO,* and Norio SAITO**

Department of Applied Physics, Osaka City University, Sumiyoshi, Osaka 558
*Department of Material Science, Himeji Institute of Technology, Shosha, Himeji 671-22
**Electrotechnical Laboratory, Umezono, Tsukuba-shi, Ibaraki 305

One of the interesting aspects of the study of dissociative double photoionization is the determination of kinetic energy release in fragmentation of AB^{2+}.[1] Because of Coulomb repulsion between two positive holes, doubly charged molecular ions are generally unstable and dissociate to fragment ions (plus neutrals) with a continuous distribution of the total kinetic energy, which reflects the energy difference of the dissociative part of the potential surface of AB^{2+} and the internal energies shared by the fragment ions, both with respect to the ground states.

In the present study, kinetic energy distributions (KED) of fragment ions produced in the dissociative double photoionization of OCS have been studied in the photon energy region 37-100 eV by use of synchrotron radiation and the photoion-photoion coincidence (PIPICO) method.[2] The most probable KED was determined for the three major dissociation channels $OC^+ + S^+$, $O^+ + S^+ + O$, and $C^+ + S^+ + O$ of OCS^{2+} at selected photon energies by analyzing the spectral profiles of the PIPICO peaks measured at the pseudo magic angle ($\sim 55°$) at which the effect of angular distribution is minimized. For the channel $OC^+ + S^+$ at $h\nu = 37$ eV, the KED ranges 3-6.3 eV with the mean energy of 4.5 eV (Fig. 1), whereas the channel $O^+ + S^+ + C$ at $h\nu = 100$ eV exhibits a wide range of KED (5-23.6eV) of two ionic fragments in the direction parallel to the

PIPICO spectrometer axis (Fig. 2). The mean kinetic energy released in this latter channel is 6.3 eV at 50 eV and increases to 12.8 eV at 100 eV. The increase in the mean kinetic energy as a function of the excitation energy can be attributed to the ejection of two inner valence electrons that causes a strong Coulomb repulsion. The first observation of nearly continuous KED released in the direct double photoionization from valence orbitals is discussed in relation to the electronic states of OCS^{2+}.

References

1) G. Dujardin, S. Leach, O. Dutuit, P. M. Guyon, and M. Richard-Viard, Chem. Phys. **88**, 339 (1984); G. Dujardin, D. Winkoun, and S. Leach, Phys. Rev. A **31**, 3027 (1985).

2) T. Masuoka and I. Koyano, J. Chem. Phys. submitted.

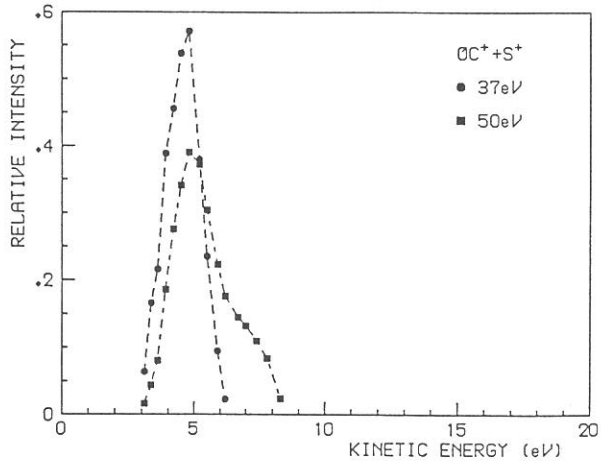

Fig. 1. Kinetic energy distribution of $OC^+ + S^+$ measured at the excitation energy of 37 and 50 eV.

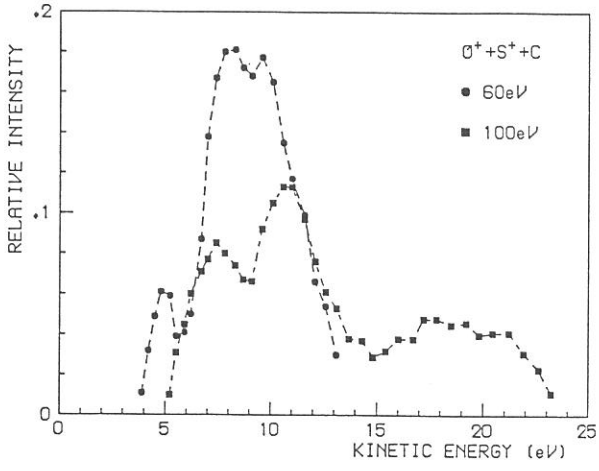

Fig. 2. Kinetic energy distribution of $O^+ + S^+ + C$ measured at the excitation energy of 60 and 100 eV.

ANISOTROPIC ANGULAR DISTRIBUTION OF FRAGMENT IONS IN DISSOCIATIVE DOUBLE PHOTOIONIZATION OF OCS

Toshio MASUOKA, Inosuke KOYANO,* and Norio SAITO**

Department of Applied Physics, Osaka City University, Sumiyoshi, Osaka 558
*Department of Material Science, Himeji Institute of Technology, Shosha, Himeji 671-22
**Electrotechnical Laboratory, Umezono, Tsukuba-shi, Ibaraki 305

The angular distribution of photodissociation products is closely related to the symmetry of the transition processes involved and the molecular dissociation dynamics.[1,2] We report here the first observation of angular distributions of fragment ions produced in the direct (not via Auger decay) double photoionization of OCS studied in the photon energy region 37-100 eV by use of synchrotron radiation and the photoion-photoion coincidence (PIPICO) method. The TOF mass spectrometer could be rotated through 90° around the photon beam in order to measure characteristic profile of PIPICO spectra.

The spectral profiles of PIPICO peaks were analyzed by a least squares fit of the simulated profiles to those measured parallel and perpendicular to the electric vector of the incident polarized light. The results of the asymmetry parameter for the channel $OC^+ + S^+$ are shown in Fig. 1, where the value ranges from 0.10 (at 37 eV) to 0.36 (the mean at 50 eV) in the photon energy region of 37-50 eV. The observed β value is a result of competition between two types of transition $\Sigma - \Sigma$ and $\Sigma - \Pi$. If the cross section ($\sigma_{//}$) for the $\Sigma - \Sigma$ type transitions is equal to that ($\sigma_{\perp}$) of $\Sigma - \Pi$, the β parameter is 0.5 from the equation[2] $\beta = (2\sigma_{//} - \sigma_{\perp})/(\sigma_{//} + \sigma_{\perp})$. The equation gives $\sigma_{//}/\sigma_{\perp} = 0.58$ at 37 eV and 0.83 at 50 eV, i.e., the $\Sigma - \Pi$ type transition is ~70% and

~20% more probable than the $\Sigma-\Sigma$ type transition at 37 and 50 eV, respectively. The β parameters for other channels are shown in Fig. 2, which shows that the β parameter for each dissociation channel differs from one another beyond the uncertainty (typically $OC^+ + S^+$, $O^+ + S^+ + C$ or $C^+ + S^+ + O$, and $O^+ + CS^+$ at 50 eV) as a natural consequence of different ionic states involved in each dissociation channel.

References
1) R. N. Zare, Mol. Photochem. 4, 1 (1972).
2) J. L. Dehmer and D. Dill, Phys. Rev. A 18, 164 (1978).

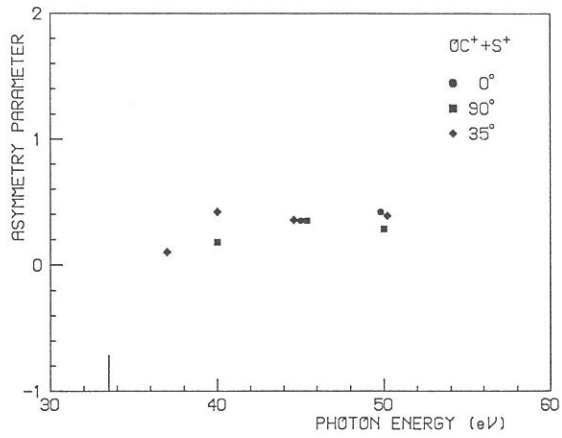

Fig. 1. Asymmetry parameter β for the channel $OC^+ + S^+$ measured at θ=0° (●), 90° (■), and 35° (◆) in the region 37-50 eV. Vertical bar indicates the dissociation channel of $OC^+ + S^+$ at 33.5 eV.

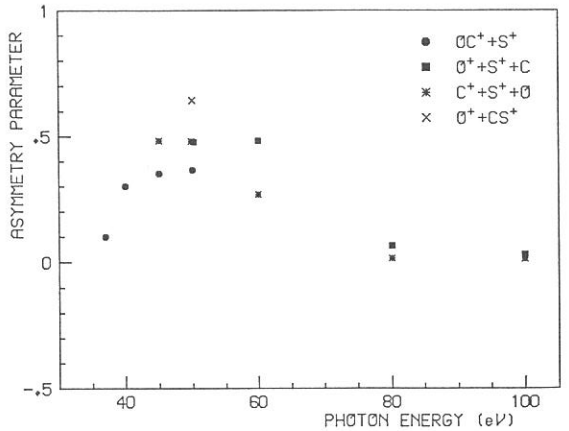

FIG. 2. Asymmetry parameter β for the channels $OC^+ + S^+$ (●), $O^+ + S^+ + C$ (■), $C^+ + S^+ + O$ (✳), and $O^+ + CS^+$ (x). For three-body dissociations, the β parameterindicated strictly holdsits meaning only in a limited dissociation mechanism.

DISSOCIATIVE SINGLE, DOUBLE, AND TRIPLE PHOTOIONIZATION OF SiF_4 IN THE VALENCE SHELL AND Si2p REGIONS ($h\nu$=33-133 eV)

Takashi IMAMURA, Chris E. BRION, and Inosuke KOYANO
Institute for Molecular Science, Okazaki 444, Japan

Toshio IBUKI
Institute for Chemical Research, Kyoto University, Uji 611, Japan

Toshio MASUOKA
Department of Applied Physics, Osaka City University,
Sumiyoshi-ku, Osaka 558, Japan

It is of particular interest to elucidate and understand the nature of the ensuing decomposition processes following the initial absorption of energetic photons by molecular targets. Above about 20eV such processes almost always lead to at least one charged species per photon absorbed. At higer energies decomposition of multiply charged ions leads to the so-called "Coulomb explosion" processes producing two or more ions and these also play an improtant role in the radiation induced decomposition of free molecules and materials.

In the present work, the photoionization of SiF_4 in the valence shell and Si2p inner shell regions has been studied using time-of-flight mass spectrometry and synchrotron radiation over the photon energy range 33-133 eV. Photoionization branching ratios are determined for stable singly and doubly charged ions arising from the various possible molecular and dissociative photoionization processes and are shown in Figure 1a for dominat ions. As seen in the figure, with increasing the photon energy from the valence shell region ($\leqq$100 eV) to the Si2p inner shell region ($\geqq$ 106 eV), the photoionization branching ratio of SiF_3^+ decreases and those of the small fragment ions such as F^+, Si^+, Si^{2+} etc. contrarily increases. Photoion-photoion coincidence

(PIPICO) techniques have been used to investigate the relative yields of Coulomb explosion decomposition products and threshold energies for dissociative double photoionization in the valence shell and Si2p regions. The PIPICO branching ratios of dominant processes are shown in Figure 1b. In going from valence shell to the Si2p inner shell regions, the dominant process changes (F^+ + SiF_3^+) into (F^+ + Si^+). This trend is correspondent with the results of TOFMS, i.e., the shapes of SiF_3^+ and (F^+ + SiF_3^+) are similar in both the valence and Si2p regions and F^+ and (F^+ + Si^+) are also similar in shape. The PIPICO spectra show additional peaks with thresholds in the Si2p region and these structures arise from the dissociation of triply charged ions into the exit channels (F^+ + SiF_2^{2+}), (F^+ + SiF^{2+}) and (F^+ + Si^{2+}). Of these the latter is the most probable process.

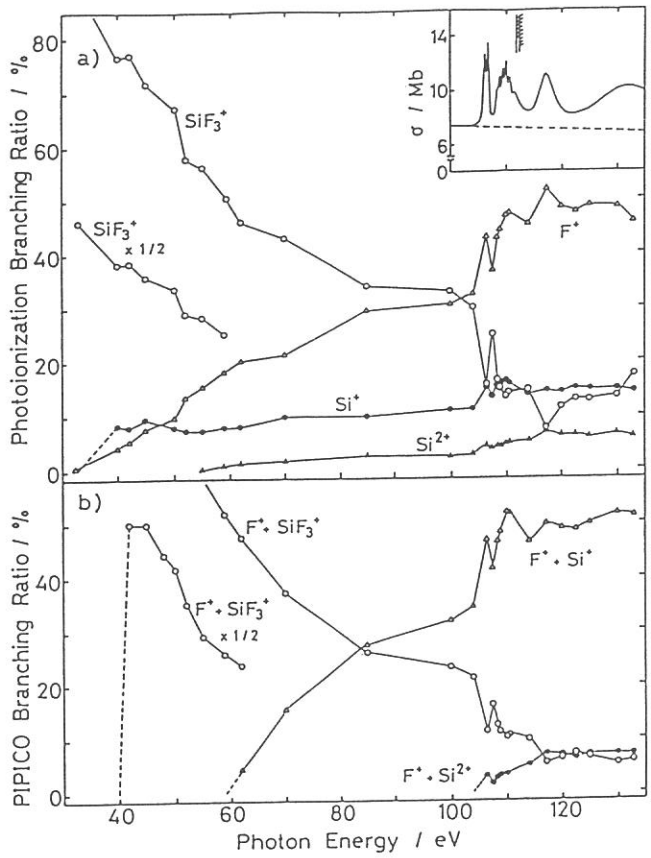

Figure 1. (a) Photoionization branching ratios for dominant stable singly and doubly charged ions. (b) PIPICO branching ratios for dominant processes.

DISSOCIATION OF DOUBLY CHARGED 1,1-DIFLUOROETHYLENE IN THE VALENCE SHELL EXCITATION ($h\nu$ = 37-80 eV)

Toshio IBUKI[a], Takashi IMAMURA[b], Inosuke KOYANO[c], Toshio MASUOKA[d] and C. E. BRION[b,e]

a Kyoto University of Education, Fushimi-ku, Kyoto 612
b Institute for Molecular Science, Myodaiji, Okazaki 444
c Department of Material Science, Himeji Institute of Technology, Himeji 671-22
d Department of Applied Physics, Osaka City University, Sumiyoshi-ku, Osaka 558
e The University of British Columbia, Vancouver, B.C. V6T 1Y6, Canada

The study of doubly-charged states of polyatomic molecules has rapidly increased in number because of the recent developments in experimental techniques to generate and detect the dications such as photoion-photoion coincidence (PIPICO), photoelectron-photoion coincidence (PEPICO) and photoelectron-photoelectron coincidence (PEPECO) measurements.

Dissociative processes of the doubly-charged $H_2C{=}CF_2^{++}$ ion has been studied by PIPICO technique in the photon energy range of 37-80 eV at the BL3A2 beam line of the UVSOR facility. Figure 1 shows a PIPICO spectrum of 1,1-$C_2H_2F_2$ excited at 55 eV. The dissociation channels into $CX_m^+ + CY_n^+$ show wide PIPICO bands while ion pairs of $H^+ + C_mX_n^+$ give narrow ones since the formed H^+ carries away the most part of the excess energy of molecule. Figure 2 shows the PIPICO branching ratios for dissociative double photoionization of 1,1-$C_2H_2F_2$ in the valence region. The threshold energies for the formation of $CX_m^+ + CY_n^+$ pairs are lower than 37 eV while those for H^+ (or F^+) + $C_mX_n^+$ channels are higher than 37 eV.

The recent theoretical investigation of the Auger spectrum of C_2H_4 reveals that a lot of two-hole ($2h$) states generated by releasing two outer valence electrons can contribute to the formation of the doubly-charged $C_2H_4^{++}$ ion and they lie in the region between 29 and 60 eV [1]. Up to the exciting energy of 37 eV, the main $2h$ channels are the outermost $(\pi_{C=C})^{-1}$ accompanied by another outer electron release [1]. In the region above 38 eV, the doubly-charged ions can be mainly formed through the $2h$ composition of $(\pi_{CH})^{-2}$, $(\pi_{CH})^{-1} + (C_{2s})^{-1}$, $(C_{2s})^{-2}$ and $(C_{2s})^{-1} + (\sigma_{C-C})^{-1}$ [1,2].

The combination of the PIPICO branching ratios in Figure 2a and the theoretical conclusion of Ref. 1 implies that the double photoionization ejecting a $\pi_{C=C}$ electron results in the formation of $CX_m^+ + CY_n^+$ pairs. The charges of 1,1-$C_2H_2F_2^{++}$ ion formed through

the $2h$ process of $(\pi_{CH})^{-2}$, $(\pi_{CH})^{-1} + (C_{2s})^{-1}$, $(C_{2s})^{-2}$ or $(C_{2s})^{-1} + (\sigma_{C-C})^{-1}$ would be strongly localized and hence these doubly-charged ions would decompose into $CX_m^+ + H^+$ (or F^+) fragments by the Coulomb explosion as shown in Fig. 2b.

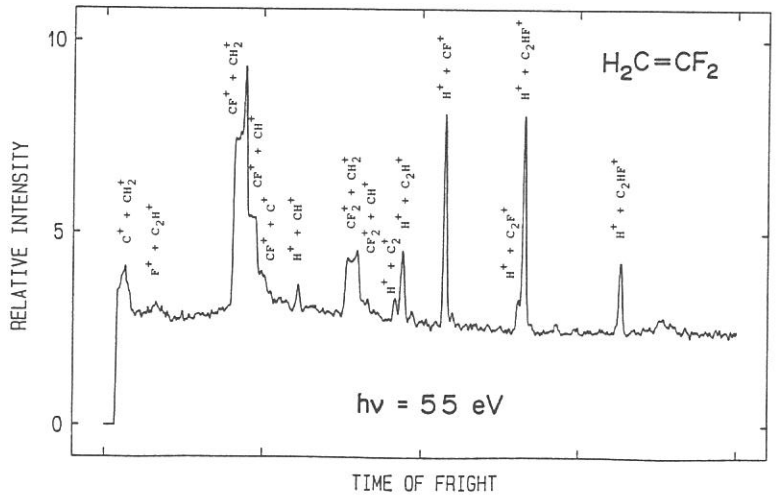

Fig. 1. PIPICO spectrum of 1,1-$C_2H_2F_2$.

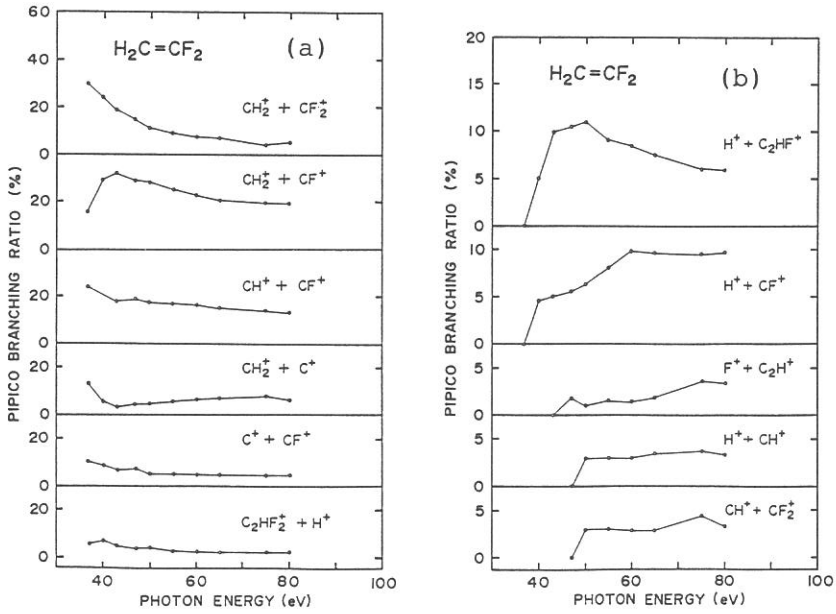

Fig. 2. PIPICO branching ratios.

[1] E. Ohrendorf, H. Köppel, L.S. Cederbaum, F. Tarantelli, and A. Sgamellotti, *J. Chem. Phys.*, **91**, 1734 (1989).

[2] K. Kimura, H. Katsumata, Y. Achiba, T. Yamazaki and S. Iwata, "Handbook of He I Photoelectron Spectroscopy of Fundamental Organic Molecules", Jpn Sci. Soc. Press, 1981.

DISSOCIATIVE PHOTOIONIZATION OF $Al_2(CH_3)_3Cl_3$ IN THE VACUUM ULTRAVIOLET

Shin-ichi NAGAOKA, Inosuke KOYANO,* Takashi IMAMURA,#
and Toshio MASUOKA+

Department of Chemistry, Faculty of Science, Ehime University, Matsuyama 790
*Department of Material Science, Himeji Institute of Technology, 2167 Shosha, Himeji 671-22
#Institute for Molecular Science, Okazaki 444
+Department of Applied Physics, Osaka City University, Sumiyoshi, Osaka 558

In recent years, relaxation processes following core excitation in molecules have been a topic of much interest. We have investigated the dissociation processes following photoionization of $Al_2(CH_3)_3Cl_3$ (MASC) in the range of valence and Al:2p core-level ionization by means of the photoelectron-photoion and photoion-photoion coincidence methods (PEPICO and PIPICO methods, respectively). MASC has a structure given by $(CH_3)_2 \cdot Al \cdot Cl_2 \cdot Al \cdot Cl(CH_3)$ and the chemical environments of the two Al atoms are different from each other. Thus, we try to examine whether or not the site-specific fragmentation is observed in MASC.

The experiments were performed using a time-of-flight (TOF) spectrometer with variable path length, coupled to a constant-deviation grazing incidence monochromator installed on the BL3A2 beam line of the UVSOR synchrotron radiation facility in Okazaki.[1]

Figure 1 shows an example of the TOF mass spectra in the PEPICO mode. The PIPICO intensity was found to be negligible throughout the energy range studied. In contrast to the case of $Al_2(CH_3)_6$,[2] dissociative double ionization does not play an important role in the fragmentation process of MASC in the energy range studied. The major relaxation process following Al:2p ionization of MASC is not the LVV Auger process which produces a

doubly charged parent ion.

Figure 2 shows plots of the ratios of the integrated intensities of the various ions in the TOF mass spectra to the total photoionization ($I_{ion}/I_{tot-ion}$) as a function of photon energy. The increase and decrease in $I_{ion}/I_{tot-ion}$ for Al^+ and $AlC_2H_6^+$, respectively, with photon energy in the range of 20–80 eV can be explained in terms of the increase in internal energy with increase of photon energy. We cannot observe the site-specific fragmentation around the Al:2p core-ionization threshold. The reason for this is that the energy resolution is not sufficient in the present experiment and/or that the difference in chemical environment between the two Al atoms in MASC does not cause so large a difference in the Al:2p energy level.

1. T. Masuoka, T. Horigome, and I. Koyano, Rev. Sci. Instr. 60, 2179 (1989); E. Ishiguro, M. Suzui, J. Yamazaki, E. Nakamura, K. Sakai, O. Matsudo, N. Mizutani, K. Fukui, and M. Watanabe, Rev. Sci. Instr. 60, 2105 (1989).
2. S. Nagaoka, I. Koyano, and T. Masuoka, Phys. Scr. 41, 472 (1990).

Fig. 1 (left-hand side) TOF mass spectrum of MASC taken by excitation at 40 eV in the PEPICO mode.
Fig. 2 (right-hand side) $I_{ion}/I_{tot-ion}$ in MASC as a function of photon energy.

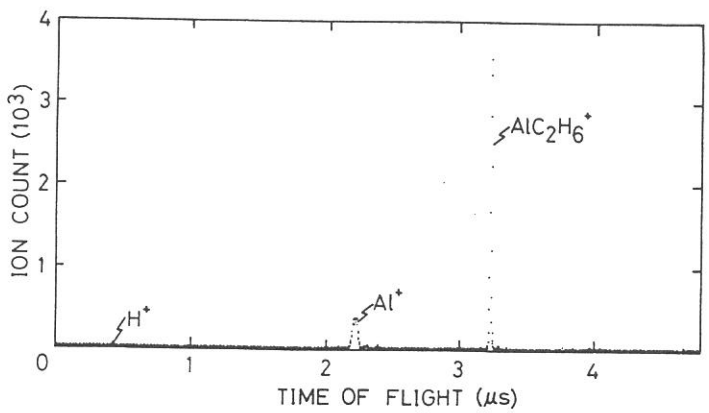

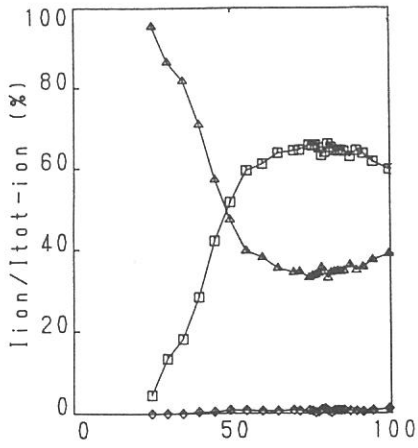

NEGATIVE-ION MASS SPECTROMETRIC STUDY OF ION PAIR FORMATION IN THE VACUUM ULTRAVIOLET. $SF_6 \longrightarrow F^- + SF_5^+$

Koichiro MITSUKE,[α] Shinzo SUZUKI,[β] Takashi IMAMURA,[γ] and Inosuke KOYANO[δ]

[α]Department of Chemistry, College of Arts and Sciences, The University of Tokyo, Komaba, Meguro-ku, Tokyo 153
[β]Department of Chemistry, Tokyo Metropolitan University, Fukazawa, Setagaya-ku, Tokyo 158
[γ]Institute for Molecular Science, Myodaiji, Okazaki 444
[δ]Department of Material Science, Himeji Institute of Technology, 2167 Shosha, Himeji 671-22

Ion-pair formation from photoexcitation of SF_6 has been studied by negative-ion mass spectrometry using synchrotron radiation in the 11.27 - 31.0 eV photon energy range.[1] Negative ions F^-, SF_6^-, and SF_5^- have been observed. Figure 1(a) shows a photodissociation efficiency curve of F^- produced from SF_6. The appearance energy of the F^- ion is about 1 eV higher than the thermochemical threshold for the formation of the pair of the ground state ions F^- (^1S_g) and SF_5^+ ($\tilde{X}\,^1A_1$). The peaks observed in the F^- efficiency curve (features *F*1 - *F*9) are interpreted as resulting from transitions to neutral excited states with the $^1T_{1u}$ symmetry which effectively couple with ion-pair states through avoided potential surface crossings. Our assignments are summarized in Table I.[1] We also perform assignments of the peak features in the previous photoabsorption spectra[2,3] [Figs. 1(b) and 1(c)] by using the term values for related Rydberg and virtual valence orbitals. The peaks assigned to diffuse Rydberg states are distinctively enhanced in the F^- efficiency curve (*e.g.* features *F*1, *F*2, *F*6, and *F*9), probably because of large transition probabilities from the dissociative Rydberg states to the ion-pair states. In contrast, the excited states of valence type autoionize in a short period and have quite small branching to the ion-pair channel. Consequently, the corresponding peaks are markedly suppressed in the F^- spectrum (*e.g.* features *F*5, *F*11 and *F*12). Other negative ions observed, SF_6^- and SF_5^-, are produced by resonance capture of low energy electrons emitted by photoionization of the parent molecules.

1) K. Mitsuke, S. Suzuki, T. Imamura, and I. Koyano, *J. Chem. Phys.* **93**, 8717 (1990).

2) (a) L. C. Lee, E. Phillips, and D. L. Judge, *J. Chem. Phys.* **67**, 1237 (1977); (b) D. Blechschmidt, R. Haensel, E. E. Koch, U. Nielsen, and T. Sagawa, *Chem. Phys. lett.* **14**, 33 (1972); (c) M. Sasanuma, E. Ishiguro, H. Masuko, Y. Morioka, and M. Nakamura, *J. Phys.* **B 11**, 3655 (1978).

3) K. H. Sze and C. E. Brion, *Chem. Phys.* **140**, 439 (1990).

TABLE I Summary of the observed features in the F^- photodissociation efficiency curve of SF_6, photoabsorption spectrum of SF_6 [Refs. 2(a)-(c)], and electron energy loss spectrum of SF_6 (Ref. 3). Photon energies and term values for transitions to the virtual orbitals are in eV.

Feature	Photon	This work	
	Energy [a]	Assignment	Term value[b]
*F*1	13.2	$1t_{1g}\rightarrow 4p$	2.5
*F*2	14.3	$5t_{1u}\rightarrow 4s$	2.6
		$3e_g\rightarrow 6t_{1u}$	4.4
*F*3	14.6	$1t_{1g}\rightarrow 5p$	1.1
*F*4	15.7	$5t_{1u}\rightarrow 5s$	1.2
		$1t_{2g}\rightarrow 6t_{1u}$	4.1
*F*5	17.0	$4t_{1u}\rightarrow 6a_{1g}$	5.7
*F*6	19.6	$4t_{1u}\rightarrow 4s$	3.1
*F*7	21.2	$4t_{1u}\rightarrow 5s$	1.5
*F*8	22.1	$5t_{1u}\rightarrow 2t_{2g}$	-5.2
		$4t_{1u}\rightarrow ns\ (n\geqq 6)$	0.6
*F*9	24.6	$5a_{1g}\rightarrow 4p$	2.4
	25.7	$5a_{1g}\rightarrow 5p$	1.3
	26.2	$5a_{1g}\rightarrow 6p$	0.8
*F*10 [c]	11.52[d]	$1t_{1g}\rightarrow 6t_{1u}$	4.2
		$5t_{1u}\rightarrow 6a_{1g}$	5.4
*F*11 [c]	23.2 [d]	$5a_{1g}\rightarrow 6t_{1u}$	3.8
		($5t_{1u}\rightarrow 2t_{2g}$)	-6.3
*F*12 [c]	28.3 [d]	$4t_{1u}\rightarrow 2t_{2g}$	-5.6

[a] The energies for features *F*1 - *F*9 are estimated from the peak maximum positions in the F^- efficiency curve.

[b] Calculated from the vertical ionization potentials for the ionic states of SF_6.

[c] Not observed in the F^- efficieny curve.

[d] Reference 3).

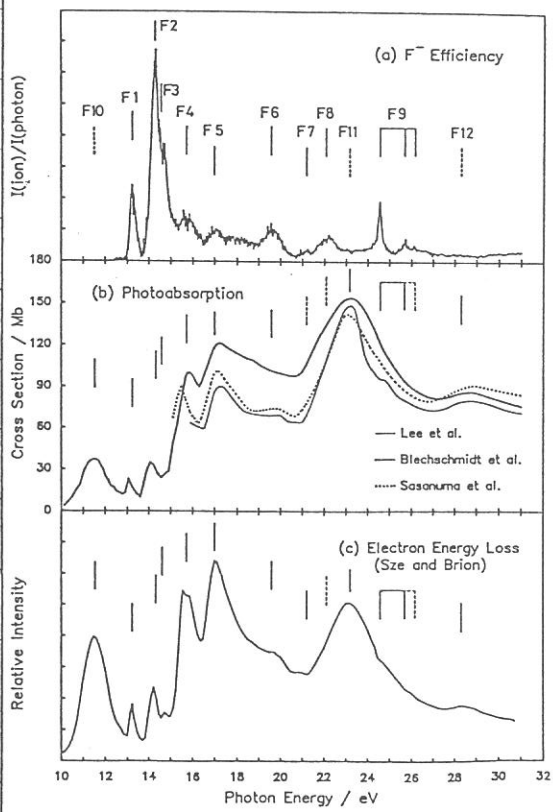

Figure 1. Comparison among (a) photodissociation efficiency curve of F^- produced from SF_6, (b) photoabsorption cross section curves [Refs. 2(a)-(c)], and (c) high resolution electron energy loss spectrum (Ref. 3).

NEGATIVE-ION MASS SPECTROMETRIC STUDY OF ION PAIR FORMATION IN THE VACUUM ULTRAVIOLET. $CH_4 \longrightarrow H^- + CH_3^+$ and $CD_4 \longrightarrow D^- + CD_3^+$

Koichiro MITSUKE,[α] Shinzo SUZUKI,[β] Takashi IMAMURA,[γ] and Inosuke KOYANO[δ]

[α]Department of Chemistry, College of Arts and Sciences, The University of Tokyo, Komaba, Meguro-ku, Tokyo 153
[β]Department of Chemistry, Tokyo Metropolitan University, Fukazawa, Setagaya-ku, Tokyo 158
[γ]Institute for Molecular Science, Myodaiji, Okazaki 444
[δ]Department of Material Science, Himeji Institute of Technology, 2167 Shosha, Himeji 671-22

Ion-pair formation from photoexcited methanes, $CH_4^* \longrightarrow H^- + CH_3^+$ and $CD_4^* \longrightarrow D^- + CD_3^+$, has been studied by measuring the efficiency curves of H^- and D^- using synchrotron radiation.[1] Figures 1 and 2(a) show typical photodissociation efficiency curves of H^- from CH_4 taken at wavelength intervals of 0.5 - 1.0 Å. Above an onset energy of 13.37 ±0.15 eV, there exists a broad peak arising from direct transitions to the ion-pair state of $^1T_2$ symmetry, which dissociates into $H^-(^1S_g) + CH_3^+(\tilde{X}\,^1A_1')$ (feature *F*1). The region above 19.8 eV contains two progressions: P1 with poorly resolved structure and P2 showing a long series of equally spaced peaks. The cross section at the 21.499 eV peak is estimated to be $\sim 1 \times 10^{-20}$ cm^2. Figure 2(b) shows the efficiency curve of D^- from CD_4 in the energy range of 19.5 - 23.0 eV. The D^- spectrum reveals a new progression (P3) starting at 21.744 eV besides P1 and P2.

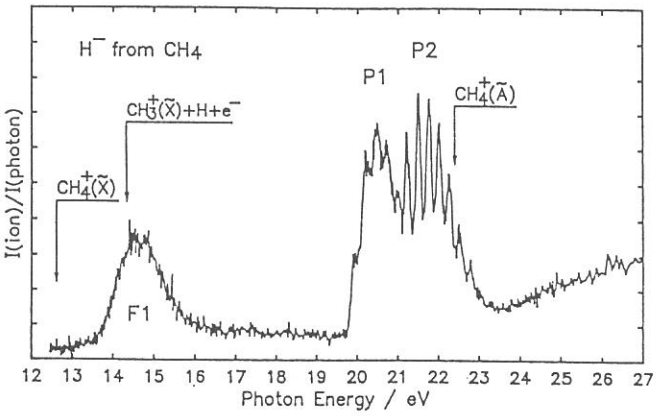

Figure 1. Photodissociation efficiency curve of H^- produced from CH_4 plotted as a function of the photon energy. The adiabatic ionization potentials for the $\tilde{X}\,^2T_2$ and $\tilde{A}\,^2A_1$ states of CH_4^+ and the appearance potential for the formation of $CH_3^+(\tilde{X}\,^1A_1') + H(^2S_g) + e^-$ are indicated.

The structures in P1 - P3 are considered to be due to the ν_1 progressions of npt_2 (n = 3 - 5) Rydberg states converging to the $\tilde{A}\,^2A_1$ state of the CH_4^+/CD_4^+. The $4pt_2$ and $5pt_2$ Rydberg states are observed here for the first time. The anomalously strong peak intensities of P2 suggest that the $4pt_2$ state interacts strongly with a neutral repulsive state *D*. Hence, we would propose the following mechanism for the formation of the ion pairs from the $4pt_2$ state: (1) passage from the Rydberg state to the *D* state, and (2) subsequent conversion of the *D* state to an ion-pair state, which dissociates into H^- (^1S_g) + $CH_3^+(\tilde{A}\,^1E'')$. The avoided surface crossing may occur at relatively long CH_3—H bond lengths between the upper *D* potential curve and the lower ion-pair curve, since the ion-pair state takes on the ionic character with the increase of the bond length and the potential curve changes from repulsive to attractive.

1) K. Mitsuke, S. Suzuki, T. Imamura, and I. Koyano, *J. Chem. Phys.* **94**, (1991), in press.

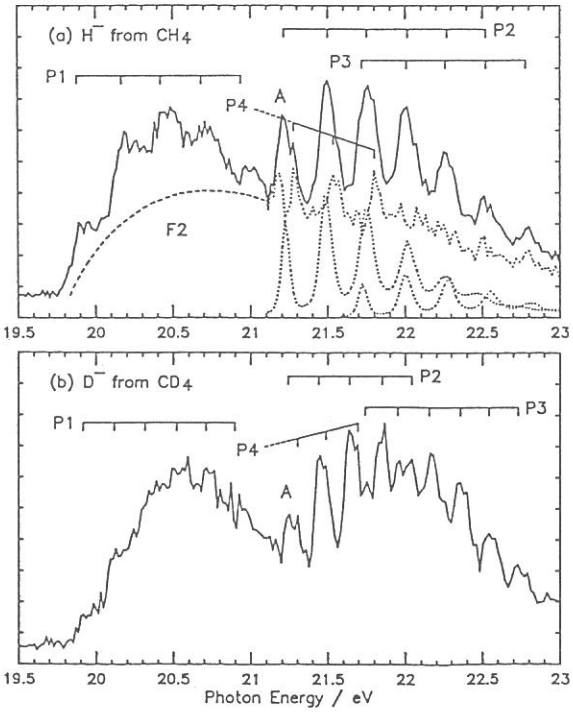

Figure 2. Photodissociation efficiency curves of (a) H^- produced from CH_4 and (b) D^- produced from CD_4. The three dotted curves represent the deconvolution of the H^- efficiency curve into two ν_1 progressions and a background.

	Progression	Term value /eV	n*	Quantum defect	Assignment
CH_4	P1	2.51	2.33	0.67	$3pt_2$
	P2	1.18	3.40	0.60	$4pt_2$
CD_4	P1	2.58	2.30	0.70	$3pt_2$
	P2	1.26	3.29	0.71	$4pt_2$
	P3	0.76	4.24	0.76	$5pt_2$

THE STUDY OF THE ION-PAIR FORMATION CH_3X --> X^- + CH_3^+ (X=F, Cl, Br) USING SYNCHROTRON RADIATION

Shinzo SUZUKI[1], Koichiro MITSUKE[2], Takashi IMAMURA[3], and Inosuke KOYANO[4]

(1)Department of Chemistry, Tokyo Metropolitan University, Setagaya-ku, Tokyo 158
(2)Department of Chemistry, College of Arts and Sciences, The University of Tokyo, Komaba, Meguro-ku, Tokyo 153
(3)Institute for Molecular Science, Myodaiji, Okazaki 444
(4)Department of Material Science, Himeji Institute of Technology, 2167 Shosha, Himeji 671-22

The ion-pair formation process from CH_3X to X^- + CH_3^+ (X=F, Cl, Br) has been investigated in the 10.0-30.0 photon energy range using synchrotron radiation at BL3B of UVSOR in Okazaki. It has been found that the efficiency curve for the formation of X^- had two components in this photon energy range. Figures 1-3 show the efficiency curves for the formation of X^- from CH_3X in the higher energy range (about 15.0-30.0 eV). The intensities of these bands are much smaller than those observed in the lower energy range (around the ionization thresholds of CH_3X). It can be seen that each band has, at least, two peaks (indicated by the arrows). Table 1 shows the summary of term values obtained from our spectra in the higher energy range and possible excitations to the Rydberg states, which was assumed by the EELS study by Hitchcook and Brion[1]. The peaks in the shorter wavelength region shown in the figures are considered to be due to $4a_1$ --> nd Rydberg transitions, while those in the longer wavelength region are considered to be due to $4a_1$ --> ns Rydberg transitions.

Reference

1)A. P. Hitchcook and C. E. Brion, J. Electron Spectrosc. and Relet. Phenom. **17**, 139(1979)

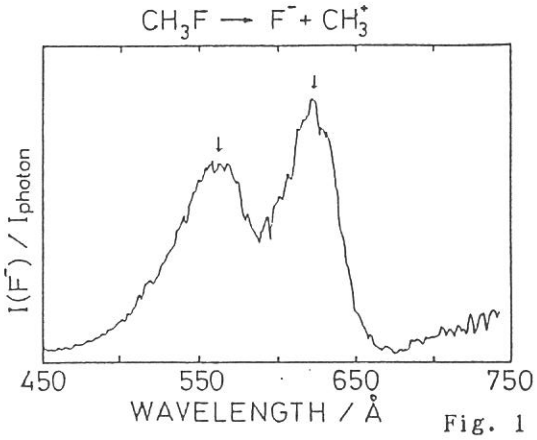

Fig. 1

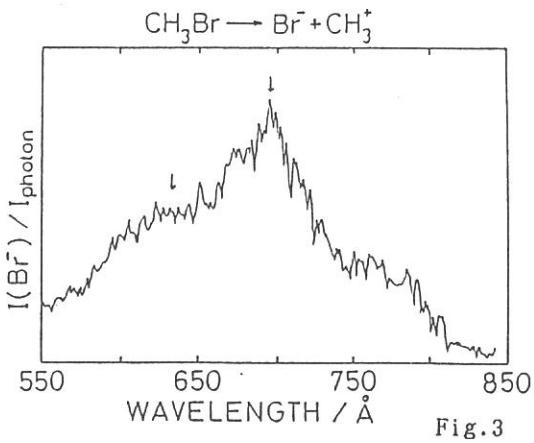

Fig.3

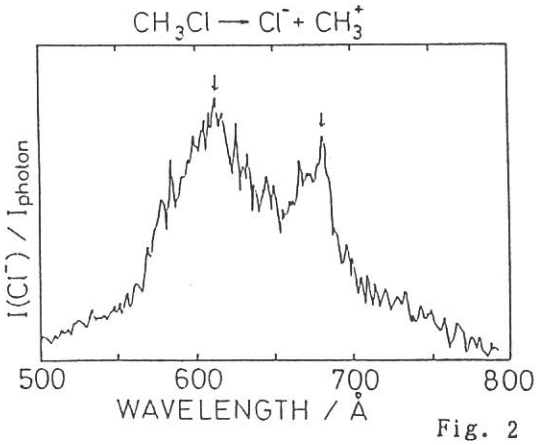

Fig. 2

Figures 1-3
The efficiency curves for the formation of X^- (X = F, Cl, Br)

Table 1

	Energy (eV)	Term Value (eV)	Possible transition
CH_3F	22.1	1.3	$4a_1 \cdots\rangle 3d$
	19.9	3.5	$4a_1 \cdots\rangle 3s$
CH_3Cl	20.2	1.3	$4a_1 \cdots\rangle 3d$
	18.2	3.3	$4a_1 \cdots\rangle 4s$
CH_3Br	19.9	1.6	$4a_1 \cdots\rangle 4d$
	17.8	3.7	$4a_1 \cdots\rangle 5s$

Table 1
The summary of term values and possible Rydberg transitions

STUDY OF ION-MOLECULE COLLISIONS BY HIGH RESOLUTION TRANSLATIONAL ENERGY SPECTROSCOPY

M. Mizutani, M. Sakurai*. M. Kimura**,
T. Imamura#, I. Koyano# and N. Kobayashi

Department of Physics, Tokyo Metropolitan University, Setagaya-ku, Tokyo 158. *National Institute of Fusion Science, Nagoya 464-01. **Department of Physics, Osaka University, Toyonaka, Osaka 560. #Institute for Molecular Science, Myodaiji, Okazaki 444.

An ion translational energy spectroscopy is a powerful technique to investigate inelastic processes in ion-atom and molecule collisions[1]. The resolution of this technique is, however, limited to several ten meV so far, since the ion beam intensity becomes very weak when we use an energy selector to get monochromatic beam. It seems necessary to develop a new technique to produce a monochromatic ion beam without an energy selector.

In this study, we have tried to develop a new technique for forming an ion beam with energy spread of less than 20 meV and intensity of larger than 10^{-10}A. Principles for this new method are as followings. 1) If ions are formed in an electric field which is usually applied in the source for extracting ions, translational energies of the ions must be depend on positions where the ions are produced. Therefore, we must form ions in a field free region. 2) Usually gas is introduced to the source in a molecular flow condition. In such case, if we produce ions in a field free region, only a small part of the ions produced can be extracted from the exit aperture. In addition to that, since the temperature of the source is much higher than the room temperature, the energy spread of the ions should be much larger than that at room temperature, about 40 meV. Therefore, a supersonic beam is adopted which is expanded from a nozzle toward an exit aperture and crosses with a photon beam. 3) The UVSOR is chosen as a light source, since the wave length is appropriate to produce singly charged ions. To get high intensity ion beams, white light is used for ionization.

An ion source, an ion accelerationg lense system and an energy analyzer of hemispherical condenser type have been

settled at about 1m back of the focusing point of BL-3A2 beam line. A diameter of the neutral beam is about 2mm at the ionization region. On the other hand, the light beam is broadened to about 15x15 mm^2, because the ion source has been set at rear of the focusing point. Therefore, an entrance aperture with the diameter of 3 mm for light source has been settled in front of the ionization region. The zeroth order light from the grating has been used.

The ions extracted from the source are mass analyzed with a Wien filter and focused to the collision center. The ions collide with a target gas beam effused from a capillary and are energy analyzed.

When Ar gas has been introduced to the source, the intensity of about 10^{-11}A has been obtained at the collision center. The energy spread of 38 meV (F.W.H.M.) has been achieved. Considering the fact that the ion source has been settled at 1m back of the focusing point of the optical system, we would be possible to get 10^{-10}A if we set the ion source just at the focusing point. On our experiences, this intensity is enough high for the translational energy spectroscopy. On the other hand, the energy spread obtained is a little larger than our expectation. However, it is better than that we have obtained. We can not understand the reason why the energy spread obtained is larger than our expected value.

Fine-structure transitions between $^2P_{3/2}$ and $^2P_{1/2}$ of Ar^+ have been studied in collisions with Ar at the collision energy of 300 eV. Although the energy difference between these states is very small, 0.18 eV, peaks due to the excitation and deexcitation between different J states have been clearly resolved from the tails of the primary beam. The angular dependences of the fine-structure transitions have been also studied at scattering angles between 0 and 3 degree.

References

1) N. Kobayashi, Electronic and Atomic Collisions. p333, ed. H. B. Gilbody, W. R. Newell, F. H. Read and A. C. H. Smith (Elsevier Science Publishers, 1988); A. Fukuroda, N. Kobayashi and Y. Kaneko, J. Phys. B At. Mol. Phys. 22 (1989) 3471.

X-Ray Microscope with Grazing Incidence Mirrors

A. Ohba[1,3], S.Ohsuka[2,3], H.Yokoyama[2,3], T. Matsumura[2,3], M. Sugiyama[3], K. Kinoshita[3], N. Watanabe[4], Y. Shimanuki[5], Y. Sano[6] and H. Kihara[2]

[1] Institute for Molecular Science, Okazaki 444
[2] Jichi Medical School, School of Nursing,Tochigi 329
[3] Hamamatsu Photonics K.K., Hamakita 434
[4] Faculty of Science, Nagoya University, Nagoya 464-01
[5] School of Dental Medicine, Tsurumi University, Yokohama 230
[6] National Food Research Institute, Tsukuba 305

To see fine structures of objects, e.g., living cells, in x-ray region, precisely fabricated x-ray optical elements and a high-resolution x-ray imaging apparatus are needed. We have evaluated Wolter type-I grazing incidence x-ray mirrors and an x-ray sensitive zooming tube which have been developed at Hamamatsu Photonics K.K. as components of an x-ray microscope [1].

Fig. 1 shows a schematic of the optical system of the x-ray microscope. The wideband SR light of the BL8A [2] was filtered by a 0.8 μm thick Al film. The calculated peak wavelength is about 1.3 nm. Two mirrors were used: one for collecting and focusing x-ray photons on a sample, and the other for magnifying the x-ray image of the sample 20 times. For the wavelength of 1.3 nm, the peak-to-valley surface roughness of a mirror with the grazing incidence angle of 26.2 mrad must be smaller than 6.2 nm according to the Rayleigh's criterion [3]. The measured peak-to-valley surface roughness and deviation from the designed profile of the mirrors are less than 4 nm and 0.5 μm, respectively. The magnified x-ray image was detected by an x-ray sensitive zooming tube and further magnified electronically 20–200 times. Since the resolution of the x-ray sensitive zooming tube is better than 1 μm at the photocathode [1], the 20-time magnification of the mirror is sufficient to observe submicron fine structure of the sample.

Fig. 2 shows the image of outermost zones of a zone plate with the outermost zone width of 0.4 14 μm. Zones are clearly resolved. From this image, resolution of better than 0.4 μm is confirmed. We also tested images of biological specimens such as diatoms, collagen and muscle. These images were shown in Fig. 3–Fig. 5.

The authors acknowledge UVSOR members of the Institute for Molecular Science for their help.

References

1 S. Ohsuka, A. Ohba, M. Sugiyama, T. Hayakawa, T. Matsumura, K. Kinoshita, N. Watanabe, Y. Shimanuki, Y. Sano and H. Kihara, X-Ray Microscopy III, in press.

2 M. Watanabe, Nucl. Instr. and Meth. A**246**, 15 (1986).

3 S. Aoki, X-Ray Microscopy II, Springer Series in Optical Science **56**, (Springer, Berlin, 1988), p.102

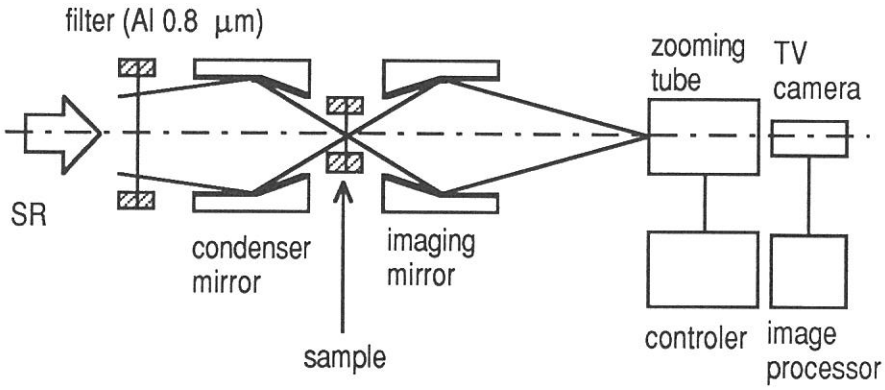

Fig. 1 Schematic of the optical system of the x-ray microscope.

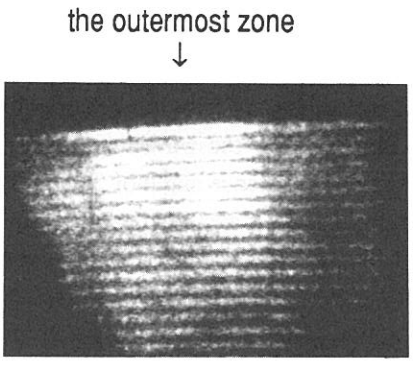

Fig. 2 A magnified image of a zone plate with the outermost zone width of 0.414 μm.

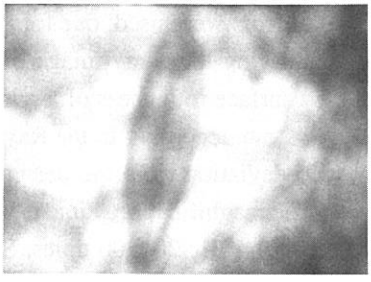

Fig. 3 A magnified image of a diatom.

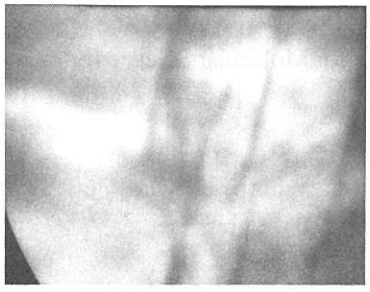

Fig. 4 A magnified image of a collagen.

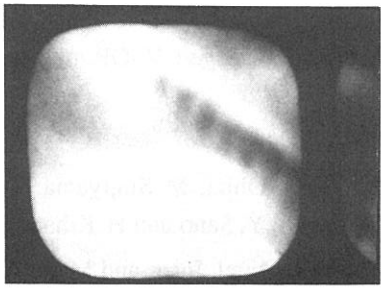

Fig. 5 A magnified image of a rabbit muscle. A shadow of the mesh supporting the photocathode of the x-ray sensitive zooming tube is also seen.

X-ray Microscope with Zone Plates

Norio Watanabe[1], Hisao Fujisaki[2,3], Yoshio Shimanuki[4], Mieko Taniguchi[1], and Hiroshi Kihara[5],

1) Department of Physics, Nagoya University, Nagoya 464-01
2) JRDC, Yoshida Nano-Mechanism Project, Tsukuba 300-26
3) Nicon Tsukuba Lab., Toukohdai 5-9-9, Tsukuba 300-26
4) School of Dental Medicine, Tsurumi University, Yokohama 230
5) Jichi Medical School, School of Nurisng, Tochigi 329-04

Abstract

An imaging microscope with two zone plates was constructed, and tested. Resolution of 0.55 u was attained with the best combination of zone plates. Several kinds of biospecimens were observed.

2. Experimental

We have tested several zone plates, of which characterizations were summarized in Table 1. They were fabricated by CANON, Mitsubishi Electric. and Heidenhein. HZP2 was designed specially for the test of phase zone plate at 1.76 nm. In Table 2, summarized X-ray microscopic systems with zone plates. Previous activities have been reported elsewhere[1,2]. This year, No. 3-5 experiments were done. They are reported below.

3. Test of phase zone plate[3] (No. 5 in Table 2)

With this system, we have tested the intensity ratio and focusing efficiency of a phase zone plate (HZP2) in comparison with the corresponding zone plate without phase gain. In theory, intensity ratio shows 2.5, whereas the ratio of the present experiment shows 1.6. Although the value is a little smaller than the theoretical one, this shows the phase zone plate gives better contrast than the normal one.

4. Test of Mitsbishi zone plates (No. 4 in Table 2)

Second series of experiments were done with two types of zone plates, both of which were fabricated by Mitsubishi Electrics. The zone plates have relatively thick support. With this reason, we used wavelength at 1.56 nm to get good contrast. Special resolution attained with a zone plate as an object was less than 1 u. Images observed had little distortion. Biospecimens such as diatom and collagen were observed.

5. Test of phase zone plate with Mitsubishi zone plate (No. 6 in Table 2)

Third series of experiments were done for the test of another series of phase zone plate. As condnser, MZP1 was used. HZP2 was used as micro zone plate. Wavelegth was set at 1.76 nm. With this set-up, we could get better resolution (0.55 u with a zone plate as an objective), probably because (i) MZP2 has better special resolution than CZP3, although the designed resolution was the same. The outermost part of CZP3 seems to be not fabricated so sharp. Biospecimens such as diatom, collagen and so on

were examined.

References

1. N. Watanabe, M. Taniguchi, Y. Shimanuki, K. Kawasaki, Y. Watanabe, Y. Nagai, and H. Kihara (1991) in "X-ray Microscopy III (A. Michette et al ed.)", Springer-Verlag, submitted.
2. N. Watanabe, M. Taniguchi, Y. Shimanuki, K. Kawasaki, Y. Watanabe, Y. Nagai, and H. Kihara (1990) UVSOR Activity Report, 1989, 94-95.
3. H. Fujisaki, N. Nakagiri, H. Kihara, N. Watanabe, Y. Shimanuki, and Y. Nagai (1991) in "X-ray Microscopy III (A. Michette et al., ed.)", Springer-Verlag, submitted.

Table 1.

zone plate	r_1 (μm)	D (mm)	n	dr_n (μm)	focus(mm) (λ=4.5nm)	mask (μmϕ)	support	material		manufacturer
CZP1	34.6	1.22	312	0.98	266.7	200	Free-standing	Au	2	CANON
CZP2	34.6	1.22	312	0.98	266.7	No	Free-standing	Au	2	CANON
CZP3	15.8	0.50	250	0.50	55.6	100	0.3μ polyimide	Au	0.3	CANON
MZP1	27.3	1.492	746	0.40	166.0	No	1.5μ SiC	W/Ti	0.5	Mitsubishi
MZP2	9.4	0.18	89	0.40	19.7	No	1.5μ SiC	W/Ti	0.5	Mitsubishi
HZP1	9.4	0.21	128	0.41	19.6	No	Free-standing	Au	0.5	Heidenhein
HZP2	9.4	0.21	128	0.41	19.6	No	Free-standing	Ni	0.43	Heidenhein
HZP3	32.7	2.4	1350	0.44	23.8	182.1	Free-standing	Au	0.5	Heidenhein

Table 2

No.	condenser ZP	micro ZP	λ (nm)	magnification	resolution (μm)	comments
1	monochromator	CZP1	10.5	10	severalμ	#1000 mesh
2	CZP1	CZP2	6.0	13.4	severalμ	heat damage of C-ZP
3	CZP3	CZP3	4.74	43.7	1.5μ	mesh, zone plate
4	MZP1	MZP2	1.7	50	1.0μ	zone plate, diatom
5	CZP3 (HZP1,	HZP2)	1.76	47	1.2μ	test of phase ZP
6	MZP1	HZP2	1.76	70	0.55μ	diatom, collagen etc.

X-ray Absorbing and Mechanical Properties of Au-C Film for X-ray Mask Absorber

H. Fukushima*, H. Yamada*, T. Matsui*, T. Tagawa*, S. Morita, and S. Hattori**

Department of Electronic Mechanical Engineering, Nagoya University
Furo-cho, Chikusa-ku, Nagoya 464

* Meitec Corporation
2-20-1, Kosei-dori, Nishi-ku, Nagoya 481

** Nagoya Industrial Science Research Institute, Dept. of Elec. Mech. Eng.
22, Ueda-Maeda, Tempaku-cho, Tempaku-ku, Nagoya 468

A X-ray absorbing compound was proposed for a X-ray mask material and evaluated experimentally. Au-Carbon compound was deposited simultaneously by evaporation of Au and plasma CVD of propylene. The X-ray transmittance of the films were measured. The mechanical stress of the films was measured befor and after the SR iradiation.

The reactor for the film deposition is shown in Fig. 1[1]. After the initiation of discharge of propylene, Au is evaporated by a basket type heater of tungsten with crucible. Atomic ratio of Au-C films were changed from pure Au to pure carbon by controlling the current of heater.

The stress of film was measured by using two layers system of Au-C film and spin coated polyimide layer on a silicon wafer as shown in Fig. 2. For the sample preparation, polyimide layer was spin coated to a thickness of 5 μm, then Au-C film with a thickness of 1 μm was deposited. Two layers system was fabricated by back-etch process. The etched hole has a diameter of 10 mm.

The stress of Au-C compound films were measured as shown in Fig. 3. Zero stress was observed at the Au composition ratio of 30 %. After the exposing to syncrotron radiation(SR) to 1500 J/cm^3, the stress shifted to tensile side.

In a future experiment, patternd Au-C films will be exposed to SR and evaluated as an X-ray mask.

References:

1) S. Ito, H. Yamada, S. Morita, and S. Hattori: Proc. of 8th Int. Symp. on Plasma Chemistry(Tokyo, Sep. 1987) pp.1353-1357, 1987.

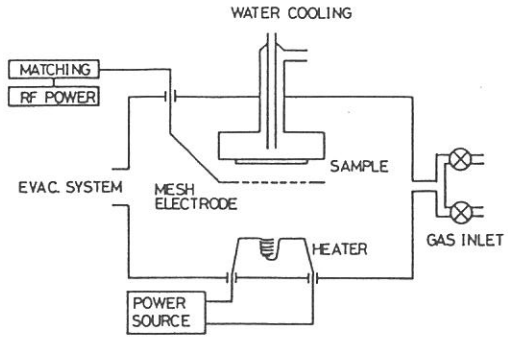

Fig. 1. Reactor for Au-C compound formation

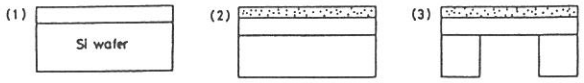

Fig. 2. Sample fabrication process for the stress measurement of Au-C film and polyimido layer system

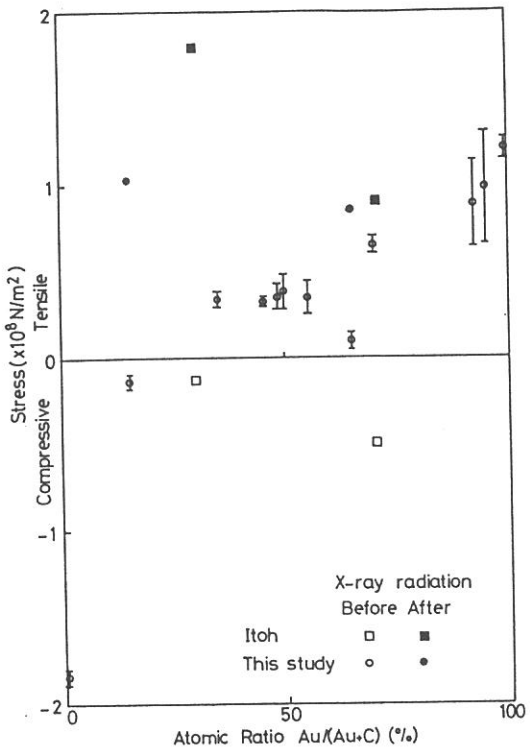

Fig. 3. Stress of Au-C compound film and the effect of SR exposure

Characteristics of CR Plate for UVSOR

Hiroki YOSHIDA and Yukio SAKAGAMI

Department of Electronics and Computer Engineering,
Faculty of Engineering, Gifu University, 1-1 Yanagido, Gifu 501-11

Extremely high-density-high-temperature state in laser-produced-plasma calls for new diagnostic methods. The emitted X-ray abounds with information about what happens in that state. The energy of the emission spectra of the photons exist almost in the soft X-ray and ultraviolet region. Nevertheless the CR(Computed Radiography) plate, Fuji HR-III, lacks any data ever published about fundamental characteristics, especially spectral sensitivity. Hitherto, the recording material has been limited mainly to X-ray film. By the authors, it was found that CR plate was superior to it in detecting the soft X-ray[1-3]. The purpose of the present study is to clarify the sensitivity in the ultraviolet region by UVSOR.

A monochromatic UVSOR was obtained by 2.2m Rowland-Circle-grating-incidence-spectrometer at the BL8B1 beamline. The CR plate was irradiated by it in the region of 80 - 130Å wavelength, typically for 10 minutes. The electron energy of the storage ring was 600MeV. The initial electron-beam-current was between 100 and 140mA. After irradiation, photostimulable luminescence was read out from the CR plate[1-5]. Fig.1 shows one of the images of luminescence. To measure the monochromatic-UVSOR-intensity, an Al_2O_3 diode was used[6]. The luminescence was referred to the intensity. From these procedures, the minimum sensitivity of the CR plate was obtained as shown in Fig.2.

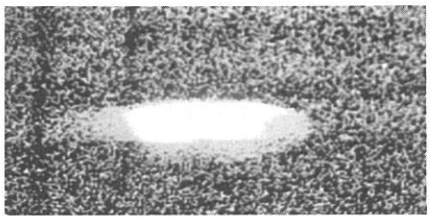

1mm

λ = 130 [Å]

Exposure Time: 10 [min]

Fig.1. Luminescence Image the CR Plate

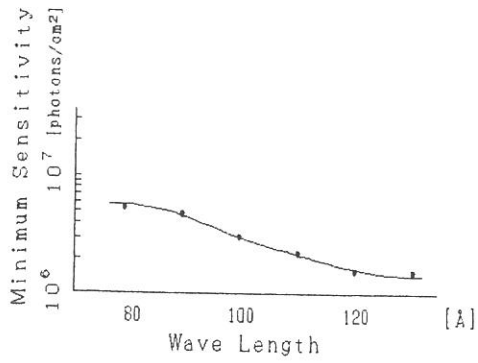

Fig.2. Minimum Sensitivity of the CR Plate

It is found that the CT plate has enough low sensitivity to measure UVSOR. It becomes clear that the CR plate is useful material for diagnostic of laser-produced-plasma.

It is our great pleasure to thank Dr. M.Watanabe and Mr. J.Yamazaki for many helpful suggestions and considerable assistance.

References

1)Y.Sakagami, M.Hattori, "Characteristics of X-ray Imaging Plate", Rev. of Laser Eng. 14, 8, 692-700(1986)

2)Y.Sakagami, Proc. 17th Joint Conf. on Image Technology, 321-326 (1986)

3)Y.Sakagami, H.Yoshida, et al., Res. Rpt. Fac. Eng. Gifu Univ. No.40, 42-44(1989)

4)H.Yoshida and Y.Sakagami, "X-ray CT Diagnostics in Laser-Fusion", Proc. of the Mtg., the Optics Div., the Jpn. Soc. Appl. Phys., p.15(1988)

5)H.Yoshida, Y.Sakagami et al., Bulletin of Convention of Tokai-District-Electric-Related-Academic-Societies, No.65(1988)

6)E.B.Saloman, "The Use of Synchrotron Radiation for Detector Calibrations", Nucl. Instrum. & Methods, 172, 79-87(1980)

SYNCHROTRON RADIATION INDUCED DEGRADATION OF MOS FIELD EFFECT TRANSISTORS

Yoji SAITO, Shinji UMEDA and Akira YOSHIDA
Toyohashi University of Technology, Tempaku-cho, Toyohashi 441

Synchrotron radiation (SR) is a promising light source for high-resolution lithography in integrated circuits. However, high energy photons have the hazard to degrade the characteristics of the electonic devices.

In this report, we show SR irradiation effects for MOS field effect transistors (FET) and their annealing effects. The p-channel poly-silicon gate MOS FETs with various thickness of passivated films (Fig.1) were irradiated with the direct SR and the Be filtered lights. Penetration wavelengths through 0.7μm and 1.8μm passivated films and 15μm Be filter are more than about 50Å, 30Å, and 15Å, respectively.

Fig.2 shows the dependence of drain current (Id) vs. gate voltage (Vg) characteristics on the irradiation dose. With incraese of the dose, the gradient of the curve decreases near the subthreshold Vg owing to the increase of interface state density (N_{it}), and the curve shifts to the direction of minus Vg due to the incresae of both N_{it} and the positive space charge (trapped holes) density in the gate oxide.

Fig.3 shows the dependence of N_{it} calculated from the Id-Vg characteristics on the dose. N_{it} increases with increase of the dose, but it scarecely depends on the thickness of the passivation films (sample A and B). Moreover, there is little difference in N_{it} between direct SR and Be filtered irradiated samples. These results indicate that the increase of N_{it} is induced mainly by short wave photons less than 30Å.

The irradiated samples were annealed in nitrogen gas for 1 hour. The relative decay of the light induced interface states $(N_{it}-N_i)/(N_o-N_i)$ is shown in Fig.4 as a function of annealing temperature, where N_i and N_o are the density of interface states of the non-irradiated sample and the as-irradiated sample, respectively. In this figure, the in-

duced interface states almost vanish by the annealing above 250 °C, and the activation energy for the decay is about 1.25eV.

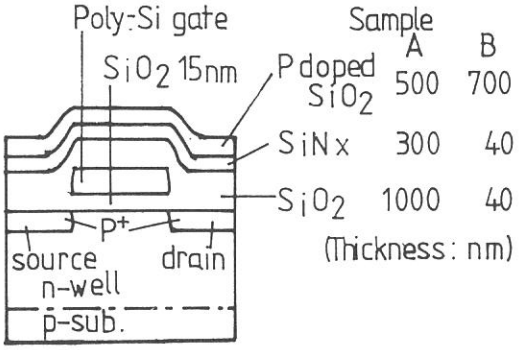

Fig.1 Schematic cross section of p-channel MOS FET

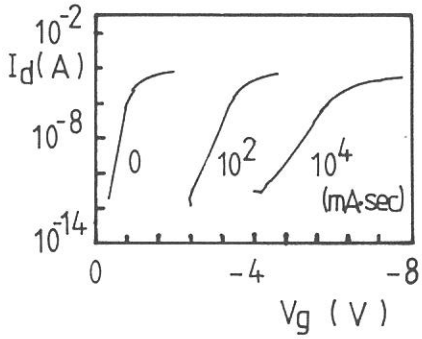

Fig.2 Dependence of Id-Vg characteristics on irradiation dose

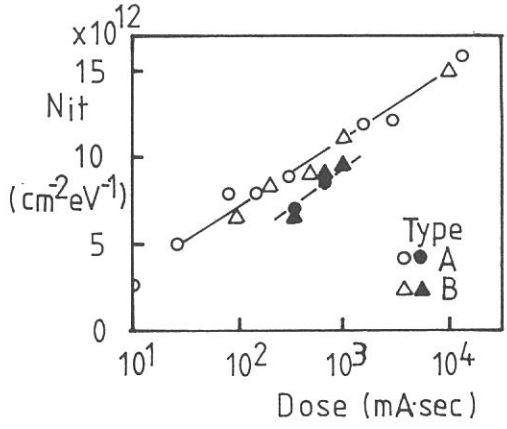

Fig.3 Dependence of Nit on irradiation dose

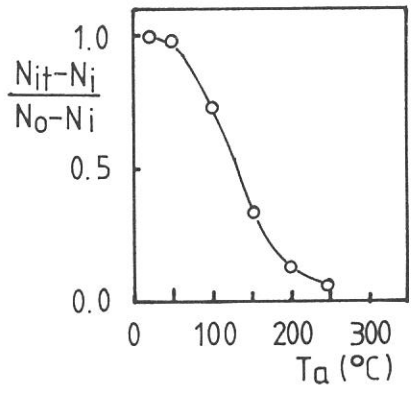

Fig.4 Decay of induced interface states by thermal annealing

SYNCHROTRON RADIATION EXCITED ETCHING OF SiO_2 WITHOUT USING AN ETCHANT

Haruhiko OHASHI,[*,] Kenichi KATO,[*,**] Akira YOSHIDA,[**] and Kosuke SHOBATAKE[*]**

[*] *Institute for Molecular Science, Myodaiji, Okazaki 444 Japan*
[**] *Toyohashi University of Technology, Tenpaku, Toyohashi 440 Japan*

Synchrotron radiation (SR) excited etching of SiO_2 and polycrystalline silicon surfaces has been actively studied in the hope of utilizing the technique for ULSI fabrication of semiconductor materials.[1-4] From the wavelength dependences of the SR-excited etching rate of SiO_2 surface, it has been proven that the excitation of the first surface layer is very crucial when the irradiation is carried out in SF_6 or F_2 atmosphere used as as an etchant.[2] In these etching reactions the main reactants are considered to be F or Cl atoms, which remove Si atoms in a form of gaseous product, SiF_4 or $SiCl_4$. Now arises a question " Can etching reactions proceed in the absence of an etchant gas? If so, how effective will they be?"

We have studied the *etchantless* etching processes of SiO_2 surfaces irradiated by SR from the bending magnet on beamline BL8A as well as the undulator radiation from the beamline BL3A1. The apparatus used for the present experiment is the same as that used for SR excited etching of semiconductor materials and SR-excited thin film formation.[1,2]

Bending magnet SR (BL8A) experiments SR is perpendicularly irradiated at ambient temperature upon thermally oxidized SiO_2 surface, so that the horizontal center of the circular sample area irradiated is in the orbital plane of the 750 MeV electron beam. The diameters of the collimating channels are 3 or 5 mm. The thickness of the SiO_2 layer was measured optically, using a film thickness measurement system (Nikon NFM-5) which determines film thickness from the interference pattern. Figure 1 illustrates angle dependences of normalized depth of the SR-irradiated SiO_2 surface, a) when the out-of-plane angle ψ is changed in the vertical plane, and b) when the in-plane angle θ is changed in the electron orbit plane. The abscissas are either angle in mrad (top) or distance from the center in mm (top). In this case the channel diameter was 3 mm. The depth profile in Figure 1a shows that i) the etch depth is the

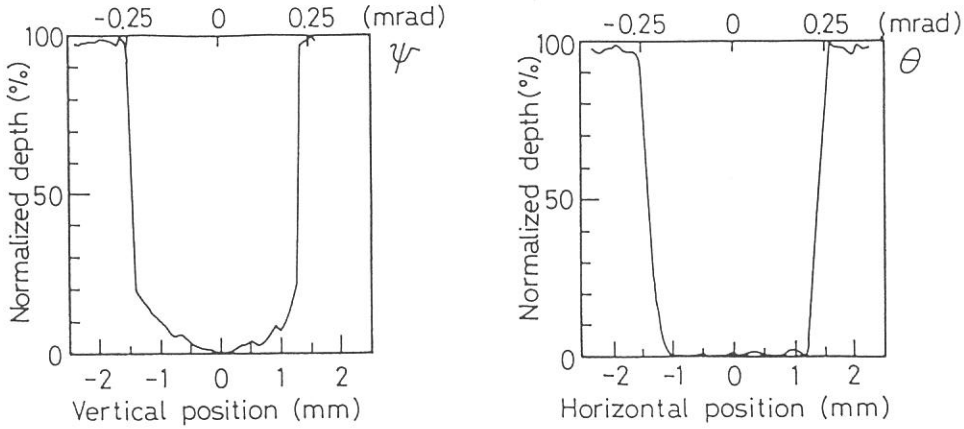

Figure 1. Angle dependences of normalized depth of the SR-irradiated SiO_2 surface, so that the monitor point is moved so that a) the out-of-plane angle ψ changes in the vertical plane, and b) the in-plane angle θ changes in the electron orbit plane. The abscissas are either angle in mrad (bottom) or distance from the center in mm(top).

deepest at the center, i.e. in the plane of the electron orbit plane and ii) becomes shallower as the monitor position moves away from the plane. On the contrary as the monitor position is moved in the orbit plane (see Figure 1b), the depth is unchanged, which is expected, and there is no reason why the depth changes with moving the monitor position where the SR is irradiated.

The out-of-plane angle dependence of the etch depth is explained as follows: a) The out-of-plane angular divergence of the light intensity depends strongly upon the wavelength of the irradiated light, i.e. the shorter is the wavelength, the narrower the angular width, and b) further-more the etch rate depends strongly upon the wavelength, too. Figure 1a shows that at the point of ψ = 2.5 mrad the etch depth decreases to less than 85% of the value at the deepest point (ψ = mrad). Assuming that only the photons, whose wavelength are shorter than a critical wavelength λ_{max} equally contribute to the the etchantless etching reaction, the angular dependence is fitted fairly well, if λ_{max} ~ 30Å is chosen. Figure 2 illustrates the theoretical angular distribution of irradiated photon numbers integrated from 1 Å to λ_{max}. It is noted that the K shell excitation of O atom is at 22.8 Å and it is within the range of the longest critical wavelength 1Å < λ < λ_{max} = 30 Å., which suggests that the K shell excitation of O atom is important in the SR-excited etching of SiO_2.

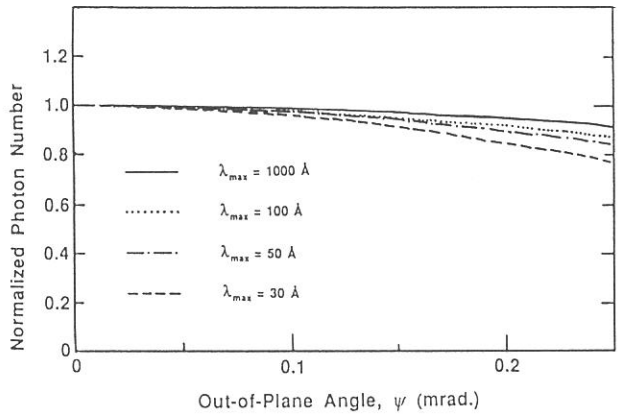

Figure 2. Normalized theoretical angular distributions of irradiated photon numbers integrated from 1 Å to λ_{max}. The observed etched surface profile fits best to the theoretical distribution for λ_{max} = ~ 30 Å.

The etch rate defined as the etch depth (in Å) divided by the accumulated beam current (in min · mA) was determined as 3.0 x 10^{-3} Å min^{-1}. mA^{-1}. Out of all the photons irradiated in the 1 -1000 Å region only 1.0 x10^{-2} % of photons are estimated to participate in etching reaction. However assuming that only the photons of the K shell excitation of O atom participate in the reaction, the quantum yield is estimated as 0.08 %. Although not described here a series of *undulator* experiments on the SiO_2 etching reaction have been carried out. Briefly the quantum yield for etching reaction done for the undulator magnet gap of 75.2 mm (the first order photon energy is 50 eV, and the second order is 97 eV which correspond to L shell excitation of Si) is measured as 0.01 %. Therefore the etch rate for the K shell excitation of O atom is found to be eight times more effective than the L shell excitation of Si atom. Using undulator radiation (gap length of 75.2 mm), the etch rate is found to increase with raising the temperature and the activation energy above 300°C is roughly estimated as about 0.3 eV. At room temperature the etch rate does not linearly increase with irradiation dose. Therefore more experiments should be done to confirm if we are observing a really etched surface or only observing nominal thickness of the irradiated sample whose optical quality has been changed upon irradiation.

References

1) N. Hayasaka, A. Hiraya, and K. Shobatake, *Jpn. J. Appl. Phys.*, **26**, L1110 (1987). 2) K. Shobatake, H. Ohashi, K. Fukui, A. Hiraya, N. Hayasaka, H. Okano, A. Yoshida, and H. Kume, *Appl. Phys. Lett.*, **56**, 2189 (1990). 3) H. Kyuragi and T. Urisu, *J. Appl. Phys.*, **61**, 2035 (1987). 4) T. Urisu, H. Kyuragi, J. Takahashi, and M. Kitamura, *Rev. Sci. Instrum.* **60**, 2157 (1989).

SYNCHROTRON RADIATION EXCITED CHEMICAL VAPOR DEPOSITION OF ALUMINUM OXIDE FILMS

Haruhiko OHASHI*, Akira YOSHIDA* and Kosuke SHOBATAKE**

* Toyohashi University of Technology, Toyohashi, Japan 440

** Institute for Molecular Science, Myodaiji,Okazaki, Japan 444

Photochemical vapor deposition (Photo-CVD) using photo-excited surface reaction has been attracting great attention because of its high potential in modern semiconductor technology[1]. Synchrotron radiation (SR) is now considered to be a suitable light source for photochemical processes[2)-3)]. In this study, aluminum oxide films were deposited on Si and SiO_2 substrates by SR-CVD at room temperature using $Al(CH_3)_3$ (TMA) gas which is known as one of the most popular organometallic materials in semiconductor industry. It is found that the carbon contamination of the aluminum oxide films deposited by SR-CVD is much lower than that deposited by thermal CVD.

Experimental The SR light through a Ni mesh (64% transmittance) was irradiated upon the substrate perpendicularly to the surface. The substrate temperature was kept at room temperature.

Results and Discussion The surface roughness of the deposited film is shown in Fig.1. Though the distance between the Ni mask and sample is 10mm, the film is deposited on irradiated area and not deposited on non-irradiated area. This fact suggests that the surface reaction is dominant in the deposition of the aluminum oxide films and that adsorbed species on the substrate surface are decomposed by irradiation of SR. Figure 2 shows Auger electron spectroscopy of aluminum oxide films by SR-CVD and by thermal CVD. The aluminum oxide film formed by thermal CVD contains carbon contamination, there are few carbon peak when using SR light. It is found that the carbon contamination from organometallic materials decreased by using SR excited CVD method.

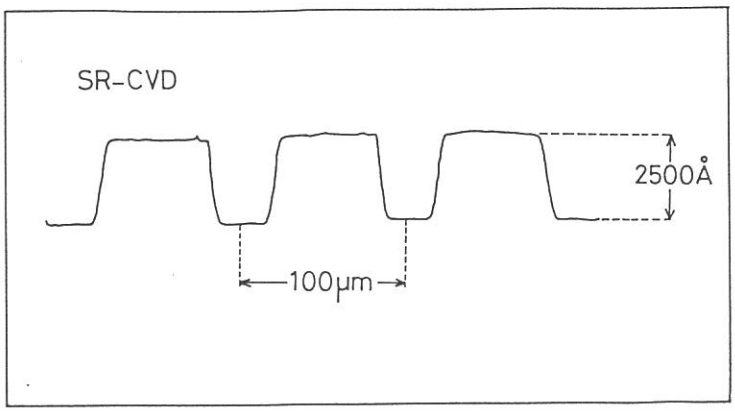

Fig.1 Surface profile of aluminum oxide film formed by SR-CVD.

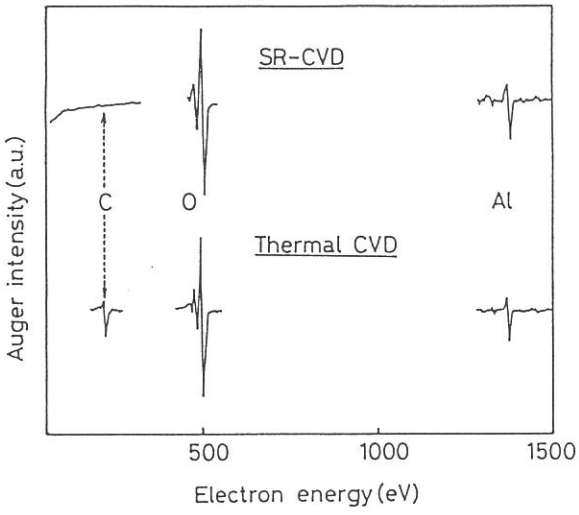

Fig.2 Comparison of AES intensities of films formed by SR-CVD and thermal CVD.

Note that the carbon contamination of the aluminum oxide film formed by SR-CVD is much lower the that by thermal CVD.

References

1) D.J.Ehrlich and J.Y.Tsao, J.Vac.Sci.Technol.**B1**, 969(1983).

2) H.Ohashi, K.Inoue, Y.Saito, A.Yoshida, H.Ogawa and K.Shobatake, Appl.Phys.Lett.**55**,1644(1989).

3) T.Urisu and H.Kyuragi, J.Vac.Sci.Technol.**B5**,1436(1987).

LOW TEMPERATURE GROWTH OF SiO_2 THIN FILM BY PHOTO-CVD USING SYNCHROTRON ORBITAL RADIATION

Masanori OKUYAMA, Yuhichi MATSUI, Ryouichi NAGAYOSHI and Yoshihiro HAMAKAWA

Department of Electrical Engineering, Faculty of Engineering Science,
Osaka University, Toyonaka 560, Osaka

SiO_2 thin films have been grown from Si_2H_6 and O_2 on Si and MgF_2 crystals by photo-CVD using the SOR. The SOR light from BL-8A was applied through a hole of diameter 3mm to the substrate surface in the reaction chamber without any spectroscopic and focussing system directly. Incident light flux is estimated to be 6.7×10^{14} photons/cm^2·s at beam current of 100mA. The background pressure was $1 \sim 2 \times 10^{-7}$Torr. O_2 was introduced into the whole chamber and Si_2H_6 was applied through a nozzle of diameter 1/16 inch to the substrate. The total pressure for the deposition of SiO_2 films was $0.05 \sim 0.2$Torr and flow rate ratio of Si_2H_6 to O_2 was $0.052 \sim 0.057$. The substrate temperature was changed from room temperature to 220 ℃.

The deposition rate on Si(100) of ρ =0.5 Ω cm below 100 ℃ under the SOR irradiation vertical to the substrate is twice larger than that in the dark area just near the irradiated circle, but these rates are almost same at 200 ℃. On the other hand, no films grow on Si(111) of ρ =0.1 Ω cm at 200 ℃. Origin of difference of the deposition is not clear, but might be resistivity difference or anisotropy of the excitation. Spatial distribution of the deposition rates under different irradiation are shown in Fig. 1. Remarkable difference of the deposition rates under or outside the irradiation is found when the SOR light is incident vertically to the substrate as shown in Fig. 1(a). The difference decreases when the light is incident horizontally to the substrate as shown in Fig. 1(b). Moreover, the spatial distribution is spread more when the light passes over the substrate horizontally. It is considered from these spatial distributions that the film deposition at low temperature region is attributed much to photo-chemical reaction of radical species on the irradiated substrate surface, but not so much to the vapor-phase reaction. Refractive indices of the films on Si(100) change a little up to 150 ℃, but decrease very much at 200 ℃.

Infrared transmission measured by FT-IR shows that absorption assigned

to Si-H and Si-OH in not found in the SOR photo-CVD film, but is found in the films of photo-CVD using D_2 lamp or Kr-He lamp. Transmission spectra in visible and ultraviolet light region were obtained using vacuum monochrometer and are shown in Fig. 2. There are two large absorption peaks both in the film deposited on MgF_2 by the vertical irradiation and in MgF_2 irradiated with the SOR light, but no absorption peaks in the film deposited on MgF_2 by the horizontal irradiation. Therefore, no large absorption is not produced in the deposited film.

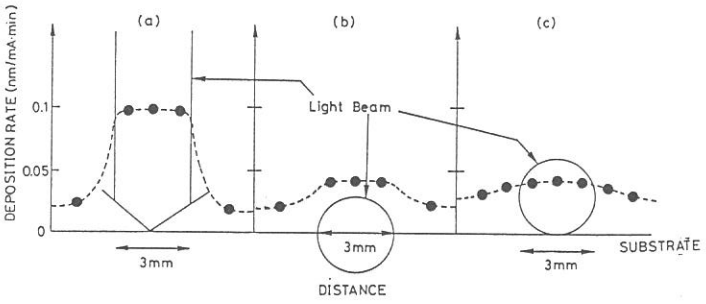

Fig. 1 Spatial distribution of thickness of films deposited under different incidences.

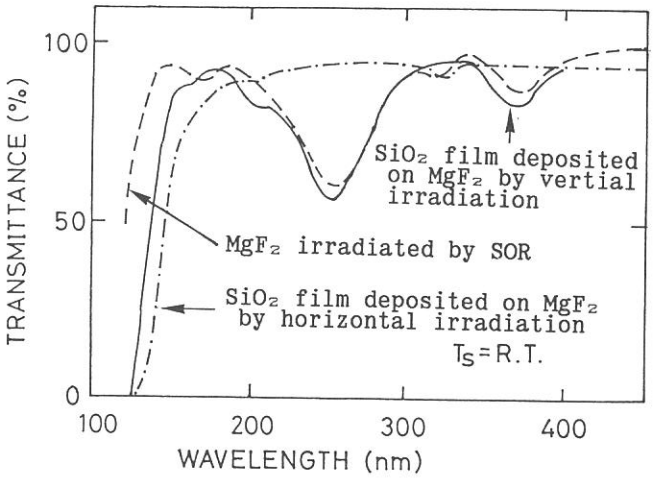

Fig. 2 Visible and ultra-violet light transmission spectra of the SiO_2 films and MgF_2.

Electrical property was characterized by the C-V and DLTS measurements. Fixed oxide charge is estimated from the flat band voltage and the minimum is $1.6\times10^{11}cm^2$. Interface state density is obtained from DLTS analysis and the minimum is $1.1\times10^{11}eV^{-1}cm^2$.

In summary, the SiO_2 film are grown from Si_2H_6 and O_2 by the photo-CVD at low temperature and shows superior optical and electrical properties as compared to the other photo-CVD films.

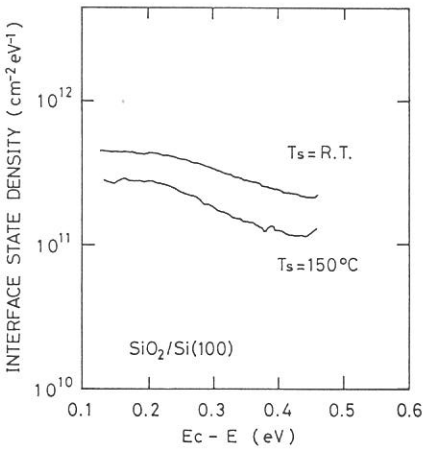

Fig. 3 Interfrace state density of SiO_2-Si structure prepared by photo-CVD.

Synchrotron Radiation Irradiated Metalorganic Chemical Vapor Deposition of The Zinc Telluride Films

Hiroshi OGAWA, Mitsuhiro NISHIO, Makoto IKEJIRI and Hideyuki TUBOI

Department of Electronic Engineering, Faculty of Science and Engineering, Saga University, 1 Honjo, Saga 840, Japan

ZnTe, one of the II-VI compound semiconductors, is promising in application to opto-electronic devices. However, it is difficult to obtain the high quality film due to the self-compensation or residual impurities. In order to overcome this problem, it is important to establish the growth technique for the preparation of the ZnTe film at low substrate temperature. In this report, we describe the low-temperature growth of ZnTe by photo-assisted metalorganic chemical vapor deposition method using the synchrotron radiation (SR) as a light source.

Figure 1 shows the schematic experimental apparatus. Diethylzinc and diethyltelluride were used as source materials. These alkyls diluted with high purity hydrogen were introduced into a stainless steel reactor and then transported toward the substrate stage controlled by the resistance heater. The ZnTe substrate with (110) plane was cut from a Bridgman-grown ingot. The MgF_2 filter was inserted between the beam line and the reactor. As a result, SR used for the excitation has a wavelength range above about 120 nm, by which the source organometallics can be dissociated in gas phase. The growth was carried out under the condition of atomspheric pressure. During the growth, the beam was irradiated onto the substrate and the substrate temperature was kept at 130℃.

After the growth, it was found that the deposition occurs only in the irradiated region on the substrate, as shown in Fig. 2. The film with smooth surface was obtained. It showed a red color characteristic of ZnTe. Thus, it was concluded that the SR irradiation is very useful for the formation of the ZnTe film at a low temperature such as 130℃, at which the pyrolysis of the source materials is very difficult. The thickness of the film was estimated as small as 0.1μm. According to the RHEED observation, the film deposited was amorphous ZnTe.

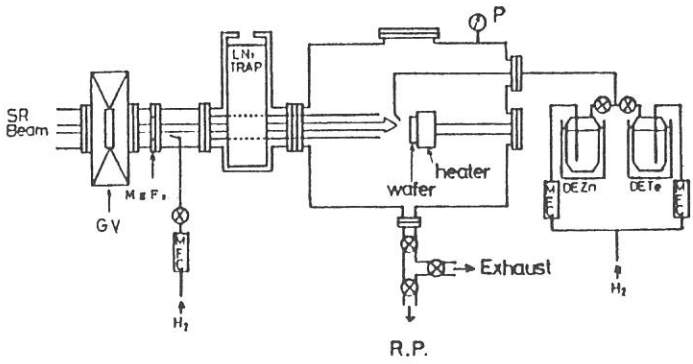

Fig. 1. The schematic experimental apparatus.

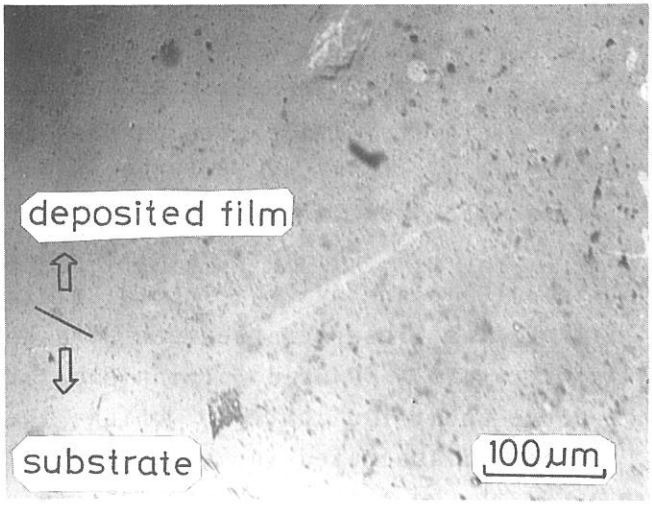

Fig. 2. The typical microphotograph of the film.

UV-SOR photoelectron spectroscopic study of κ-(BEDT-TTF)$_2$Cu(NCS)$_2$ organic superconductor

R.Itti, H.Mori, K.Ikeda,

I.Hirabayashi, N.Koshizuka, and S.Tanaka

Superconductivity Research Laboratory, International Superconductivity Technology Center, 1-10-13 Shinonome, Koto-ku, Tokyo 135, JAPAN

K.Kamiya, and H.Inokuchi

Institute for Molecular Science, Myodaiji, Okazaki 444, JAPAN

κ-(BEDT-TTF)$_2$Cu(NCS)$_2$ was first reported by Urayama et al. to be an ambient pressure organic superconductor with the critical temperature Tc=10.4K.[1] It is the organic superconductor with the highest Tc until the recent discovery of the two new ones with Tc=11.6K (at ambient pressure) and 12.8K (under a pressure of 0.3kbar), respectively.[2]

For the organic superconductors, a complete picture of the electronic structure has not yet emerged. Among various normal and superconducting characteristics of this system, some agree with the conventional theory, while others do not.[3]

In this communication, the first photoelectron spectroscopic valence band study of this compound investigated by the UV-SOR is reported.

Single crytals of κ-(BEDT-TTF)$_2$Cu(NCS)$_2$ prepared by an electrochemical method[1] with the typical size of 2x1x0.05 mm^3 were used in this study. Measurements were carried out at the beam line 8B2 of the UVSOR storage ring of the Institute for Molecular Science at ambient temperature. Photon with the energy range of 20-80 eV was used. The spectra were recorded with the total energy resolution of better than 0.6 eV. The reliability of the data was verified from the reproducibility from different samples. Because of the small sample size and in order to minimize the radiation damage, the photon was focused into the beam size smaller than the sample size and a nickel mesh of 50% nominal transmission was used in the measuremens.

Figure 1 shows the valence band spectrum from κ-(BEDT-TTF)$_2$Cu(NCS)$_2$ for hν=40 eV photon radiation. The result shows a broad

feature of the valence band arising from the Fermi level up to the binding energy of about 12 eV. Peaks at about 5, 6, and 9 eV can be observed. A continuous increase of the spectral intensity just below the Fermi level upto about 3-4 eV is also worth noting. The spectral intensity reflecting the density of states at the Fermi level comes out to be very small. Peaks due maybe to shallow core levels can also be observed at about 13 and 17 eV.

In Fig.2, the valence band spectra from $\kappa-(BEDT\text{-}TTF)_2\,Cu(NCS)_2$ as a function of photon energy are shown. Relative intensities of peaks at 5, 6, and 9 eV change as the photon energy changes. This is informative in the consideration of the characteristics of the bands (bonds) involved in the valence band structure. Detailed analysis of the results is in progress and will be reported elsewhere.

REFERENCES

1. H.Urayama, H.Yamochi, G.Saito, K.Nozawa, T.Sugano, M.Kinoshita, S.Sato, K.Oshima, A.Kawamoto, J.Tanaka, Chem.Lett. **1988**, 55 (1988).
2. A.M.Kini, U.Geiser, H.H.Wang, K.D.Carlson, J.Williams, W.K.Kwok, K.G.Vandervoort, J.E.Thompson, D.L. Stupka, D.Jung, M.-H.Whangbo, Inorg.Chem.**29**, 2555 (1990).
3. For a review of experimental and theoretical studies on organic superconductors, see: *The Physics and Chemistry of Organic Superconductors*, edited by G.Saito and S.Kagoshima (Springer-Verlag, Berlin Heidelberg, 1990).

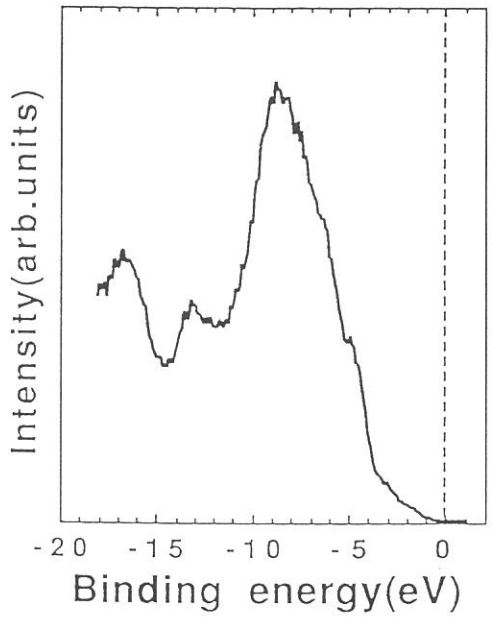

Fig.1 valence band spectrum for hν=40 eV photon radiation

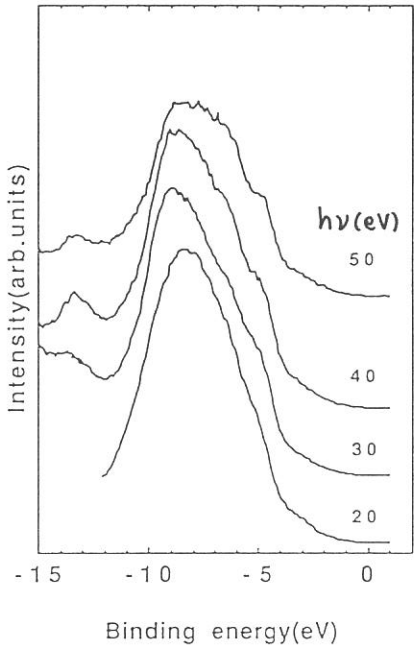

Fig.2 valence band spectra as a function of photon energy

ANGLE-RESOLVED PHOTOEMISSION FROM Cu-PHTHALOCYANINE FILM EVAPORATED ON GRAPHITE SURFACE

[a]N. Ueno, [b]K. Kamiya, [c]M. Hara, [d]K. Seki, [a]K. Sugita, [c]H. Sasabe, [c]A. Yamada and [b]H. Inokuchi

[a]Department of Materials Science, Faculty of Engineering, Chiba University, Chiba 260

[b]Institute for Molecular Science, Okazaki 444

[c]Frontier Research Program, The Institute of Physical and Chemical Research, Wako 351-01

[d]Department of Materials Science, Faculty of Science, Hiroshima University, Hiroshima 730

The angle-resolved ultraviolet photoemission spectroscopy (ARUPS) is very powerful for studying both the electronic structure and molecular orientation in the ultrathin films, since the angular distribution of the photoelectrons reflects the angular part of the wave function for the valence electrons of the films [1].

The investigation of the molecular orientation and electronic structure in an ultrathin film of organic molecule has become important in recent years. The phthalocyanine class of materials have been known as the most stable organic semiconductors, both chemically and thermally, and can be sublimed to form high quality thin films.

We have measured ARUPS spectra of thin films of copper phthalocyanine (CuPc) evaporated onto a cleaved graphite (HOPG) surface. The frequency change of a quartz thickness monitor was 62 Hz for the film deposition. The intensity of the monochromatized synchrotron radiation was reduced by introducing a nickel mesh of 50% nominal light transmission across the light path, since we observed spectral changes when the mesh was not used. This change can be ascribed to the change in the molecular orientation, since only the intensities of π bands changed by the irradiation. The incidence angle of photons (α) was fixed at 0° throughout the measurements.

The ARUPS spectra at $h\nu$=30eV are shown in Fig. 1 as a function of the electron take-off angle θ. The two features denoted by A and B, which can be ascribed to valence bands consisting of π-electrons in the molecules, show apparent θ dependence with a maximum at θ=45° (Fig. 2), while other features in larger binding energy region did not show such a clear θ dependence, probably because these peaks originate in many electronic states with different characters.

LEED measurements for CuPc films, ARUPS spectra of which showed a clear θ dependence at $h\nu$=31 eV similar to Figs. 1 and 2, gave an evidence that the molecules lie with their molecular plane parallel to the substrate surface [2,3]. It is thus concluded that CuPc molecules in the present film orient with their molecular planes parallel to the graphite surface.

As seen in Figs. 3 and 4, on the other hand, the θ dependences at $h\nu$=40 eV differ significantly from those at $h\nu$= 30 eV. This indicates that the final state affects the angular distribution of the photoelectron from the CuPc films.

References
[1] "Photoemission and the electronic properties of surfaces", Edited by B. Feuerbacher, B. Fitton and R. F. Willis, (John Wiley and Sons, New York, 1978).
[2] R. Engelhardt, R. Dudde, E. E. Koch and N. Ueno, 8th Int. Conf. Vacuum Ultraviolet Radiation Physics, 8/4-8/8 (1986), Lund, Sweden, p.632.
[3] R. Engelhardt, Ph.D Thesis, Universität Hamburg, 1985.

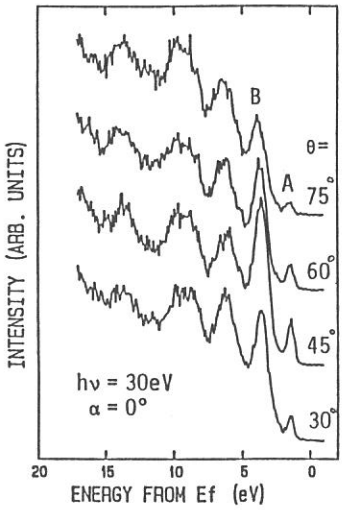

Fig. 1 θ dependence of ARUPS spectra for CuPc on graphite at $h\nu$=30eV and α=0°.

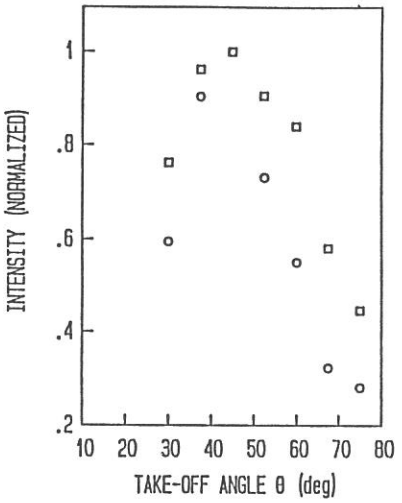

Fig. 2 θ dependence of the intensity of π bands (A and B) at $h\nu$=30eV and α=0°. ○ : π band A. □ : π band B.

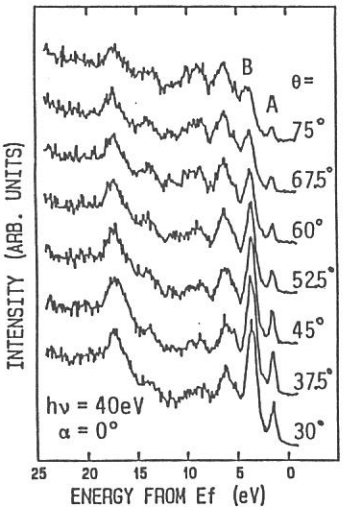

Fig. 3 θ dependence of ARUPS spectra for CuPc on graphite at $h\nu$=40eV and α=0°.

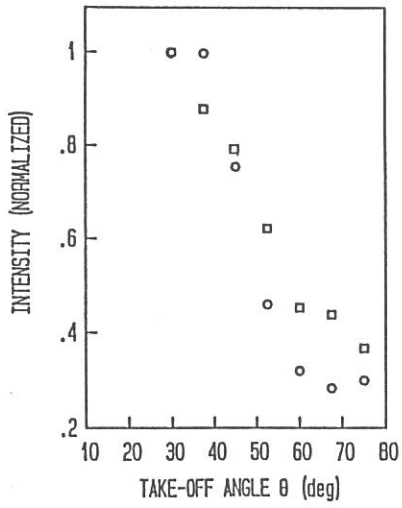

Fig. 4 θ dependence of the intensity of π bands (A and B) at $h\nu$=40eV and α=0°. ○ : π band A. □ : π band B.

UV PHOTOELECTRON SPECTROSCOPY OF POLY(p-PHENYLENE) EVAPORATED FILMS

Kazuhiko SEKI, Kunishige EDAMATSU, Satoru NARIOKA, Toshiaki OHTA, Koji KAMIYA[A], Hiroo INOKUCHI[A], and Takakazu YAMAMOTO[B]

Department of Materials Science, Faculty of Science, Hiroshima University, Hiroshima 730

[A]Institute for Molecular Science, Myodaiji, Okazaki 444

[B]Research Laboratory of Resources Utilization, Tokyo Institute of Technology, Nagatsuda, Yokohama 227

Poly(p-phenylene)(PPP) is one of the typical conducting polymers with an extended π-conjugated system. Its electronic structure has been studied by X-ray photoelectron spectroscopy (XPS) combined with molecular orbital calculations [1]. The uppermost part of the valence band, which is most important in discussing the electronic conduction on acceptor doping, has been studied in more detail by us on oligomers up to sexiphenyl (six benzene rings) using angle-resolved uv photoelectron spectroscopy (UPS) [2]. Although the UPS work revealed fine structures of the π levels on the way of forming a π band, corresponding data for the π band of PPP polymer have not been obtained. In this work we report UPS results for a thin PPP film using synchrotron radiation.

The sample material of PPP was synthesized by dehalogenation of dibromobenzene using organometallic catalysis developed by Yamamoto [3]. The UPS sample films were prepared by vacuum evaporation on Au film deposited on a Cu disk. The thickness was ca. 10 nm as monitored with a quartz oscillator. The spectra were measured on an angle-resolving UPS spectrometer at the beamline 8B2 at the UVSOR facility in the photon energy range between 20 and 90 eV.

In Fig. 1 we show the UPS spectrum at $h\nu$ = 60 eV covering the whole valence band. It agreed well with the UPS spectrum of sexiphenyl except for the topmost valence band. In Fig. 2 this topmost part is expanded. The strong peak B at ca. 8 eV is derived from one of the doubly degenerate highest occupied molecular orbitals (HOMOs) of benzene, which is not perturbed by connecting the rings due to the lack of electron density at the connecting part. The other HOMO strongly interacts by the connection, forming a wide π band. In a one-dimensional system such as PPP, the density of states concentrated at the top and the bottom of the formed band. Thus the peak A can be assigned as the top end of the delocalized π band. The A-B separation is 1.6_5 eV, corresponding to the half-width of the π band. This value is somewhat smaller than the value estimated from the data of short oligomers (2 eV). This difference may arise from the imperfect planarity or other structural irregularity in the evaporated PPP film.

REFERENCES

[1] J. Riga, J.J. Pireaux, J.P. Boutique, R. Caudano, J.J. Verbist, and Y. Gobillon, Syn. Metals, 4, 99 (1981).
[2] K. Seki, U.O. Karlsson, R. Engelhardt, E.E. Koch, and W. Schmidt, Chem. Phys., 91, 459 (1984).
[3] T. Yamamoto, Y. Hayashi, and A. Yamamoto, Bull. Chem. Soc. Jpn., 51, 2091 (1978).
[4] T. Yamomoto, T. Kanbara, and C. Mori, Chem. Lett. in press.

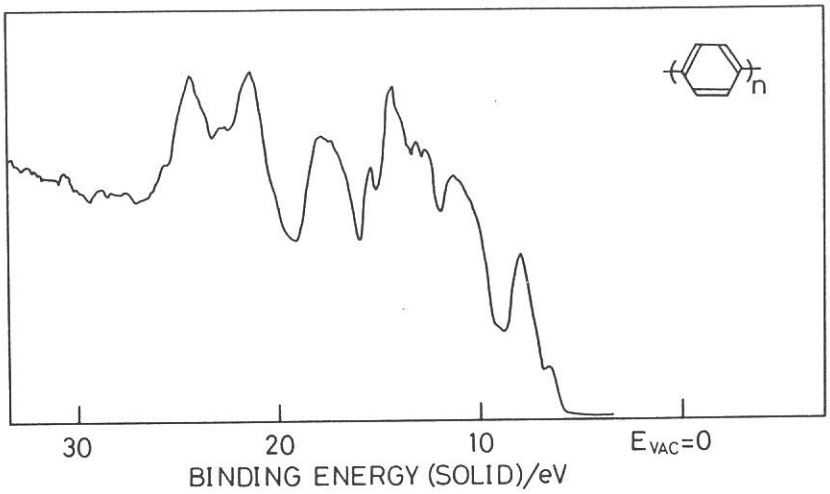

Fig.1 UPS spectrum of poly(p-phenylene) evaporated film at $h\nu$ = 60 eV covering the whole valence band.

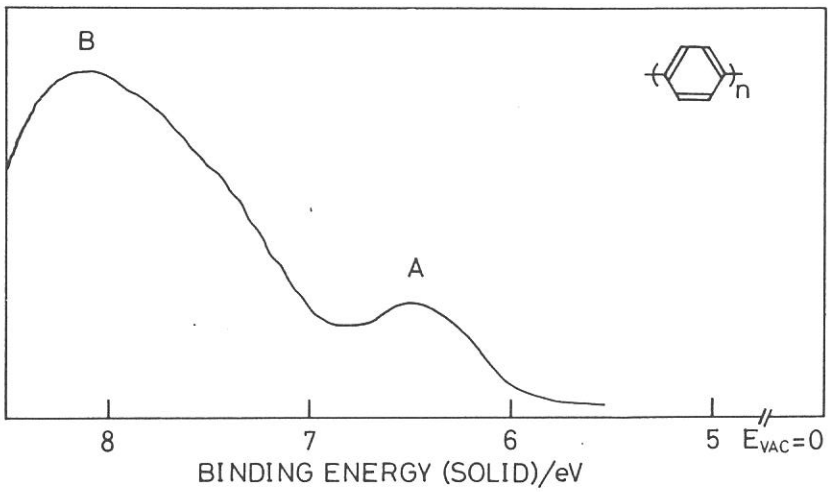

Fig.2 Expanded UPS spectrum of poly(p-phenylene) evaporated film in the topmost valence band region. The peaks A and B correspond to the top and the center of the wide π band, respectively.

Photoemission Study of an Al-Cu-Fe Icosahedral Phase

M. MORI, S. MATSUO, T. ISHIMASA, T. MATSUURA, K. KAMIYA*, H. INOKUCHI* and T. MATSUKAWA**

College of General Education, Nagoya University, Chikusa, Nagoya 464-01
*Institute for Molecular Science, Myodaiji, Okazaki 444
**Department of Physics, Naruto University of Education, Naruto 772

It has been well known that five-fold symmetry can not be present in crystals. The discovery of Shechtman et al.[1], which displayed sharp diffraction peaks with icosahedral symmetry, has made a great surprise in the world. The arrangement of the atoms in the icosahedral phase (i-phase) has still not been determined as its state differs from the ordinary crystal in the lattice periodicity. There has been increasing interest in the physical properties of i-phase materials. An Al-Cu-Fe alloy system was found to have a **stable i-phase** with high quasicrystalline quality. And it was reported that the magnetic susceptibility is proportional to T^2. This fact suggests a sharp dip (valley-like) structure in the electronic density of state (DOS) at the Fermi energy (E_F), since the T^2 dependence occurs to the Pauli paramagnetism[2]. The principal purpose of this study is the observation of DOS of the Al-Cu-Fe i-phase specimens. It is checked whether the above-mentioned anomaly in DOS at E_F exists or not.

An $Al_{65}Cu_{21}Fe_{14}$ i-phase alloy was a poly-quasicrystalline ingot[2]. All UPS studies were performed on BL-8B2 of UVSOR in IMS at room temperature. High energy resolution (0.14eV=ΔE defined as the width of Gauss function) was utilized in order to examine the detailed DOS near E_F with the incident photon energy 40eV. This specimen was so brittle that clean surfaces were easily obtained by scraping with a diamond file in a vacuum of $2\text{-}5 \times 10^{-10}$ Torr, and that the sample was transferred to the UPS chamber in a vacuum of $0.4\text{-}2\times10^{-10}$ Torr. Standard spectra of Al and Au were also measured.

Curves drawn with marks in Figs. (a), (b) and (c) is the UPS observed for pure Al, Au and Al-Cu-Fe i-phase sample, respectively. While well-defined E_F is clearly recognized for the pure Al and Au, the spectrum of Al-Cu-Fe i-phase does not give such a clear Fermi edge (Fig. (c)). This non-well-defined Fermi edge of this spectrum is an intrinsic property.

By assuming that the observed spectrum is proportional to DOS and the DOS depends linearly on the electronic energy, a model to reproduce the spectra near E_F is considered to obtain a quantitative estimation of the dip structure. The DOS of the Al-Cu-Fe i-phase alloy, additionally, has the dip of which shape is assumed to be a Lorentzian function having the center on E_F and a half width Γ as shown in Fig. (d). f(x) is the Fermi distribution function. An observed intensity I(E) is given as follows.

$$I(E)=\int (ax+b)*\{1-\frac{C\Gamma^2}{(x-E_F)^2+\Gamma^2}\}f(x)\cdot G\exp(-(x-E)^2/(\Delta E)^2)dx,$$

where $(ax+b)*(1-C\Gamma^2/\{(x-E_F)^2+\Gamma^2\}$ indicates the DOS at the energy x near E_F

with the dip of the DOS near E_F. C is the ratio of dip-depth and the normal.

The case of C=0 (normal DOS) is considered in order to treat the spectrum of pure Al and Au. Fitting results, shown as the solid curves in Figs. (a) and (b), are in good agreement with the observed data using ΔE=0.14eV and the fitting parameters a and b. No calculated curve could fit with the observed data of Al-Cu-Fe i-phase in case of C=0. The calculated drops more abruptly near E_F than the experimentals. At the next step, the parameter C is introduced to fit the spectrum of Al-Cu-Fe i-phase sample. The solid curve of Fig. (c) is the most adequately fitted calculation result using the values C=0.7 and Γ=0.35eV. The calculated curve based on the fitting model described above is in good agreement with the observed spectrum. Therefore, it is regarded that this 'dip' model is a good approximation to the DOS near E_F of this Al-Cu-Fe i-phase specimen. A width Γ of the dip is given as about 0.35±0.05eV and the DOS on E_F becomes 30±10% of the normal DOS without the dip. The model proposed by Matsuo et al.[2] is supported by the present result. The detailed UPS and CIS studies of i-phase alloys are now in progress. The partial DOS of each component atom is interesting.

The authors are indebted to K. Kimura, H. Fujimoto, M. Watanabe, O. Matsudo and K. Fukui, UVSOR, the Institute for Molecular Science.

1)Shechtman D, Blech I, Gratias D & Cahn J W, Phys. Rev. Lett. 531951(1981)
2)Matsuo S, Ishimasa T, Nakano H and Fukano Y, J. Phys. F: Met. Phys. 18 L175 (1988) and J. Phys.: Condens. Matter 1 6893 (1989)

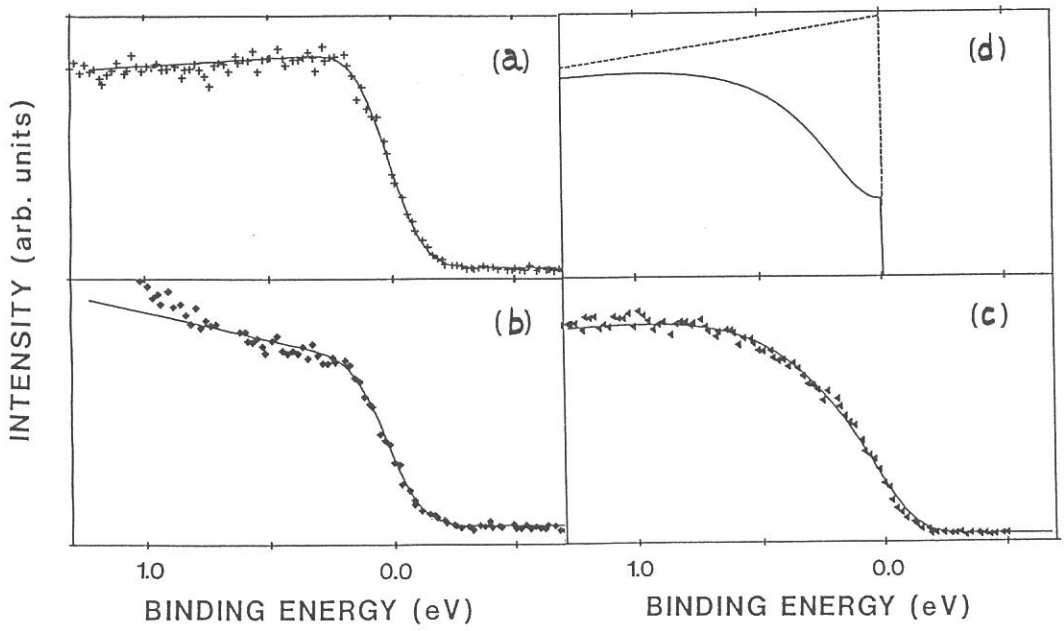

FIGURE Marked curve is the observed UPS near the Fermi edge. Solid curve is the fitted result. (a) Al, (b) Au and (c) Al-Cu-Fe i-phase. (d) The DOS model of the Al-Cu-Fe i-phase for the fitting calculation is made up by subtracting the dip from the normal DOS (broken curve). Solid curve is for the case of C=0.7 and Γ =0.35eV.

Photoemission Measurements of Crystalline and Amorphous SnTe Thin Films

Kazutoshi FUKUI, Yasuo FUJII,[1)] Masao KAMADA[2)]
and Makoto WATANABE[2)]
Department of Electrical and Electronics Engineering,
Fukui University, Fukui 910
[1)]*Department of Applied Physics, Osaka City University, Osaka 558*
[2)]*Institute for Molecular Science, Okazaki 444*

Group IV tellurides (IVTe : PbTe, SnTe, GeTe) are semiconductors having both ionicity and covalency. The IVTes become amorphous when they are evaporated on the cooled substrate and easily crystallize by raising temperature. The core absorption (Pb 5*d*, Sn 4*d*, Ge 3*d* and Te 4*d*) spectra of crystalline (*c*) and amorphous (*a*) SnTe, *c*- and *a*-GeTe and *c*-PbTe were already reported.[1-3)] In the present work, we report energy distribution curves (EDC) of *c*- and *a*-SnTe to discuss the details of the valence band in connection with the bonding nature. Experiments were performed at BL6A2 equipped with a plane grating monochromator (PGM) in the energy region from 21 to 80 eV. EDC experiments were carried out by using a cylindrical retarding field analyzer. The *a*-SnTe thin films were evaporated on cooled (about 100 K) Au substrates. After the measurements on *a*-SnTe were carried out at about 100 K, the samples were annealed at room temperature and then the measurements on *c*-SnTe were carried out at room temperature.

Figures 1 and 2 show the EDCs of *c*- and *a*-SnTe, respectively. All curves are normalized to the intensity of structure at the binding energy of 2.0 eV. The parameters in the figures represent the excitation photon energies. The EDCs of *c*-SnTe consist of three peaks I, II and III, as shown in Fig. 1. The peak I is a broad consisting of more than two structures. According to the band calculation,[4)] the peaks I, II and III correspond to the bonding *p* states, Sn *s* states and Te *s* states, respectively. The EDCs of *a*-SnTe are similar to those of *c*-SnTe except the shape of the peak I. This indicates that the crystal structure and bonding character do not drastically change with the phase transition from *a*-phase to *c*-

phase and the peaks I, II and III of the EDCs of *a*-SnTe can be attributed to the bonding *p* states, Sn *s* states and Te *s* states, respectively. It should be noted that the structure just below the top of the valence band in the peak I in *a*-SnTe is weaker than that in *c*-SnTe. This probably suggests that the Te *p* character is dominant at the top of the valence band in *c*-SnTe but decreases in *a*-SnTe, since *a*-GeTe is more covalent than *c*-GeTe.[2)]

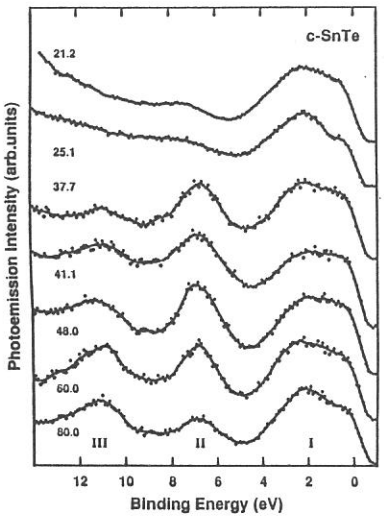

Fig. 1. Energy distribution curves of *c*-SnTe. The parameters represent the excitation photon energies.

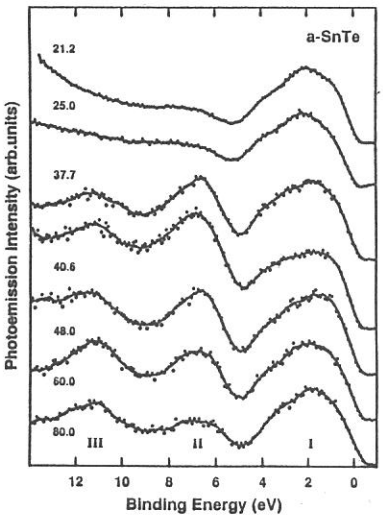

Fig. 2. Energy distribution curves of *a*-SnTe. The parameters represent the excitation photon energies.

References

1) K.Fukui, J.Yamazaki, T.Saito, S.Kondo and M.Watanabe : J. Phys. Soc. Jpn. **56** (1987) 4196.
2) K.Fukui, T.Saito, S.Kondo, Y.Fujii, Y.Sakisaka and M.Watanabe: J. Phys. Soc. Jpn. **59** (1990) 4161.
3) K.Fukui, T.Saito, S.Kondo and M.Watanabe : UVSOR ACTIVITY REPORT 1989, p54.
4) H.M.Polatoglou, G.Theodorou and N.A.Economou : Phys. Rev. B **11** (1975) 3808.

Na K-EDGE XAFS STUDIES ON SODIUM LOADED ALUMINA

Sadao HASEGAWA[1], Hiroko MAMADA[1], Nobutoshi YOSHIHARA[1], Tadashi HASEGAWA[1] and Tsunehiro TANAKA[2]

1 Department of Chemistry, Tokyo Gakugei University, Koganei, Tokyo 184

2 Department of Hydrocarbon Chemistry, Faculty of Engineering, Kyoto University, Kyoto 606

An Na-NaOH-Al_2O_3 catalyst has been found to possess basic sites with $H_0 > 35$, so-called the super base.[1] In our previous report, surface Mn^{4+} species is observed on Mn-Na-MgO and is converted to surface Mn^{2+} by evacuation.[2] The sodium ion on the surface acts as electron donor. Recently, we have found that sodium-alumina acts as a base for alkylation of 1,3-diketones and that only sodium-alumina containing less than 20 wt% of sodium shows on effective reactivity.[3]

In the present study, surface structures of sodium catalysts have been investigated by XAFS. The K-edge absorption spectra of sodium loaded Al_2O_3 catalysts were measured at the BL-7A soft X-ray beam line with UVSOR facilities. A beryl two-crystal monochrometer was used.

Sodium loaded alumina(Na/Al_2O_3: sodium contents are in the range of 5 to 40 wt%) was prepared by soaking Al_2O_3 in an ethanol solution of sodium ethoxide, and then heating at 393 K. The surface of sodium loaded alumina showed no infra red bands due to sodium ethoxide.

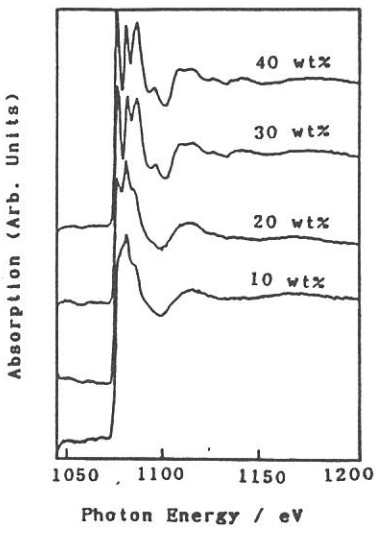

Fig. 1

Figure 1 shows the XAFS spectra of sodium loaded alumina. The peak intensity of the Na K-edge absorption at 1085 eV of photon energy is increasing with increasing the load concentration of sodium ethoxide on alumina. The results of Fourier transformation of the k^3-weighted EXAFS are shown in Figure 2. The peaks at the radial distance of ca. 2 and 3.5 A can be attributable to the Na-O (L1) and Na-Na and/or Na-Al (L2), respectively. The distances were found to decrease in high load contents of sodium on alumina. The ratio of the intensity of the peak at around 2.0 A to that at around 3.5 A is also decreased with increasing the loaded concentration of sodium as shown in Figure 3. The distances of L1 and L2 in less than 20 wt% of loaded sodium concentration are about 2.0 and 3.5 A,respectively. In above 30 wt% of sodium contents, the distances of L1 and L2 change to be 1.8 and 3.2 A, respectively. These results show that sodium ions on alumina are highly dispersed in low contents of sodium and only in these conditions the Na-O species acts as base.

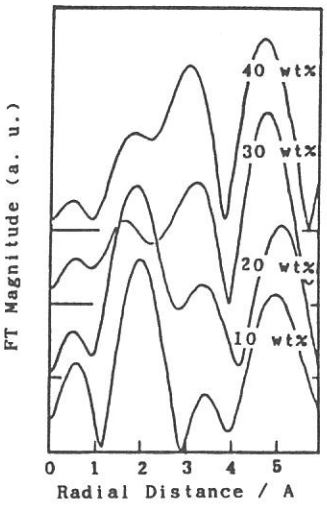

Fig. 2

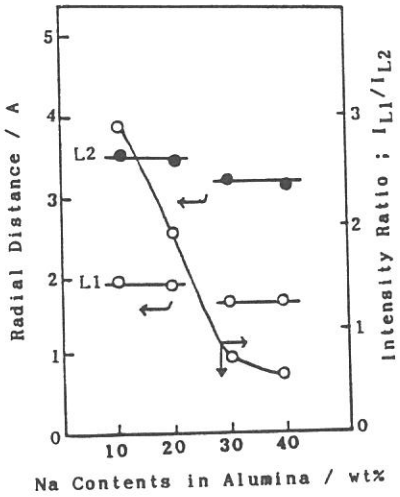

Fig. 3

References:
1 G. Suzukamo, M. Fukao, M. Minobe, Chem. Letter., 585 (1987)
2 H. Suzuka, S. Hasegawa, T. Tanaka, G. Zhang, H. Hattori, Surface Science 221, L769 (1989)
3 N. Yoshihara, T. Hasegawa, S. Hasegawa, Bull. Chem. Soc. Jpn., in press.

STUDIES ON THE STRUCTURE OF MoO_3-MgO CATALYSTS BY K-EDGE ABSORPTION SPECTRA OF Mg.

Sadao HASEGAWA, Tsunehiro TANAKA[1], Satoshi MATSUI and Hideshi HATTORI[2]

Department of Chemistry, Tokyo Gakugei University, Koganei-shi, Tokyo 184
1 Department of Hydrocarbon Chemistry and Division of Molecular Engineering, Faculty of Engineering, Kyoto University, Kyoto 606
2 Department of Chemistry, Faculty of Science, Hokkaido University, Sapporo 060

Some binary metal oxides containing MoO_3 are used as catalysts for the isomerization, oxidation, hydrogenation and metathesis of olefin. It is well known that the surface OH group on MoO_3 catalysts acts as an acid site[3], and surface Mo^{6+} is easily changed to Mo^{5+} and/or Mo^{4+} with the reduction.

In the present investigation, the surface structure on MoO_3-MgO are determined by EXAFS and XANES.

Oxidized MoO_3-MgO catalyst containing 10-90 atomic % of MoO_3 were prepared by the impregnation technique. Calculated amounts of $(NH_4)_6Mo_7O_{24} \cdot 4H_2O$ were dissolved in a volume of H_2O corresponding to the $MgCl_2 \cdot 6H_2O$ to be impregnated at the temperature of 363 K. The impregnate was air-dried for 10 hr at 383 K, and finally heat-treated at 873 K for 1 hr in air. MgO catalysts were prepared by heat-treatment of $MgCl_2 \cdot 6H_2O$ without impregnation. Reduced catalysts were prepared by the reduction with hydrogen at 773 K for 1 hr.

Mg-K absorption XAFS spectra were measured at BL 7B of the UVSOR.

Figure 1 shows Mg K-edge XANES spectra of oxidized and reduced MoO_3-MgO catalysts. From XRD results, the formation of $MgMoO_4$ is observed in the sample of oxidized MoO_3-MgO (the atomic ratio of Mo/Mg is above 0.6). While, the maximum intensity of ESR signal due to Mo_{6c}^{5+} is observed in the sample of MoO_3-MgO

containing 60 atomic % of Mo ion. By the reduction of MoO_3-MgO (Mo/Mg = 0.1-0.9) catalysts, clear XANES spectra could not observed.

The distances from Mg ion to O ion (the first ligand: L1) and to next Mg ion or Mo ion (the second ligand : L2) are calculated from Fourier transformed EXAFS data of k^3-weight of Mg K-edge in MoO_3-MgO catalysts. Figure 2 shows the values of L1/L2 ratio. From the results of Fourier transformed EXAFS on the sample of MoO_3 contents over 50 atomic % in MgO, the existence density of the first ligand is larger than that of the second ligand. In the case of MoO_3 contents under 40 atomic %, pattern of XANES and Fourier transform of Mg K-edge EXAFS are similar of non doped MgO. In the case of low contents of Mo ion, the facts suggest that MoO_3 is existed in bulk of MgO crystal.

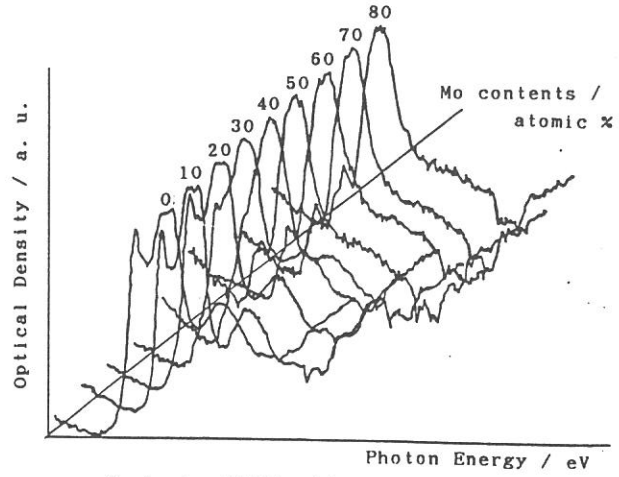

Fig. 1 Mg K-edge XANES pattern of MoO_3/MgO catalysts

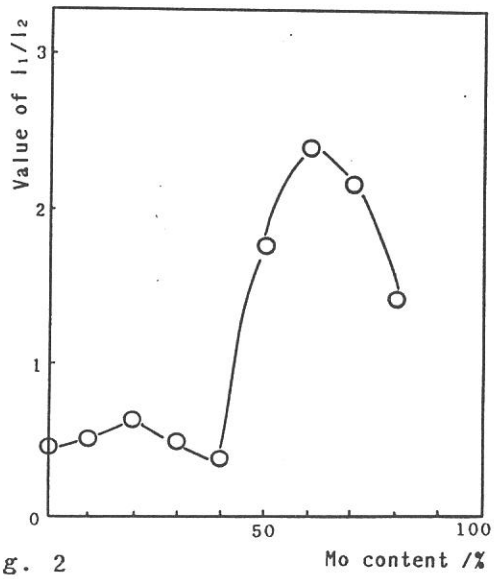

Fig. 2

Existence value of I_1/I_2 obtained Fourier transform of Mg K-edge EXAFS of MoO_3/MgO catalysts : I_1 is due to first ligand from Mg
I_2 is due to second ligand from Mg

Mg K-edge Absorption Spectra of Magnesium Oxide Species Supported on Silica.

Tsunehiro TANAKA*, Hideto TSUJI, Geng ZHANG, Mayumi SAKURABA, And Hideshi HATTORI

Department of Chemistry , Faculty of Science, Hokkaido University, Sapporo 060
**Department of Hydrocarbon Chemistry and Division of Molecular Engineering, Kyoto University, Kyoto 606*

From the views of both chemical application and basic researches, solid acid catalysts have been studied extensively and therefore mechanism of the generation of acid sites has been clarified . On the other hand, there are only a few studies of mechanism of generation of solid base. Except a special kind of combination of metal oxides, mixing of plural metal oxides only results in forming acid sites. The stable materials which exhibit explicit basicity are alkaline earth metal oxides. However, these materials lose the basicity easily when they are mixed with another metal oxides. Recently, we have found that MgO/SiO_2 shows certain basicity when Mg ions are loaded from magnesium dimethoxide. When the sample is calcined in air at higher than 1073 K, basic sites vanish.

In this material, surface magnesium oxide species are found to be in amorphous state and it is difficult to characterize the change of the phases of surface magnesium oxide species by thermal treatment. In the present study, K-edge absorption spectroscopy was utilized to characterize such species.

The catalyst samples were prepared by impregnation of silica with a methanol solution of $Mg(OCH_3)_2$ followed by calcination at several temperatures in air. MS500 and MS800 stand for Mg/SiO_2 calcined at 773 K and 1073 K, respectively. MS500 possess both acid and base sites while MS800 exhibit no apparent acid and base properties. X-Ray diffraction patterns of both samples show that they are in amorphous state.

X-Ray absorption experiment was carried out at beam line 7A in UVSOR facility. A beryl two-crystal monochromator was used. Energy calibration was made by using Al K-edge absorption in beryl. Spectra of Mg K-edge absorption were collected in the electron yield mode because the concentration of magnesium is small in the sample.

Fig. 1 shows Mg K-edge XANES spectra of MS500 and MS800. At 1310 eV, a sharp and narrow absorption due to 1s - 3p transition can be seen for MS500 XANES. This proves that Mg in MS500 is located at the center of an oxygen octahedron without distortion. On the other hand, this absorption band becomes broader in the case of

MS800. Calcination at higher temperatures changes the phase of surface species. The broadening of absorption due to 1s - 3p transition is thought to be caused by breaking the symmetry around magnesium ions. In short, XANES of MS500 is identical with that of MgO and XANES of MS800 is similar to that of Mg_2SiO_4. In MS500, Mg 3p atomic orbitals are degenerated to result in very sharp absorption, while in MS800, energy levels of the Mg 3p orbitals are split by the distorted ligand field accompanied by the split of orbitals resulting in broad absorption at 1300 - 1320 eV.

From the results of XANES, we may conclude that in MS500 very small particle of MgO is formed resulting in the presence of basic site. By raising the temperature of calcination, the surface MgO species changes to Mg_2SiO_4-like species. It is known that binary oxide comprizing MgO and SiO2 lose its acidity when it is crystallized by calcination. The same phenomenon may occur for the present sample. However, differential thermal analysis of the present sample show that no change of the states in the region of 323 - 1073 K. Therefore, we are not assured of the formation of Mg2SiO4, or rather, we conclude that precursor of Mg_2SiO_4 is formed by calcination at 1023 K.

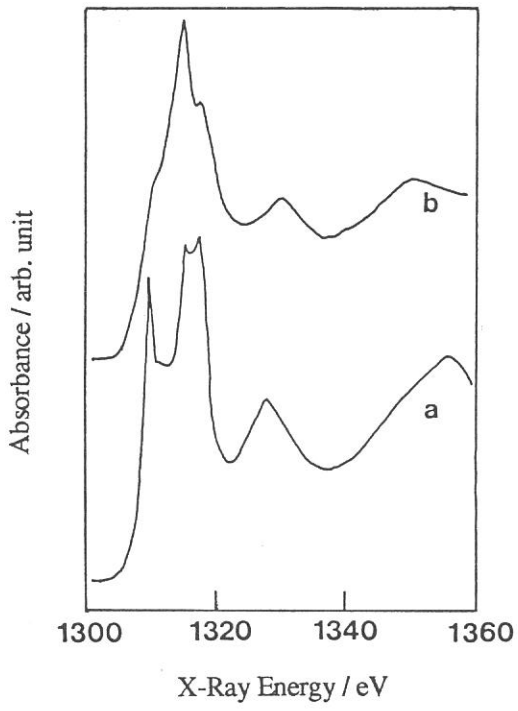

Figure 1 Mg K-edge XANES spectra of (a) MS500 and (b)MS800.
MS500, MS800, see text.

SURFACE Mg-K XANES STUDY OF MgO IN RELATION TO BASIC PROPERTY GENERATION

HIDETO TSUJI, TSUKASA HISAZAKI, TSUNEHIRO TANAKA*and HIDESHI HATTORI

Department of Chemistry, Faculty of Science, Hokkaido University, Sapporo, 060
**Department of Hydrocarbon chemistry, Faculty of Engineering, Kyoto University, Kyoto, 606*

INTRODUCTION In spite of it's simple lattice and electronic structure, MgO crystal is important from the view point of heterogeneous catalysis. Base-catalyzed reactions occur on MgO at the protruded regions such as edge and corner of the MgO crystal[1)], and the localized electronic states are considered to be associated with the catalytic behaviors. In addition, the study of electronic structure by application of DV-Xα cluster calculation method[2)] to the surface of ionic crystal indicates that the corner and edge should interact more strongly with gaseous molecules than the ideal surface, because of protrusion of the gap state wave function and their flexibility to the adsorbate perturbation. Although spectroscopic investigations of electronic structure have been made by use of ELS, LEED etc[3)], surface-XANES method is one of the suitable methods for investigation with polycrystal in relation to catalytic property. In the present study, we have characterized various types of magnesium oxide by means of photoelectron yield spectra (surface-XANES spectra), and discussed the correlation of the electronic structure of magnesium oxide with the generation of the basic property.

EXPERIMENTAL The main samples used in this work are supported magnesium oxide . They were prepared by depositing the corresponding nitrate onto Al_2O_3 from aqueous solution followed by drying at 373K for 12h, and calcination at 773K for 5h. The resulting samples are denoted as MAL followed by the number representing MgO content by wt%. The other samples NaOH-MgO and $NaNO_3$-MgO, were prepared by adding aqueous solution of NaOH and $NaNO_3$ to MgO respectively. Reference MgO was prepared from magnesium hydroxide by outgassing at elevated temperature. Photoelectron yield spectra were taken near the Mg-K edge at EXAFS facility installed at the UVSOR BL7A Institute for Molecular Science. Fine powder samples were evacuated at 773K for 2h prior to mesurement and put on the first dinode of an electron multiplier. Catalytic behaviors in base-catalyzed reaction were examined by mesurement of the activity for 1-butene isomerization at 273K.

RESULTS AND DISCUSSION Although the total electron yield spectroscopic method contains imformation not only at the surface but also in the region of several tensÅ from the surface, we obtained fairly good signals at low concentration of Mg by using this method. Fig. 1 shows photoelectron yield spectra of the samples, magnesium oxide dispersed on Al_2O_3 by different amounts. MAL15 shows Mg-K XANES similar to MgO(Fig. 2). However the peaks in the region below 1320eV are broad as compared with those observed with MgO or MAL20, indicating that the Mg cations of MAL15 have symetrical distortion. With MAL15, MgO(200) diffraction peaks appeared in XRD, but the catalytic activity did not appear. The catalytic activity appeard on MAL20. Fig. 2 shows photoelectron yield spactra of Na^+ doped magnesium oxide.

The first peak increases in intensity and broadens on Na^+ doping. It is well known that doping of alkali metal ion to magnesium oxide significantly enhances the basic strength of matrix oxide for the reason that Na^+ increases unsaturated sites of MgO[4]. Near the edge, the Kossel structure ~10eV is expected to reflect the distribution of unoccupied quantum states for the absorbing atom. On the other hand, the Madelung potential on the surface is decreased from that in the bulk so that the band gap narrows. In this connections, it is suggested that the first peak is attribute to unsaturated Mg cations. Therefore, it is expected that the electronic structure of the surface defects mesured by surface-XANES has close relation with the catalytic activity. Actually, the intensity of the first peak on MAL15 and MAL20 correlates with the catalytic activity for base catalyzed reaction. Satoko et al. reported[2] that the surface states of partially ionic crystal are determined as a result of intricately combined effects. The behaviors of the series of MAL lead us to consider that the generation of basicity needs the MgO particle larger than a certain size which has symetrical MgO lattice and effective unsaturated sites.

ACKNOWLEDGEMENT The authors thank Prof. M. Watanabe and Drs. K. Fukui, A. Hiraya, O. Matsudo, J. Yamazaki, E. Nakamura and the staffs of the UVSOR for their continuous encouuragements and technical support and suggestion.

REFERENCES 1) H. Hattori, Mater. Chem. Phys., Vol.18, 533 (1988). 2) C. Satoko et al., Ann. Rev. Inst. Mol. Sci., 22 (1978).3) V. E. Henrich et al., J. Vac. Sci. Tech., Vol. 18, 416 (1981).4) G. Zhang et al., J. Phys. Chem., Vol. 94, 506 (1990).

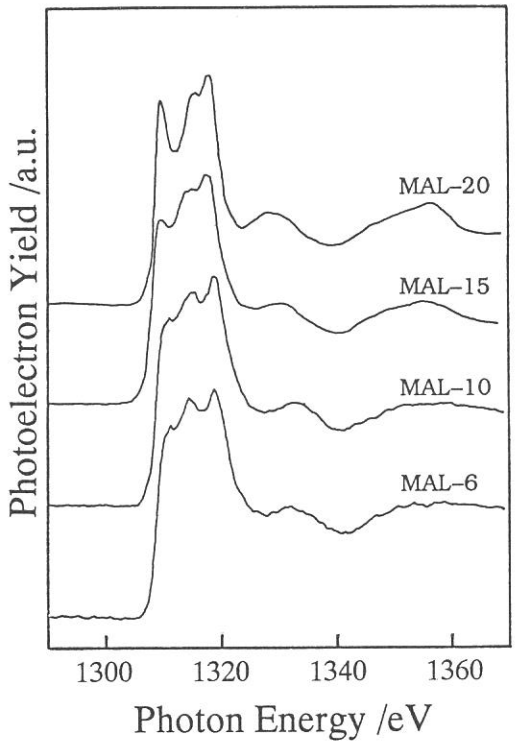

Fig. 1 Photoelectron yield spectra of MgO/Al2O3.

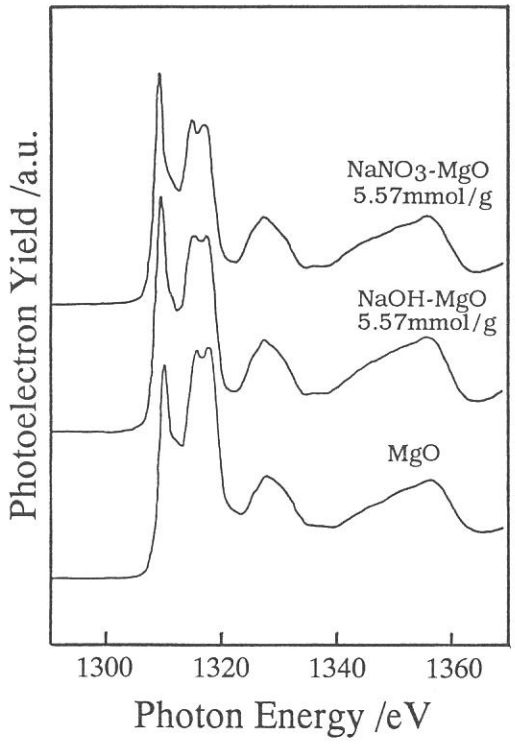

Fig. 2 Photoelectron yield spectra of MgO and Na^+doped MgO.

POLARIZED Cu L_{III} ABSORPTION STUDY OF $Bi_2Sr_2Ca_{1-x}Y_xCu_2O_8$ (x=0.0 and 0.6)

S. Suzuki, T. Takahashi, T. Kusunoki, S. Sato, and H. Katayama-Yoshida
Department of Physics, Tohoku University, Sendai 980, Japan

Copper L_{III} absorption spectra were measured for $Bi_2Sr_2Ca_{1-x}Y_xCu_2O_8$ (x=0.0 and 0.6) single crystals at various incident angles with linearly polarized synchrotron radiation. The absorption spectrum of either superconductor (x=0.0) or non-superconductor (x=0.6) shows no energy difference between the z ($3d3z^2-r^2$) and the x,y ($3dx^2-y^2$) component, while the intensity of the z component is much smaller that of the x,y component.

1. Introduction

Oxygen K (1s→2p) XAS [1] and electron-energy-loss spectroscopy (EELS) [2] results have shown that the O2p hole just above E_F has a x,y symmetry parallel to the CuO_2 plane. With respect to the Cu L_{III} (2p→3d) absorption, however, the results from these two methods do not necessarily agree with each other. XAS studies [3,4] reported a slight energy shift of the Cu L_{III} absorption peak between parallel and perpendicular to the c-axis, namely the z and the x,y component, while EELS result [2] shows no energy difference between the two.

Although the importance of two-dimensionality of a CuO_2 plane has been generally accepted, some theories place another importance on a Cu $3d3z^2-r^2$ orbital directing to the c-axis in the pairing mechanism [5,6]. According to the model, two oxygen holes form a Cooper-pair through a virtual excitation between the Cu $3dx^2-y^2$ and the Cu $3d3z^2-r^2$ orbital (d-d* excitation) through the quadrupole interaction.

2. Experimental

Single crystals of $Bi_2Sr_2Ca_{1-x}Y_xCu_2O_8$ (x=0.0 and 0.6) were grown with a self-flux method. Magnetization measurement showed that the Tc of x=0.0 is about 80K and the sample of x=0.6 is non-superconductive even at 4K.

Cu L_{III} XAS measurement was performed at BL7A. The full width at half maximum of a main Cu L_{III} peak is about 1.2eV, which indicates that the energy resolution was 0.3-0.4 eV [3]. Absorption spectrum was recorded with a total-electron-yield method. Samples were cleaved along the a-b plane under vacuum of $\sim 5 \times 10^{-8}$ Torr in the spectrometer to obtain a clean and smooth surface for polarization measurement.

3. Results and Discussion

Figure 1 shows the polarized Cu L_{III} spectra of $Bi_2Sr_2CaCu_2O_8$ measured at two incident angles, θ=0 and 70 . The main peak at 931eV is due to optical transitions from $2p^63d^9$ to $2p^53d^{10}$ and $2p^63d^9L \rightarrow 2p^53d^{10}L$. The asymmetric feature reflects the metallic nature of the crystal. As shown in Fig. 1, no energy shift is found in the main peak between the two incident angles of light. This is consistent with the previous EELS result [2] but contradicts the XAS studies [3,4]. Some possible reasons for this discrepancy will be discussed later. The intensity of the main peak is much weaker at θ=70 than at θ=0 , as reported previously [3,4]. A step-like feature appears at about 936 eV only for the measurement of θ =70 , in good agreement with a previous report [4]. This small structure in the Cu L_{III} spectrum has been assigned to the Cu 4p state.

As for the non-superconductor (x=0.6), we obtained a similar result (spectra not shown) to that of the superconductor; no detectable difference in the energy position of Cu L_{III} peak and a remarkable reduction of the intensity of the z component.

As shown in Fig. 1, the main Cu L_{III} peak is much larger at θ=0 than θ=70 , meaning that holes on Cu site are accommodated dominantly in the $3dx^2-y^2$ orbital. Extrapolation of the

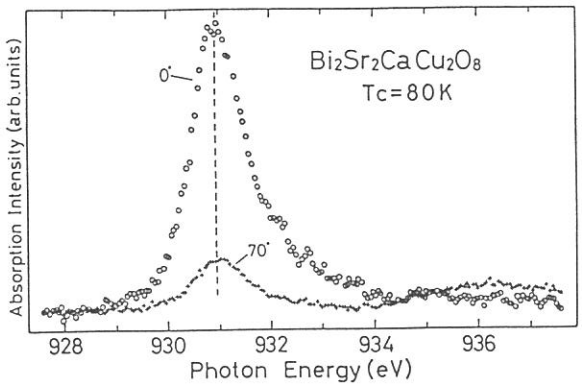

Fig. 1 Polarized Cu LIII absorption spectra of Bi2Sr2CaCu2O8 measured at incident angles of light relative to the surface normal θ =0 and 70 .

intensity-variation from θ =0° to 70° shows that the population-ratio of Cu $3d3z^2-r^2$ holes in a Cu site is less than 10%. Although the origin of such contribution from the $3d3z^2-r^2$ orbital in the Cu LIII spectrum is not clear at present, some local distortions in a CuO2 plane as observed by EXAFS [7] may be responsible for mixing of the $3d3z^2-r^2$ and the $3dx^2-y^2$ orbital.

As described above, no energy difference was observed in the Cu LIII main peak between θ =0° and 70° in the present study, which is in agreement with the EELS experiment [2] but different from XAS studies [3,4]. We should note that although the previous two XAS studies reported a substantial energy shift in the Cu LIII peak between the two extreme angles θ=0° and 90°, the amount of energy-shift is obviously different from each other; 300 meV for Bianconi et al.[3] and 500 meV for Abbate et al.[4]. Although origin(s) of these discrepancies is not finally clear at present, we discuss some possible origins. The quality of sample, especially the single-crystallinity, is essential for the polarization measurement, since we assume in the interpretation of the spectra that each crystal axis is perfectly aligned in one direction. Abbate et al.[4] and we used a single crystal while Bianconi et al.[3] used a oriented film and a pressed pellet. It is well known that a "single-crystal" film is not so perfect as a bulk single crystal, as demonstrated by a fact that a "single crystal" film is not so easily cleaved as a bulk crystal. In a pressed pellet, the crystal axis has some preferential orientation, but it is far from the perfect alignment as in a bulk single crystal. Difference in the experimental technique (XAS and EELS) may cause a discrepancy. When we measure a spectrum of the z component, we have to align the sample surface parallel to the light-path in XAS measurement while such a procedure is not necessary in EELS [2]. Therefore, a large and homogeneous single crystal surface is necessary in a polarized XAS measurement. In a case with a small sample, an elongated light spot in a grazing-angle measurement may stray out from the sample surface and as a result photoemission from a boundary of the sample which is not single crystal nor superconductor would distort the spectrum. We found in this study that the Cu LIII peak of CuO is situated a few tenths eV below that of the high-Tc superconductor. This suggests that if the boundary of the sample is polycrystalline CuO-like compound and an elongated light spot strays out from the sample surface, an apparent shift of a few tenths eV would be observed in the polarized Cu LIII XAS measurement.

References

1. F.J. Himpsel et al., Phys. Rev. B38, 11946 (1988).
2. N. Nücker et al., Phys. Rev. B39, 6619 (1989).
3. A. Bianconi, et al., "Earlier and Recent Aspects of Superconductivity" edited by K.A. Muller and J.G. Bednorz (Springer, Berlin, 1989), p.407.
4. M. Abbate et al., Phys. Rev. B42, 7914 (1990).
5. W. Weber, Z. Phys. B70, 323 (1988).
6. D.L. Cox et al., Phys. Rev. Lett. 62, 2188 (1989).
7. J. Röhler and A. Larich, to be published in Proc. International Winterschool on Electronic Properties of High Temperature Superconductors (Kirchberg, 1990).

Na K-edge XANES Studies on Structure of Sodium Catalyst for Coal Gasification

Hiromi Yamashita,* Satohiro Yoshida+ and Akira Tomita*

*Chemical Research Institute of Non-Aqueous Solutions, Tohoku University, Katahira, Sendai 980, Japan

+Department of Hydrocarbon Chemistry, Faculty of Engineering, Kyoto University, Kyoto 606, Japan

In order to clarify the local structure of sodium catalyst for steam-gasification of brown coal, Na-loaded coals prepared by various methods and their heat-treated chars have been examined by X-ray absorption near edge structure (XANES) using soft X-ray with EXAFS fasilities at BL-7A. The chemical form of sodium species in the Na-loaded samples prepared by the ion-exchange with NaCl was almost the same as that prepared by the impregnation with Na_2CO_3 at all temperatures examined. Na species are atomically dispersed with disordered local structure in the coal and in the char heat-treated at 350°C. Upon the heat-treatment at 550°C, Na species aggregated to form fine Na_2CO_3 particles which are likely active species for the steam gasification. On the other hand, crystalline NaCl particles were observed in the NaCl-impregnated coal and the aggregation of NaCl took place upon heat-treatment. A low catalytic activity of this species can be attributed to this strong affinity between Na ion and Cl ion.

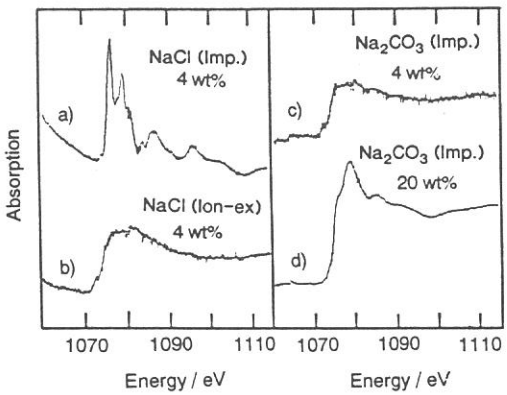

Fig. 1. XANES spectra of the dried coals.

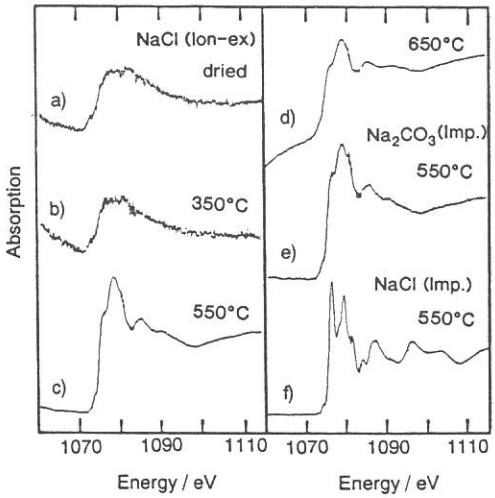

Fig. 2. XANES spectra of Na-loaded samples heated at various temperatures. Samples (a-d) ion-exchanged with NaCl, (e) impregnated with Na_2CO_3 and (f) impregnated with NaCl.

K-Absorption Spectrum of Solid Argon

Atsunari HIRAYA, Kazutoshi FUKUI[†], Poh-Kun TSENG[††], Takatoshi MURATA[†††] and Makoto WATANABE

Institute for Molecular Science, Myodaiji, Okazaki 444
[†]Department of Electrical and Electronics Engineering, Fukui University, Fukui 910
[††]Department of Physics, National Taiwan University, Taipei 10764, Taiwan
[†††]Department of Physics, Kyoto University of Education, Kyoto 612

The absorption spectra of solid and gaseous argon were measured in the 3000 - 4200 eV region at BL7A equipped with a double crystal monochromator. A pair of germanium crystals were used for this energy range. For the measurement of solid argon a He cryostat with a refrigerator was installed in the vacuum chamber. Solid argon was deposited on an Al foil (0.8 μm). A gas cell with organic-polymer windows was used for gas phase experiments.

Figure 1 shows the absorption spectra of solid and gaseous argon in the photon energy region of 3205 - 3215 eV. Only one peak is observed in gaseous argon at 3208.7 eV which correspond to the 1s→4p transition. From the observed (1.85 eV) and the known natural band width (0.58 eV),[1] the instrumental band width was estimated to be 1.27 eV. In solid argon the first peak was observed at 3210.2 eV with 1.5 eV shift toward high energy from the gaseous argon. Taking into account the instrumental band width, natural band width in solid argon was estimated to be 1.51 eV which is 2.6 times wider than in gaseous argon. Figure 2 shows the absorption spectrum of solid argon in 3000 - 4200 eV region. XANES is observed below 3400 eV.

1) L.G. Parratt, Phys. Rev. **56**, 295 (1939).

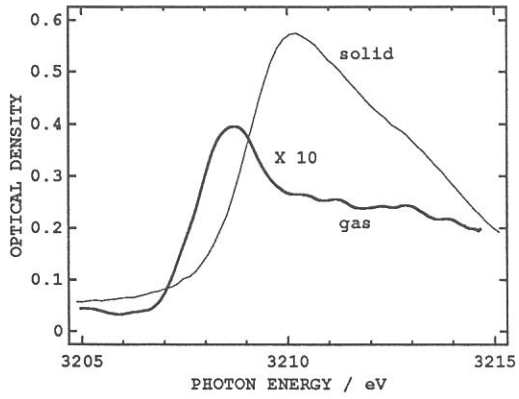

Figure 1. *K*-absorption spectra of solid and gaseous Ar. Deposition temperature was 32.9 K. Ar gas pressure was 1024 mTorr.

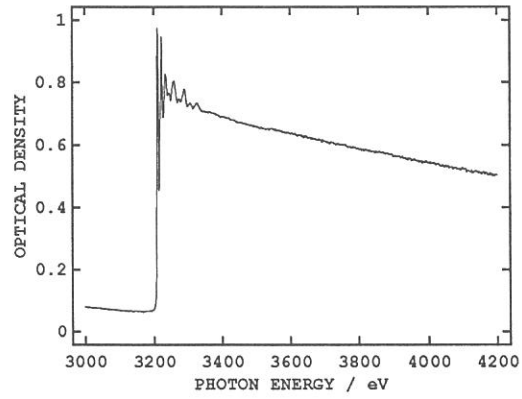

Figure 2. *K*-absorption spectrum of solid Ar in 3000 - 4200 eV region. Deposition temperature was 32.3 K.

THE HYSTERESIS IN THE PRESSURE DEPENDENCE OF THE PHONON ENERGY OF KBr IN THE B1-B2 PHASE TRANSITION

Takao NANBA and Makoto WATANABE*

Department of Physics, Faculty of Science, Kobe University, Kobe 657

*Institute for Molecular Science, Myodaiji, Okazaki 444

Alkali halides with crystal structure of rock salt undergo a well known B1 phase (rock salt) - B2 phase (cesium chloride) transition under high pressure as depicted in Fig. 1, which is reversible. The purpose of the present experiment is to observe the hysteresis in the pressure dependence of the energy of the TO (transverse optic) phonon of KBr. Hysteresis means that the pressure of the transition from the B1 to B2 phases is different from that from the B2 to B1 phases.

Using the transmission measurement system under high pressure in the far infrared region at the beamline BL6A1[1], we measured the change in the optic phonon spectrum of evaporated film of KBr with pressure at room temperature. The pressure up to 5.5 GPa was obtained by using a diamond anvil cell. The pressure was determined within the accuracy of ± 0.05 GPa by measuring the energy shift of the fluorescence R1 line of a ruby chip which was immersed together with a specimen in liquid paraffin which served as the pressure transmitting material.

Fig. 2 shows the plot of the energies of the TO phonon of KBr observed in the transmission spectrum as the function of the pressure. The open circles correspond to the data in the pressure increasing process and the closed circles to the data in the

pressure-decreasing process. In the increasing process, the phase change from the B1 to B2 was found to occur at 1.8 GPa where we can see clearly the sudden decrease of the phonon energy. At both phases of B1 and B2, the phonon energy increases linearly with the increase in the pressure. In the decreasing process, on the other hand, the phonon energy decreases with the decrease in the pressure and jumps at about 1.3 GPa. This sudden jump means the change of the crystal structure from the B2 to the B1 phase. From this result, we determined that the amount of the pressure-hysteresis in the B1-B2 phase transition of KBr is about 0.5 GPa.

References

[1] T. Nanba: Rev. Scient. Instrum. 60(7) (1989) 1680.

Fig. 1

B1-B2 phase transition of alkali halide crystal. Open circles present halide ions and closed ones alkali ions.

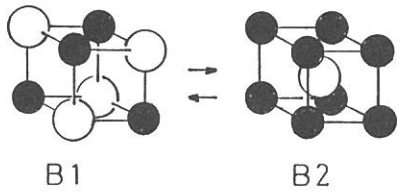

Fig. 2

The observed peak energy of the TO phonon of KBr versus pressure. Broken vertical lines correspond to the pres-sures from the B1 to B2 and the B2 to B1 phases.

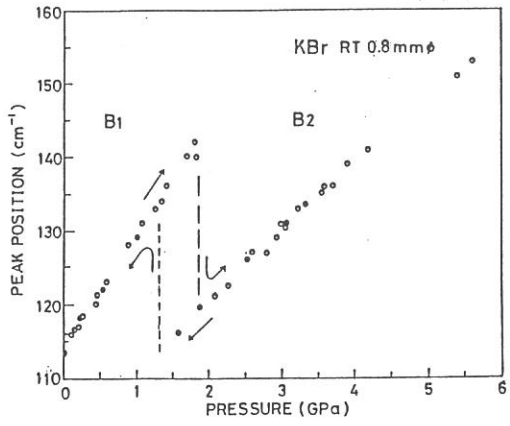

FIR TRANSMISSION SPECTRA OF SmB_6

T. NANBA, H. OHTA, R. TANAKA, M. MOTOKAWA, S. KIMURA*, S. KUNII* and T. KASUYA*

Dep. of Phys., Fac. of Science, Kobe Univ., Kobe 657

**Dep. of Phys., Fac. of Science, Tohoku Univ., Sendai 980*

SmB_6 is one of the valence fluctuating materials and at low temperature shows very small energy gap at the Fermi level due to the strong correlation between conduction electrons (5d) and 4f electrons. The purpose of the present study is to determine the magnitude of the energy gap by measuring the transmission spectrum of SmB_6.

The magnitude of the energy gap was first reported as about 32 cm^{-1} by von Molnar et al [1] and seemed consistent with other experiments like specific heat, point contact, resistivity and so on. Recently , however, the development of the preparation of the highly purified specimen made clear that the experimental results is strongly dependent on the condition of the sample preparation and our spectrum shows one order higher resistivity than that used by von Molnar et al.

Fig. 1 shows the temperature dependence of the transmission spectra of SmB_6 with thickness of 86 μm. We can see that the sample is transparent only below 110 cm-1. This means the magnitude of the gap is about 110 cm-1. As the temperature increases, we can see that a new absorption band appears at about 30 cm-1 and grows in intensity with temperature. At 18 K the gap seems to be nearly smeared out. Considering the data obtained by our

other experiments, specific heat, resistivity and point contact spectroscopy with the high quality specimens, we can assign that the gap energy of 110 cm-1 corresponds to the energy between the 4f-4f transition at the Fermi level. And also we understand that the absorption band which locates at about 30 cm-1 misled von Molnar et al to estimate the magnitude of the gap energy.

References

[1] S. von Molnar et al: Valence Instabilities, eds. by P. Wachter and H. Boppart, North-Holland (1982), p. 389.

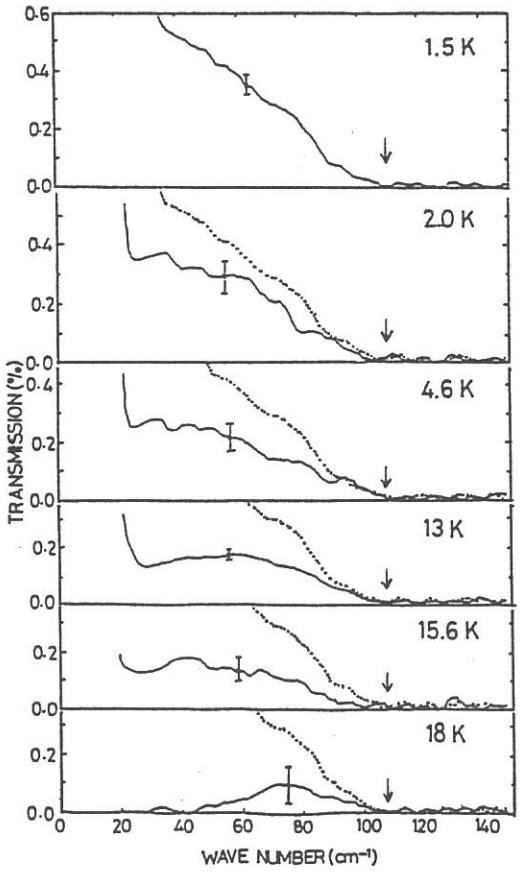

Fig. 1

Temperature dependence of the transmission spectrum of SmB_6. Broken curves shows the spectrum at 1.5 K. The downward arrow indicates the onset of the 4f-4f transition.

Far infrared spectroscopy of hydorogen-bonded ferroelectrics

Shinji SAITO, Shik SHIN, Yuki CHIBA, Mareo ISHIGAME

Research institute for scientific measurements,
Tohoku University, Sendai 980

The central modes have been found in the infrared ,Raman and hyper-Raman spectra of the hydrogen-bonded ferroelectrics KH_2PO_4 (KDP), RbH_2PO_4 (RDP), CsH_2PO_4 (CDP), and $PbHPO_4$ (LHP). In this report, the origin of the central modes are studied by means of infrared(IR) reflectance measurements using synchrotron radiation.

The central modes of CDP and RDP have been investigated from the standpoints of whether they are relaxational modes or overdamped modes by infrared, Raman, and hyper-Raman spectra. However, in infrared spectroscopy, the observation of central mode is very difficult, because there has been no suitable light source in the far-IR region. Far-IR spectroscopy by synchrotron radiation is thought to be very powerful for [1]
(1) continuous low frequency measurements with polarized light (because it is polarized in horizontal plain),and
(2) the reflection measurements on small sample (because of its high brightness).

The far-IR spectra of CDP and RDP were measured by using the beam-line BL6A in the frequency region from 5 to 250 cm^{-1}.

Figure 1 shows the temperature dependence of the reflectivity spectra of CDP. Spectra clearly show the central mode below 50 cm^{-1} in high temperature phase and below 30 cm^{-1} in low temperature phase. These spectra are analyzed by factorized form[2]. By this analysis, these modes are found to be overdamped modes, which do not become soft toward Tc (figure 2), in contrast to that of KDP. The origin of the central mode is not well understood at present.

Figure 3 shows the temperature dependence of the reflectivity spectra of RDP. The very strong central mode is clearly seen below 100 cm^{-1}. It has been suggested that the central mode in RDP is assigned to be an A_1 librational mode. However, it is clear that the A_1 livrational mode around 125 cm^{-1} and central mode are observed at the same time. Thus, the central mode is not assigned to be the A_1 librational mode. The origin of the central mode ,however, is not understood.

References

1). T.Nanba, Y.Urashima, M.Ikezawa, M.Watanabe, E.Nakamura, K.Fukui and H.Inokuchi : Int.J.Infrared and Millimeter Waves 7 1769 (1988).
2). Patrick Simon, Francois Gervais and Eric Courtens : Phys.Rev.B 37 1969 (1988).

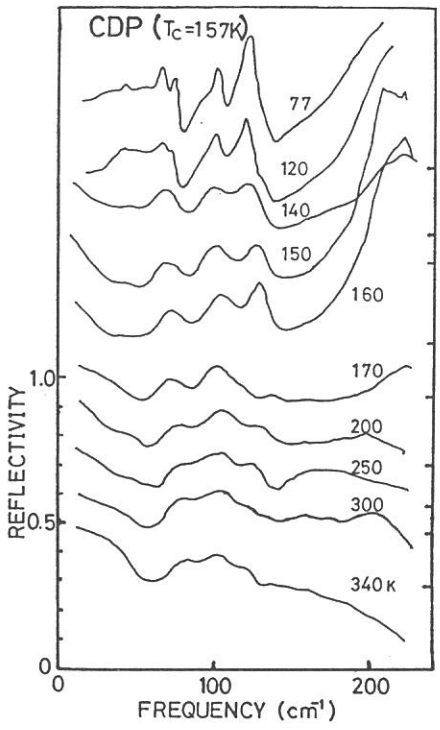

Fig. 1 The temperature dependence of the reflectance spectra of CDP.

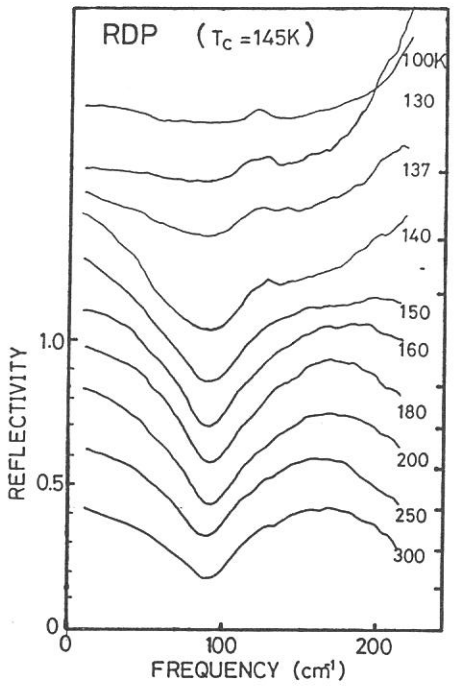

Fig. 3 The temperature dependence of the reflectance spectra of RDP.

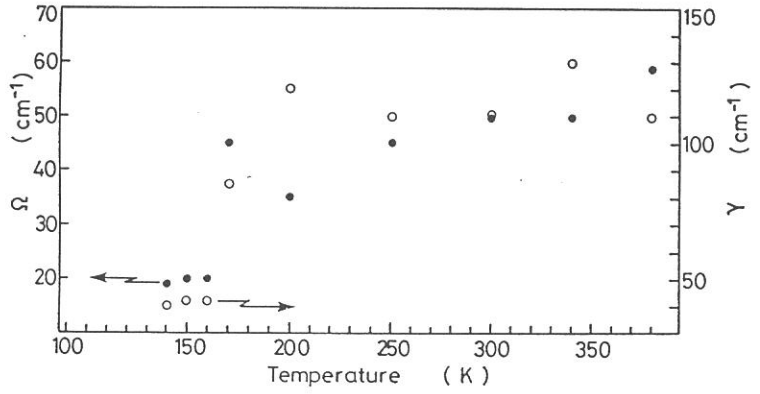

Fig. 2 The temperature dependence of frequency and FWHM of the overdamped mode of CDP.

MILLIMETER WAVE SPECTROSCOPY OF SUPERIONIC CONDUCTORS

Teruyoshi AWANO, Takao NANBA* and Mikihiko IKEZAWA**

Department of Applied physics, Tohoku Gakuin University, Tagajo 985
* Department of physics, Kobe University, Kobe 657
** Research Institute for Scientific Measurements, Tohoku University, Sendai 980

Alkali silver iodide super ionic conductors MAg_4I_5 ($M=Rb,K,NH_4$) have the high ionic conductivity at temperature above 122 K ($RbAg_4I_5$), 139 K (KAg_4I_5) or 135 K($NH_4Ag_4I_5$).[1]

An absorption band which is caused by diffusive motion of Ag^+ ions is expected to appear in a spectral region of several wave numbers. But millimeter wave absorption spectra of these crystals and their temperature dependence have not been studied in detail because of experimental difficulties.[2]

We have measured reflectivity spectra of single crystals of MAg_4I_5 in the spectral region from 3.5 to 200 cm^{-1} at temperatures between 15 K and 470 K. Optical constants were calculated by the Kramers-Kronig analysis.

Fig. 1 shows dielectric constants of $NH_4Ag_4I_5$. These spectra are similar to those of $RbAg_4I_5$ and KAg_4I_5. About 70 absorption bands were observed at 15 K. At 300 K, increase of ε_2 toward low energy side was observed in the spectral region below 30 cm^{-1}. This absorption structure disappeared at low temperatures and seems to be due to the diffusive motion of Ag^+ ions.

Energy loss function spectra of $RbAg_4I_5$ in this spectral region at temperatures of superionic phase are shown in fig. 2. A structure near 18 cm^{-1} seems to be due to attempt vibrations of Ag^+ ions in each iodine cage. Shoulder peaks were observed near 8 cm^{-1} in each spectrum. These peaks are possibly interpreted as being due to ionic plasmon. A curve calculated from the Drude model is in agreement with the experimental curve at 420 K in the spectral region below 10 cm^{-1}. The plasma frequency and the damping frequency increase when the temperature decrease. The large value of the damping frequency seems to be due to strong scattering of Ag^+ ions by potential barriers.

References
1) B.B.Owens and G.R.Argue: Science 157, 308 (1967)
2) K. Funke and R.Hoppe: Solid State Ionics 40/41, 200 (1990)

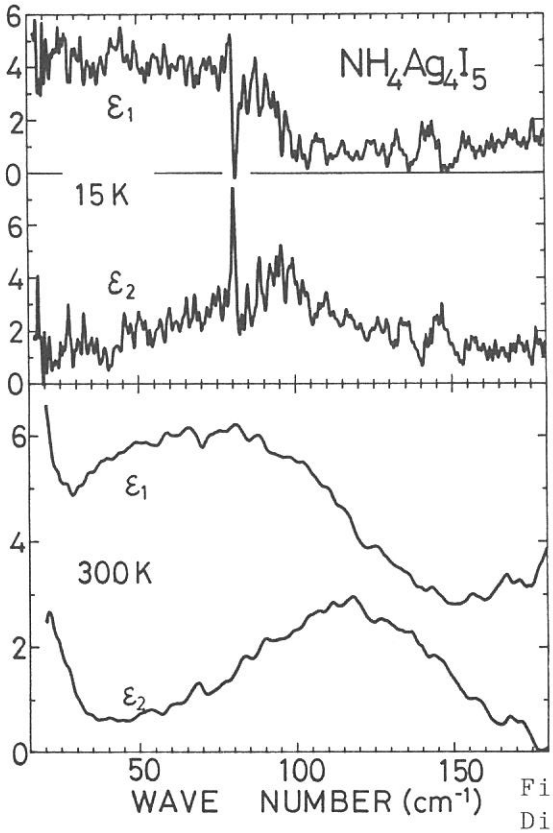

Fig. 1
Dielectric constants of $NH_4Ag_4I_5$ at 15 K (upper) and 300 K (lower).

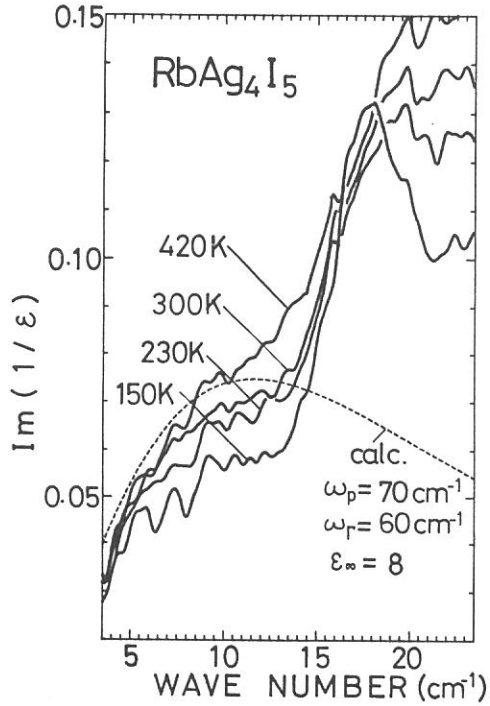

Fig. 2
Energy loss function spectra of $RbAg_4I_5$ (solid line) and a calculated curve from the Drude model (dashed line, plasma frequency ω_p = 70 cm^{-1}, damping frequency ω_r = 60 cm^{-1}, ε_∞ = 8)

Effect of pressure on the far-infrared collision-induced absorption of liquid CS_2 and CCl_4

Yoshitaka FUJITA and Shun-ichi IKAWA

Department of Chemistry, Faculty of Science, Hokkaido University, Sapporo 060

Far-infrared absorption of non-polar liquids is caused by the dipole moments transiently induced during molecular collisions. Effect of pressure on these collision induced absorption is expected to provide a clue to the intermolecular interactions. Previously, we measured the far-infrared absorption bands of liquid carbon disulfide and carbon tetrachloride at pressures from 1 bar to 1.8 kbar, and analyzed the effect of pressure on the spectral moments of the bands.[1,2] However, absorption intensities at frequencies below 20 cm^{-1} had large uncertainty owing to the limit of the sensitivity of a Ge bolometer detector used. The intensities at this low frequency region are particularly important to the calculation of the zeroth moments. The purpose of the present experiments is, therefore, to reduce the uncertainty of the intensities in the low frequency region as largely as possible by use of a InSb detector. Using the same pressure cell as used before[1,2], we have obtained fairly reliable intensities in the 8-50 cm^{-1} range. These parts of the absorption bands were joined to the intensities at the higher frequencies, which were measured previously with the Ge bolometer, and the resulting composite bands are shown in Fig. 1. The absorption profiles at frequencies below 20 cm^{-1} are approximately independent of the pressure. The zeroth and the second moments of the bands were obtained by the same procedure as before[2], and are plotted against the pressure in Fig. 2. The pressure dependence of the zeroth moments of CCl_4 is significantly less than that of CS_2. This difference in the pressure dependence is probably due to the difference in the local structure between the two liquids. The dashed lines in Fig. 2 show theoretical moments calculated on the basis of a theory of the multipole-induced absorption[3] by use of an analytical expression for the radial distribution functions of Lennard-Jones fluids. Contributions of the two and three body terms to the moments are also shown in the figure. Discrepancies between the experimental and calculated moments

suggest that both the L-J potential and the superposition approximation of the three body distrbution function used are not satisfactory to represent the local structure of the liquids. However, possibility of contribution of other induction mechanisms to the discrepancies can not be excluded at present. It is also shown in Fig. 2 that the three body terms are always negative and cancel the two body terms to a considerable extent. This cancellation effect indicates the importance of the multibody effect on the collision-induced absorption in the liquid phase.

References

1) Y. Fujita, T. Ohba and S. Ikawa, UVSOR Activity Report 1988,p122.

2) Y. Fujita and S. Ikawa, UVSOR Activity Report 1989, p100.

3) C.G. Joslin, S. Singh and C.G. Gray, Mol. Phys., 55, 1075 (1985).

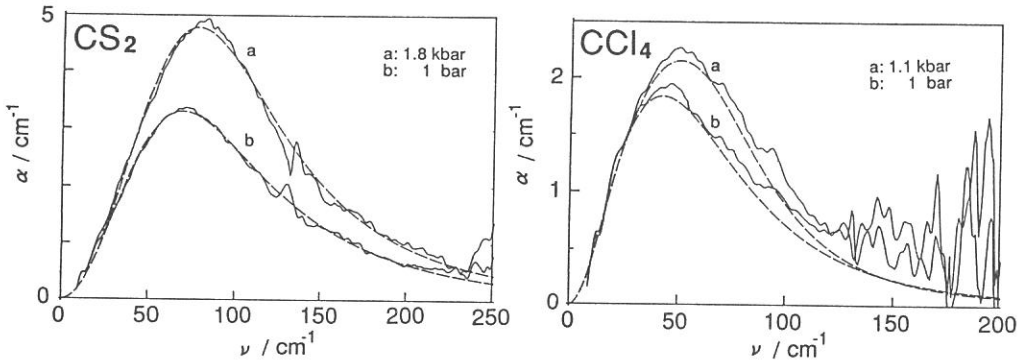

Fig. 1 Effect of pressure on the far-infrared spectra of liquid CS_2 and CCl_4.

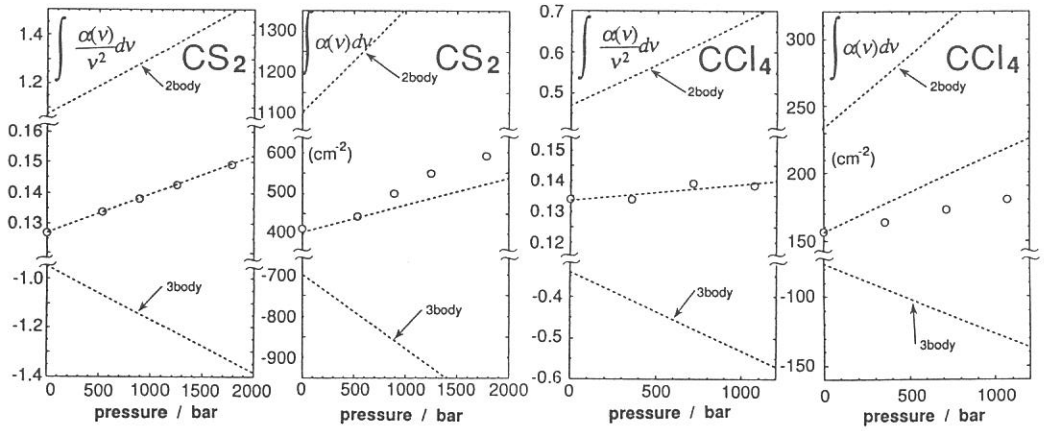

Fig. 2 Pressure dependence of the zeroth and second spectral moments of liquid CS_2 and CCl_4.

FAR-INFRARED STUDY OF FERROELECTRIC PHASE TRANSITION IN $Li_2Ge_7O_{15}$

Mitsuo WADA

Department of Physics, Faculty of Liberal Arts,
Shinshu University, Asahi, Matsumoto 390

In some ferroelectrics the critical slowing down of the dielectric constant has been observed as well as the soft phonon mode. In order to interpret the dynamics of this kind of phase transition, the following two models should be proposed: A) There is only one phonon which concerns the transition. As transition temperature is approached, the soft phonon becomes overdamped and then in the vicinity of T_c becomes a pseudo-relaxational mode. B) There exists a relaxational mode as well as the soft phonon. Firstly, the frequency of the phonon decreases as T_c is approached, by the coupling effect with the soft phonon the relaxational mode becomes soft near T_c.

Ferroelectrics lithium heptagermanate $Li_2Ge_7O_{15}$ (abbreviated to LGO) undergoes the phase transition such as mentioned above at T_c=283.5K[1]. The space group in paraelectric phase belongs to D_{2h}^{14}-Pbcn and that in the ferroelectric phase to C_{2v}^{5}-$Pbc2_1$ with the spontaneous polarization along the c-axis. The size of the unit cell does not change at the transition (Z=4), so that the soft mode should locate at Brillouin zone center. From the symmetry consideration of the space group, the soft mode should be both infrared and Raman active in the ferroelectric phase, whereas it should be infrared active and Raman inactive in the paraelectric phase[2-3].

The far-infrared measurements have been performed to investigate the mechanism of the phase transition in LGO. The transmission spectra in the frequency region to 60 cm^{-1} have been measured at various temperatures around transition point. Fig.1 shows a typical transmission spectrum of LGO at 293K for the orientation corresponding to the B_{1u} mode. The hard phonon mode at 50 cm^{-1} was observed clearly. The soft phonon should be observed in the frequency region below 10 cm^{-1}. Unfortunately, the soft phonon was not observed in the present measurements. However, it is expected that if a high sensitive detector which is available in the long wave region will be used the soft phonon mode must be observed.

References

1) Wada M.,Sawada A.& Ishibashi Y.: J. Phys. Soc. Jpn. 50 (1981) 1811.
2) Wada M. & Ishibashi Y.: J. Phys. Soc. Jpn. 52 (1983) 193.
3) Sawada A., Wada M., Fujita K.,& Toibana H.: Jpn. J. Appl. Phys. 24 (1985) (Suppl.24-2), 534.

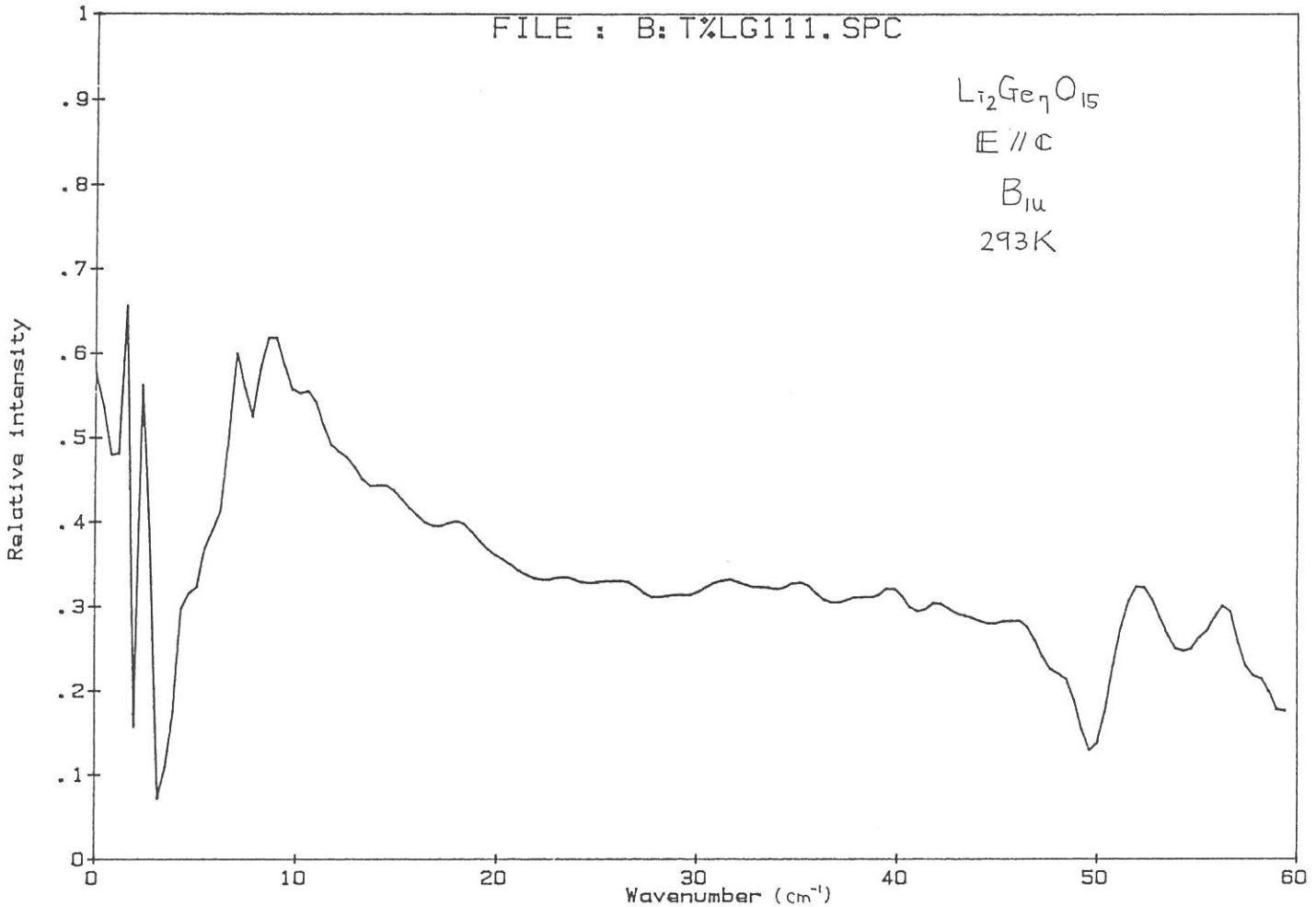
FILE : B:T%LG111.SPC
$Li_2Ge_7O_{15}$
E // c
B_{1u}
293K
Relative intensity
Wavenumber (cm^{-1})
0
.1
.2
.3
.4
.5
.6
.7
.8
.9
1
0
10
20
30
40
50
60

DEFECT-INDUCED FAR-INFRARED ABSORPTION IN DIAMONDS

T.HATTORI, Y.HAMANAKA, Y.NISIDA,* Y.OHONO,* and M.KAMADA§

Faculty of Engineering, Osaka University, Suita, Osaka, 565
* Engineering Science, Osaka University, Toyonaka, Osaka, 560
§ Institute for Molecular Science, Myodaiji, Okazaki, 444

A new far-infrared absorption band at 75.6cm^{-1} has been found first in irradiated and annealed type Ib diamonds with good reproducibility. The purpose is to elucidate the property of this absorption band and its origin. Several crystals of synthetic type Ib diamonds were irradiated by neutron at Kyoto University Research Reactor, and were isochronally annealed at every 200℃ upto 1100℃ for each one hour. Type Ib diamonds were supplied from Sumitomo Electric Industries Ltd., and contains isolated nitrogen impurities at about 100ppm.

Figure 1 shows a typical spectrum of a sample which was annealed at 900℃ after neutron dose, 2.8×10^{18}cm^{-2}. The peak appears at 75.6cm^{-1} and the tail extends towards the higher energy side, which arises from the phonon side band. The full width at half maximum of the main peak is 3.8cm^{-1} at temperatures below 20K. This band is observed only for samples annealed around 900℃ after the heavy dose. In Fig.2, the temperature dependence of this absorption is shown. The absorption is observed even at a high temperature of 77K, but not at room temperature. The peak height is gradually decreased with increasing temperature. These observed features indicate a characteristic of the resonant mode absorption, whose origin is not yet known at present. The absorption was not observed for natural type IaA diamond treated with the same conditions, which

contains nitrogen impurities in a pair form. Therefore the defect responsible for this absorption is probably a complex center including an isolated nitrogen, and exists stably only in the temperature region around 900℃. farther study is now undertaken on correlation between the absorption and other measurements, vsible absorption and ESR, with respect to the annealing temperature.

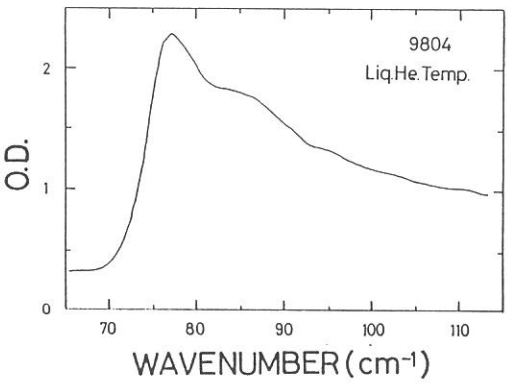

Fig.1 Far-infrared absorption spectrum of type Ib diamond neutron-irradiated followed by annealing at 900℃, observed at liquid helium temperature.

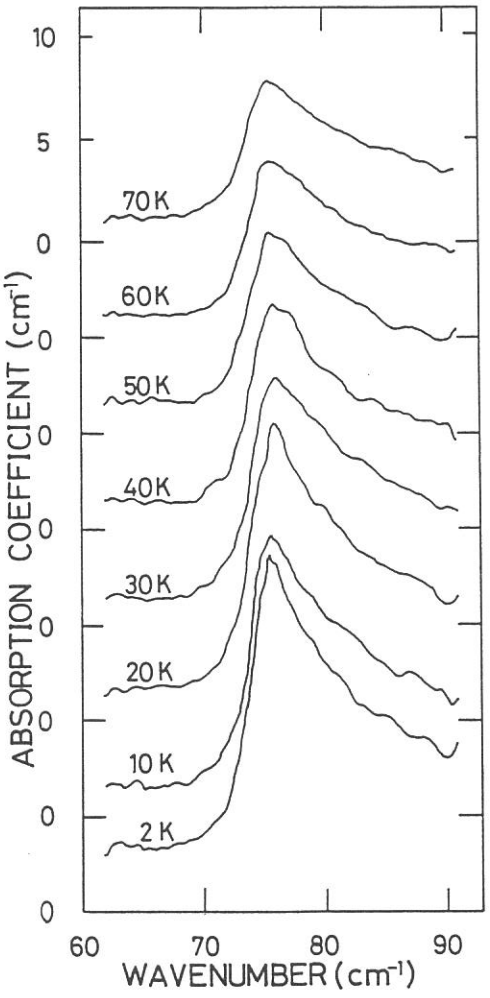

Fig.2 Change in the spectrum with temperature.

STABILITY AND TIME RESOLUTION OF THE TIME CORRELATED SINGLE PHOTON COUNTING SYSTEM IN UVSOR

Tadashi OKADA and Shinya NISHIKAWA

Department of Chemistry, Faculty of Engineering Science, Osaka University, Toyonaka, Osaka 560

In the course of studies on the mechanisms of energy transfer from a excited state of liquid alkane to a solute aromatic molecule, we have obtained some characteristics for the time correlated emission measurements system in UVSOR facility. We believe that these characteristics would be useful as a typical standard for some users who wish to analyze emission time profiles by using UVSOR as a pulsed light source.

The system shown in Fig. 1 was used at BL-1B and BL-7B.

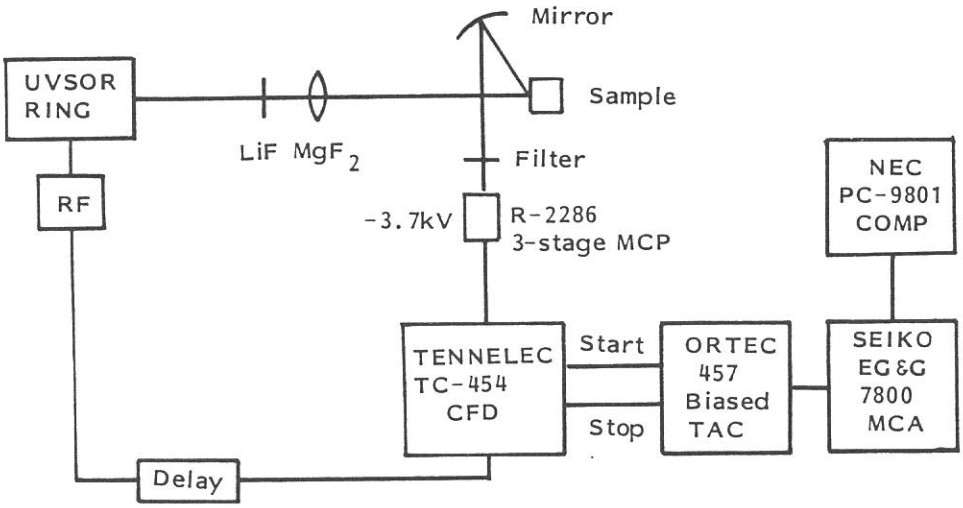

Fig. 1. Block diagram of the time correlated single photon counting system.

Typical time profiles of the exciting light pulse are indicated in Fig. 2. The bunch lengthening of the beam in the storage ring was reported by H. Yonehara et al. [1)]

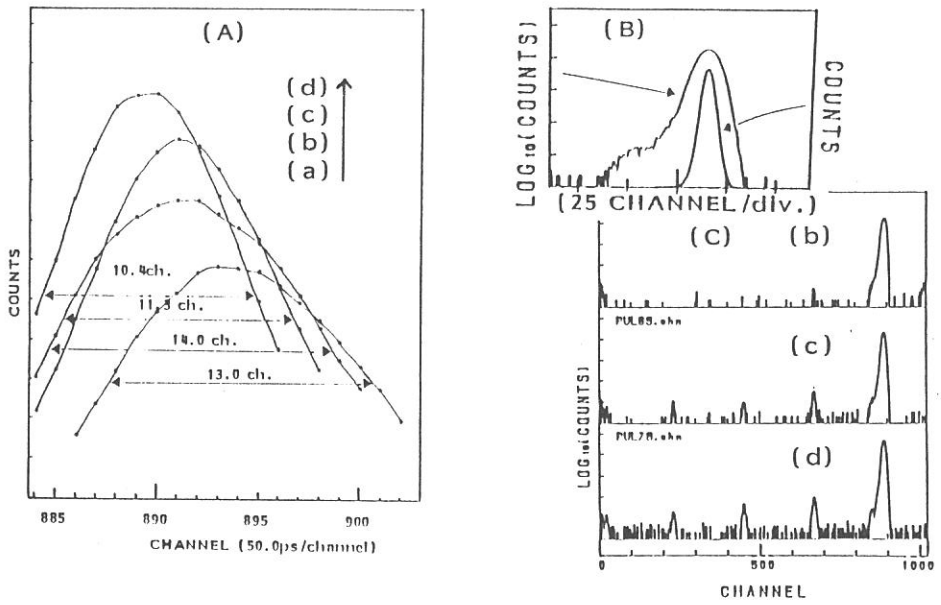

Fig. 2. The time profiles of exciting light pulses measured at BL-1B.
(A) Expanded profiles measured at (a) 9:36, (b) 13:24, (c) 16:15, and (d) 17:55, Sept. 26, 1990.
(B) Logarithmic and linear plots of the pulse (c) in (A).
(C) Full-range profiles indicating a leak of electrons to the following bunches. (b), (c), and(d) correspond to (b), (c) and (d) in (A), respectively.

Obtained results are as follows.

- Time walk for whole system: 50-150 ps/9 hr
- Time resolution with a least square deconvolution analysis for decay time of a single exponential: less than 100 ps. for rise time: 200-300 ps, depends strongly upon the time walk between the exciting pulse and the emission curve and also depends upon a ratio of the photon density of emission and stray light.
- Observed pulse width: 500-700 ps (FWHM) depending on beam current. See Fig. 2(A).
- Application of the system to the measurements of very weak emission.

S/N ratio was improved by accumulation of the signal synchronized with the bunches of SR light pulse. The emission whose quantum yield is as low as 10^{-6} was detected.[2)]

1) H. Yonehara, T. Kasuga, M. Hasumoto, and T. Kinoshita, UVSOR Activity Report, 1988, 5.
2) Y. Inoue, Y. Daino, A. Tai, T. Hakushi, and T. Okada, J. Am. Chem. Soc., 1989, 111, 5584.

LUMINESCENCE PROCESSES IN PARA-TERPHENYL CRYSTALS

K.Uchida, S.Sato, Y.Takahashi* and E.Ishiguro**

Fukui Institute of Technology, Gakuen, Fukui 910

*Aichi Institute of Technology,Yakusa,Toyoda 590-02

**Department of Applied Physics, Faculty of Engineering, Osaka City University, Osaka 558

Para-terphanyl(PTP) molecules consists of three phenyl rings joined by single bond. According to X-ray diffraction studies, the central phenyl rings of PTP molecules rotate between two bottoms of double well potential for the libration of its ring[1]. At low temperature, the ring is in one of the two bottoms and twisted by an angle about 15 - 26 degree from the plane formed by the two outer phenyl rings. Accordingly, we measured the emission spectra and decaytimes in order to clarify the effect of the molecular libration on luminescence processes of PTP crystals.

Fluorescence decay times were measured by the time-correlated single photon counting system under the single bunch peration of UVSOR, using 1 m Seya-Namioka monochromator in BL7B beam line. A vacuum of a cryostat chamber was separated from the beam line by LiF window, since vapor pressure of para-terphenyl crystals is very high.

Figure 1 shows the excitation spectrum of the 370 nm emission from 120 nm to 360 nm at room temperature. This spectrum is very broad and structureless, and similar to the absorption

spectrum of PTP molecules in a solution[2]. Meanwhile, the fluorescence spectra show vibrational structure[3] . Therefore, in the crystalline states, molecules is non-planar in the ground state and in the excited state is planar . Also, since the long wavelength region of the figure 1 overlaps with the emission spectrum of PTP crystals, the emission of PTP is self-absorbed at room temperature.

Figure 2 is the temperature dependence of the fluorescence decay times between 90K and 300 under the 320 nm excitation. At room temperature, the decaytime is about 3 nsec. This temperature dependence is probably due to the reabsorption effect of the emission.

[1] P.J.L.Baudour and H.Cailleau, Acta Cryst. B33(1977)1773

[2] I.B.Berlman J.Phys.Chem. 74(1970)3085

[3] K.Uchida et al. UVSOR ACTIVITY REPORT 1989

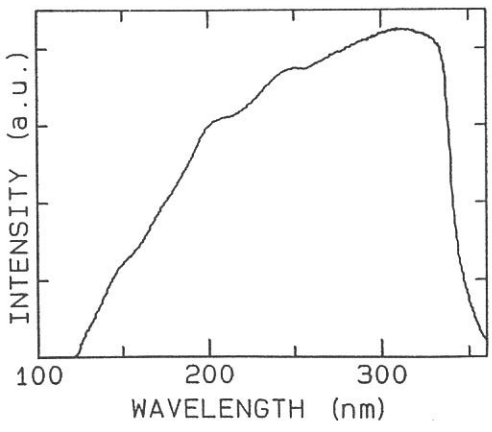

Fig.1 The excitation spectrum of 370 nm emission at R.T..

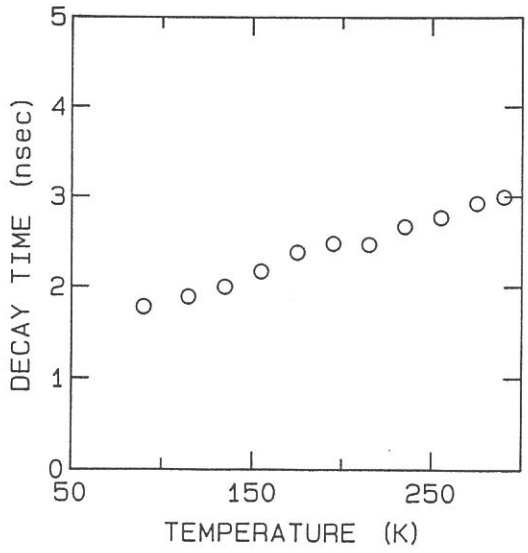

Fig.2 Temperature dependence of of the fluorescence decay times.

DENSITY DEPENDENCE OF STRUCTURE IN PHOTOCONDUCTIVITY EXCITATION SPECTRA OF SUPERCRITICAL XENON DOPED WITH ANTHRACENE

Kazumichi NAKAGAWA, Arisato EJIRI*, and Kazuie KIMURA+

Physics Division, Faculty of Education, Kobe University,
Tsurukabuto, Nada-Ku, Kobe 657, Japan.
*Department of Pure and Applied Sciences, University of Tokyo,
3-8-1 Komaba, Meguro-Ku, Tokyo 153, Japan.
+The Institute of Physical and Chemical Research,
Wako, Saitama 351, Japan.

Recently, photoconductivity excitation spectra of nonpolar fluids doped with anthracene have been extensively studied with a focus on the origin of photocurrent structure. Three groups have suggested different interpretations: (I)due to molecular Rydberg transitions of anthracene converging to the first ionization potential with no energy shift from gas phase values (Holroyd et. al.[1]), (II)due to vibrational states of anthracene ion (Tweeten and Lipsky[2]), and (III)due to second Rydberg states of anthracene with the same energy shift with photoconductivity threshold (Nakagawa et. al.[3]). In this work, we have reinvestigated the photoconductivity excitation spectra of supercritical xenon doped with anthracene in detail and re-examined our previous data where densities of xenon were changed somewhat sporadically.

Experiments were performed at BL1B beam line of UVSOR. We used a new type of photoconductivity cell with parallel plate electrodes with a gap of ~3 mm and MgF_2 windows with 2 mm opening diameter and 4 mm thickness which allow us to measure spectra up to 7.8 eV where strong fundamental absorption of xenon steps up. Monochromatic light with a bandwidth of 0.8 nm from a 1m Seya-Namioka monochromator was used. Obtained spectra at 300 K are shown in Fig. 1. Concentration of anthracene was less than 1 ppm.

Although complete interpretation is not obtained at the present time, we can point out following points:

(1)A strong peak at 7.4 eV and a shoulder at 7.1 eV for xenon density of 2.25×10^{21} cm^{-3} show no significant energy shift; Shift is less than 0.2 eV to lower energy side from 1.55 to 5.40×10^{21} cm^{-3}

(2)At densities higher than 5.0×10^{21} cm^{-3}, strong absorption due to bulk xenon from 6.8 to 7.8 eV, makes photocurrent structure unclear.

(3)For the energy region from 6.4 to 7 eV, it is difficult to pick up each shoulder and to correlate each other. But some of them can be correlated with shoulders reported previously[3].

(4)Spectral shapes for higher densities are different from those reported

in our previous paper[3] where spectra were obtained for the higher anthracene concentration. Low concentration in this work may be a reason of less structure spectra observed here.

At the present time, we have no conclusive idea for the origin of photocurrent structure. Simultaneous measurement of absorption and photocurrent spectra done by HASYLAB group[4,5] may yield a useful information for this problem.

The authors thank to Dr. R. Reininger of HASYLAB for offering UHU adhisive to make MgF_2 windows. This work was supported by by a joint study programm of the Institute for Molecular Science No. 2-A806.

References:[1]R.A.Holroyd, J.M.Preses, E.H.Böttcher and W.F.Schmidt, J. Phys. Chem. 88(1984)744. [2]D.W.Tweeten and S.Lipsky, J.Phys.Chem. 93(1989) 2683. [3]K.Nakagawa, A.Ejiri, M. Nishikawa and K.Kimura, Chem. Phys. Lett. 155(1989)278. [4]A.M.Köhler, V.Saile, R.Reininger and G.L.Findley, Phys. Rev. Lett. 60(1988)2727. [5]R.Reininger, E.Morikawa and V.Saile, Chem.Phys. Lett. 159(1989)276.

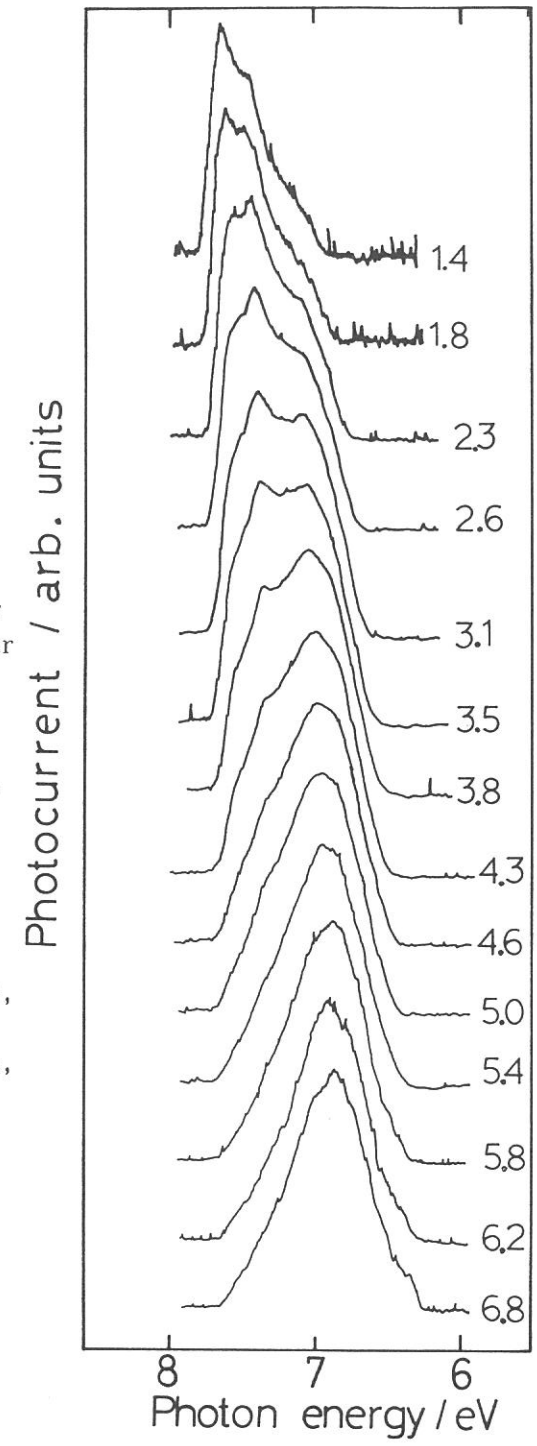

Fig.1. Photocurrent spectra at 300 K of supercritical xenon doped with anthracene. Numbers near each curve show xenon density in the unit of 10^{21} cm^{-3}. Base lines of spectra are shifted each other.

PHOTOIONIZATION QUANTUM YIELD OF TMAE(TETRAKIS-DIMETHYLAMINO-ETHYLENE) DOPED IN XENON SUPERCRITICAL FLUIDS

Kazumichi NAKAGAWA, Kazuie KIMURA*, and Arisato EJIRI+

Physics Division, Faculty of Education, Kobe University, Tsurukabuto, Nada-Ku, Kobe 657
*The Institute of Physical and Chemical Research(RIKEN), Wako, Saitama 351
+Department of Pure and Applied Sciences, University of Tokyo, 3-8-1 Komaba, Meguro-Ku, Tokyo 1

TMAE has attracted some attention of high energy physicist as a sensitizer of particle detectors[1] owing to its very low gas phase ionization potential of ~5.36 eV[2]. In this work we measured photoionization quantum yield of TMAE doped into supercritical xenon as a function of photon energy in an attempt to obtain a basic information for development of a particle detector using the doped rare gas systems.

We used a high pressure photoconductivity cell with parallel plate electrodes with 1.65 mm gap and fused silica windows with opening diameter of 10 mm and thickness of 6 mm. Extra pure TMAE was supplied by Dr. R. A. Holroyd of the Brookhaven National Laboratory. Research grade xenon from Tokyo Kaseihin Co. was used after purification by passing through a silica-gel column activated at 720 K in a vacuum line. Monochromatic light beam from a 1 m Seya-Namioka monochromator with bandwidth of ~0.8 nm was introduced to the photoconductivity cell (see Fig. 1). Magnitude of incident light intensity I_0 and scattered light intensity M by a beam splitter (BS) at each wavelength λ was first measured without rare window (RW) by a calibrated phototube (Hamamatsu R645) and a sodium-salicylate-coated photomultiplier (SS and PMT), and a conversion factor from M to I_0 was calculated. A filter (F) of fused silica was necessary to eliminate short wavelength light and to make a estimation of I_0 from M value possible. After filling the cell by 94 atm xenon at 300K (density ~8 x 10^{21} cm^{-3}) doped with and without TMAE, transmitted light intensity T was measured, and a magnitude of the light absorbed by TMAE was calculated. Value of photocurrent i was simultaneously measured by a Keithley electrometer 617 and values of i, M, T and λ were recorded and manipulated by a NEC computer. A similar measurement was also made for vapor TMAE.

Obtained result is shown in Fig. 2 by a curve B. In the figure, curve A is a quantum yield spectrum reported by Holroyd et. al.[3] and a curve C is an emission spectrum of BaF_2 scintillator reported by Schotanus et. al.[1]. As seen from the figure magnitude of quantum yield of TMAE/Xe system is fairly large when one compares it with vapor values. Two humps observed in vapor spectrum at 6.7 and 7.2 eV seem to shift in xenon by ~1.3

eV to lower energy side, which value of energy shift is comparable with the value ~1.2 eV of shift in ionization threshold of TMAE in xenon from vapor phase[4]. The magnitude of overlap of the emission spectrum of BaF_2 with the quantum yield curve of TMAE is larger for TMAE doped in xenon than that for vapor because of the shift in the photoionization threshold. A large value of electron mobility of xenon may be useful to get a fast and strong signal when this system is applied to a particle detector.

Authors thank to Dr. R. A. Holroyd for his offering of the ultra pure TMAE. This work was supported by a joint study program of the Institute for Molecular Science No. 1-E833.

References:[1]P.Schotanus, C.W.E.van Eijk, R.W.Hollander and J.Pijpelink, IEEE transaction on Nuclear Science, NS-34(1987)272. [2]Y.Nakato, M.Ozaki, and H.Tsubomura, Bull. Chem. Soc. Jpn. 45(1972)1299. [3]R.A.Holroyd, J.M.Preses, L.Woody and R.A.Johnson, Nucl. Instr. and Meth. A261(1987)440. [4]K.Nakagawa, A.Ejiri, K.Kimura and M.Nishikawa, Physica Scripta 41(1990)140.

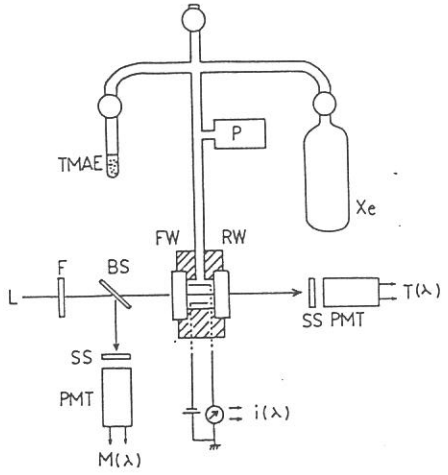

Fig. 1. Schematics of experimental system. Details are in the text.

Fig. 2. Quantum yield curves of TMAE vapor (A) by Holroyd et. al.[3] and of TMAE in xenon (B) obtained in this work, and a emission spectrum of MgF_2 scintillator in arbitraly units by Schotanus et. al.[1].

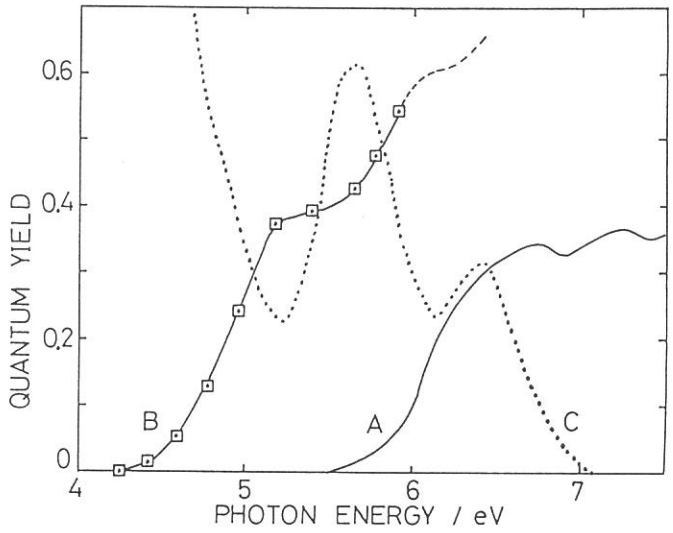

Simultaneous generation of the 7.6eV optical absorption band and F_2 molecule in fluorine doped silica glass under annealing in He

Koichi AWAZU and Hiroshi KAWAZOE
Research Laboratory of Engineering Materials
Tokyo Institute of Technology
Nagatsuta, Midori-ku, Yokohama 227

and
Ken-ichi MUTA
Showa Electric Wire & Cable Co., Ltd.
Minami-Hashimoto, Sagamihara 229

We examined chemical state of fluorine doped silica glasses and its thermal behavior. Samples were prepared with the VAD (vapor phase axial deposition) method. SF_6 gas was used as a source gas of fluorine. Estimated concentration of fluorine was $2.9\times10^{20}cm^{-3}$ (1.3mol%) and $6.2\times10^{20}cm^{-3}$ (2.8mol%), namely FS and FL samples, respectively.

Almost all of the fluorine atoms were found to have the ≡SiF structure with Raman spectroscopy (Fig.1).[1] In the measurements of optical absorption, no absorption in the region of 3-9eV was detected in the glass. When the glasses were annealed in a He atmosphere at 1000°C, absorption bands peaking at 7.6eV (Fig.2) and 4.3eV (Fig.3) appeared. These two bands are attributed to the ≡SiSi≡ structure[2] and to F_2 molecules,[3] respectively. We proposed a thermal decomposition reaction expressed as ≡SiF + FSi≡ → ≡SiSi≡ + F_2. The concentrations of the reaction products, ≡SiSi≡ and F_2, estimated from the absorption cross sections were equal to each other within the errors of measurements.

We also examined the radiation damage with γ-ray (Fig.2). The concentration of E′ center was almost the same for the same dose in silica glasses having different concentrations of FSi≡ and ≡SiSi≡. We suggest that FSi≡ and ≡SiSi≡ were found to be stable for γ-irradiation at room temperature.

References

1. P.Dumas, J.Corset, W.Carvalho, Y.Levy and H.Neuman, J. Non-Crystalline Solids, 47, 239 (1982).
2. U.Itoh, Y.Toyoshima, H.Onuki, N.Washida and T.Ibuki, J. Chem. Phys. 85, 4867 (1986).
3. G.Gibson and N.Bayliss, Phys. Rev. 44, 188 (1933).

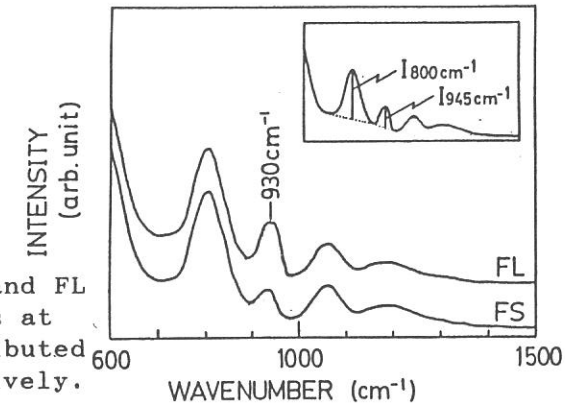

Fig.1 Raman spectrum for FS and FL samples. The scattering peaks at 800cm^{-1} and 945cm^{-1} are attributed as Si-O-Si and Si-F, respectively.

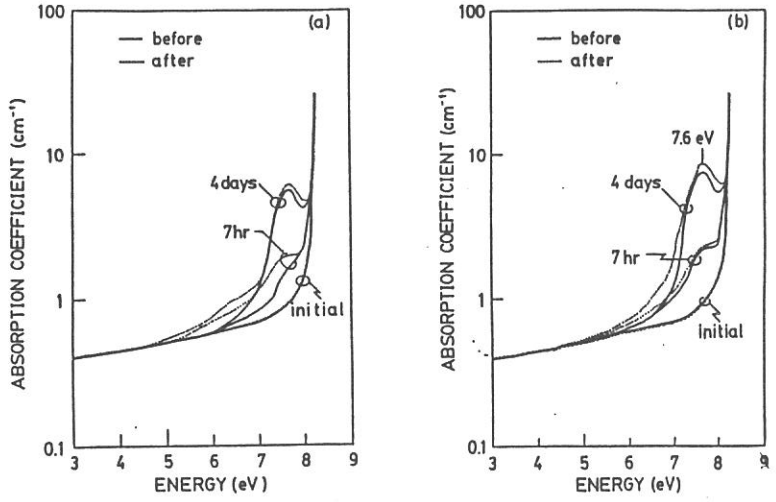

Figs.2 The optical absorption spectra in the region of 3-9eV. The (a) shows the spectrum for FS and the (b) shows that for FL. Solid and dotted lines show them before and after irradiation, respectively. The initial shows the one before annealing and 7hr and 4days show the spectra after annealing at 1000°C in He ambient for 7hr and 4days, respectively.

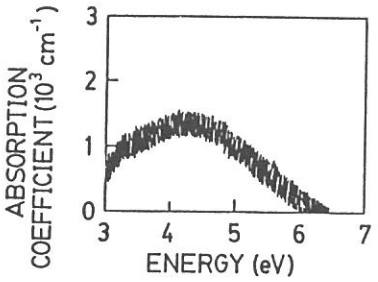

Fig.3 shows the absorption spectrum measured with JASCO SS-25GD for the detection of a weak absorption. The sample had 10mm thickness and annealed in He for 4days at 1000°C.

MAGNETIC FIELD EFFECTS ON THE LUMINESCENCE OF PERYLENE SINGLE CRYSTAL EXCITED WITH VUV RADIATION

Yoshinobu TAKEDA, Ryuzi KATOH, Masataka TSURUTA,
Hiroyuki KOBAYASHI and Masahiro KOTANI

Faculty of Science, Gakushuin University
Mejiro, Tokyo 171

Motivated by the notion that there is no single report on the triplet exciton in perylene crystal, we have started a search for the reason why. A very weak delayed fluorescence could be observed so far by exciting a perylene crystal with a powerful laser diode operating in the 800 nm region, which will be reported elsewhere.

Another approach to study triplet exciton T* is to make use of exciton fission:

$$S^{**} \longrightarrow T^* + T^*,$$

where S** is a higher excited singlet state which can be generated by absorption of a VUV photon. This process is sensitive to the external magnetic field, since the total spin has to be conserved in the process.

A small vacuum chamber was constructed which allows measurements of luminescence from a solid sample, which is positioned between pole pieces of an electromagnet. The sample specimen could be rotated so that anisotropy of the magnetic field effects can be measured. It has been found that the fission of a singlet exciton into two triplet excitons commences at an energy equal to twice that of a triplet exciton and becomes very efficient with

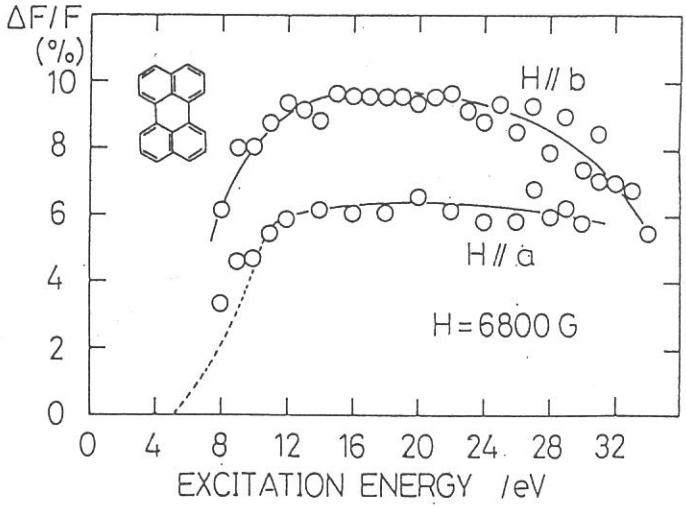

Fig. 1 Luminescence modulation vs. photon energy.

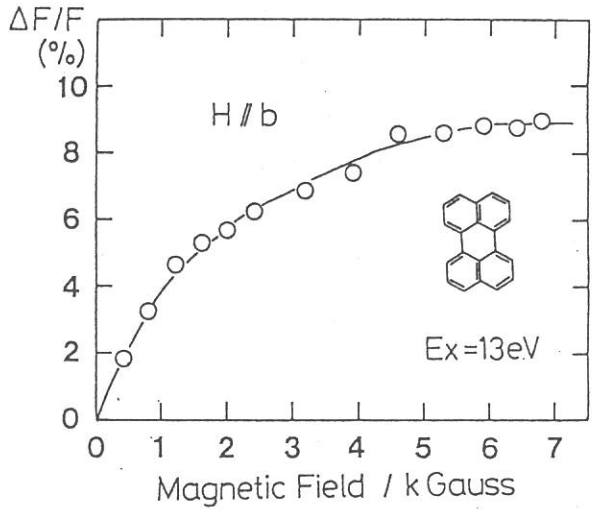

Fig. 2
Luminescence modulation vs. magnetic field strength. Excitation photon energy is 13 eV.

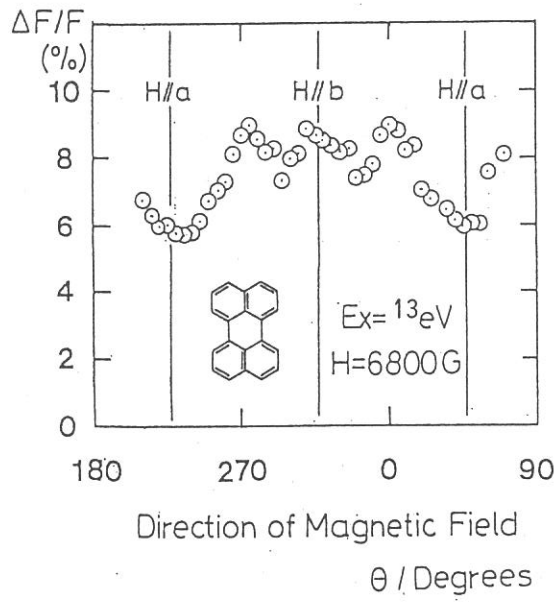

Fig. 3
Anisotropy of the magnetic field effect on the luminescence. The structure reflects the fine structure interaction in the triplet exciton.

excitation energy toward ~13 eV and then flattens. The field strength dependence and the angular dependence of the magnetic field effect could be measured. The very low intensity of the delayed fluorescence seems to be due to the short lifetime of the exciton.

Electronic structures and their anisotropy of polysilanes as investigated by synchrotron radiation spectroscopy

Hiroaki Tachibana ,Yasujiro Kawabata, Shin-ya Koshihara*, Takayoshi Arima*, Yutaka Moritomo*, and Yoshinori Tokura*

National Chemical Laboratory for Industry, Tsukuba, Ibaraki 305, JAPAN
*Department of Physics, University of Tokyo, Tokyo 113, JAPAN.

1.INTRODUCTION

Polysilanes are extended Si-polymers with organo-substituents, in which σ-electrons are considered to be delocalized along the Si-backbones. The σ-electrons on the Si-backbones are responsible for opto-electronic properties characteristic of polysilanes, such as excitonic one-photon and two-photon absorption bands in the near-UV region, sharp photo-luminescence band, photo-conduction and fairly large nonlinear optical properties.

However, detailed features of electronic structures in polysilanes are still to be experimentally investigated. For this purpose, optical spectroscopy on highly oriented samples over the wide photon energy region may be useful, since the polarization-dependent absorption spectra can bring about information on the symmetry and character of relevant electronic states.

Among a variety of polysilanes, investigated in this work was poly(dihexylsilane) (PDHS) which is known to have the all-trans planar zig-zag conformation. To examine the higher-lying exited states arising from the large dispersion of the σ-electron bands, the measurements were extended to the vacuum ultraviolet region (up to ca. 10 eV) by utilizing polarized synchrotron radiation (UV-SOR, IMS). We have prepared highly oriented films of PDHS, which has enabled us to investigate polarization-dependent features of transitions. The experimental results, which are analyzed on the basis of theoretical band structures, indicates large dispersion of σ-electrons.

2. RESULTS AND DISCUSSION

Absorption spectra of PDHS films with the all-trans backbones at 77 K are shown in Fig. 1; (a) for as-cast unoriented thin film and (b) for oriented film prepared by the rubbing method. (Solid and dotted curves in Fig. 1(b) represent the polarized spectra for the light E-vector parallel and perpendicular to the polymer chain direction, respectively.) Four distinct absorption peaks, denoted as F, A, B, and C in Fig.1, were observed below 8 eV, while broad absorption bands showed up in the higher energy region. As clearly seen in Fig.1(b), the four peaks show well polarization-dependent features: The peak F, A, and C are polarized parallel to the chain, while the peak B perpendicular to the chain.

We reproduce in Fig.1(c) the theoretical band structure of unsubstituted all-trans polysilane with D_{2h} symmetry calculated by Takeda and Shiraishi (NTT). Considering the

selection rules for optical transitions between the valence and conduction bands, one may elucidate the anisotropy in the polarized absorption spectra. We assume that the optical absorption is dominated by the electronic transitions at the k=0 (Γ) point. The selection rule for dipole transitions is as follows: The σ_p-σ_p^* transitions are polarized parallel to the polymer chain, while the σ_p-σ_s^*, π-σ_s^* are allowed for perpendicular polarization. Therefore, the observed absorption bands, F, A, and C, with the polarization parallel to the polymer chain should be attributed to the σ_p-σ_p^* transitions. Among these, the band F positions at the lowest energy and hence has been assigned to the σ_p-σ_p^* transition between HOVB and LUCB state. Another σ_p-σ_p^* transition allowed for parallel polarization is expected to be located at ca. 7 eV as indicated by the arrow labeled C in Fig. 1(c). This transition is likely to correspond to the observed absorption peak C around ca. 7.3 eV. The energy separation of the parallel-polarized F and C bands (ca. 3.9 eV) give a measure of the large dispersion width of σ-electron band. As an origin of the peak B showing the polarization perpendicular to the backbone chain, one may consider the lowest σ_p-σ_s^* transition as indicated by the arrow B in Fig. 1(c).

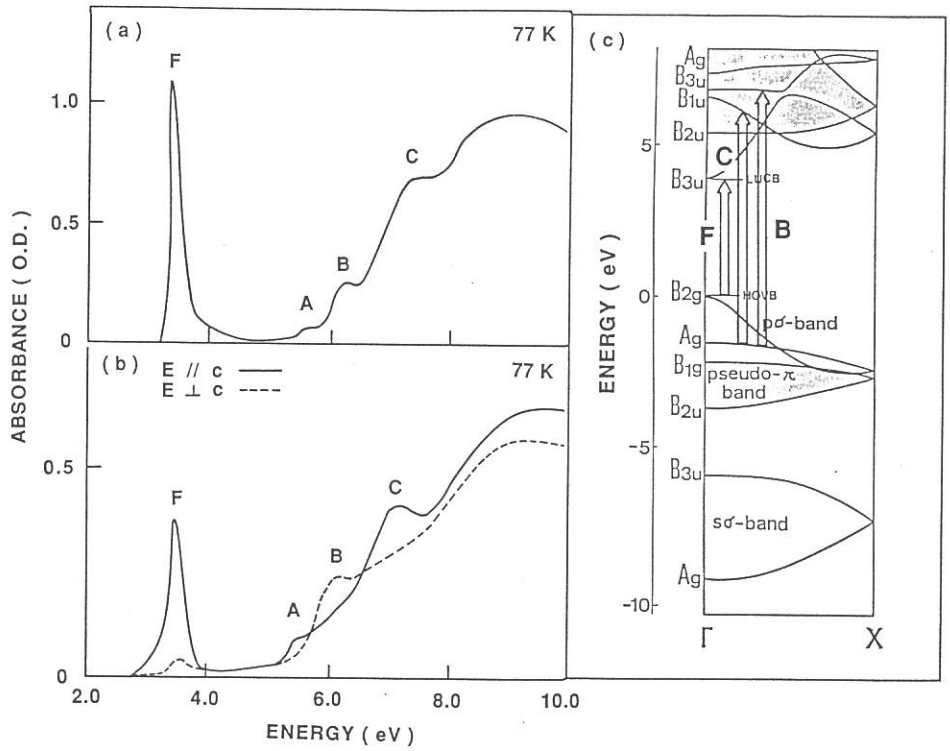

Fig.1. Absorption spectra of polydihexylsilane (PDHS) films; (a) for the as-cast (unoriented) films and (b) for the oriented film with polarizations parallel (a solid line) and perpendicular (a broken line) to the backbone direction, (c) Electronic band-structures for all-trans planar zig-zag polysilane $(SiH_2)_n$.

Optical and Mechanical Properties of Hard Hydrogenated Amorphous Carbon Films Deposited by Plasma CVD

Haruki YOKOYAMA, Masaki OKAMOTO, Toshifumi YAMASAKI, Katsumi TAKAHIRO, and Yukio OSAKA

Department of Electrical Engineering, Hiroshima University, Saijo, Higashihiroshima, Hiroshima 724

Hydrogenated amorphous carbon (a-C:H) films were deposited by plasma chemical vapor deposition from pure CH_4 at a low pressure of the order of 10^{-4} Torr under a magnetic field to confine the plasma on negatively self-biased electrode. The reflectance spectra were measured in a wide range of 0.5-25 eV by using synchrotron radiation and a usual light source. The dielectric constants were determined by applying the Kramers-Kronig relation. Using an effective medium approximation, volume fractions of diamond-like, graphite-like and polymeric (polyethylene) components were derived. The results for the volume fraction v_j of the various components as the function of annealing temperatures are plotted in Fig. 1. It can be seen that the polymeric component is nearly constsnt and the diamond-like and graphaite-like components quickly decrease and increase, respectively, following the 400 °C anneal. Figure 2 shows relationships between the Vicker's hardness and the annealing temperature, where the volume fractions v_d of diamond-like component for various annealing temperatures are also shown. The

Vicker's hardness increase slightly at an annealing temperature of 400 ·C. Following 400 ·C anneal, the Vicker's hardness gradually decrease up to 600 ·C anneal, but the volume fraction v_d of diamond-like component rapidly decrease. This suggests that the contribution of graphite-like component to the hardness of films can not be neglected.

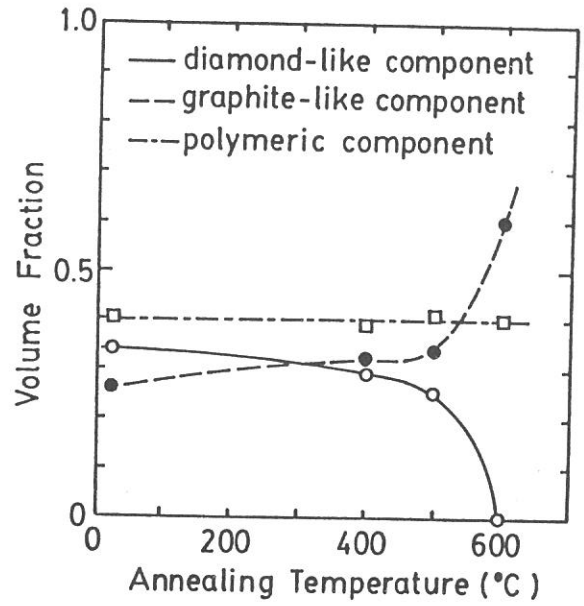

Fig. 1.
The dependence of volume fractions of diamond-like, graphite-like and polymeric components on annealing temperatures.

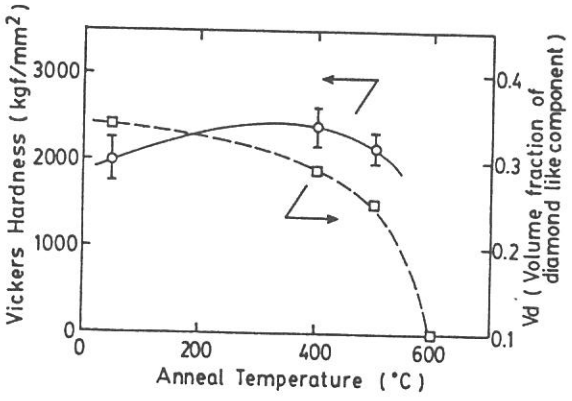

Fig. 2.
The dependence of Vicker's hardness and v_d (volume fraction of diamond-like component) on annealing temperatures.

FLUORESCENCE MICROSPECTROSCOPY OF MUSCLE FIBERS USING SYNCHROTRON RADIATION FROM UVSOR

M. Taniguchi, S. Toyonaga, K. Osada and N. Watanabe
Department of Physics, Faculty of Science, Nagoya University
Chikusa-Ku, Nagoya (Japan)

Sliding theory for muscle contraction postulates that the contractile force is generated by rotational motions of cross-bridges of myosin molecules interacting with F-actin. Therefore, it is important to obtain information concerning the segmental flexibility of interacting domains of myosin cross-bridges and F-actin. We are now able to monitor the rotational motions of tryptophan residues in muscle fibers, because the light source from UVSOR has high intensity in the ultraviolet region . The light pulse under single bunch mode is feasible to measure rotational motions in the nanosecond time range, because the light pulse has very short width with high repetition rate. We described the effects of excitation wavelength on the fluorescence intensity and excited-state lifetime of tryptophan residues in different states of muscle fibers. The fluorescence measurements were carried out at the beam line BL7B. The setup for the fluorescence microspectroscopy was described previously [1]. A bundle of glycerinated muscle from crab Portunus puber was used. The excitation and emission spectra of the fibers were measured during contraction. The excitation spectrum has mainly two bands peaking at 235 nm and 300 nm, when emitted at 330 nm (see Fig. 1). The emission spectrum has a peak at 330 nm, when excited at 280 nm. Fig.2 (A), (B) and (C) show fluorescence decays of the fibers in rigor, relax and contraction solutions, respectively. When excited at 300 nm, the fluorescence decay at 350 nm during contraction was fitted with three exponentials (τ_1 = 0.4 ns, I_1 =35 %, τ_2 = 3.1 ns, I_2 = 59 %, τ_3 = 7.0 ns, I_3 = 5 %). When excited at 280 nm, the decay was two exponentials (τ_1 = 0.4 ns, I_1 = 98 %, τ_3 = 7.0 ns, I_3 = 2 %). The observed changes of fluorescence spectra and lifetimes suggest that the structural and functional interactions between the cross-bridges of myosin and F-actin significantly correlate with local conformational changes in the subnanosecond time range.

The authors thank Prof. M. Watanabe and Prof. M. Kamada for the help and encouragements. We are very grateful to Mr. K. Sakai, Mr. O. Matudo, Mr. J. Yamazaki, Mr. E. Nakamura and the staffs of the Institute for Molecular Sciences for technical assistance.

1. M. Taniguchi, S. Toyonaga, K. Osada & N. Watanabe, "2nd Europ.Conf. Prog. in X-Ray Synchrotron Radiation Research, 25, 999 (1990)

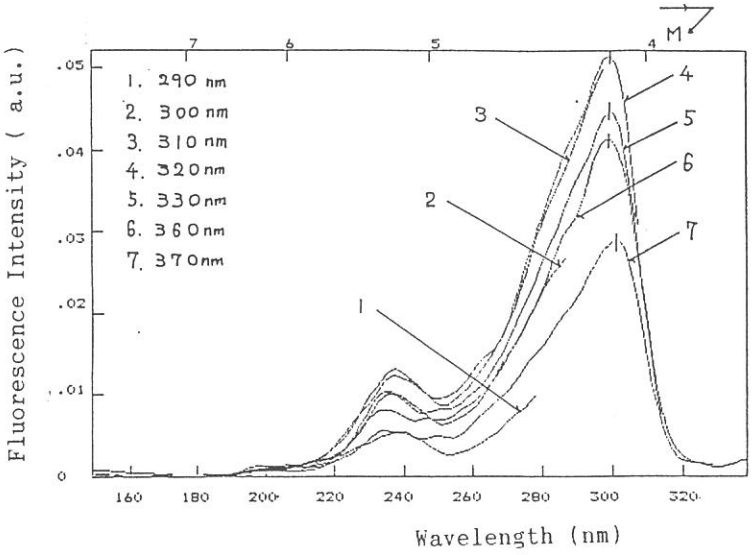

Fig. 1 (A) Excitation spectra of contracting muscle with emission at 340 nm. Emission wavelengths were shown in figure.

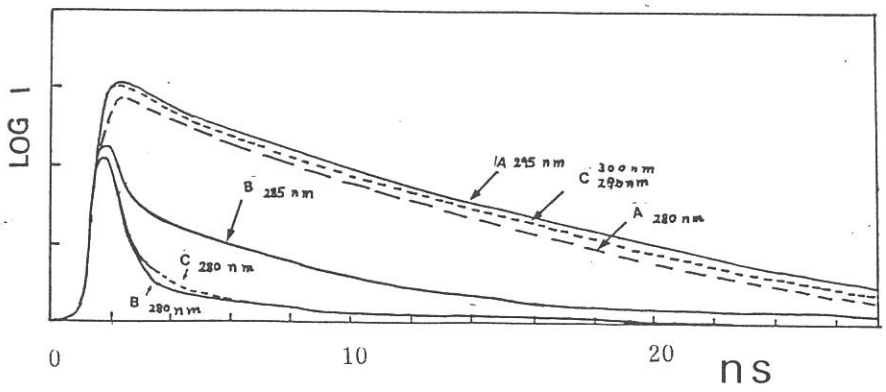

Fig. 2. Decay curves of the fibers at the emission wavelength of 350 nm. The exciting wavelengths are shown in this figure. (A)rigor, (B) relax and (C) contraction.

POLARIZED REFLECTION SPECTRA OF ORTHORHOMBIC $PbBr_2$ CRYSTAL

Masami FUJITA, Hideyuki NAKAGAWA[+], Norio KITAGATA[+], Kazutoshi FUKUI[+], Hiroaki MATSUMOTO[+], Takeshi MIYANAGA[++], and Makoto WATANABE[+++]

Maritime Safety Academy, Wakaba, Kure 737
[+]Department of Electrical and Electronics Engineering, Faculty of Engineering, Fukui University, Fukui 910
[++]Department of Physics, Faculty of Education, Wakayama University, Sakaedani, Wakayama 640
[+++]Institute for Molecular Science, Myodaiji, Okazaki 444

The crystal structure of $PbBr_2$ is orthorhombic $PbCl_2$ structure which belongs to the D_{2h}^{16} space group. The lattice constants are a_0=4.767A, b_0=8.068A and c_0=9.466A. The optical property of the single crystal of $PbBr_2$[1] has not so well been understood as that of the hexagonal PbI_2 crystal.[2,3] In the present study, polarized reflection spectra of $PbBr_2$ single crystal have been measured.

Single crystals of $PbBr_2$ were grown from the melt by the Bridgman method. The crystals were cleavable only in a plane perpendicular to the c-axis.

Figure 1 shows reflection spectra of cleaved surfaces of $PbBr_2$ single crystals at 27 K for polarization parallel to the a-axis (E//a) and b-axis (E//b). Reflection spectrum of PbI_2 crystal is also shown for the sake of comparison. The spectra of $PbBr_2$ show the dichroism due to the anisotropy of the crystal. The structures below 18 eV are attributed to the transitions from the valence band of Pb^{2+} 6s and Br^- 4p states. First exciton band is observed at about 4 eV. As shown in Fig. 2, the exciton band has a single peak for E//a, while it has two peaks for E//b. This result corresponds to the polarization dependence of the first exciton peak of $PbCl_2$ single crystals.[4] A characteristic dip is found at 8.5 eV. The structures around 10 eV are assigned to the transitions from the lower valence band.

At about 20 eV sharp peaks are found. As shown in Fig. 3, five peaks are observed for each polarization. The peaks are attributed to the excitonic transition from Pb^{2+} 5d core level to

6p level. The site symmetry around Pb^{2+} ion is C_s in $PbBr_2$, while it is D_{3d} in PbI_2. In spite of different symmetry around Pb^{2+} ion, spectral feature of $PbBr_2$ is similar to that of PbI_2 crystal as shown in Fig. 3. This indicates that the crystal field effect on the Pb^{2+} 5d core excitons in lead halides is small and the excitons are highly localized.

References

1) V. G. Plekhanov: Phys. Status Solidi B 68(1975)K35

2) J. H. Beaumont, A. J. Bourdillon and J. Bordas: J. Phys. C 10(1977)761.

3) T. Hayashi, K. Toyoda and M. Itoh: J. Phys. Soc. Jpn. 57(1988)18.

4) J. Kanbe, H. Takezoe and R. Onaka: J. Phys. Soc. Jpn. 41(1976)942.

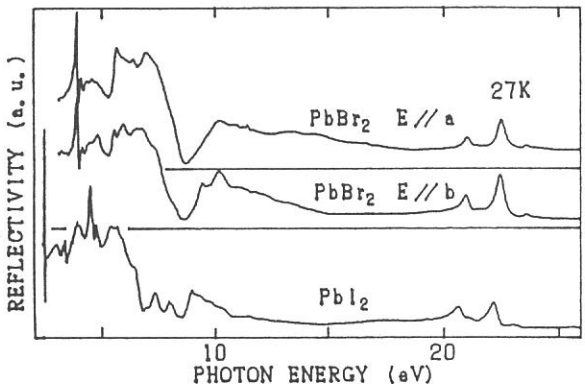

Fig. 1
Reflection spectra of $PbBr_2$ crystal at 27K for polarization E//a and E//b. Reflection spectrum of PbI_2 is also shown.

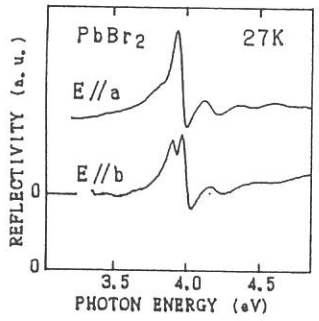

Fig. 2
Reflection spectra of $PbBr_2$ crystal around the first exciton band for E//a and E//b.

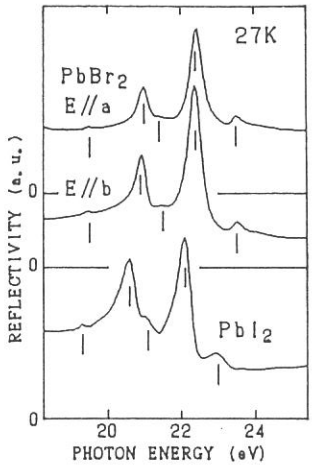

Fig. 3
Reflection spectra of $PbBr_2$ and PbI_2 crystals in the core exciton region.

AUGER-FREE LUMINESCENCE FROM $K_{1-x}Cs_xCl$ AND $Rb_{1-x}Cs_xCl$ MIXED CRYSTALS

Satoshi HASHIMOTO, Shinzou KUBOTA* and Jian-zhi RUAN(GEN)*
Kyoto University of Education, Fushimi-ku, Kyoto 612
* Rikkyo Univsersity, Nishi-Ikebukuro 3, Tokyo 171

The Auger-free luminescence is due to interatomic radiative transition of valence band electrons to outermost-core-hole states in alkali halides in which the band gap energy E_g is larger than the energy difference E_{vc} between the top of the valence band and the outermost-core-hole state.[1] The crystals with the condition of $E_g > E_{vc}$ are referred as type L. If $E_g < E_{vc}$, the interatomic Auger process is dominant (type A).

It is expected that the Auger-free luminescence can be observed in mixed crystals of type A and type L. Study of luminescence from such mixed crystals is important for developing new scintillation materials with nano second life time.

The purpose of this study is to confirm the Auger-free luminescence from $K_{1-x}Cs_xCl$ and $Rb_{1-x}Cs_xCl$ mixed crystals ($0 < x < 0.1$). Here, KCl and RbCl are type A and CsCl is type L. In these crystals, the luminescence would be induced from Cl^- 3p to Cs^+ 5p states, not to K^+ 3p or Rb^+ 4p states.

The experiment was carried out by using a 1-m Seya-Namioka monochromator at BL7B beam line of UVSOR. The experimental set up is similar to that described in Ref. 1. The fast luminescence band of 210 - 320 nm having peaks at 245 and 265 nm is observed in $K_{0.95}Cs_{0.05}Cl$ crystal at room temperature. This spectrum is almost similar to that from pure CsCl.[1] At liquid nitrogen temperature, the fast luminescence of 230 - 360 nm band having peak at 275 nm is observed.

By using 5.632 MHz UVSOR single bunch and by a single-photon counting method, the energy resolved luminescence photon were detected by an MCP photomultiplier. The output pulses from this photomultiplier were used to start a time-to-amplitude converter. The fast luminescence intensity was obtained as output pulses from a single channel analyzer which accepts the pulses corresponding to luminescence decay within 10 nsec for the output pulses from the time-to-amplitude converter. Figure 1 shows a

photo-excitation spectrum for the fast luminescence intensity of 275 nm band from $K_{0.95}Cs_{0.05}Cl$ crystal at liquid nitrogen temperature. The spectrum has the threshold energy of 13.4 ± 0.1 eV, which is slightly smaller than that for pure CsCl(i.e. 14.1 ± 0.2 eV). The luminescence intensity decreases with increasing incident photon energy in the region above ∿ 18 eV, in which K^+ 3p level can be excited. The decay time is measured to be 2 ns for 275 nm luminescence band from $K_{0.95}Cs_{0.05}Cl$ crystal at liquid nitrogen temperature.

The similar results for the luminescence spectra and photo-excitation spectra were observed for $RbCl_{0.999}Cs_{0.001}$, $Rb_{0.995}Cs_{0.005}Cl$ and $Rb_{0.99}Cs_{0.01}Cl$ crystals at room temperature and liquid nitrogen temperature. The decay time is measured to be 2 ns for 275 nm luminescence band from $Rb_{0.995}Cs_{0.005}Cl$ crystal at liquid nitrogen temperature.

In conclusion, present observations strongly suggest the fast luminescence band from mixed crystals of type A and type L is due to Auger-free luminescence.

Reference

1. S.Kubota et al. Phys. Rev. Lett. 60 (1988)239.

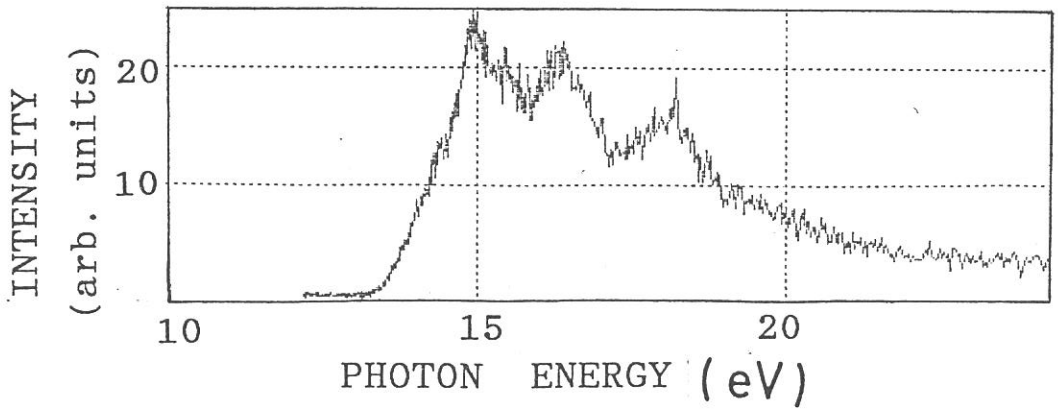

Figure 1. Photo-excitation spectrum for fast luminescence intensity of 2 nsec lifetime for 275 nm band from $K_{0.95}Cs_{0.05}Cl$ crystal at liquid nitrogen temperature.

Characteristics of Self-Trapped Exciton Luminescence in Lithium Halides

Sadao TANAKA, Hideaki Fujita, Koji FUJIWARA, Shunji NAGATA, Masaaki NAKAYAMA, Hitoshi NISHIMURA, Teruo KOMATSU* and Satoshi HASHIMOTO**

Department of Applied Physics, Osaka City University, Sumiyoshi-ku Osaka 558
* Department of Physics, Osaka City University, Sumiyoshi-ku Osaka 558
** Kyoto University of Education, Fushimi-ku Kyoto 612

We have investigated the characteristics of the self-trapped exciton (STE) luminescence in lithium halides. The luminescence spectra are shown in Fig. 1. LiI, LiBr and LiCl show only one STE luminescence band, and LiF two bands. The 3.0 eV band in LiI and 5.4 eV band in LiBr have been assigned to impurities [1,2]. Peak energies E_{STE}, decay times τ and half-widths W_0 of STE luminescence at low temperature, and relaxation energies E_{LR} of STEs in 16 alkali halides are listed together with the 1s exciton energies E_{1s} in Table I. We estimated the relaxation energies from $E_{LR}=(E_{1s}+B-E_{STE})/2$, in which 2B stands for exciton band width.

The STE states in lithium halides are expected to be of on-center type, on account of the small values of the Rabin-Klick (R-K) parameter (Fig. 2) defined by S/D (S is the space between adjacent halogen ions, and D is the diameter of halogen atom) [3]. Considering the large Stokes shift energies and long decay times of the STE luminescence in lithium halides, however, the STE states may be of off-center type similar to the π states in NaCl and KBr rather than of on-center type similar to the σ states in them. The STE luminescence bands of LiI, LiBr and LiCl do not show σ like fast decay component, but show π like slow decay component only, which is different from the STE luminescence consisting of fast and slow components in NaI and NaBr [4]. Two luminescence bands in LiF, in which the value of the R-K parameter is a little larger than those in NaCl and KI, may be σ and π bands, though the ratios of the Stokes shift energies to the 1s exciton energies are larger than those expected (dotted lines in Fig. 2).

Half-widths of STE luminescence bands are much wider in alkali fluorides than in alkali iodides; the width in LiF (1.1 eV) is about 4 times as large as the width in RbI (0.28 eV). Taking exciton-acoustic phonon interaction (the matrix element is V_k) into acount, we write the width as $W(T)^2=8\ln 2 \cdot D(T)^2 = 8\ln 2 \cdot \Sigma V_k^2(2n_k+1)$. The width at low temperature ($n_k=0$) is approximately given by $W_0^2=4\hbar\omega_D \cdot E_{LR}$, where ω_D stands for Debye frequency. The calculated values W_0^{cal} are a little smaller than the values W_0. However, the ratios R of both values are nearly constant 1.4～1.5 for on-center σ bands and for some π bands with small Stokes shift energy (in NaI and NaBr), though for the π bands with large Stokes shift energy (in KBr and RbBr) the ratios deviate from the constant probably because of additional off-center relaxation (Table I). The half-widths are thus explained by using $\hbar\omega_D$ and E_{LR}.

The temperature dependence of the half-widths is given by $W(T) \sim W_0[\coth(\hbar\omega_D/2k_BT)]^{1/2}$. The frequencies of phonons responsible for the luminescence broadening are obtained from the fitting of this formula to the results. The frequencies ω obtained are listed in Table I. For σ bands ω is close to ω_D, while for π bands ω is very smaller than ω_D. Particularly, for the π bands in rubidium halides and alkali fluorides with large values of R-K parameter, we cannot find the frequency because of unfitness of the formula to the results. For the STE luminescence bands in lithium halides, this fitting is capable, but ω is fairly smaller than ω_D (Table I). These results suggest that the STEs in lithium halides are not of on-center type but of off-center type, and that the on-center STE state is unstable in LiI, LiBr and LiCl. This may be caused by a relaxation of anions surrounding the $(\text{halogen})_2^{2-}$.

References: [1] H. Nishimura et al.: J. Phys. Soc. Jpn. 56 (1987) 3715. [2] K. Fujiwara et al.: J. Luminescence 48/49 (1991) 107. [3] H. Rabin et al.: Phys Rev. 117 (1960) 1005. [4] K. Kan'no et al. Rev. Solid State Science 4 (1990) 253.

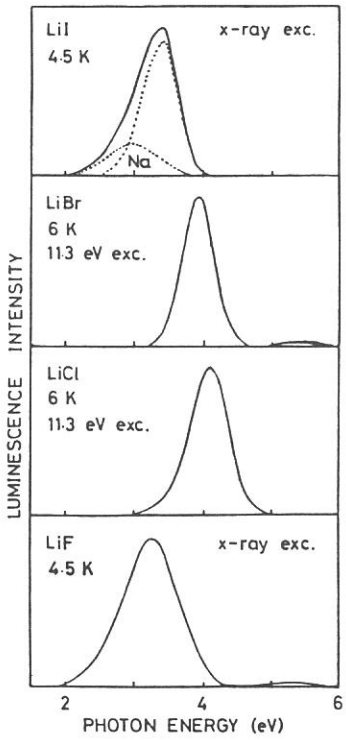

Fig. 1.

Table I.

	E_{1s} (eV)	E_{STE} (eV)		τ (10^{-6}s)	E_{LR} (eV)	W_0 (eV)	W_0^{cal} (eV)	R	ω ($10^{13}s^{-1}$)	ω_D ($10^{13}s^{-1}$)
LiI	5.98	3.4	π	10	1.62	0.46	0.33	1.4	1.31	2.61
LiBr	7.2	3.95	π	4.5	1.87	0.62	0.41	1.5	2.5	3.35
LiCl	8.7	4.1	π	120	2.5	0.76	0.61	1.27	3.51	5.52
LiF	12	5.3		--	3.7	1.1	0.9	1.22	--	9.58
		3.3	π	--	4.7	1.12	1.09	1.03	--	9.58
NaI	5.62	4.2	πσ	0.16	0.88	0.34	0.23	1.5	1.83	2.15
NaBr	6.68	4.6	πσ	0.5	1.21	0.43	0.31	1.41	2.83	2.95
NaCl	7.96	5.34	σ	0.003	1.53	0.61	0.41	1.48	5.26	4.20
		3.35	π	295	2.53	0.62	0.53	1.17	1.26	4.20
NaF	10.7	2.6	π	6700	4.32	0.97	0.85	1.14	--	6.44
KI	5.83	4.1	σ	0.002	0.96	0.3	0.21	1.44	1.81	1.73
		3.3	π	4	1.37	0.32	0.25	1.28	--	1.73
		3.0	E_x	4	1.51	0.31	0.26	1.19	--	1.73
KBr	6.78	4.4	σ	0.003	1.29	0.4	0.27	1.46	1.90	2.28
		2.3	π	130	2.34	0.42	0.37	1.13	--	2.28
KCl	7.65	2.3	π	5000	2.82	0.61	0.48	1.27	--	3.08
KF	9.9	2.7	π	38000	3.78	0.88	0.67	1.30	--	4.40
RbI	5.73	3.9	σ	0.003	1.03	0.28	0.19	1.46	1.60	1.35
		3.0	E_x		1.48	0.30	0.23	1.30	0.58	1.35
		2.3	π	10	1.83	0.30	0.25	1.20	--	1.35
RbBr	6.6	4.1	σ	0.003	1.37	0.38	0.25	1.53	1.72	1.71
		2.1	π	180	2.37	0.34	0.33	1.03	0.5	1.71
RbCl	7.5	2.2	π	5500	2.77	0.51	0.40	1.28	--	2.16
RbF	9.5	3.0	π	--	3.45	0.79	--	--	--	--

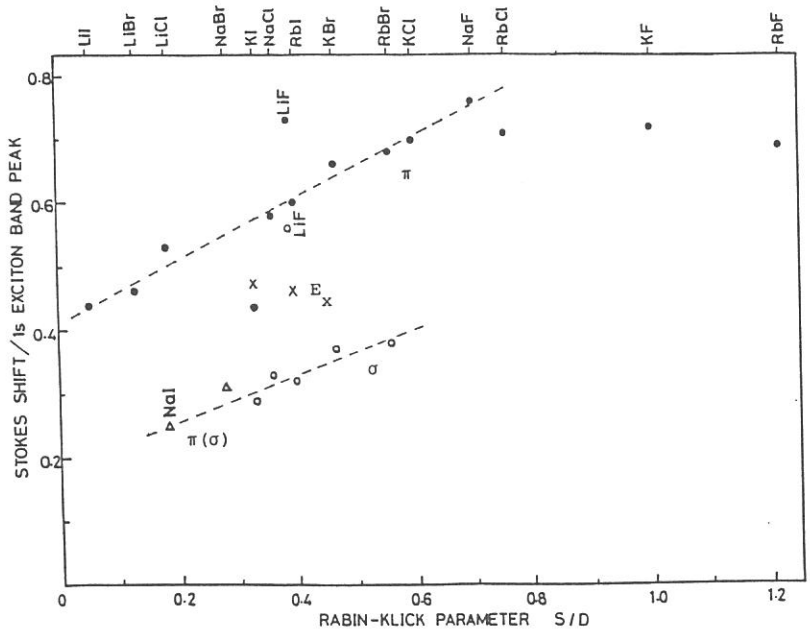

Fig. 2.

RELAXATION OF EXCITONS IN SODIUM IODIDES

M. ITOH, S. HASHIMOTO† and N. OHNO‡

Faculty of Engineering, Shinshu University, Nagano 380

† *Kyoto University of Education, Fushimi-ku, Kyoto 612*

‡ *Faculty of Engineering, Osaka Electro-Communication University, Neyagawa, Osaka 572*

Annihilation of self-trapped excitons (STE) in alkali halides results in broad emission bands with large Stokes shift. According to recent studies,[1–3] the relaxed configuration of the STE is very sensitive to a geometrical factor such as the Rabin-Klick parameter S/D. Among the alkali halides, NaI is a particular material since it exhibits only one emission band (π band) of the STE. Another interesting feature of the STE in NaI comes from recent finding of a fluorescent component with a short lifetime (1.2 ns) in addition to the long-lived phosphorescent component ($\sim$ 100 ns),[4] which reveals that the initial state of the π band in NaI consists of a singlet-triplet pair slightly split by the exchange interaction.

In the present work, we have investigated an effect of dilatational strain on the STE luminescence of NaI by using thin crystals grown inside a narrow gap of the quartz cell at 11 K. The dilatational strain is caused by the large difference in thermal contractions between NaI and quartz; its magnitude increases for thinner samples.

Figure 1 shows luminescence spectra of thin NaI crystals measured under band-to-band excitation at 5.90 eV. As the crystal thickness d decreases, a new luminescence appears around 3.05 eV accompanied by a complementary decrease of the π emission at 4.17 eV. The NaI has $S/D = 0.17$, which is very small value. This suggests that in the matrix of NaI, the V_K core is stable against an axial shift along a <110> direction, leading to the π emission from the STE of on-center type. However, when the lattice constant is expanded with decreasing d, the STE relaxes spontaneously to a new STE configuration from which the 3.05 eV band is emitted. A reasonable candidate for this is a weakly displaced off-center configuration, similarly to the case of NaBr.[3]

The decay profile of the 3.05 eV band was found to consist of a fast component ($\sim$ 6.7 ns) and a slow component ($\geq$ 2 μs), as shown in Fig. 2. These lifetimes are significantly longer than the respective values of the π band. This is probably because the electron-hole overlap becomes smaller for the off-center configuration. The transient behavior of the π emission was not affected by the dilatational strains.

Figure 3 shows excitation spectra for the singlet (open) and triplet (closed) components obtained by a time-resolved analysis of the π emission (4.17 eV) in NaI. It appears that both curves are parallel to each other, except for a small hump around the $n = 2$ exciton band at 5.8 eV. This means that the relaxation path of free excitons into a singlet or triplet STE state does not depend on the exciting photon energy.

1) K.S. Song and C.H. Leung: Rev. Solid State Sci. **4** (1990) 357.

2) K. Kan'no, K. Tanaka and T. Hayashi: Rev. Solid State Sci. **4** (1990) 383.

3) M. Itoh, S. Hashimoto and N. Ohno: J. Phys. Soc. Jpn. **59** (1990) 1881.

4) K. Kan'no, K. Tanaka, H. Kosaka, T. Mukai, Y. Nakai, M. Itoh, T. Miyanaga, K. Fukui and M. Watanabe: Phys. Scr. **41** (1990) 120.

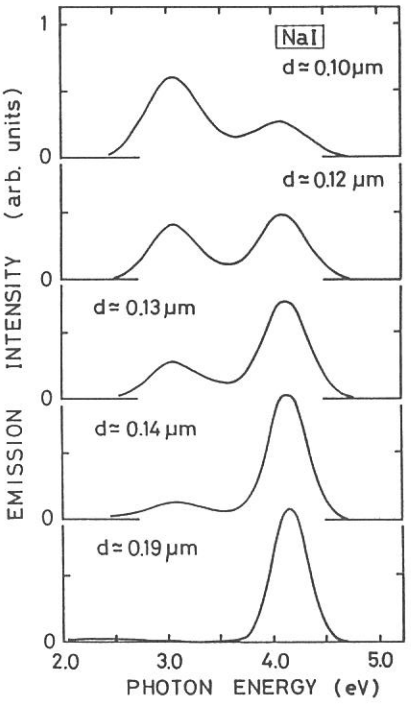

Fig.1

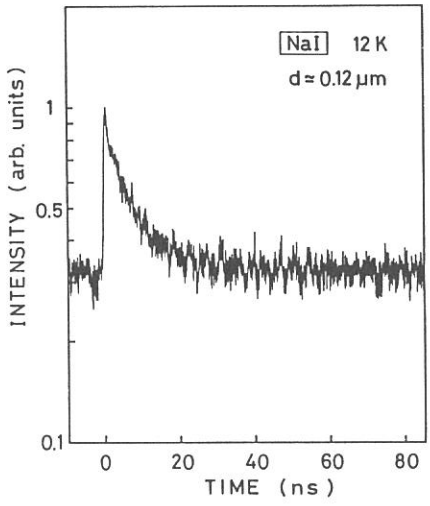

Fig.2

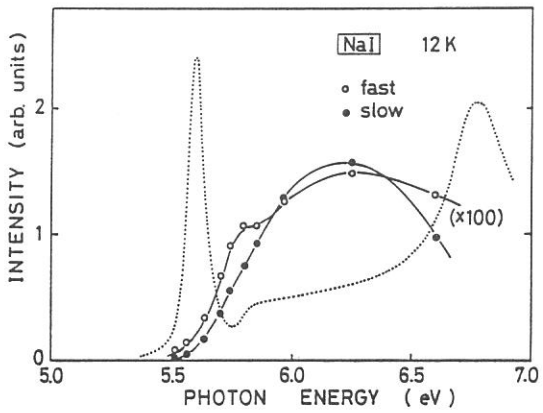

Fig.3

Lifetime Studies on STE-luminescence of Alkali Halide Crystals

Hideyuki NAKAGAWA, Atsushi FUKUMOTO, Kazutoshi FUKUI, Hiroaki MATSUMOTO, Masami FUJITA*, Takeshi MIYANAGA** and Makoto WATANABE***

Department of Electrical and Electronics Engineering, Fukui University, Fukui 910
* Maritime Safety Academy, Wakaba, Kure 737
** Department of Physics, Faculty of Education, Wakayama University, Sakaedani, Wakayama 640
***Institute for Molecular Science, Okazaki 444

The STE (self-trapped exciton) luminescence of alkali halide crystals is classified into three types, I, II and III, according to the spectral pattern[1]. In the present study, the decay profiles were investigated on the type I STE luminescence, that is, the σ emission in NaCl, KBr, KI, RbBr and RbI and the π emission in NaBr and NaI. Decay curves were measured at 7 K with a time correlated single photon counting method by using a micro-channel plate photomultiplier R2287U-06 and a TAC system. Excitation was made with single-bunched pulses at 31.5 nm from an undulator of UVSOR which have about 0.5 ns pulse duration and 178 ns time interval of successive pulses. The delayed luminescence over 178 ns is superposed on the successive repeated events and results in a piled-up background level.

In Fig.1 are shown decay curves obtained at 7 K for the type I luminescence of seven crystals. As for the σ emission of NaCl, KBr, KI, RbBr and RbI, long decay components ($\tau > 100$ ns) were observed in addition to the short decay components ($\tau <$ 10 ns) which are essentially the same as those[1-3] reported already and have been regarded as a basis to connect the σ emission to the spin singlet STE. Although the intensity levels of the long decay components are 2 or 3 order lower than the short ones on the decay curves, the integrated intensities amount to 10 to 30 % of the total integrated intensities. On the other hand for the π emission in NaBr and NaI, the short decay components (1.5 ns for NaBr and 1.0 ns for NaI) appear on the initial stage of main long components which have attributed the π emission to the spin triplet STE.

The luminescence intensity at the peak (0 ns) and at the time after 170 ns on each decay curve was plotted against the emission energy to obtain the time-resolved emission spectrum. The results are shown in Fig.2. The steady emission spectra (drawn with lines) were obtained under the same condition with the decay measurements except that the out-put of the photomultiplier were fed to a DC pico-ammeter. The time resolved spectra at 0 ns (●) and at 170 ns (▲) were plotted on the steady spectra in the normalized manner at each emission peak. Agreement among three spectra is fairly good.

These results clearly show that the type I STE luminescence consists of short and long decay components. Thus, the traditional understanding that the σ and π emission correspond to the spin singlet and triplet STE's, is not accurate any longer. The type I luminescence are attributed to the on-center type of "V_K + e" STE[1]. It is concluded that both singlet and triplet states are responsible to the type I luminescence from the on-

center STE.

1)K.Kan'no et al.:Rev. Solid State Science 4 (1990) 383.
2)K.Kan'no et al.:Physica Scripta 41 (1990) 120.
3)I.M.Blair et al.:J. Phys. C Solid State 5 (1972) 1537.

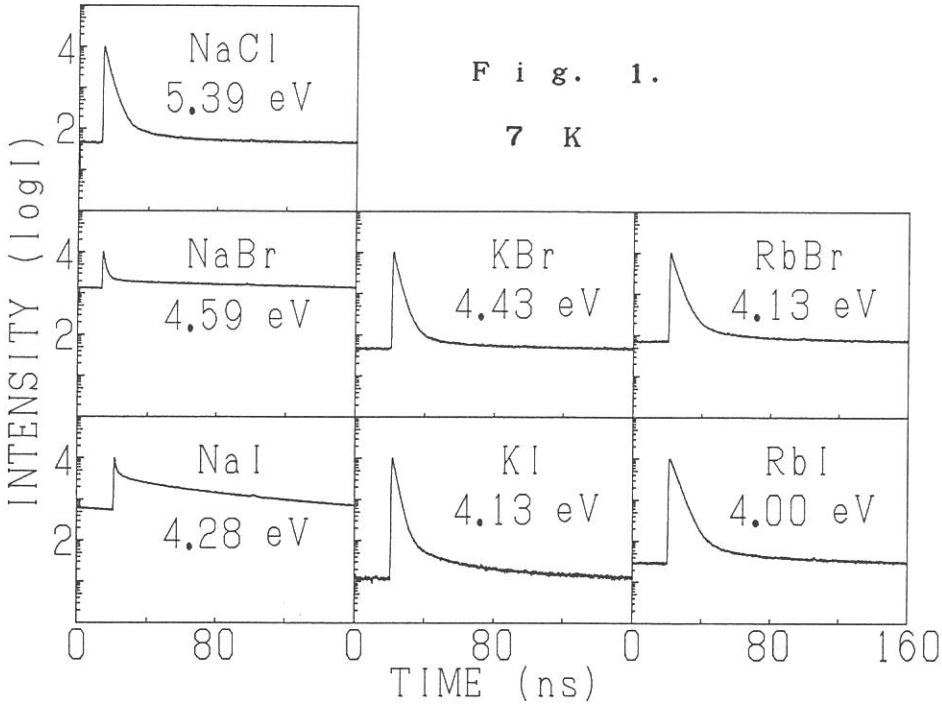

Fig. 1.

7 K

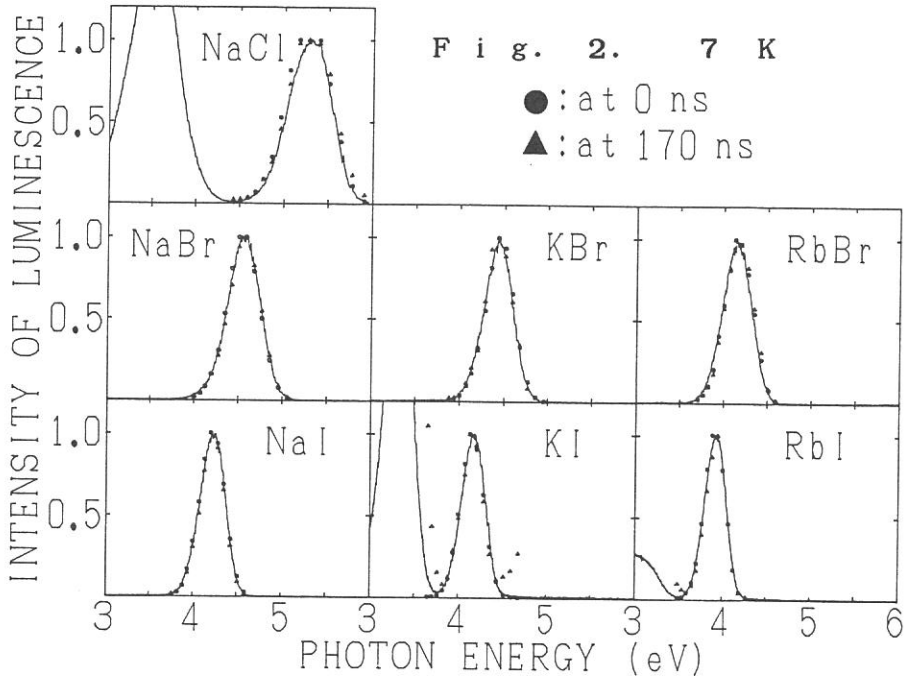

Fig. 2. 7 K

●:at 0 ns

▲:at 170 ns

$N_{4,5}$ EMISSION SPECTRA OF SOME RARE-EARTH HEXABORIDES

Kouichi ICHIKAWA, Takashi UMEHARA, Katsuhito Aoki and Masao KAMADA*

College of Engineering, University of Osaka Prefecture, Mozu-Umemachi, Sakai 591
*Insitutute for Molecular Science, Myodaiji, Okazaki 444

There have been many studies on the absorption spectra and the photoemission spectra of rare-earths (RE) and their compounds in the region of 4d excitation because the 4d-4f interaction gives characterestic features in the spectra. The absorption spectra show weak lines with widths of several tenths of an electron volt and giant bands with 15-70 eV widths. The final states of the absorption decay radiatively and/or nonradiatively. The former process emits soft-x-rays in the region of 4d absorption and is distinct from ordinary x-ray emission.[1] The latter process ejects electrons with different kinetic energies corresponding to the various decay channels such as the Auger decay processes and the direct recombination of the excited electron and the 4d hole.[2,3] The observation of these phenomena is useful for understanding the electronic structure of RE compounds and the decay mechanism of the $4d^9 4f^{n+1}$ excited states, where n is a number of 4f electrons in the ground state.

In the present study we measured RE $N_{4,5}$ emission and photoelectron spectra of PrB_6, NdB_6, EuB_6 and GdB_6. Thin samples were prepeared in situ by evaporation to reduce intensity loss due to the self-absorption in the measurements of soft-x-ray emission. In the case of photoemission, polycrystalline samples were scraped in situ with a diamond file to obtaine clear surface.

The Eu $N_{4,5}$ emission spectra of EuB_6 with electron excitation mode were shown in Fig. 1 (a)-(c). Excitation voltage is indicated at a right hand side of each spectrum. The total yield spectrum measured with a plane-grating-monochromator at a beam line 6A2 was also shown at a bottom of Fig.

1. The intense peak A at about 110 eV in the emission spectrum is caused by the transition between Eu 5p and 4d inner-core levels, and thus spectra were normalized at this peak. The intensity of the peak D relative to the peak A increases with decreasing the incident electron energy. This result suggests that the emission spectra are affected by the self-absorption. In fact, strong absorption due to the transition from the 4d level to the empty 4f level is observed in this energy region as shown at the bottom of Fig. 1. In a common sense, ordinary x-ray emission cannot appear in the energy region where the absorption is observed. Thus, we think that the peak D in the emission spectra is caused by the radiative decay of the $4d^9 4f^{n+1}$ excited states as observed previously in LaB_6 and CeB_6.[1] In the present case, however, the emission feature does not agree well in shape with the absorption. Therefore, there is a possibility that the peak D is caused by the transition from $4d^9 4f^n$ states because of large 4d-4f interaction.

Similar results were obtained for other RE hexaborides. However, there are close resemblance in shape between the emission and absorption spectra with decreasing atomic number. Detailed analysis of the spectra is under way.

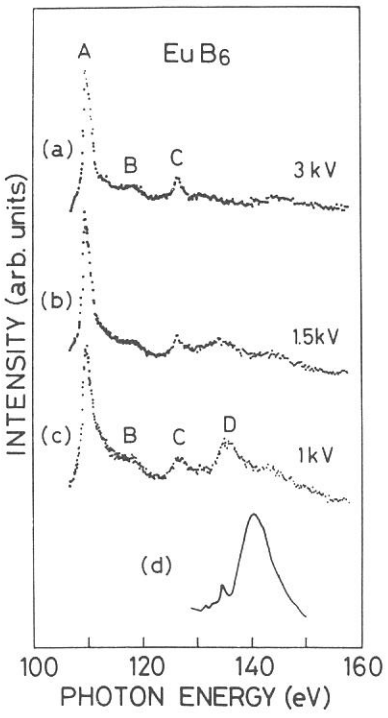

Fig. 1 Eu $N_{4,5}$ emission spectra (a)-(b) and total yield spectrum (d) of EuB_6. Emission spectra were obtained with the electron excitation mode and excitation voltage is indicated at a right hand side of each spectrum.

REFERENCES

1) K. Ichikawa, A. Nisawa and K. Tsutsumi, Phys. Rev. B 34 (1986) 6690.
2) J. W. Allen, L. I. Johansnon, I. Lindau and S. B. Hagstrom, Phys. Rev. B 21 (1980) 1335.
3) M. Aono, T. -C. Chiang, F. J. Himpsel and D. E. Eastman, Solid State Commun. 37 (1981) 471.

4d CORE PHOTOABSORPTION SPECTRA OF BaF_2 AND SOME RARE-EARTH COMPOUNDS

Osamu AITA, Sayumi HIROSE, Katsuhito AOKI and Masao KAMADA*

College of Engineering, University of Osaka Prefecture, Mozu-Umemachi 4-cho, Sakai 591
*Institute for Molecular Science, Myodaiji, Okazaki 444

The investigation of the effect of 4f orbital collapse on the spectra of cesium, barium and light rare-earths in the 4d $\rightarrow$nf,εf excitation is a interesting subject of theoretical and experimental studies because the properties of rare-earth elements depend on the sudden collapse of the 4f wave function at the biginning of this group. The 4d X-ray absorption spectra (XAS) of these substances show sharp lines near the threshold and a broad and intense band above the threshold.[1,2] These sharp lines are interpreted as originating from the electronic transition of 4d electron to the unoccupied 4f state which is localized into small orbitals inside the potential barrier. Owing to the exchange interaction between a 4d hole and a 4f electron the resulting multiplet states of the $4d^9 4f^{n+1}$ configuration spread over several tens of electron volts, where n equals the number of 4f electrons in the ground state. Recent theoretical results have shown that the effect of hybridization between 4f and valence band states on multiplet structures is important in the prethreshold region of the 4d XAS for metallic Ce compounds.[3] In the present work we measure the 4d XAS of some Ba-, La-, and Ce-halides for comparison with the results of resonant photoemission to know the extent of localization of $4d^9 4f^{n+1}$ excited states.

The experiments were carried out using a 2-m Grasshopper monochromator at BL2B1 beam line of UVSOR. Samples were prepared on a collodion substrate coated with a thin aluminum film by a vacuum evaporation method. A filter made of TbF_3 with a thickness of about 2000 Å was used to reduce overlapping of the second-order light to the spectral region studied.

The 4d XAS of BaF_2, LaF_3, $LaCl_3$ and CeF_3 are shown in Fig.

1. Sharp absorption lines appear near the threshold and a broad and intense band follows them. In La compounds absorption peaks are interpreted as being due to the transitions to the multiplet states of the $4d^9 4f^{n+1}$ configuration in the atomic picture. The peaks appeared around 97 and 102 eV and the broad and intense band around 118 eV are attributed to the $^3P_1$, $^3D_1$ and autoionized $^1P_1$ states, respectively. The spectrum of BaF_2, whose Ba^{2+} ion has no 4f electron in the ground state as the La^{3+} ion, is similarly interpreted. The Ce 4d XAS of CeF_3 is interpreted by the multiplet states of the $4d^9 4f^2$ configuration. It is noted that the spectral profiles of the broad and intense band of BaF_2 and La compounds are much different each other. This indicates that these spectra are not interpreted only by the atomic model. We suppose that this difference arises from the difference in hybridization between 4f and conduction states which is closely related to crystal structure.

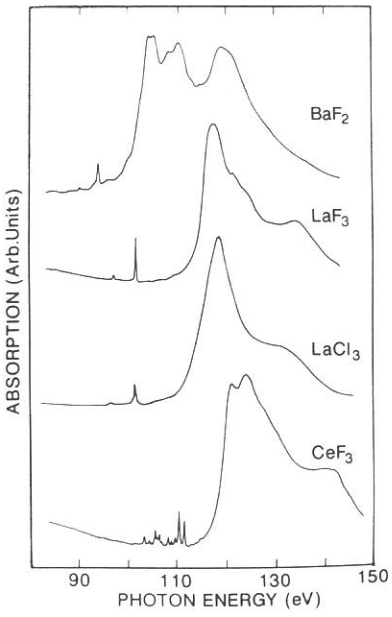

Fig. 1. 4d XAS of BaF_2, LaF_3, $LaCl_3$ and CeF_3.

We measured the resonant photoemission of the present substances except for CeF_3. As one of results, for example, the photoemission intensity of the valence band was enhanced in the broad and intense band region in LaF_3 but not enhanced in BaF_2. This feature may indicate the extent of localization of the excited states is different between these substances. Detailed discussion on the resonant photoemission spectra will be given elsewhere.

References
1) S. Suzuki et al.: J. Phys. Soc. Jpn. 38 (1975) 156.
2) T. Miyahara et al.: J. Phys. Soc. Jpn. 55 (1986) 408.
3) T. Jo: J. Phys. Soc. Jpn. 58 (1989) 1452.

Te 4d Core Absorption of p- and n-type SnTe

Kazutoshi FUKUI,* Tadaaki SAITO,[1)] Shin-ich KONDO,[1)]
and Makoto WATANABE
Institute for Molecular Science, Okazaki 444
[1)]*Department of Applied Physics, Fukui University, Fukui 910*

We have been investigating the relation between the electronic structure and the core absorption spectral feature of crystalline (*c*) and amorphous (*a*) group IV (Pb, Sn, Ge) tellurides (IVTes). The *c*-IVTes are degenerate semiconductors, that is, the electrons (holes) exist in the conduction (valence) band.[1)] Therefore, they are all metallic, and the usual *c*-PbTe samples show *n*-type character, and *c*-SnTe and *c*-GeTe samples, *p*-type characters. On the other hand, the *a*-IVTes are insulator-like because their conductivity are of thermal activation type. In the Te 4*d* absorption,[2-4)] broad structures are observed above 40 eV in all *c*- and *a*-IVTes. However, a small peak at lower energy side of this broad structures has been found only in *c*-SnTe and *c*-GeTe. One possible interpretation of the small peak is that it is due to the excitonic transition. However, since the small peak is only found in *p*-type degenerate semiconductors, there is another interpretation that it is due to the transition from Te 4*d* level to the hole state which is located at the top of the valence band. In the present work, since the total photoelectron yield (TY) spectra reflect absorption spectra,[5)] the TY spectra of both *p*- and *n*-type polycrystalline SnTe are measured around Te 4*d* transition at BL2B1 equipped with a Grasshopper monochromator. The *p*-type samples were prepared so that the stoichiometric composition deviates to Te rich side, and the *n*-type samples, to Sn rich side. Figure 1 shows the TY spectra of *c*-SnTe both of *p*-

* Present address : Department of Electrical and Electronics Engineering, Fukui University, Fukui 910

and *n*-type in the energy region from 38 to 46 eV. As shown in the figure, the small peak at 39.6 eV is found in the spectra of *c*-SnTe of *p*-type, but not in that of *n*-type. Since the small peak is found only in the IVTes of *p*-type (*c*-GeTe, *p*-type *c*-SnTe), the small peak is characteristics of *p*-type degenerate semiconductors. Therefore, it is concluded that the small peak is due to the transition from Te 4*d* level to the top of the valence band (hole states). Since Te 4*d* level is split by the spin-orbit interaction (about 1.5 eV), the other small peak should be found around 41.1 eV. However, it seems to be difficult to found it because of the overlap of the broad structures.

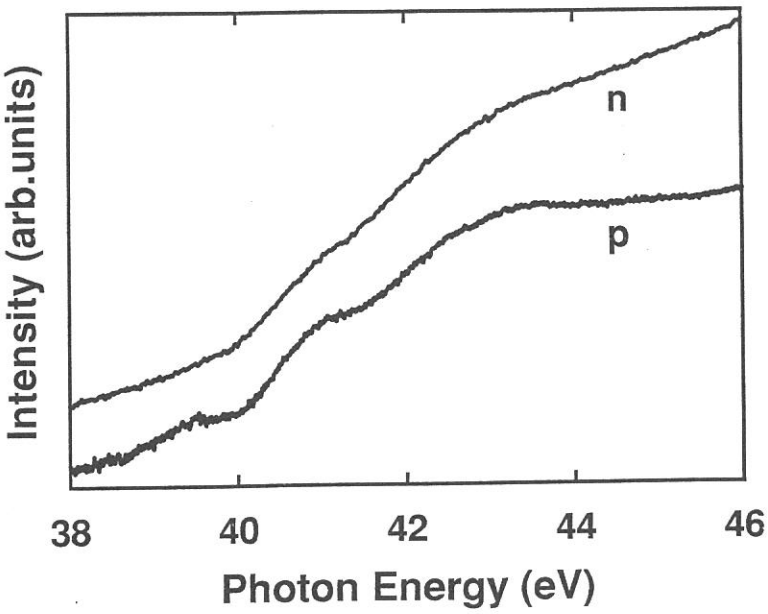

Figure 1. The total yield spectra of *c*-SnTe of *p*- and *n*-type around Te 4*d* transition.

References

1) N.J.Parada : Phys. Rev. B **3** (1971) 2042.
2) K.Fukui, J.Yamazaki, T.Saito, S.Kondo and M.Watanabe : J. Phys. Soc. Jpn. **56** (1987) 4196.
3) K.Fukui, T.Saito, S.Kondo, Y.Fujii, Y.Sakisaka and M.Watanabe : J. Phys. Soc. Jpn. **59** (1990) 4161.
4) K.Fukui, T.Saito, S.Kondo and M.Watanabe : UVSOR ACTIVITY REPORT 1989, p54.
5) W.Gudat and C.Kunz : Phys. Rev. Lett. **29** (1972) 169.

Orientation of Oxygen Admolecules on Platinum(110)(1x2) Surfaces; A Near-Edge X-Ray Absorption Fine-Structure Study

Yuichi Ohno, Tatsuo Matsushima, Shin-ichiro Tanaka, Eriko Yagasaki, and Masao Kamada

Institute for Molecular Science, Okazaki National Institutes, Myodaiji, Okazaki 444, Japan

The orientation of oxygen admolecules on Pt(110)(1x2) reconstructed surfaces was studied with the near-edge X-ray absorption fine-structure (NEXAFS). The molecular axis was concluded to be lying on the surface and oriented along the surface trough.

NEXAFS spectra of oxygen admolecules on Ag(110) and Pt(111) have been reported to be dominated by intramolecular scattering resonances from the oxygen core level(1s) to the unfilled molecular orbitals, $3\sigma^*$ and $1\pi^*$[1]. The transitions are governed by dipole selection rules, and then analysis of the subsequent Auger electron yield as a function of the E vector orientation of incident X-ray allows the determination of the molecular orientation. This method was applied to oxygen on Pt(110)(1x2) surfaces, where the adsorption was well characterized[2]; it is adsorbed molecularly below 150 K.

Experiments were carried out on Beam Line 2B1 of UVSOR, IMS, with the use of a Grasshopper monochrometer(Mark XV). The photon energy was calibrated with the sharp photoemission spectra due to the Pt 4f level. The spectra were recorded by a partial Auger-yield mode at an electron kinetic energy of 520 eV after saturation with O_2(a) at 120 K. The yield was normalized to the incident photon flux. The sample crystal was rotated around the axis perpendicular to the photon incidence, to change the angle between the E vector and the surface plane. The surface was first cleaned by Ar^+ bombardments and oxygen treatments in a separate chamber, and characterized with AES and LEED. The crystal was again cleaned in a similar way after the transfer into a chamber of the beam line.

Figure 1 shows typical spectra when the E vector is oriented in the [1$\bar{1}$0] direction (along the trough). Both resonances (σ^*, and π^*) were enhanced when the photon incidence was normal. The

former resonance was attenuated when the incidence was glancing(Fig.2). This indicates that the O-O axis is parallel to the surface plane. Noticeable differences were found in spectra, when the E vector was oriented in the [001] direction. Yields in both resonances were significantly reduced. Less incident angle dependence was observed. In this case, the molecular axis is always perpendicular to the E vector. In conclusion, oxygen molecules are lying down on the surface and oriented along the trough.

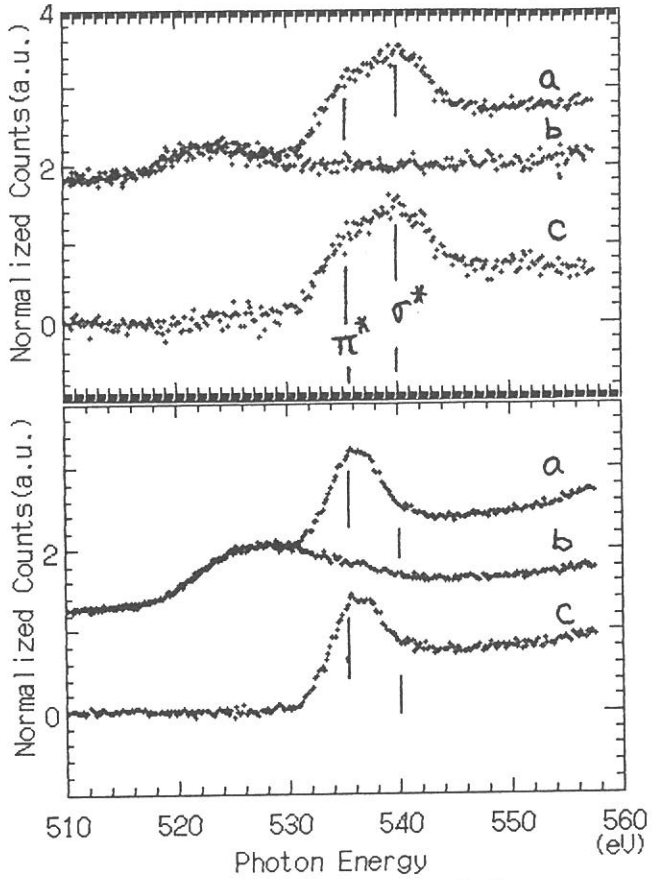

Fig.1 NEXAFS spectra of O_2(a), when the E vector is in the [1$\bar{1}$0] direction and θ = 0° . θ is the angle between the surface normal and the photon incidence. (a) O_2(a) saturated, (b) clean surfaces, and (c) the difference, (a)-(b).

Fig.2 NEXAFS spectra when the E vector is almost perpendicular to the surface plane(θ =80°) and in the (1$\bar{1}$0) plane. The notations are the same as those in Fig.1.

[1](a)J.Stöhr, J.L.Gland, W.Eberhardt, D.Outka, R.J.Madix, F.Sette, R.J.Koestner, U.Doebler, Phys. Rev. Lett. 51(1983) 2414;(b)D.A.Outka, J.Stöhr, W.Jark, P.Stevens, J.Solomon, and R.J.Madix, Phys. Rev. B, 35(1987) 4119;(c)W.Wurth, J.Stöhr, P.Feulner, X.Pan, K.R.Bauchspiess, Y.Baba, E.Hudel, G.Rocker, and D.Menzel, Phys. Rev. Lett. 65(1990) 2426.
[2]Y.Ohno and T.Matsushima, Surface Sci. (1991) in press.

Sputtering of Excited-State Na Atoms from Sodium-Halides Irradiated with Undulator Radiation

M. Kamada, S. Hirose,* and O. Aita*
Institute for Molecular Science, Myodaiji, Okazaki 444
* College of Engineering, University of Osaka Prefecture

Bombardment of solids by energetic electron- or photon-beams causes the ejection of constituent species from the surface. This sputtering phenomenon is much attractive, because of its applicability to microfabrication and its close relation to the radiation damage of the solids. However, most previous studies of electron- or photon-induced sputtering have been limited primarily to ionized species and ground-state species, while few groups have studied the photon-induced sputtering of excited species.[1] The purpose of the present study is to get a well understanding of the sputtering process of the excited-state alkalis from ionic crystals irradiated with undulator radiation.

Experiments were performed at the BL-3A1 of the UVSOR facility. Undulator radiation of about 1.7 eV in full-width at half-maximum was used as an exciting light source. Alminum filters of about 1300 Å were inserted between the undulator and samples to eliminate visible and higher energy photons. Single crystals were cleaved with a knife edge in the sample chamber, of which base pressure was about 2×10^{-7} Pa. Undulator radiation was incident at surface normal, and the optical emission was obtained at 45° from the surface normal. The spectra shown here have been corrected for the spectral sensitivity of the detecting system including monochromator and photomultiplier by using a tungsten standard lamp.

Figure 1 shows a set of optical emission spectra of sodium-halides, which were irradiated at 300 K with undulator radiation of 36 eV. The spectra are composed of a sharp line at about 2.1 eV and broad bands. The broad bands may be due to the recombination between bulk defects and are not concerned in the present context. The energy position and the shape of the sharp line in the emission spectra coincide well with those of the atomic emission line (so-called Na D-line) from a discharge lamp. It should be noted that the intensity of the Na D-line

from NaF is larger than that from NaCl, and that the Na D-line is not appreciable on NaBr and NaI. This result is different from the existing result of the photon-induced sputtering of ground-state sodium atoms from sodium halides,[2] where the intensity of the ground-state sodium atoms is almost the same among sodium halides. It is generally accepted that the electronic excitation of halogen ions results in the halogen-ion vacancies, and that the production efficiency of the halogen defects is in the order of NaF to NaI, depending on Rabin-Klick parameters.[3] This tendency is in good agreement with that of the Na D-line intensity shown in the figure. Thus, we propose that surface defects play important roles in the sputtering of excited-state sodium atoms from sodium halide crystals. It should be also stressed that temperature dependence of the Na D-line intensity from NaF and NaCl shows a maximum at 316 and 303 K, respectively. This result is not interpreted in terms of an existing thermal-evaporation mechanism, but can be explained with the thermal instability of the surface defects. Detailed discussion will be reported in near future.

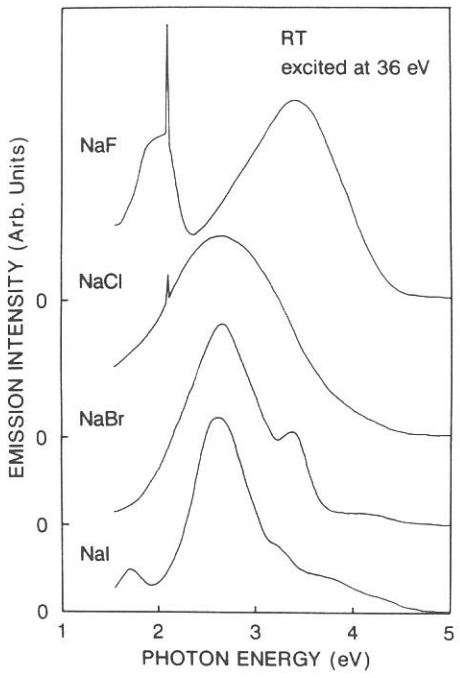

Fig. 1. Emission spectra of sodium halides irradiated with undulater radiation of 36 eV.

References

1) Desorption Induced by Electronic Transitions (DIET IV), edited by G. Betz and P. Varga (Springer, Berlin, 1990).
2) N. G. Stoffel, R. Riedel, E. Colavita, G. Margaritondo, R. F. Haglund, Jr., E. Taglauer, and N. H. Tolk, Phys. Rev. B **32**, 6805 (1985).
3) H. Rabin and C. C. Klick, Phys. Rev. **117**, 1005 (1960).

Photon Stimulated Desorption from the Surface of Rare Gas Solids

Ichiro ARAKAWA, Takato HIRAYAMA, and Makoto SAKURAI[1]

Department of Physics, Gakushuin University, Mejiro, Toshima, Tokyo 171
[1] National Institute for Fusion Science, Furo-cho, Chikusa, Nagoya 464-01

Studies on Photon Stimulated Desorption(PSD) processes using Synchrotron Radiation(SR) have been increasingly reported[1,2]. As an agent of primary excitation, photons have some advantages over the other kind of probes on account of their state selective nature, minimum momentum transfer, and feasibility to both surface-localized and bulk excitation for a primary step in Desorption Induced by Electronic Transitions(DIET). In this report, we present some results of the experimental study on the desorption of Ar metastables[3].

Photo-desorbed species, ions and excited neutrals, from the surface of a solid rare gas, which is condensed on a cold substrate, are detected by secondary electron multipliers and their kinetic energies are analyzed by using Time-of-Flight(TOF) technique[4]. The experimental apparatus is build in an ultra-high vacuum chamber which is installed on the beamline BL5B of UVSOR.

A TOF spectrum of PSD Ar excited neutrals(Ar*) from the surface of solid Ar is shown in Fig. 1, where photon energy is 13.8 eV (wavelength λ = 90 nm). The kinetic energies of Ar*, 0.6 eV and 0.04 eV, at the two peaks and the shape of distribution are almost identical with those of ESD Ar*[5], except for their relative intensity of the two peaks. The Ar* peak with the higher energy (0.6 eV) disappears when the excitation photon energy is 12.2 eV (λ = 102 nm). When the photon energy is lower than 11.7 eV (λ >106 nm), the peak with the lower energy (0.04 eV) also disappears and no Ar* signals are detected. The dependence of the total Ar* PSD yield on the photon energy, from 11.3 eV to 15.5 eV, is shown in Fig. 2. This spectra exhibits a clear correlation between the photon energies at the peaks of desorption yield and the excitation energies of the first and second surface (1s and 2s) and bulk (1b and 2b) excitons[6].

The TOF spectrum of Ar* shown in Fig. 1 was obtained at the energy corresponding to the excitation of the second bulk exciton. The comparison of the TOF spectra at several photon energies shows that the excitation of the second order exciton leads to desorption of Ar* with the kinetic energy around 0.6 eV and that the Ar* with the lower kinetic energy around 0.04 eV originates from the first order exciton. The present result suggests a different desorption channel for each Ar* group (0.04 eV and 0.6 eV) and supports the following two models of the desorption mechanism[7]. The lower kinetic energy of Ar* originates from an

exciton trapped at a surface where an excited atom is ejected by a repulsive potential around an exciton. The desorption of the higher energy Ar* is induced by the relaxation of highly excited dimer: Ar_2^{**} -> Ar* + Ar.

References

1) P. Feulner, T. Müller, A. Puschmann, and D. Menzel, Phys. Rev. Lett. **59**, 791 (1987).
2) T. Kloiber, W. Laasch, G. Zimmerer, F. Coletti, and J.M. Debever, Europhys. Lett. **7**, 77 (1988).
3) I. Arakawa and M. Sakurai, in *Desorption Induced by Electronic Transitions, DIET IV*, ed. by G. Betz and P. Varga (Springer, Berlin, 1990) p. 246.
4) M. Sakurai, T. Hirayama, and I. Arakawa, Vacuum **41**, 217 (1990).
5) I. Arakawa, M. Takahashi, and K. Takeuchi, J. Vac. Sci. Technol. **A7**, 2090 (1989).
6) V. Saile, M. Skibowski, W. Steinmann, P. Gürtler, E.E. Koch, and A. Kozevnikov, Phys. Rev. Lett. **37**, 305 (1976).
7) S.T. Cui, R.E. Johnson, and P.T. Cummings, Phys. Rev. **B 39**, 9580 (1989).

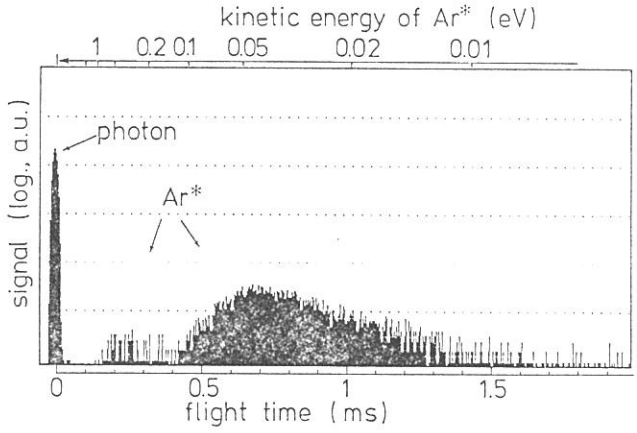

Fig. 1. Ar* PSD TOF spectrum at a excitation photon energy of 13.8 eV.

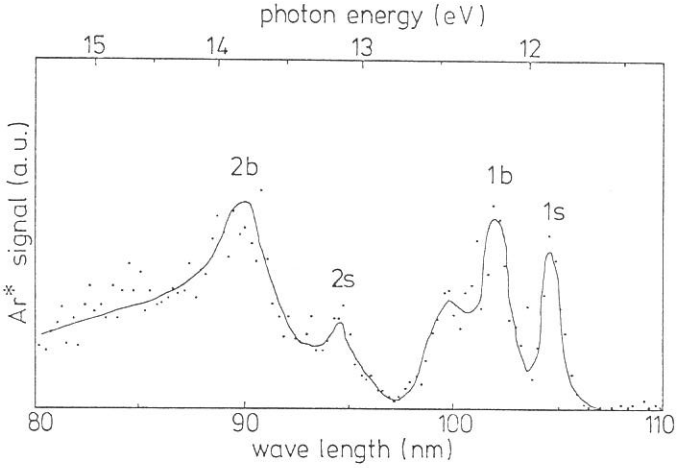

Fig. 2. Dependence of the Ar* PSD signal intensity on the photon energy from 11.3 eV (110 nm) to 15.5 eV (80 nm).

Time-Resolved Measurement of Photoemission after Pulsed VUV Irradiation

Tatsuo Okano and Makoto Sakurai*
Institute of Industrial Science, University of Tokyo, Tokyo 106
* National Institute for Fusion Science, Nagoya 464-01

We have recently developed an apparatus for the time-resolved measurement of photoemission process. To examine the ability of the apparatus, we have made preliminary measurement of photoemission from Au, stainless steel, and GaAs. The outline of the apparatus is shown in Fig.1 The vacuum chamber is attached at the end of BL-5B beamline of UVSOR. Samples of solid surface is mounted on a XYZ translator. The cleaning of surfaces is made by electron beam heating of the sample holder. The surface is irradiated by synchrotron radiation of 450ps in pulse duration which comes through a port of the ultra-high vacuum chamber. The detection system of photo-emitted electrons consists of a series of electrostatic lenses and a particle-counting type streak-camera. The streak-camera system is a newly built one for the time-resolved measurement of charged particles. It is basically a windowless optical streak-camera. The photocathode was replaced by a metal-seal vacuum flange. Charged particles are focused on the entrance aperture of the streak tube and detected by a triple microchannel plate (MCP) after high-speed deflection. The multiplication factor of the MCP and the sensitivity of the CCD camera is high enough to make single electron counting possible. The time-resolution of the system was estimated to 50ps.

Time-resolved measurements of photoemission in picosecond region have become necessary in several field of experimental physics such as;

1. Charge transport in semiconductor,
2. Dynamics in core-excitation process,
3. Development of advanced accelerator.

Before concentrating on a specific material, we have measured the photoemission from various materials by using the newly developed apparatus. The following three materials were used.

Gold: Polycrystalline wire.

Stainless steel: SUS316L, mirror-polished by ECB process.

GaAs(100): p-type (Zn, $1.96 \times 10^{19}/cm^{3}$).

The photoemission from GaAs(100) is shown in Fig.2. The decay of photoemission from the GaAs(100) surface was much slower than those of other two materials. We are planning to measure the correlation between the decay of photoemission and the condition of the the surfaces.

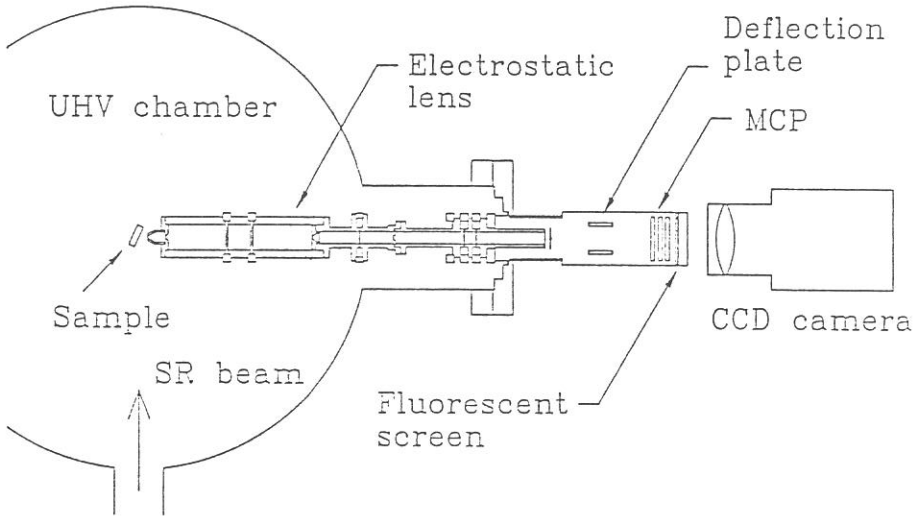

Fig.1. Apparatus for the measurement of time-resolved photoemission.

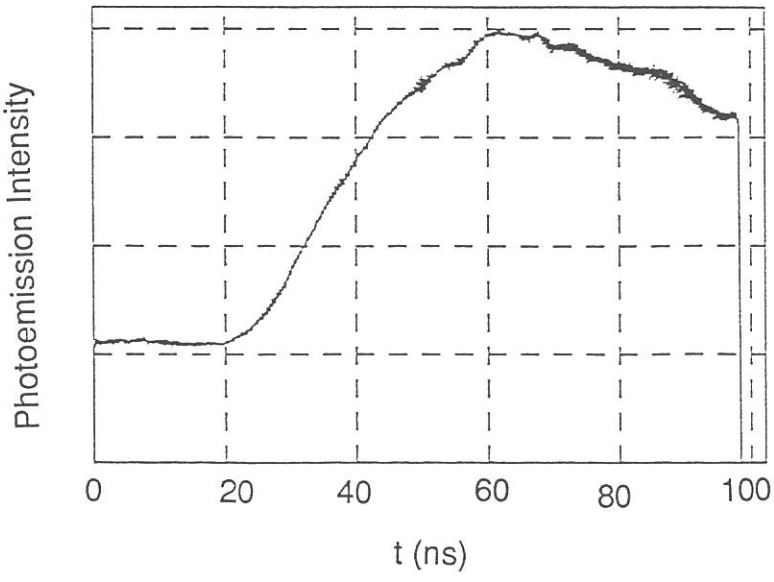

Fig.2. Photoemission from GaAs(100) after irradiation of VUV light, λ=100nm.

Sensitivity Calibration of Surface Barrier Diodes in the Soft X-Ray Region

Makoto SAKURAI, Nobuyuki ASAKURA * and Yoshihiro SHIMAZU *

National Institute for Fusion Science, Nagoya 464-01
*Faculty of Science, University of Tokyo, Tokyo 113

Abundant radiation in the soft X-ray (SX) region is emitted from magnetically confined plasmas, and the measurement of space distribution of the emission make it possible to obtain informations on equiliblium and instability of the plasma. The two-dimensional distribution is computationally reconstructed from the signals of surface barrier diode (SBD) detectors which observe integrated radiation flux along the line of sights. Then, it is important to know relative sensitivities between the detectors precisely, however, reliable calibration procedure has rarely been performed due to luck of convenient light sources in the SX region.

We measured sensitivities of 33 SBD's using monochromatized synchrotron radiation (SR) at BL5B. Fig.1 shows the experimental setup for calibration. SR was chopped into pulses of 20μs duration using a rotating wheel to simulate the experimental condition for SX observation from the plasma of REPUTE-1 [1]. Ten SBD's were mounted on a sample holder, and both spatial and incident angle distributions of sensitivity could be measured for each detector. Signals were stored and averaged using boxcar integrator (EG&G Princeton Applied Research, 4402 + 4421).

Fig.2 shows the spectral response of a SBD and a proportional counter which was used for standard photon detector. Both dectors show similar absorption edge profiles of C-K since they have 4 μm polypropylene filters. Fig.3 shows the incident angle dependence of SBD signal. The signal decreases faster than cosϕ curve with the rotation. Relative sensitivities of 33 SBD's at 5.2nm are listed in Fig. 4. Experimental error of the sensitivity exists at 2-4%. Groups of the serial number of each SBD are shown as '24-xxx', '25-xxx', etc., and those SBD's with the same number, which are made from the same wafer, are expressed with the identical symbol.

Reference

1) N. Asakura et al., Nucl. Fusion **29**, 893 (1989).

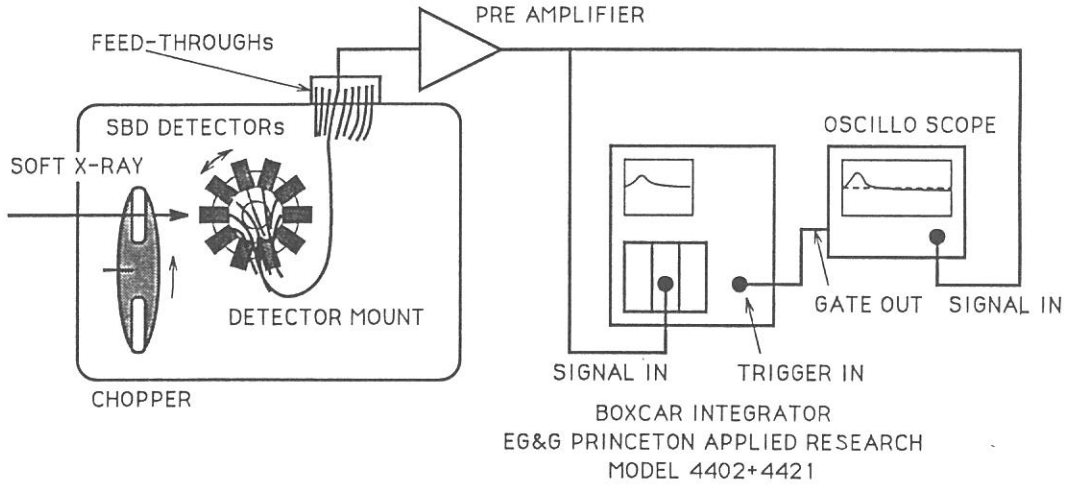

Fig. 1. Schematic diagram of the experimental setup.

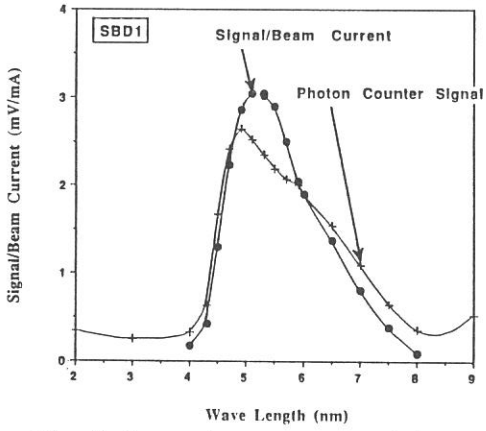

Fig. 2. Spectral responses of the SBD detector and proportional counter.

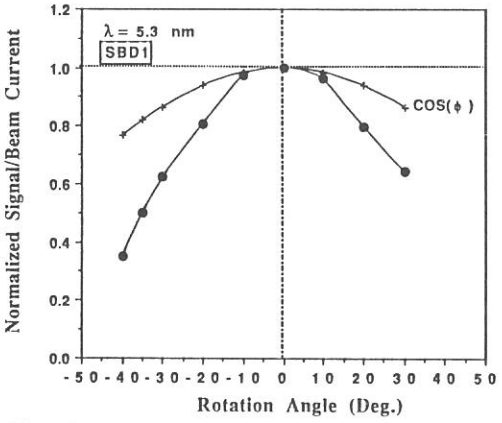

Fig. 3. Incident angle dependence of the SBD detector.

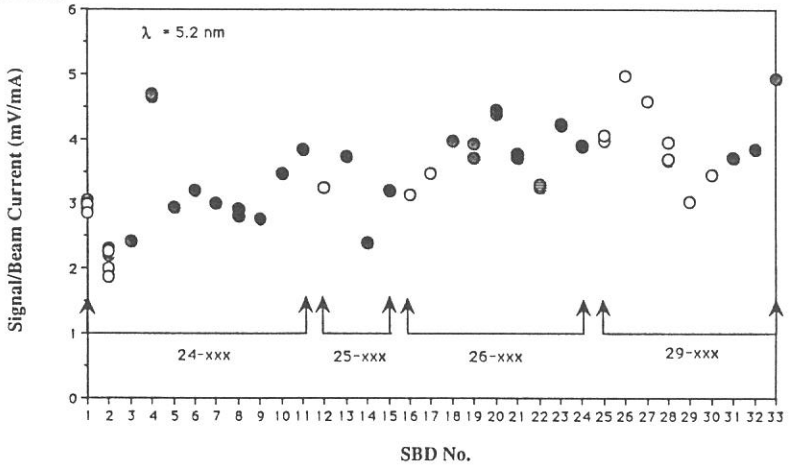

Fig. 4. Relative sensitivities of SBD detectors.

CHARACTERIZATION OF MULTILAYER REFLECTORS AND DETECTORS ON BL-5B

Koujun YAMASHITA*, Shunji KITAMOTO, Keisuke TAMURA, Shin-ichiro TAKAHAMA, Isamu HATSUKADE** and Makoto SAKURAI***

Department of Physics, Osaka Univershity, Toyonaka 560
*Institute of Space and Astronautical Science, Sagamihara 229
**Faculty of Engineering, Miyazaki University, Miyazaki 889-20
***National Institute for Fusion Science, Nagoya 464-01

We carried out the characterization of multilayer reflectors of Ni/C, Mo/si and Hf/Si, and position sensitive detectors of micro-channel plate(MCP) in the wavelength region 45 - 500A using BL-5B which is specially designed for the calibration of optical elements and detectors used for the plasma diagnostics in the wavelength region 20 - 2000A(1). Incident beam is monochromatized by PGM and a sensitive wavelength band is selected by a combination of grating and mirror.

The measurement of reflectivities of multilayer reflectors was done at the incidence angle of 20 - 80 deg. to the reflecting surface for s and p polarization. A thin window proportional counter and windowless photomultiplier were used for this measurement. Multilayers are Ni/C(2d=115A,N=20) used for paraboloid mirror, Mo/Si(2d=146A, N=20) for spherical mirror, and Mo/Si and Hf/Si(2d=330A, N=5) specially designed for HeII(304A) observation(2,3). One of these results is shown in Fig.1 for Mo/Si(2d=330A, N=5) at 70 deg.. There exist 1st order Bragg reflection around 300A and 2nd peak at 155A. This indicates that multilayer is useful for broad band filter.

The detection efficiency of MCP coated with CsI was measured against wavelength and incidence angle in the wavelength region 45 - 80A. Fig.2 shows the efficiency and gain vs. incidence angle

at 55A. The bias angle is set at 27 deg. Incident beam is parallel to channels at -27deg., where gain becomes lower and efficiency higher. MCP was also used for the reflectivity measurement to get the beam profile.

(1) M. Sakurai et al., Rev. Sci. Instrum., 60, 2089(1989).
(2) M. Sakurai et al., Vacuum, 41, 1234(1990).
(3) K. Yamashita et al., Rev. Sci. Instrum. 60, 2006(1989).

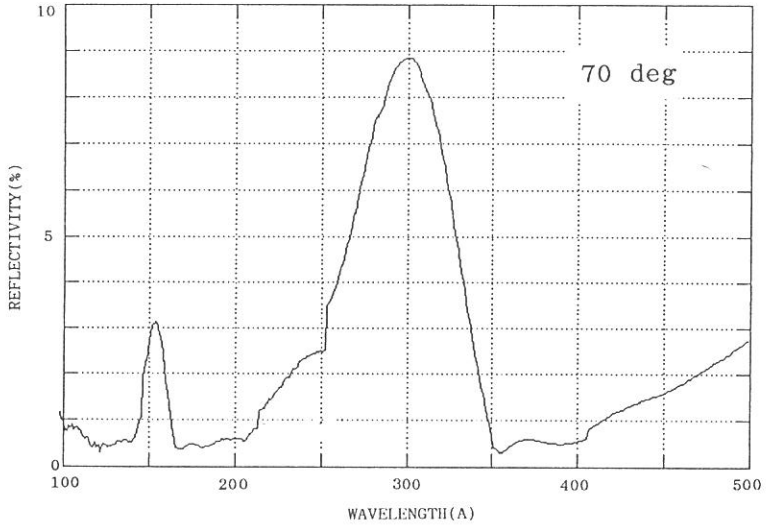

Fig.1 Reflectivity of Mo/Si(2d=330A, N=5) vs. wavelength.

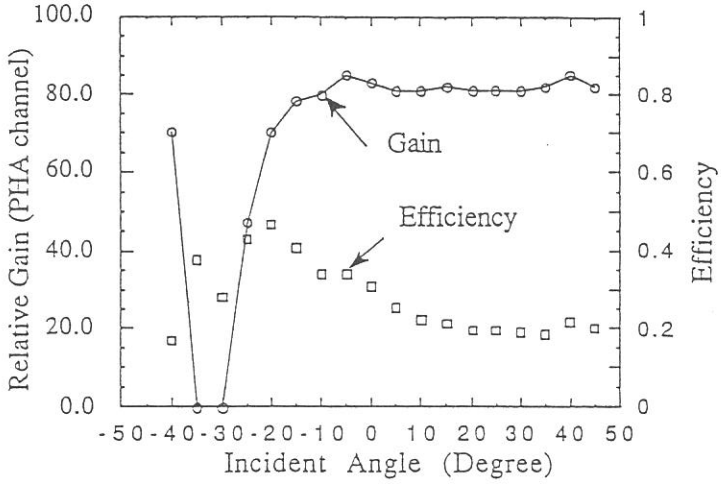

Fig.2 Efficiency and gain vs. incidence angle at 55A

APPENDIX

ORGANIZATION

Staff

Director

Katsumi	KIMURA	Professor

Scientific Staff

Light Source

Goro	ISOYAMA	Associate Professor
Hiroyuki	HAMA	Research Associate
Shirou	TAKANO	Research Associate

Beam Line

Makoto	WATANABE	Associate Professor
Masao	KAMADA	Associate Professor
Atsunari	HIRAYA	Research Associate
Shin-ichiro	TANAKA	Research Associate

Technical Staff

Kusuo	SAKAI	Section Chief Engineer
Osamu	MATSUDO	Unit Chief Engineer
Toshio	KINOSHITA	Engineer
Masami	HASUMOTO	Engineer
Jun-ichiro	YAMAZAKI	Engineer
Eiken	NAKAMURA	Engineer

Secretary

Yasuno	YAMAGUCHI	

Guest Scientist

Kazuhiko	SEKI	Adjunct Associate Professor from Hiroshima Univ.
Koichiro	OBA	Visiting Research Fellow from HAMAMATSU PHOTONICS K. K.

Representative of Beam Lines

BL1A	Makoto	WATANABE	UVSOR
BL2A	Kosuke	SHOBATAKE	Dept. Molecular Assemblies

BL2B2	Katsumi	KIMURA	Dept. Molecular Assemblies
BL3B	Kosuke	SHOBATAKE	Dept. Molecular Assemblies
BL4A	Shinri	SATO	Dept. Molecular Assemblies
BL4B	Kosuke	SHOBATAKE	Dept. Molecular Assemblies
BL6B	Kyuya	YAKUSHI	Dept. Molecular Assemblies
BL6A2	Masao	KAMADA	UVSOR
BL8B2	Hiroo	INOKUCHI	IMS
Others	Makoto	WATANABE	UVSOR
	Masao	KAMADA	UVSOR

Steering Committee (April 1990 - March 1992)

Katsumi	KIMURA	IMS Chairman
Jun-ichi	CHIKAWA	Nat. Lab. High Energy Phys.
Junji	FUJITA	Nat. Inst. Fusion Science
Masao	KOTANI	Gakushuuin Univ.
Kaizo	NAKAMURA	Okayama Univ.
Yukinori	SATO	Tohoku Univ.
Tadamase	SHIDA	Kyoto Univ.
Shigemasa	SUGA	Osaka Univ.
Kazuhiko	SEKI	IMS and Hiroshima Univ.
Ichiro	HANAZAKI	IMS
Kyuya	YAKUSHI	IMS
Kosuke	SHOBATAKE	IMS
Norio	MORITA	IMS
Makoto	WATANABE	IMS
Goro	ISOYAMA	IMS
Masao	KAMADA	IMS

JOINT STUDIES (fiscal year 1990)

Special Project	: 3
Cooperative Research	: 28
Use of Facility	: 104
Users' Meeting	: 1
Workshop on Beam Dynamics and Free Electron Laser	: 1
Users' Time	: 39 Weeks

LIST OF PUBLICATION

1)"Anisotropic Reflectivity of Black Phosphorus in the Far-Infrared Region"

T.Nanba, M.Ikezawa, I.Shirotani and H.Inokuchi

Proc. 12th Int. Conf. Infrared and Millimeter Waves (IEEE, 1987) p.231.

2)"Phonon Polaritons in Thin Films and Microcrystals of MnO"

S.Mochizuki

J. Phys.: Condens. Matter **1** (1989) 10351.

3)"Na K-XANES and EXAFS Studies in Sodium Halides"

T.Murata, T.Matsukawa and S.Naoe

Physica B **158** (1989) 610.

4)"Decay of the 4d Hole States of Xe Studied by Photoelectron-Photoelectron Coincidence Spectroscopy"

K.Okuyama, J.H.D.Eland and K.Kimura

Phys. Rev. A **41** (1990) 4930.

5)"Energy-Band Dispersion in Oriented Thin Films of Pentatriacontan-18-One by Angle-Resolved Photoemission with Synchrotron Radiation"

N.Ueno, K.Seki, N.Sato, H.Fujimoto, T.Kuramochi, K.Sugita and H.Inokuchi

Phys. Rev. B **41** (1990) 1176.

6)"Optical Spectra of Cadmium Halide Crystals in 3-30 eV Region"

M.Fujita, H.Nakagawa, H.Matsumoto, T.Miyanaga, M.Watanabe, K.Fukui, E.Ishiguro, Y.Fujii and Y.Sakisaka

J. Phys. Soc. Jpn. **59** (1990) 338.

7)"Lattice Relaxation of Self-Trapped Excitons in Binary Mixed Crystals of KCl and KBr"

K.Tanaka, K.Kan'no and Y.Nakai

J. Phys. Soc, Jpn. **59** (1990) 1474.

8)"Effect of Dilatational Strain on the Self-Trapped Exciton Luminescence of Alkali Halides"

M.Itoh, S.Hashimoto and N.Ohno

J. Phys. Soc. Jpn. **59** (1990) 1881.

9)"Core Absorption Spectra of Crystalline and Amorphous GeTe Thin Films"

K.Fukui, T.Saito, S.Kondo, Y.Fujii, Y.Sakisaka and M.Watanabe

J. Phys. Soc. Jpn. **59** (1990) 4161.

10)"Self-Trapped Exciton Luminescence in Mixed $K_{1-x}Rb_xI$ Crystals"

M.Itoh, N.Ohno and S.Hashimoto

J. Phys. Soc. Jpn. **59** (1990) 4534.

11)"Identity of Self-Trapped Exciton Configurations for the π Emission of NaI and the σ Emission of KI"

M.Itoh, S.Hashimoto, N.Ohno and K.Kan'no

J. Phys. Soc. Jpn. **60** (1991) 61.

12)"Photoionization Efficiency Curves in the Threshold Region for $Bi_n(n < 4)$ Molecules"

Y.Saito, A.Kajita, T.Yasue, M.Hayashi, A.Ichimiya, T.Gotoh, Y.Shigeta, S.Takagi, Y.Tazawa and S.Ohtani

Physica Scripta. **41** (1990) 51.

13)"Electronic and Geometric Structures of Oligothiophenes Studied by UPS and MNDO: π-Band Evolution and Effect of Disorder"

H.Fujimoto, U.Nagashima, H.Inokuchi, K.Seki, N.Nakahara, J.Nakayama, M.Hoshino and K.Fukuda

Physica Scripta. **41** (1990) 105.

14)"Decay Time Measurements of Intrinsic Luminescence in Alkali Halides Using Single-Bunched Light Pulses from UVSOR"

K.Kan'no, K.Tanaka, H.Kosaka, T.Mukai, Y.Nakai, M.Itoh, T.Miyanaga, K.Fukui and M.Watanabe

Physica Scripta. **41** (1990) 120.

15)"Density Effect on Photoionization Process in Supercritical Xenon Fluids Doped with TMAE (Tetrakis-Dimethylaminoethylene)"

K.Nakagawa, A.Ejiri, K.Kimura and M Nishikawa

Physica Scripta. **41** (1990) 140.

16)"Angle-Resolved Photoemission from Oriented Thin Films of Long Alkyl Molecules: Valence Band Dispersion"

N.Ueno, H.Fujimoto, N.Sato, K.Seki and H.Inokuchi

Physica Scripta. **41** (1990) 181.

17)" Dissociative Double Ionization Following Valence and Al: 2p Core Level Photoexcitation of $Al(CH_3)_3$"

S.Nagaoka, I.Koyano and T.Masuoka

Physica Scripta. **41** (1990) 472.

18)"Photochemical Reactions of Molecules on Alkali Halide Surfaces Induced by Undulator Radiation"

M.Watanabe, H.Nakagawa, T.Miyanaga, H.Matsumoto, M.Fujita and K.Fukui

Physica Scripta. **T31** (1990) 154.

19)"Polystyrene Thin Film Formed by Synchrotron Radiation Chemical Vapor Deposition"

H.Yamada, M.Nakamura, H.Katoh, T.Hayakawa, S.Moita, S.Hattori, H.Ohashi and K.Shobatake

J. Appl. Phys. **67** (1990) 2613.

20)"Simultaneous Generation of Optical Absorption Bands at 5.14 and 0.452 eV in 9 SiO_2:GeO_2 Glasses Heated under an H_2 Atmosphere"

K.Awazu, H.Kawazoe and M.Yamane

J. Appl. Phys. **68** (1990) 2713.

21)"O_2 Molecules Dissolved in Synthetic Silica Glasses and Their Photochemical Reactions Induced by ArF Excimer Laser Radiation"

K.Awazu and H.Kawazoe

J. Appl. Phys. **68** (1990) 3584.

22)"Formation of NH(c $^3\Pi$), NH(A $^3\Pi$), and NCO(A $^2\Sigma$) in the VUV Photolysis of HNCO"
K.Uno, T.Hikida, A.Hiraya and K Shobatake
Chem. Phys. Lett. **166** (1990) 475.

23)"Photoionization of $(O_2)_2$, $(O_2)_3$, and Ar-O_2 in the 50-100 nm Region: State Selective Ionization of O_2 in a Framework of Van Der Waals Molecules"
M.Ukai, K.Kameta, K.Shinsaka, Y.Hatano T.Hirayama, S.Nagaoka and K.Kimura
Chem. Phys. Lett. **167** (1990) 334.

24)"Ionic Fragmentation Processes in Organometallic Molecules of Group II-V Elements Following (n-1)d Core Photoionization"
S.Nagaoka, S.Suzuki, U.Nagashima, T.Imamura and I.Koyano
J. Phys. Chem. **94** (1990) 2283.

25)"Super-Polished silicon Carbide Mirror for High-Power Operation of Excimer Lasers in a Vacuum Ultraviolet Spectral Range"
K.Kurosawa, W.Sasaki, M.Okuda, Y.Takigawa, K.Yoshida, E.Fujiwara and Y.Kato
Rev. Sci. Instrum. **61** (1990) 728.

26)"Si-O Bond Breaking in SiO_2 by Vacuum Ultraviolet Laser Radiation"
Y.Takigawa, K.Kurosawa, W.Sasaki, K.Yoshida, E.Fujiwara and Y.Kato
J. Non-Crystal. Solids **116** (1990) 293.

27)"Photoexcitation of $M(CH_3)_2$ (M=Zn, Cd, Hg) compounds in the 106-270 nm region"
T.Ibuki, A.Hiraya and K.Shobatake
J. Chem. Phys. **92** (1990) 2797.

28)"Ultraviolet Photoemission Study of Oligothiophenes: π-Band Evolution and Geometries"
H.Fujimoto, U.Nagashima, H.Inokuchi, K.Seki, Y.Cao, H.Nakahara, J.Nakayama, M.Hoshino and K.Fukuda
J. Chem. Phys. **92** (1990) 4077.

29)"Vacuum Ultraviolet Photochemistry of $CHFCl_2$ and $CHFBr_2$. Absorption Spectra and CHF($\tilde{A}$ ^{1}A") Radical Formation"
T.Ibuki, A.Hiraya, K.Shobatake, Y.Matsumi and M.Kawasaki
J. Chem. Phys. **92** (1990) 4277.

30)"Negative-ion Mass Spectrometric Study of Ion Pair Formation in the Vacuum Ultraviolet. I. $N_2O \rightarrow O^- + N_2^+$"

K.Mitsuke, S.Suzuki, T.Imamura and I.Koyano

J. Chem. Phys. **92** (1990) 6556.

31)"Negative-ion Mass Spectrometric Study of Ion-Pair Formation in the Vacuum Ultraviolet. II. $OCS \rightarrow S^- + CO^+$, $O^- + CS^+$ and $CO_2 \rightarrow O^- + CO^+$

k.Mitsuke, S.Suzuki, T.Imamura and I.Koyano

J. Chem. Phys. **93** (1990) 1710.

32)"Visible and UV Spectra of a Polydiacetylene with a Side Group Conjugated to the Main Chain"

K.Ichimura, T.Kobayashi, H.Matsuda, H.Nakanishi and M.Kato

J. Chem. Phys. **98** (1990) 5510.

33)"A New Type of Luminescence Mechanism in Large Band-Gap Insulators: Proposal for Fast Scintillation Materials"

S.Kubota, J.Ruan(Gen), M.Itoh, S.Hashimoto and S.Sakuragi

Nucl. Instrum. Methods Phys. Res. A **289** (1990) 253.

34)"Far-Infrared Absorption in Nickel and Copper Microcrystals"

S.Mochizuki, K.Ishi and A.Johgo

Phys. Stat. Sol. (b) **157** (1990) K137.

35)"Suppression of Increase in Impurity in Single-Bunch Mode for the UVSOR Storage Ring"

M.Tobiyama, T.Kasuga, H.Yonehara, M.Hasumoto, T.Kinoshita, O.Matsudo, K.Nakamura, K.Sakai and J.Yamazaki

Jpn. J. Appl. Phys. **29** (1990) 210.

36)"Optical and Mechanical Properties of Hard Hydrogenated Amorphous Carbon Films Deposited by Plasma CVD"

H.Yokoyama, M.Okamoto, T.Yamasaki, K.Takahiro, Y.Osaka and T.Imura

Jpn. J. Appl. Phys. **29** (1990) 2815.

37)"Synchrotron Radiation-Excited Etching of SiO_2 with SF_6 at 143 and 251 Å Using Undulator Radiation"

K.Shobatake, H.Ohashi, K.Fukui, A.Hiraya, N.Hayasaka, H.Okano, A.Yoshida, and H.Kume

Appl. Phys. Lett. **56** (1990) 2189.

38)"New Aspects of Intrinsic Luminescence in Alkali Halides"

K.Kan'no, K.Tanaka and T.Hayashi

Rev. Solid State Sci. **4** (1990) 383.

39)"Auger-Free Luminescence Under Core Level Excitation of Ionic Crystals"

M.Itoh, S.Kubota, J.Ruan(Gen) and S.Hashimoto

Rev. Solid State Sci. **4** (1990) 467.

40)"Photo-Induced Production of CN^--Ions on the Crystal Surface of KCl"

H.Nakagawa, M.Fujita, T.Miyanaga, H.Matsumoto, K.Fukui and M.Watanabe

Rev. Solid State Sci. **4** (1990) 741.

41)"Time-of-Flight Measurement of Desorbed Particles from Solid Rare Gases Using Synchrotron Radiation"

M.Sakutai, T.Hirayama and I.Arakawa

Vacuum **41** (1990) 217.

42)"Characterization of Multilayer Reflectors for the Soft X-Ray Region Using Synchrotron Radiation"

M.Sakurai, J.Fujita, K.Yamashita, M.Ohtani, I.Hatsukade, K.Tamura, H.Nagata, Y.Suzuki and S.Seki

Vacuum **41** (1990) 1234.

43)"Photon Stimulated Desorption of Excited Neutrals from the Surface of Solid Ar"

I.Arakawa and M.Sakurai

Desorption Induced by Electronic Transitions DIET IV (Springer-Verlag Berlin, Heidelberg, 1990) p. 246.

44)"Surface Alterations of SiO_2 optics by 9.8 and 8.5 eV Laser Photons"

Y.Takigawa, K.Kurosawa, W.Sasaki, M.Okuda, K.Yoshida, E.Fujiwara, Y.Kato and Y.Inoue

J. Non-Crystalline Solids **125** (1990) 107.

45)"Time- and Spacial-Resolved Luminescence Spectroscopy of Muscle Fibers Using Synchotron Radiation from UVSOR"

M.Taniguchi, S.Toyonaga, N.Watanabe and K.Osada

2nd Europ. Conf. Prog. in X-Ray Synchrotron Radiation Research **25** (1990) 999.

46)"Growth of SiO_2 Thin Film by Photo-CVD Using Synchrotron Orbital Radiation"

M.Okuyama, M.Nakamura and Y.Hamakawa

Solid-State Electronics **33** (1990) 149.

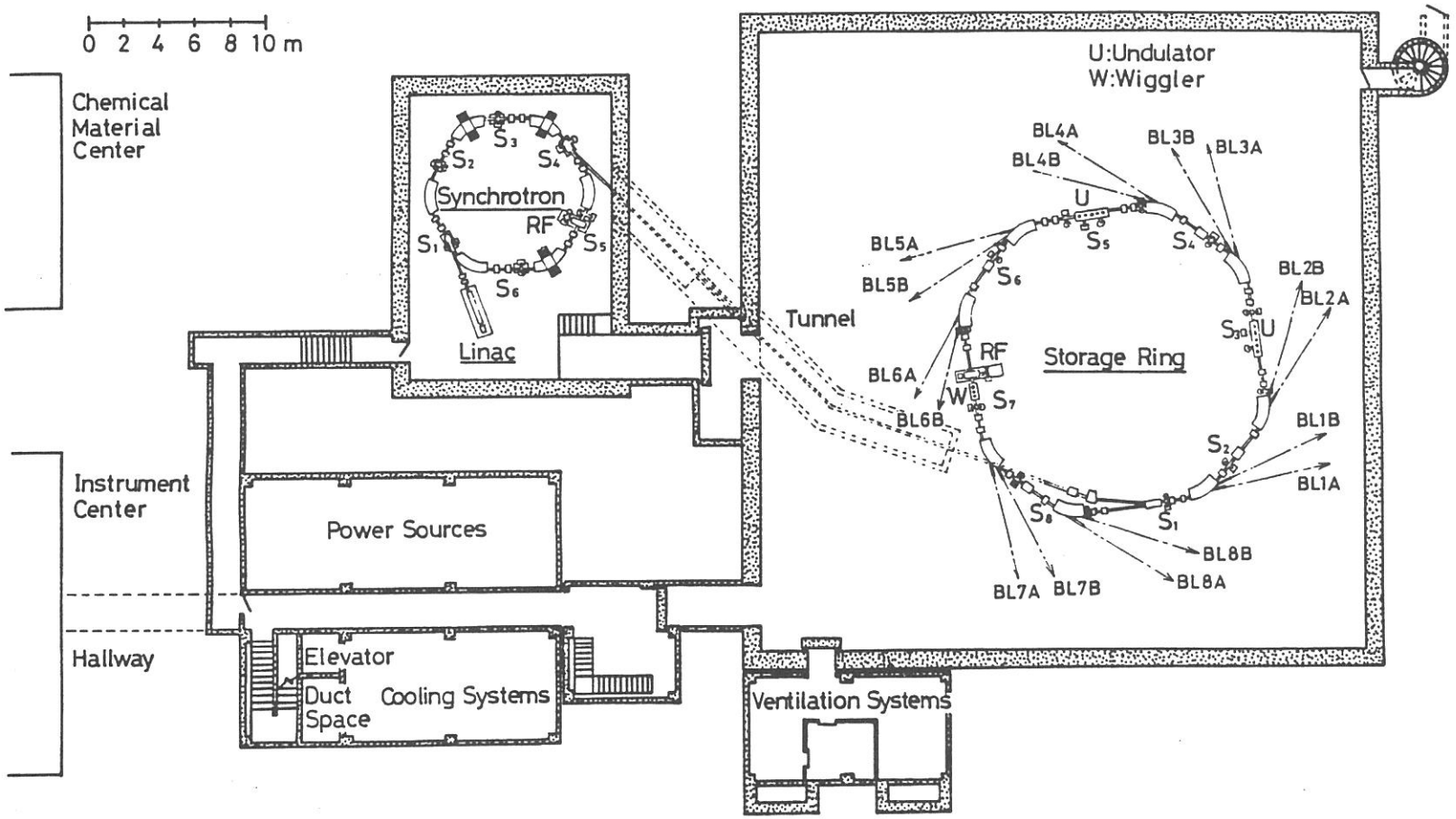

Plan view of the basement of the UVSOR Facility.

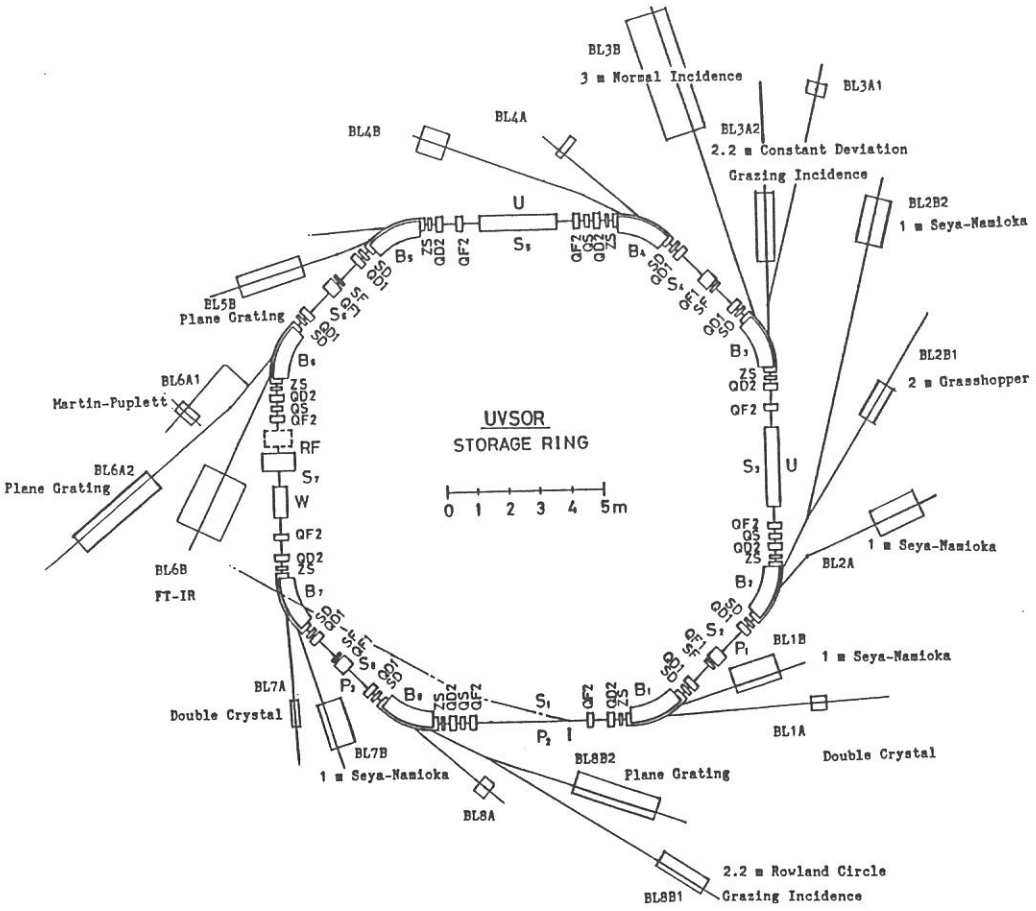

The UVSOR storage ring and the beam lines.

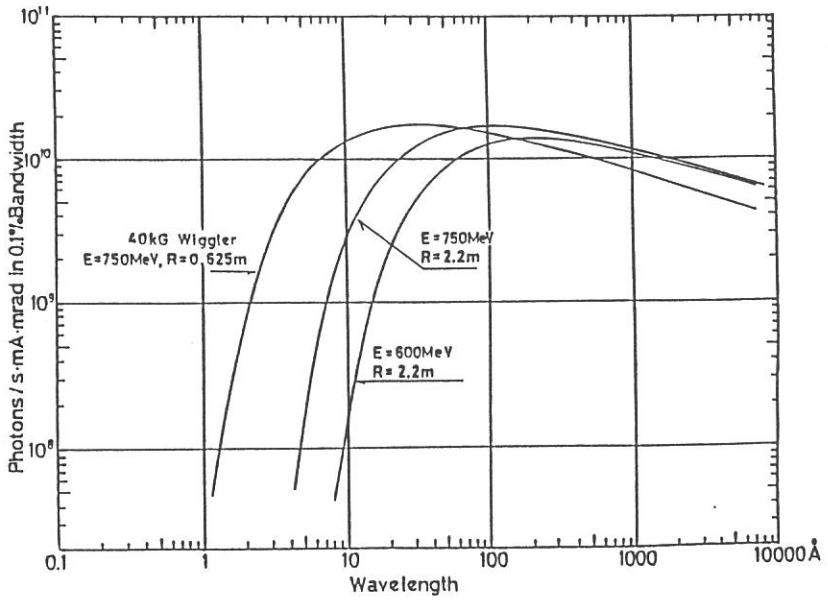

Intensity distribution of the UVSOR radiation.

Table I. Main Parameters of the UVSOR Accelerator Complex

Linac	
Energy	$E = 15$ MeV
Frequency	$f_{RF} = 2.856$ GHz
Synchrotron	
Energy	$E = 600$ MeV
Beam Current	$I = 32$ mA
Circumference	$C = 26.6$ m
Superperiodicity	$N_{superperiodicity} = 6$
Bending Radius	$\rho = 1.8$ m
Harmonic Number	$h = 8$
RF Frequency	$f_{RF} = 90.115$ MHz
Repetition Rate	$f_{rep} = 2.6$ Hz
Storage Ring	
Energy	E=750 MeV
Critical Energy of SR	$\varepsilon_c = 425$ eV
Beam Current (Nominal)	
Multi-Bunch	$I = 200$ mA
Single-Bunch	$I = 60 \sim 70$ mA
Beam Lifetime	$\tau = 180$ min.at I=200mA
Circumference	$C = 53.2$ m
Superperiodicity	$N_{superperiodicity} = 4$
Bending Radius	$\rho = 2.2$ m
Betatron Wave numbers	
Horizontal	$Q_x = 3.19$
Vertical	$Q_y = 2.22$
Momentum Compaction Factor	$\alpha = 0.032$
RF Frequency	$f_{RF} = 90.115$ MHz
RF Voltage	$V_{RF} = 50$ kV
Natural Emittance	
Horizontal	$\varepsilon_x = 1.15 \times 10^{-7}$ π m rad
Vertical[a)]	$\varepsilon_y = 1.15 \times 10^{-8}$ π m rad
Beam Sizes	
Horizontal	$\sigma_x = 0.39$ mm
Vertical[a)]	$\sigma_y = 0.27$ mm
Bunch Length	$\sigma_l = 170$ psec

a) 10 % coupling is assumed.

Table 2. Beam Lines at UVSOR

Beam Line	Monochromator, Spectrometer	Wavelength Region	Acceptance Angle(mrad)		Experiment
			Horiz.	Vert.	
BL1A	Double Crystal	15 - 8 Å	4	1	Solid
BL1B	1m Seya-Namioka	6500 - 300 Å	60	6	Gas &Solid
BL2A	1m Seya-Namioka	4000 - 300 Å	40	6	Gas
BL2B1	2m Grasshopper	600 - 15 Å	10	1.7	Gas & Solid
BL2B2	1m Seya-Namioka	2000 - 300 Å	20	6	Gas
BL3A1	None (Filter, Mirror)		(U) 0.3	0.3	Gas & Solid
BL3A2	2.2m Constant Deviation	1000 - 100 Å	10	4	Gas & Solid
	Grazing Incidence		(U) 0.3	0.3	
BL4A	None		6	6	Irradiation
BL4B	None		8.3	6	Irradiation
BL3B	3m Normal Incidence	4000 - 300 Å	20	6	Gas
BL5B	Plane Grating	2000 - 20 Å	10	2.2	Calibration[#]
BL6A1	Martin-Pupplet	5 mm - 50 μm	80	60	Solid
BL6A2	Plane Grating	6500 - 80 Å	10	6	Solid
BL6B	FT-IR	200 - 1.7 μm	70	25	Solid
BL7A	Double Crystal	15 - 8 Å	2	0.3	Solid
		15 - 2 Å	(W) 1	0.15	Solid
BL7B	1 m Seya-Namioka	6500 - 300 Å	40	8	Gas & Solid
BL8A	None (Filter)		25	8	Irradiation, User's Instrm.
BL8B1	2.2 m Rowland Circle Grazing Incidence	440 - 20 Å	10	2	Gas & Solid
BL8B2	Plane Grating	6500 - 80 Å	10	6	Solid

[#] National Institute for Fusion Science

U: with an undulator, W: with a wiggler

LOCATION

Ultraviolet Synchrotron Orbital Radiation (UVSOR) Facility, Institute for Molecular Science (IMS) is located at Okazaki. Okazaki (population 300,000) is 260 km southwest of Tokyo, and can be reached by train in about 3 hours from Tokyo via New Tokaido Line (Shinkansen) and Meitetsu Line.

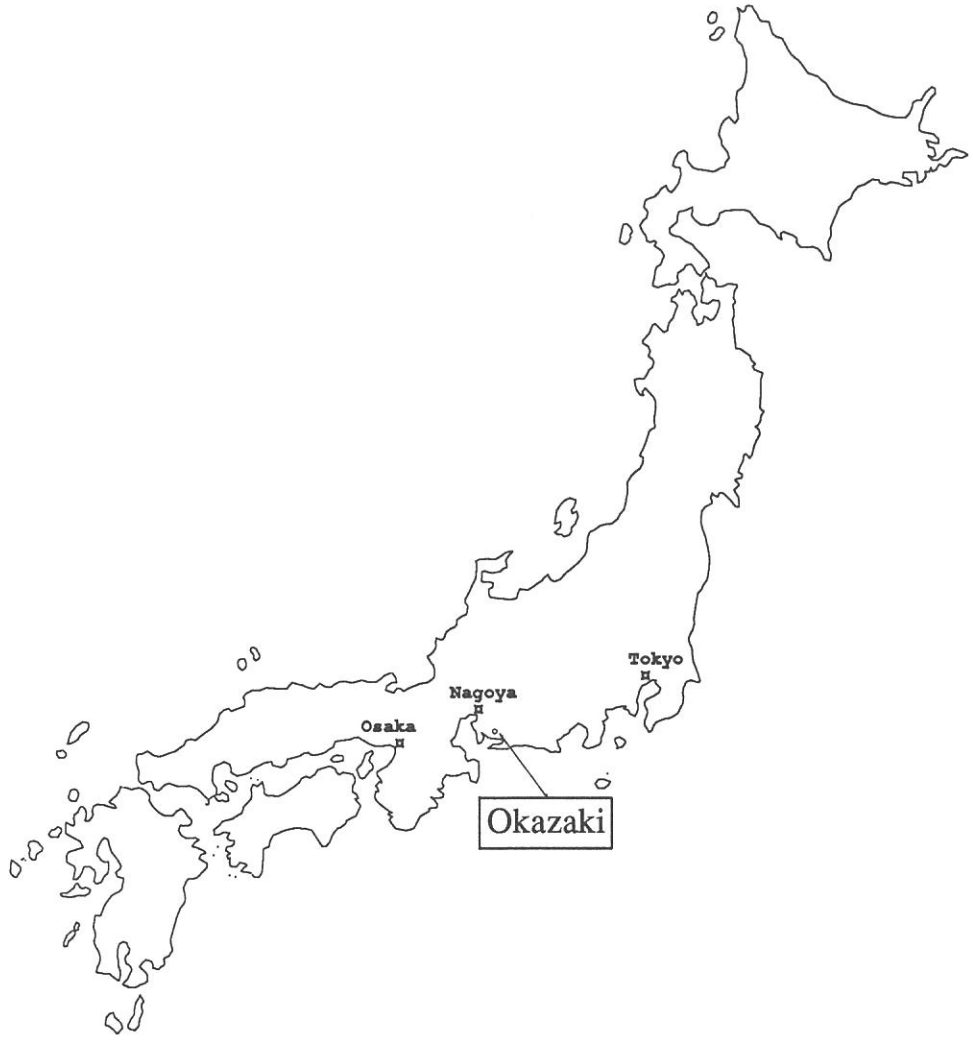

Address
UVSOR Facility, Institute for Molecular Science
Myodaiji, Okazaki 444, JAPAN

Telephone 0564-52-6101 (UVSOR)
Fax 0564-54-7079 (UVSOR)
Telex 4537475 KOKKEN J (IMS)

Editors: M. Kamada and S. Tanaka